SURFACE-RELATED MULTIPLE ELIMINATION, AN INVERSION APPROACH

PROEFSCHRIFT

ter verkrijging van de graad van doctor
aan de Technische Universiteit Delft,
op gezag van de Rector Magnificus,
prof. drs. P.A. Schenck,
in het openbaar te verdedigen
ten overstaan van een commisie,
aangewezen door het College van Dekanen
op dinsdag 3 december 1991 te 16.00 uur door

DIRK JACOB VERSCHUUR

geboren te Alphen aan den Rijn

natuurkundig ingenieur

Gebotekst Zoetermeer / 1991

Dit proefschrift is goedgekeurd door de promotor:

prof. dr. ir. A.J. Berkhout

CIP-DATA KONINKLIJKE BIBLIOTHEEK, DEN HAAG

Verschuur, Dirk Jacob

Surface-related multiple elimination, an inversion approach / Dirk Jacob Verschuur
[S.l. : s.n.] (Zoetermeer : Gebotekst)
Thesis Technische Universiteit Delft. - With ref. - With summary in Dutch.
ISBN 90-9004520-1
Subject heading: seismology

SUPPORT
The research for this thesis has been financially supported by the Dutch Technology Foundation S.T.W. (project DTN 58.0879) and the DELPHI consortium.

Printed in The Netherlands by: N.K.B. Offset bv, Bleiswijk

PREFACE

The research that formed the basis of this thesis has been carried out in the Laboratory of Seismics and Acoustics of the Physics department at the Delft University of Technology.

The research has been financially supported by the Dutch Technology Foundation (S.T.W., DTN 58.0879) for the first four and a half years and by the Delphi consortium for the last half year. Being involved in the pre-processing team of the Triton project first and in the Delphi project later on gave me the opportunity to do research within a larger context and have contacts with the international geophysical industry.

Although it may seem that this thesis is the work of one person alone, the discussions with and cooperation of many members of the laboratory have substantially contributed to the final result. Therefore, I would like to express my appreciation to the following people.

First of all I would like to thank my promotor prof. A.J. Berkhout, whose never ending enthusiasm for this research has always been a source of inspiration. His ability to see things in a broader prospective resulted in many constructive suggestions.

Next I want to express my sincere thanks to my direct supervisor dr. Kees Wapenaar. The many fruitful discussions with him have always been helpful to improve the theoretical background of this research.

Also I want to thank all the colleagues of the laboratory for the many pleasant conversations, the good discussions and the helpful hands. The pleasant atmosphere has had a positive influence on the scientific output. In this respect I want to thank my former colleagues Niels, Gerrit, Henk, René, Alex, Gerd-Jan and Wim as well as my present Delphi colleagues Greg, Cees, Phillippe, Johan, Walter, Berend and Jan-Willem.

The research involved a large amount work being carried out on the computer and the assistance of the computer support team, Edo and Leen, is also highly appreciated.

Apart from doing research, working in a research group also brings in many practical arrangements that have to be made. For this, I want to thank Hanneke for her help.

The Dutch Technology Foundation and the Delphi sponsors are thanked for their support on this research. I am especially grateful to SAGA Petroleum A.S. for providing the field data.

Finally, I would like to express my appreciation for my wife Margreet, for her moral support, attention and patience.

TABLE OF CONTENTS

5 *FROM SIMULATED DATA TO FIELD DATA, PRACTICAL CONSIDERATIONS*

6 *IMPLEMENTATION AND APPLICATION ASPECTS*

7 *FIELD DATA EXAMPLES*

8 *SURFACE-RELATED MULTIPLE ELIMINATION, A CMP VERSION*

9 *CONCLUSIONS AND DISCUSSION*

1

INTRODUCTION

1.1 SEISMIC EVENTS

1.1.1 Primaries, multiples and surface waves

In the noise-free situation surface seismic responses consist of three main types of events, as illustrated in Fig. 1.1:

- *direct and surface waves*

  Waves that do not propagate downward, but travel laterally, just below the surface. In the marine case this is the direct P-wave, which propagates from the source to the receivers without reflection. On land there are more wave types involved that travel along the surface, normally referred to as ground roll. In this thesis direct waves and surface waves are not addressed; it will be assumed that they are removed in a first processing step.

- *primary events*

  Waves that propagate in the subsurface (downward and upward) and have bounced (reflected, diffracted or refracted) only once.

- *multiple events*

  Waves that propagate in the subsurface (downward and upward) and have bounced at least twice before detection.

  In the *surface* seismic situation, multiples defined by *vertical* bounces are more important than multiples defined by *lateral* bounces. Therefore, in this thesis we will address only the multiples that have bounced up- and down at least three times (up, down, up); see Fig. 1.1.

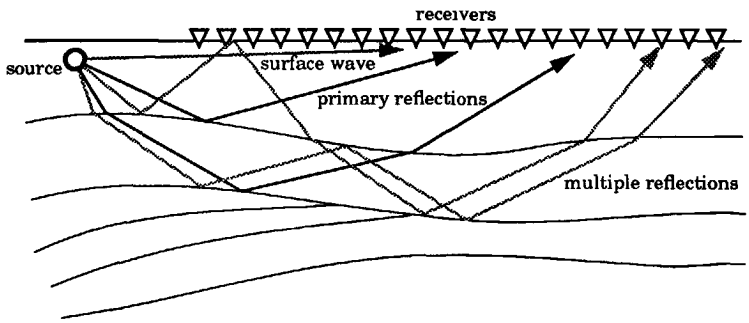

Fig. 1.1 The different type of waves that are measured in a seismic experiment.

In most seismic processing methods the seismic data is considered to consist of primary events only. The influence of multiples, however, may generally not be neglected and should be removed in a separate step.

For an example we consider the acoustic subsurface model of Fig. 1.2. Fig. 1.3a shows the primary response (no surface waves, no multiples) as a function of time for a source (frequency content of 10-50 Hz, mixed phase) located at 2000m. The receivers are positioned along the surface with a separation of 20m. The shot record experiment is repeated for different source locations (separation of 20m) in order to illuminate the subsurface from different angles. Fig. 1.3b shows the multiple free pre-stack migration result for the shot records with the sources located from 1000 to 3000m. The 4 primary reflections from Fig. 1.3a (marked with numbers corresponding to the 4 interfaces in Fig. 1.2) have been properly imaged at the correct depths, as can be observed when comparing Fig. 1.3b with Fig. 1.2.

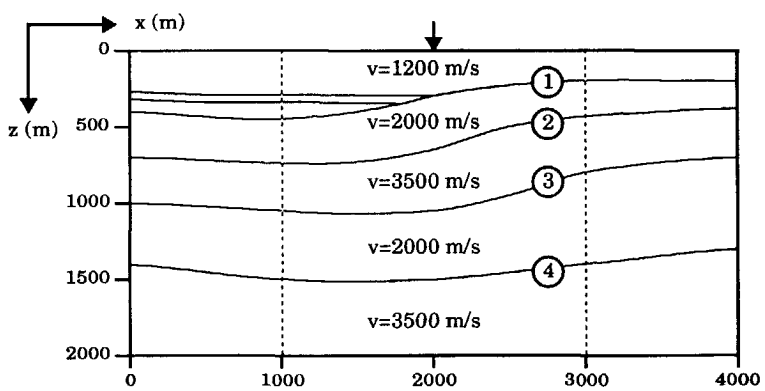

Fig. 1.2 Subsurface model for the simulation of seismic surface data. The sources are located between 1000 m and 3000 m with a separation of 20 m.

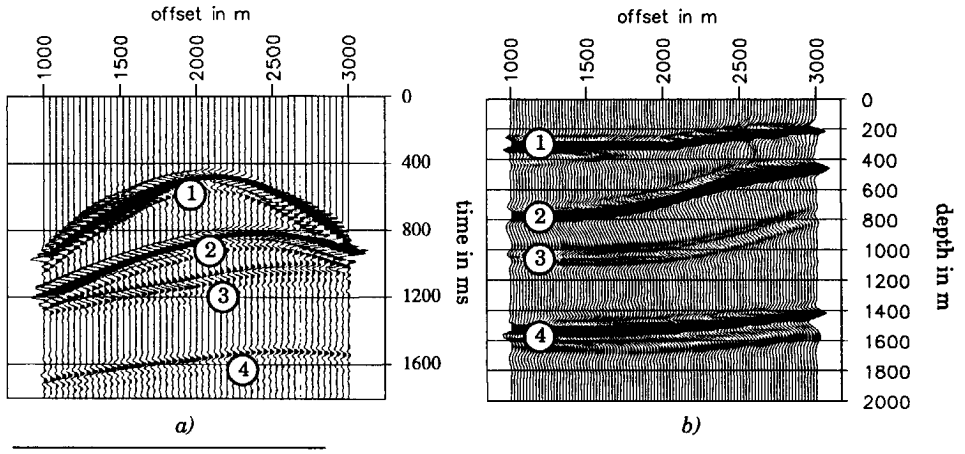

Fig. 1.3 *a) Shot record without multiples for a source located at the marked position in Fig. 1.2*
b) Multiple free pre-stack migration result for the shot records located between 1000 m and 3000 m.

As already mentioned, in reality a measured response from the earth consists of more events than primaries only. Particularly, a large number of multiple reflections are present in the data. One might argue that multiple reflections have lower amplitudes than the primary reflections (as each bounce reduces the amplitude) and may therefore be neglected. Unfortunately this negligence is not allowed in many situations, as for strong reflectors this amplitude reduction is only moderate, especially when the free surface is involved. However, even more important is the fact that the *number* of multiple reflections is much larger than the *number* of primary reflections.

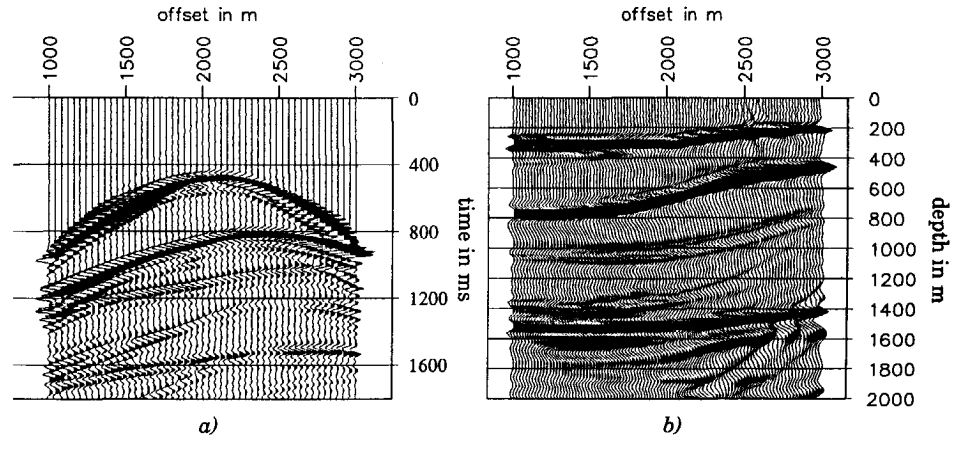

Fig. 1.4 *a) Shot record with multiples for a source located at the marked position in Fig. 1.2*
b) Pre-stack migration result with multiples for the shot records located between 1000 m and 3000 m.

In many situations primaries of the deeper reflectors can be totally obscured by the large number of multiples generated at the shallower reflectors. As a consequence, it is very difficult to make a reliable interpretation of the seismic data, particularly with respect to amplitudes. To illustrate this Fig. 1.4a shows a shot record at the same position as in Fig. 1.3a, but now with all the multiples included. Even for this simple four-reflector example the number of events has increased significantly and it may be difficult to distinguish between the primary and multiple events, particularly at the level of reflector 4 (target). After pre-stack migration of the shot records with multiples the result is shown in Fig. 1.4b. Apart from the well imaged primary reflections, a number of false images from the multiples can be observed at the target, which may lead to a seriously wrong interpretation. As seismic processing gradually changes to *pre-stack* imaging, in stead of the standard *post-stack* processing, the correct amplitudes in *pre-stack* data is becoming very important. As the influence of multiples in single-source data is much larger than in a multi-source image, one of the first steps in a seismic processing sequence should be to remove the multiple events from the shot records, in order to end up with pre-stack seismic data that contains primaries only.

1.1.2 Different types of multiples

It is important to make a distinction between different types of multiples. For our purpose an organization into two types will be made: the *surface-related* multiples and the *internal* multiples. Surface-related multiples are those reflection events that have at least one bounce against the free surface, i.e. they are those events that would disappear if the surface was totally absorbing. Internal multiples are those events that have bounced at least three times (up, down, up), without any reflection against the surface being involved.

The surface-related multiples can be subdivided into first layer multiples, first layer reverberations and "remaining" surface-related multiples:

- The first layer multiples are those multiple reflections that have *not* propagated in the subsurface below the first layer; they are trapped in the first layer bouncing between surface and first layer bottom, as is shown in Fig. 1.5a.

- The first layer reverberations are those multiple reflections that have propagated in the subsurface below the first layer; they start and/or end with at least one extra round trip in the first layer, see Fig. 1.5b.

- The remaining surface-related multiples are those events that start *and* end with a reflection in the subsurface below the first layer, with at least one bounce against the surface in between (Fig. 1.5c).

- Finally Fig. 1.5d shows some internal multiples, being multiple reflections for which the free surface is not involved.

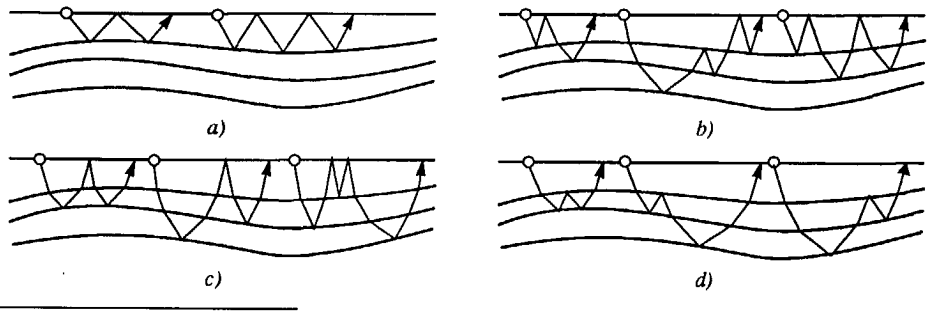

Fig. 1.5 *a) First layer multiples b) First layer reverberations c) "Remaining" surface-related multiples d) Internal multiples.*

For marine data the first layer is the water layer and surface-related multiples, in particular the water layer reverberations, play a very important role.

1.1.3 The reflecting surface

The method described in this thesis aims at removing all surface-related multiples from the seismic surface data and leaves the primaries and internal multiples. It is important to realize that the major amount of *multiple* energy in almost all seismic situations is produced by the free surface (sometimes the major amount of *all* energy in the data is caused by surface-related multiples). This is because the reflection coefficient of the free surface is -1, which causes each upgoing event to be totally reflected at the surface, generating an additional (complex) illuminating wave field. This is repeated over and over again. It causes a major train of surface-related multiples in the seismic section (see Fig. 1.6).To see the influence of the free surface on seismic data Fig. 1.7 shows a zero offset section with and without surface-related multiples that are simulated in the model of Fig. 1.6. Note the enormous reduction of events and the improvement of the ability to make an interpretation of the data in Fig. 1.7b. The primary reflections can be easily identified. The internal multiples (indicated with the arrows in Fig. 1.7b) are of minor importance.

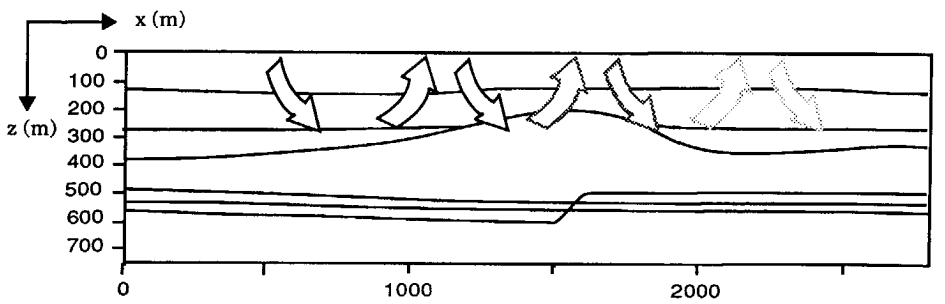

Fig. 1.6 *The free surface fully reflects all upgoing energy, giving rise to a major sequence of surface-related multiples.*

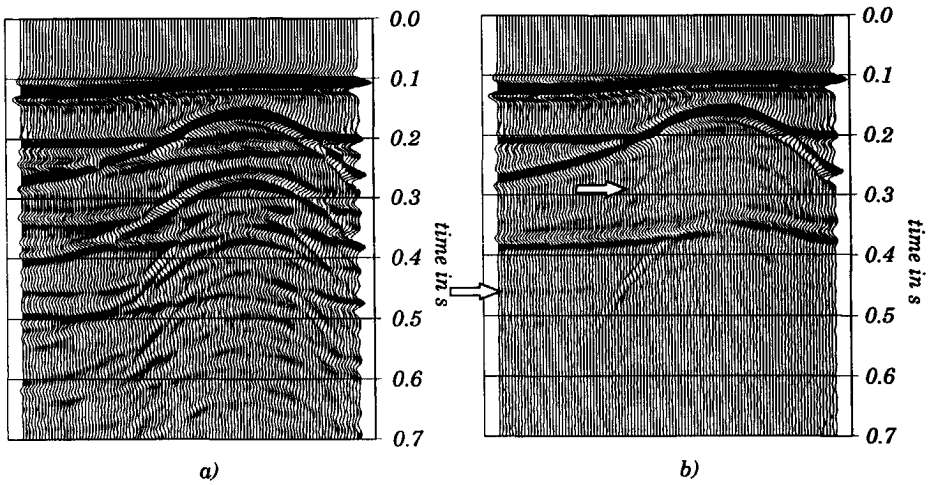

Fig. 1.7 *a) Simulated zero offset section with surface-related multiples*
b) Simulated zero offset section without surface-related multiples.
The two arrows indicate the (much weaker) internal multiples that are not removed.

In many of the simulated and field data examples, that have been investigated so far, a similar major improvement is achieved by removing the free surface multiples from the data. The detrimental effect of *surface-related* multiples on seismic data is not always realized in the seismic industry.

1.2 OVERVIEW OF MULTIPLE ELIMINATION METHODS

The problem of multiples and how to deal with them is as old as the seismic method itself. Many efforts have been made to remove multiples from the data and to preserve the primary events. We have subdivided multiple suppression methods into filtering methods and wave field methods.

The *filtering methods* assume that in seismic data the primary reflections and the multiples have different properties. Based on those differences both groups are separated by a special filtering process. The difference in properties, on which the discrimination is based, rely on assumptions which are generally not fully met (e.g. whiteness of reflectivity series, different move-out properties, 1D subsurface model). Therefore they might be risky to apply, removing primary energy as well. On the other hand, they are very attractive in situations where those assumptions are (approximately) valid, because of their efficiency.
We will review the predictive deconvolution and the differential move-out filtering methods.

In *wave field methods* multiples are predicted using wave theory as well as subsurface information related to the multiple generating layer. After the prediction step the multiples are subtracted from the data. In general the wave field methods are more effective, but they are also more expensive. Surface-related multiple elimination, which is the topic of this thesis, belongs to this category. A unique property of the proposed surface-related method is that *sub*surface information is not used for predicting the surface-related multiples.
We will discuss the wave field extrapolation and subtraction technique and, of course, the newly developed wave field based surface-related multiple elimination technique.

For an overview of a multiple elimination strategy as part of a standard seismic data processing sequence, see Hardy and Hobbs (1991). However, note that their strategy is based on the objective to generate a multiple-free *stack*. The surface-related multiple elimination method on the other hand yields multiple-free *pre-stack* data; it is therefore very suited as one of the first steps in a pre-stack data imaging and inversion scheme, like the method proposed by the DELPHI project, see Berkhout and Wapenaar (1990). But also the seismic inversion technique as described by Tarantola (1987), which uses fitting of simulated with field data, can take advantage of introducing an absorbing free surface. On post-stack stratigraphic inversion techniques, like Duijndam (1988) or Gelfand and Larner (1983), remaining stacked multiple energy may have a very negative effect and multiple elimination is an essential pre-processing step.

1.2.1 Predictive deconvolution

Predictive deconvolution is a statistical technique that is generally used for two purposes: wavelet shortening (wavelet shaping) and multiple elimination. It is based on the assumption that a seismic trace consists of a deterministic and a statistical part. The deterministic part consists of the source signature and the multiple generating process. The statistical part contains the primary reflection sequence, that is assumed to be white, i.e. a flat power spectrum in the frequency domain. The separation of these two is based on the assumption that the autocorrelation function of the seismic trace at non-zero shifts is only defined by the deterministic part, as a white time series has a autocorrelation function which is equal to a scaled delta pulse.
A large number of publications on predictive deconvolution can be found in the literature. For a clear description see Robinson and Treitel (1980). The deterministic part, which is the combination of the wavelet and the multiple generating operator, is assumed to be minimum phase. If the deconvolution is applied as a so-called gapped deconvolution, the wavelet is left (largely) unchanged and only the multiple generating process is being corrected for. In that case the wavelet does not need to be minimum phase. However, the separation of the wavelet and the multiple generating operator is only possible if the gap (the periodicity of the multiples to be removed) is larger than the wavelet length. For the gapped predictive deconvolution there are in fact two variants: single- and double-gap filters. The first one is based on the removal of the first layer *multiples*, being ideally $\delta(t)+r_1\delta(t-t_1)$, r_1 being the reflectivity of the first reflector at traveltime t_1.

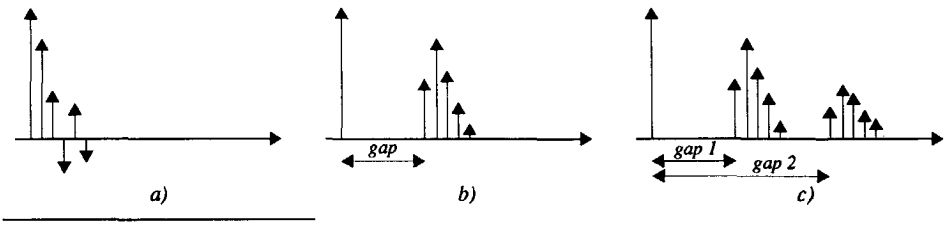

Fig. 1.8 Three variants of the predictive deconvolution operator a) Wavelet shaping deconvolution operator b) Single-gap deconvolution operator c) Double-gap deconvolution operator.

The double-gap deconvolution filter is designed for removing the first layer *reverberations*, being ideally $\delta(t)+2r_1\delta(t-t_1)+r_1^2\delta(t-2t_1)$. However, for small first interface reflection coefficients, the second term in the double gap deconvolution will be small, which causes the two variants to give comparable results. Fig. 1.8 shows the three discussed variants of the predictive deconvolution operators. Predictive deconvolution is generally applied to remove the first layer multiples and reverberations simultaneously with a single-gap deconvolution. The gap is designed to be roughly equal to the two-way traveltime in the first layer. A classical reference for periodic multiple removal is Backus (1959). The predictive deconvolution method is still very popular in seismic processing.

Fig. 1.9 shows an example of predictive deconvolution on a 1-D modeled data set (horizontal plane wave response from a horizontally layered medium). Fig. 1.9a shows a 4-reflector model in which a horizontal plane wave response is simulated with all multiples included, see Fig. 1.9b. Even for this simple model it is difficult to distinguish primaries from multiples. After applying single-gap predictive deconvolution the result is shown in Fig. 1.9c. For this example the exact first layer multiple periodicity has been used (0.4 s) with a filter length of 1, and the autocorrelation function is calculated from the first 2 seconds of data only. The latter accomplishes that the predictive deconvolution process concentrates on the first layer *multiples*, which are well removed (see the arrows in Fig. 1.9b). If the removal of the reverberations is the main objective, a double-gap deconvolution is applied, resulting in Fig. 1.9d. Now the autocorrelation function is computed from the full trace. Note that the first layer *multiples* (e.g. at 0.8 s) are overcorrected now. The arrows point at suppressed first layer *reverberations*. From this example it is clear that with predictive deconvolution no complete suppression of both first layer *multiples* and *reverberations* can be done, due to the different generation systems. However, knowing the exact first layer multiple period t_1 and reflection coefficient r_1, the multiple removal could be done deterministically by applying the (frequency domain) operator $(1+r_1e^{-j\omega t_1})$, then mute the first primary and apply this operator for the second time. With the first filtering step one half of the first layer reverberations are removed plus the first layer multiples, the second filtering step removes the other half of the reverberations. The result of this deterministic approach is shown in Fig. 1.9e. This is exactly the 1D variant of the wave field based extrapolation and subtraction technique (see section 1.2.3). Finally Fig. 1.9f shows the response modeled without surface-related multiples. This would also be the result of our surface-related multiple elimination scheme. Note that only the *internal* multiples are left.

The main advantages of the predictive deconvolution technique are:

* It is computationally very fast, as it is applied on a single trace basis.
* It is very simple to apply, as it needs a minimum of user interaction.

The drawbacks of this method are:

* A reflectivity series is never perfectly uncorrelated, certainly not over a limited time interval.
* The multiple generating system is assumed to be one-dimensional, resulting in a multiple periodicity which is constant along the trace. Therefore this method is most effective on zero offset traces in an approximately horizontally layered medium.
* In situations were the underlying assumptions are not met, primary reflections may be distorted and multiples are only partly removed.

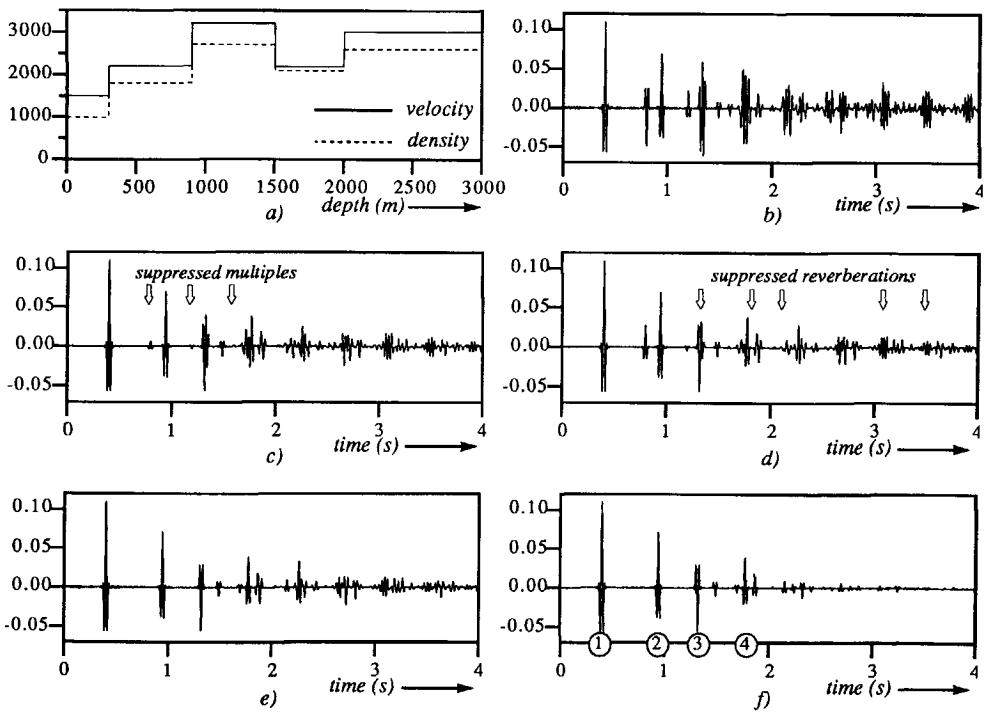

Fig. 1.9 *a) Velocity and density function of a 1D 4-Reflector model b) Horizontal plane wave response with all multiples included c) Response after applying single-gap predictive deconvolution d) Response after applying double-gap predictive deconvolution e) Response after deterministic removal of the first layer multiples and reverberations f) Horizontal plane wave response modeled without surface-related multiples (resulting in primaries and internal multiples).*

Efforts have already been reported to extend the single trace predictive deconvolution technique to a multi-trace (pre-stack) deconvolution procedure, by which the varying character of the multiple periodicity as a function of offset may be taken into account. This can be done in the space-time domain where 2-dimensional deconvolution operators are designed and applied, see Taner (1990). Another way to handle the multi-offset situation is to apply predictive deconvolution in the tau-p domain. In this domain the periodicity of the multiples is constant per p value for a horizontally layered model. This is investigated by Taner (1980) and Durrani (1991). In section 1.2.5, Fig. 1.17, an example of deconvolution using the tau-p transform is showed. However, note that an accurate forward and backward tau-p transform is required to end up with the correct primaries in the space-time domain. Results show that those extended predictive deconvolution methods improve the result for non-zero offset traces indeed.

1.2.2 Differential move-out filtering and stacking

Another very popular type of multiple elimination is based on discrimination of primaries and multiples by their different move-out velocities. The underlying idea is the assumption that for a given zero offset arrival time a primary has a higher move-out (stacking) velocity than a multiple. In order to make a separation of events with different move-out velocities possible, the data is transformed to another domain, e.g. with a spatial Fourier transform or with a (linear or quadratic) Radon transform. In the new domain the separation step is done and the inverse transformation is applied on the "primary" data.

A refined version of the Fourier based velocity filtering procedure is described by Ryu (1982). He applies NMO correction on the CMP gathers with velocities that are in between primary and multiple velocities. Primary events are therefore slightly overcorrected and multiples undercorrected. In that way primary and multiple events map onto the positive and negative k_x-plane respectively. By zeroing the negative k_x-plane, applying an inverse spatial Fourier transform and removing the NMO correction, the multiples are suppressed. The velocity filtering procedure is applied on pre-stack data, but in standard processing a stacking process will always follow. In fact stacking alone has also velocity filtering capabilities, as the events will be added along the primary stacking curves. All events with move-out properties which differ from the primaries will destructively interfere by the stacking process. Generally the k_x-plane velocity filtering procedure is applied when stacking, together with predictive deconvolution, is not sufficient; see also Hardy and Hobbs (1991).

A more recent approach of the velocity filtering technique takes advantage of the generalized Radon transform, which adds the data along parabolic trajectories (after applying a rough NMO correction to the data, which allows a parabolic description of the residual move-out curves). In this way a better separation of primaries and multiples can be achieved compared to the k_x-plane filtering technique, see Hampson (1986), Yilmaz (1989) and Kelamis et al (1990).

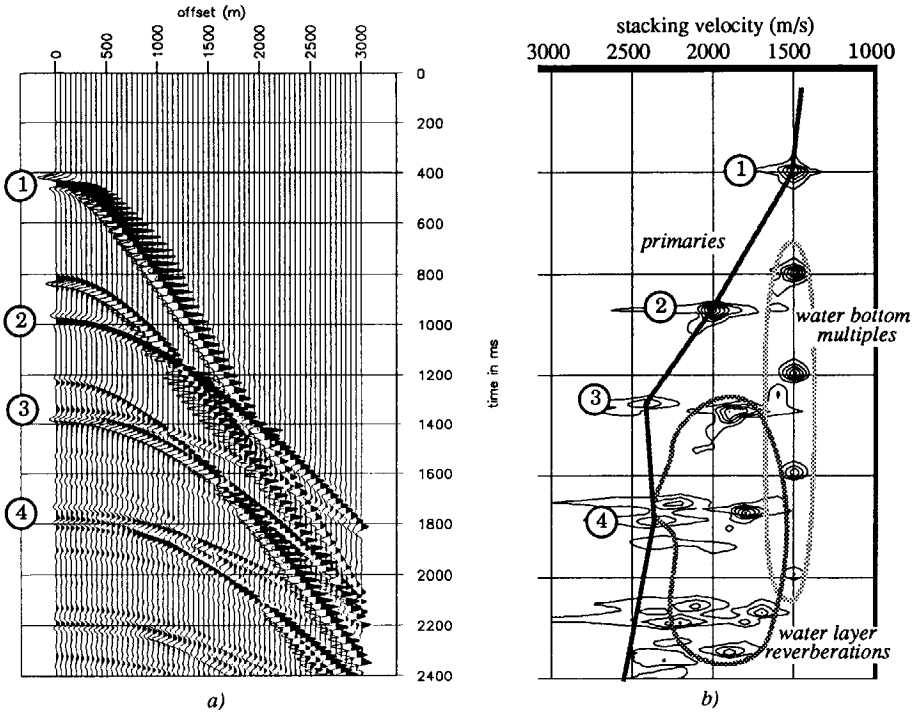

Fig. 1.10 *a) Simulated CMP gather with primary and multiple events related to the model of Fig. 1.9a b) Velocity panel related to a).*

To illustrate the k_x-plane filtering technique, Fig. 1.10a shows a CMP gather simulated in the horizontally layered model, which has been built with the velocity and density function of Fig. 1.9a. The simulation has been done with an acoustic finite difference algorithm. Also a velocity panel of this CMP gather has been calculated, which is shown in Fig. 1.10b. The four primaries have been indicated in Fig. 1.10. The important multiples in Fig. 1.10 have been classified in the velocity panel. The water bottom multiples have the lowest stacking velocity. The water layer reverberations have higher stacking velocities, somewhere in between the water velocity and the primary stacking velocities. The surface-related multiples without the first layer involved (the "remaining" surface-related multiples) have the highest stacking velocities, but still lower than the primary velocities. The internal multiples have stacking velocities in the neighbourhood of the primary velocities.

In the example of Fig. 1.10 the events can be separated in the velocity domain, except for the fourth primary reflection around 1.8 s. There the primary and multiple are almost fully overlapping due to the velocity inversion in the model at 1500 m. On this dataset the velocity filtering method via the k_x-plane was applied, rejecting all the events with stacking velocities less than 90% of the primary stacking velocity curve (which is depicted in Fig. 1.10b).

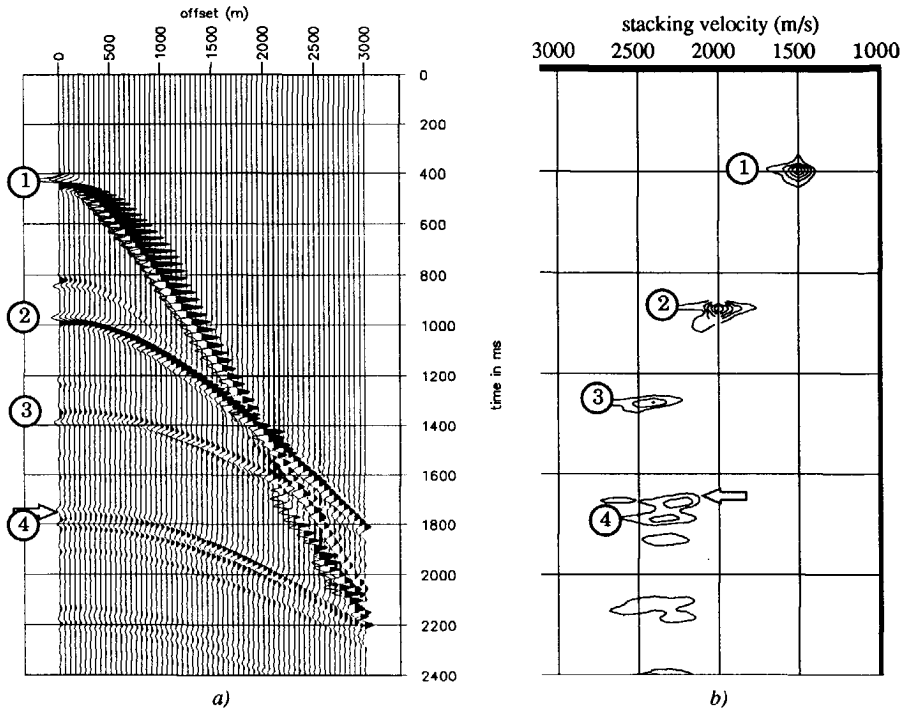

Fig. 1.11 *a) Seismic CMP gather of Fig. 1.10a after applying the velocity filtering method, rejecting all events with velocities lower than 90% of the primary event b) Velocity panel related to a).*
Note that the reverberation at the arrow can not be separated from the primary interfering with it.

Fig. 1.11 shows the filtering result, together with its velocity panel. A lot of multiple energy has been removed, although at the small offsets there are some remainings of multiple energy; also the primaries have been distorted there. Note that the method described by Hampson (1986) using the generalized Radon transform would have produced a better result at the smaller offsets. However, those events that are overlapping in the velocity domain can never be separated by any velocity discrimination method.

The advantages of the move-out filtering methods are:

* The calculations involved are rather simple, although it takes significantly more time than predictive deconvolution. Using the generalized Radon transform involves more elaborate calculations than the Fourier transform methods.

* It is possible to remove internal multiples, provided sufficient move-out differences with respect to the primaries occur.

* The output is pre-stack data (normally CMP gathers), allowing pre-stack processing of the data after multiple elimination.

The disadvantages of the move-out methods are:

* If there is no sufficient move-out difference between primaries and multiples (e.g. in areas with a significant velocity inversion), move-out related multiple elimination does not work satisfactory.

* For the small offsets all events are approximately flat (the top of the hyperbolas). Therefore, move-out techniques tend to destroy primary information at small offsets.

* For laterally inhomogeneous media, for which both primary and multiple events have complex move-out curvatures, move-out separation is not practical.

* User interaction is necessary in order to make a distinction in the velocity panels between primaries and multiples.

1.2.3 Wave field extrapolation and subtraction

The wave field based multiple elimination methods predict the multiples with extrapolation techniques based on wave theory. They can be considered as a *layer*-oriented approach (in contrast with our surface-related multiple elimination method, which is an *interface*-oriented approach). References for this extrapolation method can be found in Bernth and Sonneland (1983), Berryhill and Kim (1986) and Wiggins (1988).

With the wave field extrapolation and subtraction method the multiples related to the first layer (i.e. the water layer in the marine case) are eliminated. If we consider the subdivision of multiples as discussed in section 1.1.2, this method will eliminate the multiples of Fig. 1.5a and Fig. 1.5b. This is achieved by extrapolating the seismic data one round trip through the first layer (down and up), by which primaries become first order reverberations, first order reverberations become second order etc. By subtracting these from the original data all first layer reverberations will be eliminated. In fact the wave field extrapolation and subtraction method is the deterministic counterpart of predictive deconvolution.

The application of this method is shown in Fig. 1.12. The same data of Fig. 1.10a is considered. A shot record of this horizontally layered medium is identical to the CMP gather of Fig. 1.10a. After one extra round trip through the first layer, all events become one order higher (Fig. 1.12a). If those events are subtracted from the original shot record (Fig. 1.10b), the result is Fig. 1.12b. We see that the water bottom multiples (indicated with the arrows in Fig. 1.12a) have been removed.

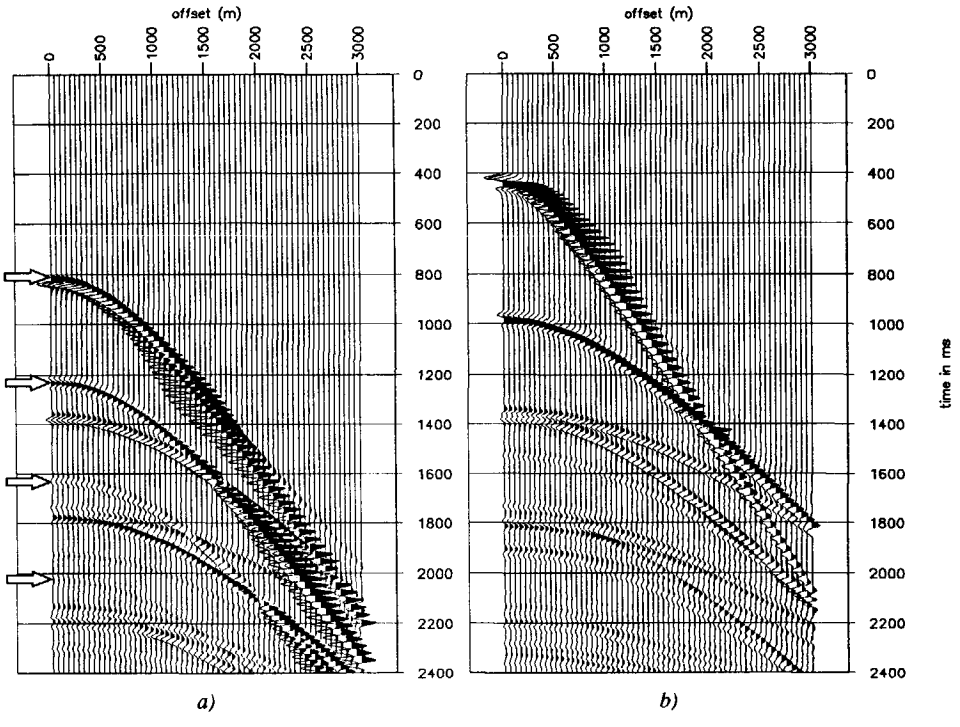

Fig. 1.12 *a) Seismic shot record of Fig. 1.10a after extrapolation one round trip through the first layer, predicting the first layer multiples and part of the reverberations b) Shot record after subtracting the predicted multiples from the original shot record. The arrows indicate predicted water bottom multiples.*

However, the water layer *reverberations* have been reduced to only half the original amplitudes, as each reverberation occurs twice, see Fig. 1.13. For a horizontally layered medium these dual reverberations exactly overlay (see Fig. 1.13a), but for laterally inhomogeneous media they appear as separate events (Fig. 1.13b). Note also that higher order reverberations have also an increasing number of ways to occur; e.g. for a second order reverberation there are three possibilities, for a third order reverberation there are four possibilities etc.

Actually, a second extrapolation at the source side should be applied to predict the other half of the reverberations. To do this properly, the primary of the water bottom should be removed in advance, in order to prevent the water bottom *multiples* to be overcorrected.
The fact that two separate extrapolations with an intermediate removal of the first primary is needed to do a perfect first layer-related multiple removal has already been mentioned by Bernth and Sonneland (1983); we also discussed this aspect in section 1.2.1. Wiggins (1988) used the *one-step* prediction to remove the water bottom multiples only.

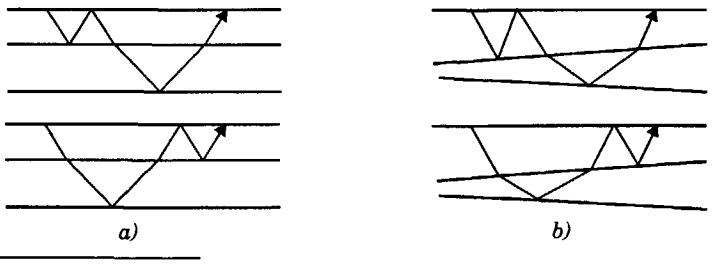

Fig. 1.13 Each first order reverberation of a reflection from a deeper interface occurs twice. In a horizontally layered medium these reverberations overlap exactly in time (a), but for a laterally inhomogeneous model these events do not overlap (b).

The discrepancies between the multiples predicted by only one extrapolation step and the true multiples in the data can be (partly) overcome by applying the subtraction adaptively. By introducing a space and time varying (complex-valued) scalar that is applied to the predicted multiples prior to subtraction, they will adapt to the multiples as they appear in the data.

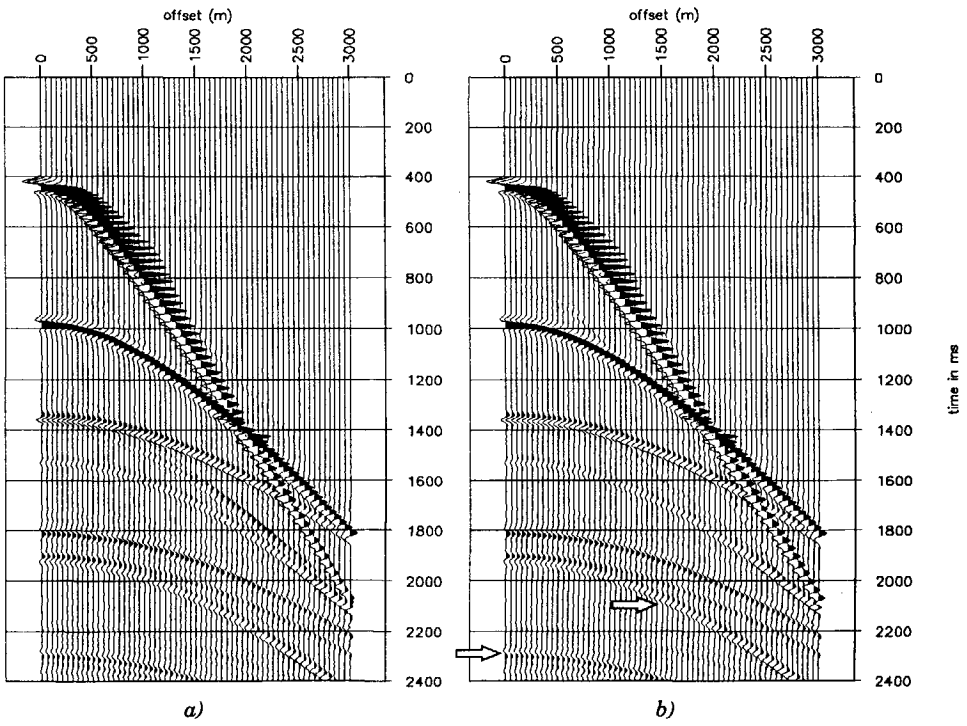

Fig. 1.14 a) Seismic shot record of Fig. 1.10a after adaptive subtracting of the predicted multiples of Fig. 1.12a b) Seismic shot record of Fig. 1.12b after a second prediction and subtraction step. The two arrows indicate surface-related multiples that are not related to the water layer.

The (complex-valued) scalar may also account for the inaccuracies in the information that is needed to do the extrapolations, i.e. position and reflection characteristics of the first layer bottom. This adaptive subtraction can yield good results, as has been shown by Berryhill and Kim (1986), Julien and Raoult (1989) or Monk (1991), all using different adaptive subtraction procedures. Note that the danger of adaptive subtraction is that if too much freedom is allowed for the predicted multiples to match the data (in stead of a scalar a transfer function is used), primary energy may easily be removed as well. Therefore it is important to take as few adaptive parameters as possible.

The *adaptive* subtraction of multiples after only one prediction step has also been applied to the example under consideration (Fig. 1.10). A smooth, time dependent weighting factor has been allowed during the subtraction stage. The result is shown in Fig. 1.12a. The result has indeed improved considerably. Only at the position where the water bottom multiples and water layer reverberations cross (at the larger offsets) a compromise had to be found.

The *two-step* extrapolation and subtraction technique has also been applied to the dataset of Fig. 1.10. After the first stage (Fig. 1.12b) (i.e. after the *deterministic* subtraction) the water bottom primary has been removed, and a second multiple prediction is applied. After subtraction of these multiples from that data, and replacing the water bottom primary at its original position, Fig. 1.12b is the result. Indeed all water layer related multiples have been removed. The arrows indicate two events that are surface-related multiples, but not water layer-related (belonging to the group of Fig. 1.5c). The first arrow indicates a multiple bounce of the second interface via the surface with itself. The second arrow points at a surface-related multiple, which is a combination of the second and third interface. The rest of the "remaining" surface-related multiples occurs at larger traveltimes.

Note that an adaptive approach of the two-step extrapolation and subtraction technique is not feasible as after the first stage only half of the reverberations should be removed. Also the fact that removal of the first primary will not be easy in practice, the two-step method is not applied adaptively. Berryhill and Kim (1986) described a very good alternative. By using reciprocity only one extrapolation is needed to predict both source and receiver reverberations. Those multiples are combined and then adaptively subtracted from the data.

The advantages of the wave field extrapolation and subtraction methods are:

* Strong water bottom related multiples can be removed, even in a more complex area where standard methods fail.

* The output is pre-stack data (normally common shot gathers), which allows pre-stack processing of the data after multiple elimination.

The disadvantages of the wave field extrapolation and subtraction methods are:

* The water bottom structure and reflectivity must be known. Therefore the method is always applied adaptively, with the water bottom position and reflectivity as parame-

ters. This introduces a difficult parametrization, as those parameters often vary laterally in a significant way.

* As pre-stack wave field extrapolations are involved the methods are time consuming. A faster application in the k_x-ω domain has the restriction of an approximately 1D water layer.

* First layer-related multiples are removed only (see also section 1.2.4).

1.2.4 The surface-related multiple elimination method

Surface-related multiple elimination, the subject of this thesis, removes all multiples related to a certain *interface* (generally the free surface), in stead of multiples related to a certain *layer*. This has the advantage that *more* type of multiples are eliminated with a *simpler* method. If we consider again Fig. 1.5 all the multiples in Fig. 1.5a to Fig. 1.5c are removed. It may seem that the removal of the "remaining surface-related multiples" (as denoted in section 1.1.2) is not a significant advantage. As we saw in the example of Fig. 1.12 only two surface-related multiples, which are not related to the first layer, were left in the data. But going deeper in the section, the number of these multiples increase considerably. The surface-related multiples with the first layer being involved are the strongest, but the number is less. However, the large number of weaker "remaining surface-related multiples" may give significant problems in the *deeper* part of a seismic section (generally our target).

This is also visible in the 1D example of Fig. 1.9. The events in Fig. 1.9b for times larger than 2s are mainly due to the "remaining surface-related multiples". Comparison of the data without the water layer related multiples in Fig. 1.9e with Fig. 1.9f (data without surface-related multiples) for the interval between 2 and 4s shows that the "remaining" surface-related multiples still have a disturbing effect on the data, which could easily mask (weak) primaries from the target.

To illustrate how the balance between water layer related multiples and "remaining" surface-related multiples depends on the number of reflectors, some simple 1D examples have been generated. Fig. 1.15a shows a *primary* plane wave response of a 20 reflector model. The primary reflections occur within 2s traveltime. The reflection coefficients of the reflectors (modeled with a random generator) have been chosen to have an average absolute value of 0.05, except for the first reflector (simulating the water bottom) which has a reflectivity of 0.2. In Fig. 1.15 the different type of multiples have been displayed separately with the amount of energy (normalized on the total energy in the response of primaries with multiples) is indicated in the right-hand corner.
Looking from 0-4 s, the total amount of multiples (Fig. 1.15b) contains 16% of all energy; the amount of energy in the water layer-related multiples (Fig. 1.15c) is 11%; the amount of "remaining" surface multiples (Fig. 1.15d) is 5% of the total amount of energy and the internal multiples (Fig. 1.15e) account for less than 1%.

However, looking at 2-4 s the total amount of multiples (Fig. 1.15b) is 100% of all energy in this primary free interval; the amount of energy in the water layer-related multiples (Fig. 1.15c) is 41%; the amount of "remaining" surface multiples (Fig. 1.15d) is 78% of the total amount of energy and the internal multiples (Fig. 1.15e) account for 2%.

For the energy calculations the interference of the multiples with each other, when added together, has not been incorporated.

Fig. 1.15f shows a smoothed version of the envelopes of the different groups of multiples, corresponding to Fig. 1.15b to e.

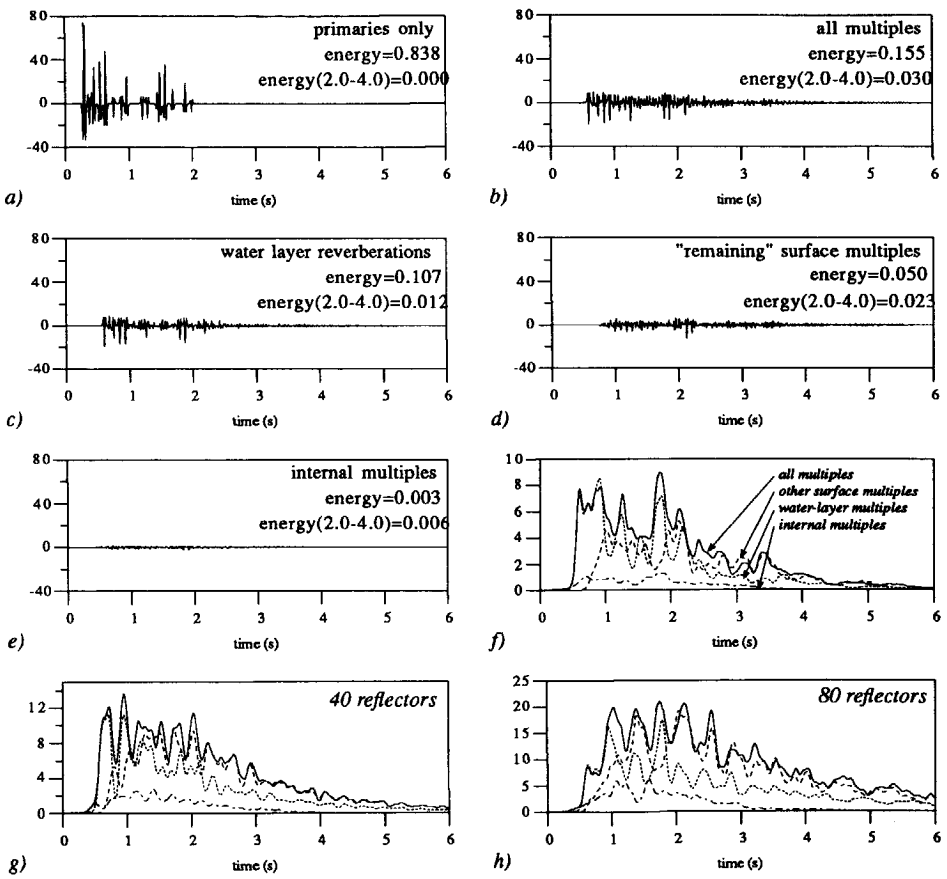

Fig. 1.15 Horizontal plane wave response of a model consisting of 20 reflectors.
a) Response with primaries only b) Response with all multiples only c) Water layer related multiples and reverberations d) The "remaining" surface-related multiples e) Internal multiples f) Smoothed envelopes of the responses with the different type of multiples separately displayed g) Similar envelope plot as f) for a 40 reflector model h) Envelope plot for a 80 reflector model.
Note the different scales for the envelope plots.

In total 12 simulations have been made with a 10, 20, 40 and 80 reflector model. In each model the average reflection coefficient was 0.05, apart from the first reflector which took the values 0.1, 0.2 and 0.3. A similar envelope plot as in Fig. 1.15f for the 40 and 80 reflector model has been added in Fig. 1.15g and Fig. 1.15h; note the different scalings.

In Table 1.1 the percentages of the primaries and the different groups of multiples with respect to the total energy in the response have been gathered for those models. It shows that the influence of the "remaining" surface-related multiples is significant and becomes more important when the number of reflectors increases. The amount of water layer related multiples strongly depends on the water bottom reflectivity, as could be expected. In Table 1.1 the energy distribution of the different groups of multiples are given for a time gate without primary reflections in what could be the target zone (2 - 4 s). It shows the strong dependence of the reverberations on the water bottom reflectivity.

Table 1.1 *Percentages of the energy of primaries and multiples for the complete trace length (0-4 s).*

number of reflectors	10			20			40			80		
reflection coefficient of the water bottom	0.1	0.2	0.3	0.1	0.2	0.3	0.1	0.2	0.3	0.1	0.2	0.3
primaries	89	85	80	87	84	79	81	79	76	60	58	54
all multiples	9	13	18	12	16	21	21	24	29	37	41	46
reverberations	3	10	16	3	11	18	4	13	23	4	14	26
other surface multiples	5	2	1	8	5	3	18	14	10	33	27	19
internal multiples	0	0	0	0	0	0	1	1	1	1	2	2

Table 1.2 *Percentages of the energy of primaries and multiples in a time gate without primaries (2-4 s).*

number of reflectors	10			20			40			80		
reflection coefficient of the water bottom	0.1	0.2	0.3	0.1	0.2	0.3	0.1	0.2	0.3	0.1	0.2	0.3
primaries	0	0	0	0	0	0	0	0	0	0	0	0
all multiples	100	100	100	100	100	100	100	100	100	100	100	100
reverberations	6	27	60	10	41	73	8	28	54	5	18	37
other surface multiples	94	70	38	104	78	41	96	84	66	96	80	58
internal multiples	1	2	2	1	2	2	1	2	2	1	2	2

The contribution of the other surface-related multiples decreases with increasing water bottom reflectivity, although the absolute amount of this energy stays more or less the same (which cannot be seen in the tables). Note the interference effects, which yield that the sum of the energies is not the same as the energy of the sum. Of course, these percentages are dependent on the realizations of the reflectivity models.

The general conclusion of the two tables is that especially in the lower part of the seismic section the "remaining" surface-related multiples account for an important part of the total multiple energy; removing the first layer related multiples is therefore not enough for a clear picture of the primaries. Note that the internal multiples have much lower amplitudes than the surface-related multiples. Of course the latter is not always the case, e.g. when a low velocity layer is enclosed between higher velocity layers.

Besides the fact that with the surface-related multiple elimination more multiples are removed than with the prediction and subtraction techniques, it is very important to realize that the surface-related multiple elimination method does not need *any* information about the subsurface. The seismic data itself is used to predict the surface-related multiples. Information about the *surface* is needed only, i.e. surface reflectivity and source/receiver characteristics.

The historical development of the surface-related multiple elimination procedure starts with Anstey (1967), who observed that with the autoconvolution of a trace multiples were enhanced. Kennett (1979) described an inversion scheme in the k_x-ω domain to eliminate multiples for a horizontally layered elastic medium and for ideal source/detector properties. Berkhout (1982) redefined the multiple problem for laterally varying media and practical acquisition conditions by using a wave theory based matrix formulation. An adaptive version with examples has already been shown by Verschuur et al. (1989) and (1990). The method described here, based on Berkhout's approach, handles both the acoustic and the elastic situation. In the latter case, by taking the full elastic reflection at the free surface into account, all surface-related multiply reflected *and* converted events can be eliminated.

The surface-related multiple elimination method is especially suited for situations where other multiple suppressing schemes fail: in situations where the move-out of primaries and multiples are close, and in any complex situation. In addition the method is particularly beneficial for deeper data (say > 2 s). Therefore, it fits very well in *reservoir-oriented* seismic processing. In both the acoustic and elastic case the theory assumes that the measured response should represent upgoing reflected waves, related to downgoing source waves. Hence, before applying the surface-related multiple elimination procedure a decomposition of the measured seismic data into up- and downgoing waves has to be applied.
It is important to realize that the surface-related multiple elimination procedure means application of an *inversion* process to the seismic data (as will be shown in Chapter 3), which replaces the *reflecting* surface by a *transparent* surface. As a result any upgoing event will vanish after being detected once. This means that only primaries and internal multiples are left after the surface-related multiple elimination procedure.

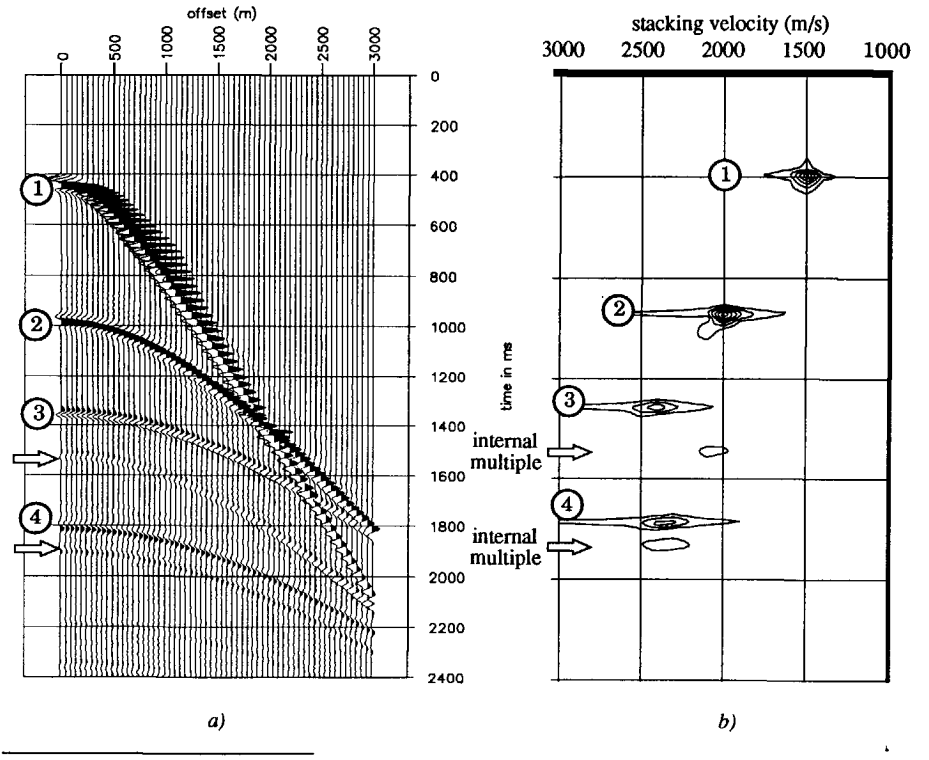

Fig. 1.16 *a) Seismic CMP gather of Fig. 1.10a after applying the surface-related multiple elimination procedure b) Velocity panel corresponding to a). The arrows indicate internal multiples, that are not removed by the surface-related multiple elimination procedure. Compare this result with Fig. 1.10a.*

In fact, the examples at the beginning of this chapter (Fig. 1.2 to Fig. 1.4 and Fig. 1.7) are already a showcase of the surface-related multiple elimination procedure, as the data without surface-related multiples were acquired by applying the multiple elimination method.

When the example of Fig. 1.10 is considered again and the surface-related multiple elimination procedure is applied to this data, Fig. 1.16 is the result. From the shot record in Fig. 1.16a as well as the velocity panel in Fig. 1.16b it can be clearly observed that all surface-related multiples have been perfectly eliminated. The primaries are left unharmed; they have been restored from interference with multiples (see for example the event at 1800 ms). Apart from the 4 primaries 2 internal multiples can be indicated (at the arrows in Fig. 1.16) which have not been removed by this method. These internal multiples are both related to the second layer. In Chapter 3 we will show that even these internal multiples can be removed after a downward continuation of the data to the first reflector level and applying a second interface-related multiple elimination.

The advantages of the surface-related multiple elimination method are:

* There is no need to specify any information about the *sub*surface.
* No assumption on the move-out properties have to be made.
* In stead of suppressing multiples related to the first layer only (i.e. first layer bottom multiples, first layer reverberations), *all* surface-related multiples are removed.
* The output is pre-stack data, allowing further processing on pre-stack data.
* In an adaptive version it is possible to estimate the source signature, including the scaling factor. This is a very important feature, considering *true amplitude inversion* after multiple elimination.

Disadvantages are:

* The method is computationally intensive; it may be compared with a pre-stack redatuming step.
* As the data itself is used as multiple prediction operator, the quality of the data with respect to remaining surface waves and missing traces is of particular importance.

1.2.5 Summary

To summarize, the example of the 4 reflector model (Fig. 1.9a) is used. The resulting CMP gathers/shot records after the application of the different multiple elimination techniques are shown in Fig. 1.17. Fig. 1.17a shows the CMP gather/shot record with all multiples included (identical to Fig. 1.10a). After applying predictive deconvolution on all traces in the tau-p domain, and displaying the result in the space-time domain, the result is Fig. 1.17b (not shown before). Indeed a lot of multiple energy has been removed by this (simple) procedure, although primary reflections have been distorted. The result of velocity filtering in the wave number domain is shown in Fig. 1.17c (identical to Fig. 1.11a), which produces a better result than predictive deconvolution, except at the small offset traces. In many processing applications these two methods are therefore combined. The wave field prediction and subtraction technique can either be applied in a single step adaptive mode (Fig. 1.17d, identical to Fig. 1.14a) or in a two-step mode (Fig. 1.17e, identical to Fig. 1.14b). Both yield good results, but leave the surface-related multiples that are not water layer related. Finally Fig. 1.17f shows the result of surface-related multiple elimination. The four primaries have been perfectly restored from interference with the multiples. Some weak internal multiples are left in the data.

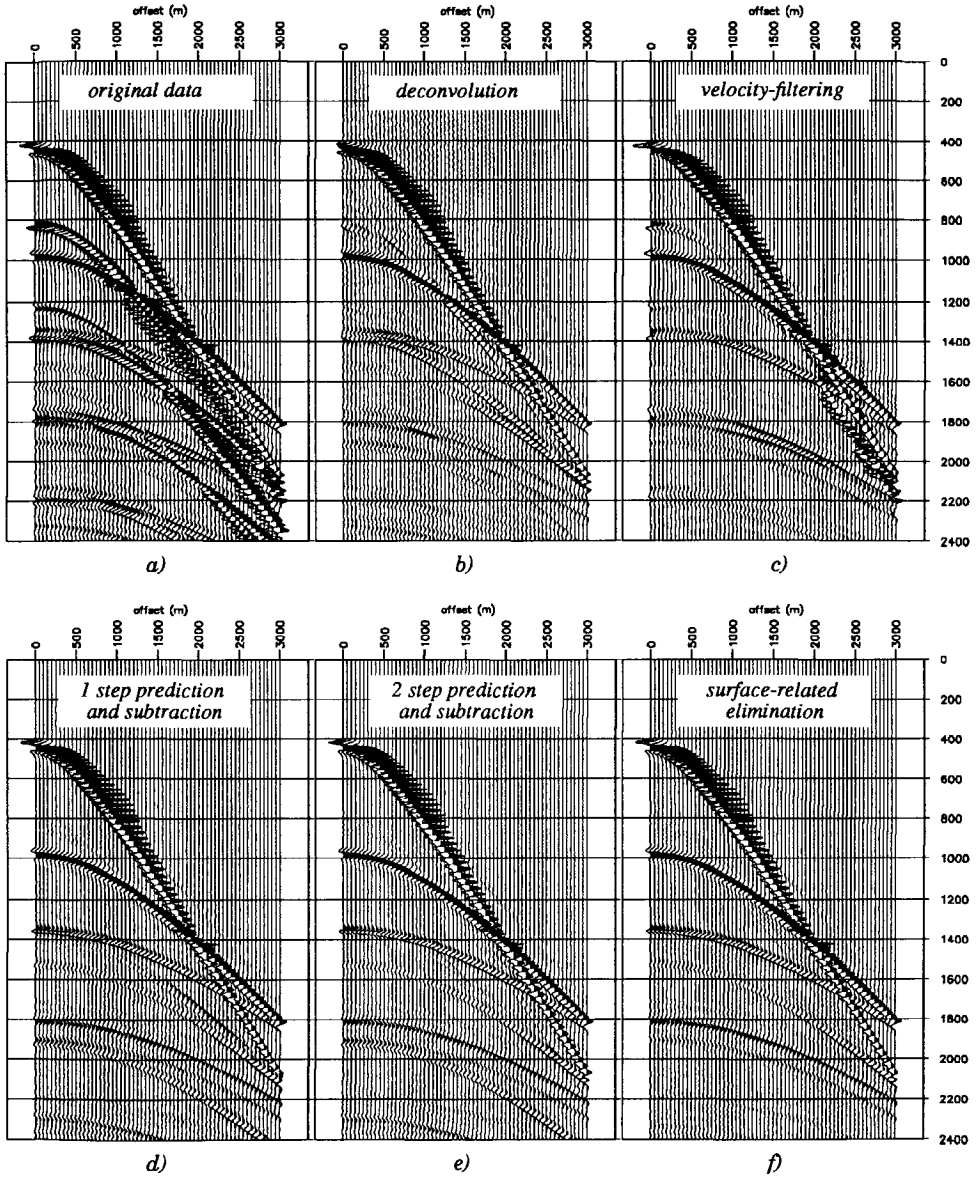

Fig. 1.17 *Comparison of the results of the different multiple elimination techniques on a 1D example. a) The original CMP gather b) CMP gather after predictive deconvolution via the tau-p domain c) CMP gather after move-out filtering via the wave number domain d) CMP gather after wave field prediction and adaptive subtraction using one prediction step e) CMP gather after wave field prediction and subtraction using two prediction steps f) CMP gather after surface-related multiple elimination.*

Note that for this simple 1D example all methods yield acceptable results, except if accurate pre-stack amplitude inversion is the final goal. Then the wave field based solutions are to prefer. Furthermore, if the subsurface structures are more complex the filtering methods will loose effectiveness very soon and the wave field based methods are the only proper solution to the multiple problem. Taking into account the fact that for a somewhat deeper target zone (say larger than 2s) the amount of surface-related multiples, that are not related to the first layer, is at least as important as the amount of first layer related multiple energy, the surface-related multiple elimination method will yield the most satisfactory results.

To illustrate the effect of complex subsurface structures, we consider a simulated data set for the subsurface model of Fig. 1.18, with an irregular water bottom. Due to the synclinal shapes the multiple behavior is very complex, as can be observed in a simulated shot record with the source at x=0 m, as shown in Fig. 1.19a. For the larger offsets the multiples of the synclines have a significant larger complexity than the primaries; with each bounce the complexity will increase. The velocity based separation of primaries and multiples will certainly fail. This is also true for predictive deconvolution. The wave field extrapolation and subtraction method can only be successful if an accurate description of the water bottom is available, and if a correct extrapolation procedure is used.

The surfac-related multiple elimination method does not have any difficulties with this data, as the data perfectly predicts the multiples without any additional information: the information about the complexity of the multiples is *in* the data. The result for the shot record at x=0 m is shown in Fig. 1.19b, in which the four primaries can be easily identified. For this dataset the zero offset section is shown in Fig. 1.20a. Note again the complex multiple behavior. For example, the left side synclinal structure around x=500 m produces multiples that are spread out over a very large offset range. After the surface-related multiple elimination method has been applied to all shot records, the zero offset section is extracted again. Note from Fig. 1.20b that the four primary reflections can be easily identified.

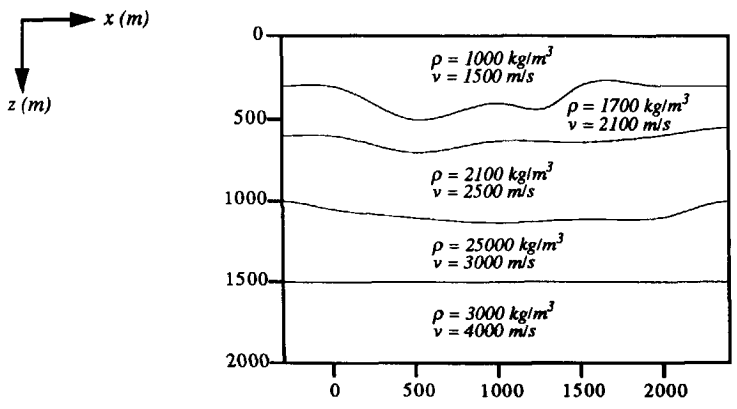

Fig. 1.18 *Subsurface model with a complex sea bottom.*

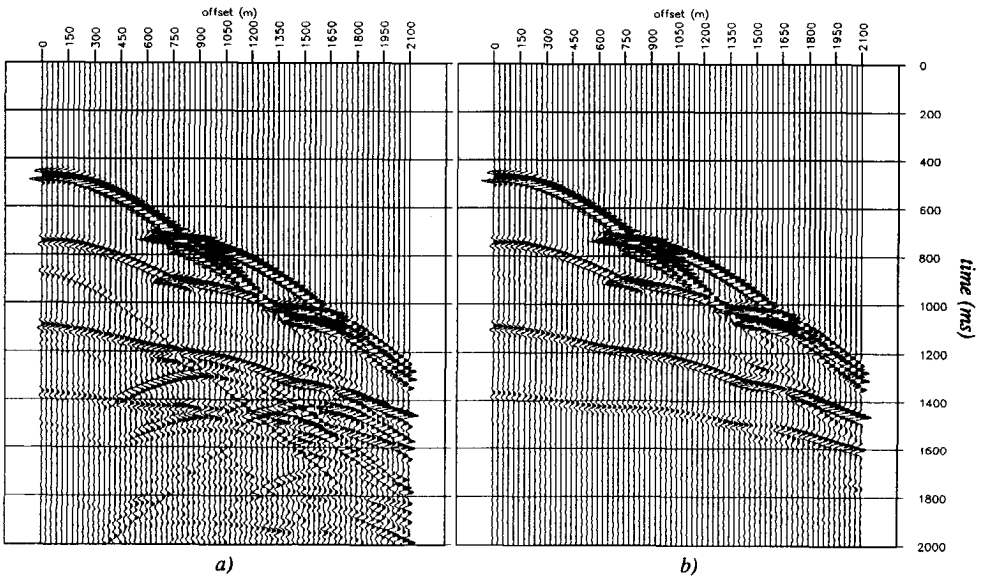

Fig. 1.19 Shot record related to the subsurface model of Fig. 1.18 with the source position at x=0 m. a) All multiples are included b) After surface-related multiple elimination.

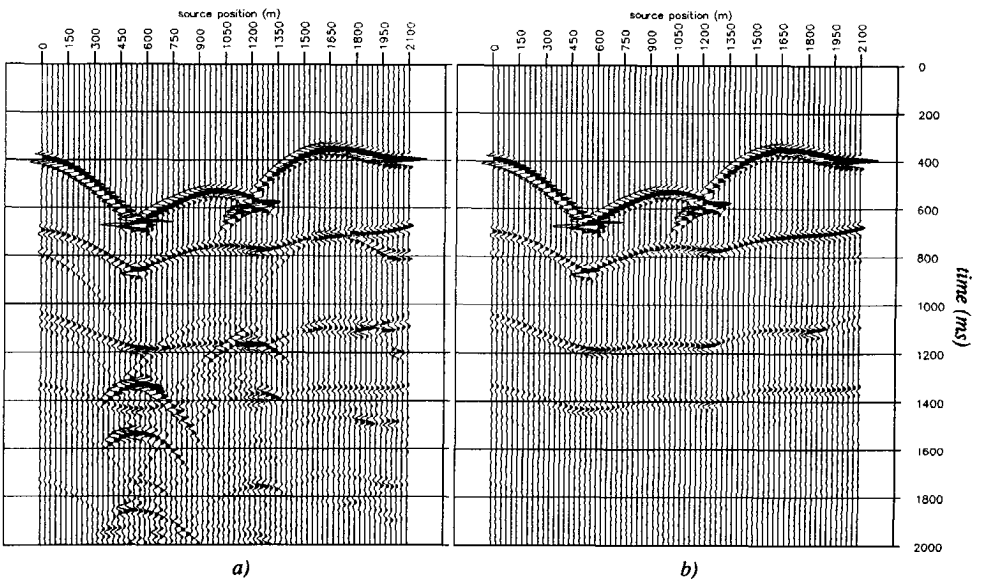

Fig. 1.20 Zero offset section related to the subsurface model of Fig. 1.18. a) All multiples are included b) After surface-related multiple elimination.

Finally in Table 1.3 an overview of the performance of the aforementioned multiple elimination methods has been gathered. In the table the methods are compared on the following characteristics:

* *Speed*: how fast is the application of the method with respect to computer time.
* *Small offsets*: quality of the result for small offsets.
* *Large offsets*: quality of the result for large offsets.
* *Effectiveness*: how many (types of) multiples are removed by the method.
* *Reliability of result*: how confident can we be on the result of the multiple elimination method; are primaries well restored from interference with multiples.
* *Subsurface independency*: independency of the multiple elimination method on assumptions and/or knowledge about the subsurface.

In this overview we see that the surface-related multiple elimination method outperforms any other method except for the calculation speed, which is the price to be paid. To overcome this drawback a more efficient scheme, applicable in more or less 1D media, will be proposed in Chapter 8. It is a very attractive alternative when the calculation time is a constraint. However, we may expect that with the increasing capabilities of the computer hardware the relatively large computation costs will not be problematic anymore in the near future.

Table 1.3 Overview of the main characteristics of the discussed multiple elimination techniques.

elimination method	speed	small offsets	large offsets	effectiveness	reliability of result	subsurface independency
predictive deconvolution	++	+	−−	+/−	−	−−
velocity filtering	+	−−	+	+	+/−	−
extrapolation & subtraction	−	++	++	+	++	−
surface-related elimination	−	++	++	++	++	++

2

FORWARD MODEL OF SEISMIC DATA

2.1 INTRODUCTION

In this chapter the theory of multiple elimination will be anticipated by reviewing a suitable version of the seismic forward model. First a recursive version of the forward model is discussed, starting at the deepest depth level. With this model the surface seismic data is described by recursively extrapolating the response from the deepest depth level to the surface, including multiples at each depth level. Hence, it contains all *surface-related* multiples as well as all *internal* multiples. A special version of this forward model is used in the case of a thin surface layer. It is shown that in the thin surface layer situation the surface-related multiple elimination method should consider the surface as one reflector with a complex reflectivity. This means a.o. that an extra pre-processing step is needed to remove the thin surface layer reverberations before the actual surface-related multiple elimination process is applied.

In the first part of this chapter the assumption of an acoustic medium is made, meaning that only one type of wave is considered, i.e. the longitudinal or P-wave (marine data). However, in the second part a description of multi-component data in an elastic medium is given, meaning that transversal or S-waves are included (land data).

If we assume that each subsurface layer may be considered as *locally* homogeneous, decomposition of the total wave field into down- and upgoing waves is well defined (no interactions between down- and upgoing wave fields, except at the reflecting boundaries).

For the description of seismic wave fields the matrix notation proves to be extremely useful because of its simplicity and its close relation to the actual implementation in a computer. The matrix notation for seismic wave fields has been introduced by Berkhout (1982) and will be

used extensively throughout this thesis. It is explained in detail in Appendix A. Concerning the notation we can make the following distinctions (2D):

$P^-(x,z_0,t)$: time domain representation of a shot record.

$P^-(x,z_0,\omega)$: frequency domain representation of a shot record.

$\tilde{P}^-(k_x,z_0,\omega)$: wave number domain representation of a shot record.

$\vec{P}^-(z_0)$: data vector for one frequency related to one shot record.

$\mathbf{P}^-(z_0)$: data matrix, one column being related to one shot record.

The positive z-axis is chosen downward. Therefore a minus sign will denote upgoing waves, like $\vec{P}^-(z_0)$.

All matrix formulations can be interpreted as both 2D and 3D descriptions, as the matrix notation is designed to be identical for both 2D and 3D data. Only the interpretation of this notation makes it a 2D or 3D description, as described by Kinneging et al. (1989). However for simplicity reasons, the description will be 2D for the moment and, therefore, all illustrations and references to the coordinate system will be 2D in this chapter. The extension of the theory to 3D is straightforward. Furthermore, in Chapter 5 an example of full 3D multiple elimination is shown. A nice feature about the matrix notation is that all formulations, stated for the acoustic 2D case, stay the same if we introduce multi-component elastic data, even in the 3D situation. It is the interpretation of the matrices that changes.

It should be pointed out that the recursive forward model as described in this chapter should not be considered as a modeling algorithm. It is only introduced as a starting point for the multiple elimination theory.

2.2 FORWARD MODEL OF ACOUSTIC SEISMIC DATA

The forward model can be described in a recursive or a non-recursive way. The recursive description starts at the deepest depth level of interest. The response at the deepest depth level is extrapolated upwards, adding the influence of each shallower depth level to this response, until the surface is reached. Finally, the data acquisition parameters are included. The non-recursive forward model considers the seismic response as a summation of individual reflections.

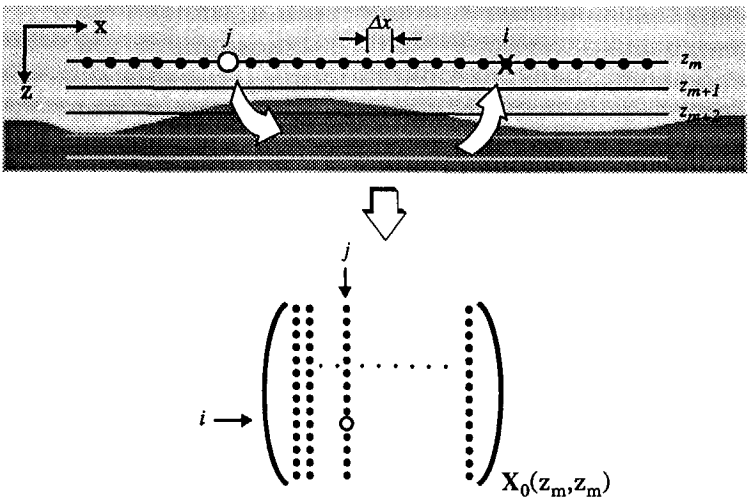

Fig. 2.1 *Each element of matrix $X_0(z_m,z_m)$ describes the monochromatic spatial impulse response of lower half space $z>z_m$ at a detector position at z_m due to a unit point source (dipole) at z_m, the upper half space $z \leq z_m$ being considered to be homogeneous.*

For the description of the recursive forward model the work of Berkhout (1982) is followed. In fact this recursive model is a multi-dimensional variant of what is known as the reflectivity method, see Fuchs and Muller (1971) and Ursin (1983).

For the recursive description the medium is divided into a number of depth levels, from the surface until the deepest level of interest. Note that one depth level does *not* generally coincide with a reflector. If we consider a certain depth level z_m, matrix $\mathbf{X}_0(z_m,z_m)$ describes one Fourier component of the total spatial impulse response of lower half space $z>z_m$, the upper half space $z \leq z_m$ being considered to be homogeneous. More specific, one element of $\mathbf{X}_0(z_m,z_m)$ describes the monochromatic subsurface impulse response at z_m from all depth levels below z_m for a unit point source at $x_j=j\Delta x$, measured by a receiver at $x_i=i\Delta x$ (see Fig. 2.1). This response is located in the i^{th} element of the j^{th} column in the matrix $\mathbf{X}_0(z_m,z_m)$.

The relation between a monochromatic downgoing pressure wave field $\vec{P}^+(z_m)$ at this depth level and the corresponding monochromatic upgoing wave field $\vec{P}^-(z_m)$ is given by:

$$\vec{P}^-(z_m) = \mathbf{X}_0(z_m,z_m)\, \vec{P}^+(z_m)\,. \tag{2.1}$$

The monochromatic downgoing wave field $\vec{P}^+(z_m)$ is represented by a vector which contains the discretized version of this wave field at depth level z_m as a function of the lateral coordinate. In the same way $\vec{P}^-(z_m)$ contains the discretized monochromatic upgoing wave field at depth level z_m. Fig. 2.2a shows equation (2.1) in a diagram.

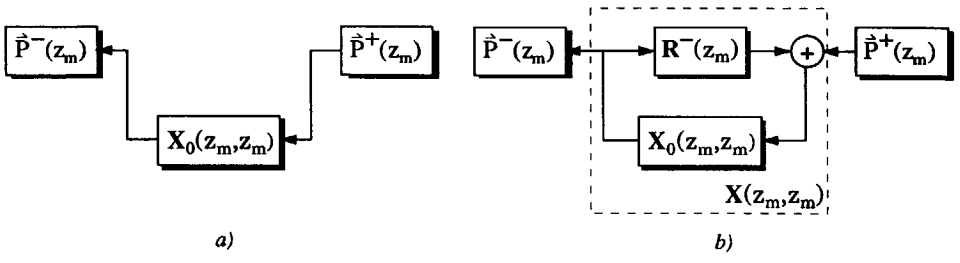

Fig. 2.2 *a) Response at depth level $z=z_m$ assuming a homogeneous half space $z \leq z_m$ (no reflecting surface). b) Response at depth level $z=z_m$ assuming a homogeneous half space $z < z_m$ (reflecting surface).*

When the reflectivity effect of depth level z_m itself is included (see Fig. 2.2b) the upgoing wave field is reflected by the inhomogeneities at depth level z_m and transformed into an additional downgoing wave field. In this way z_m-related multiples are generated. Hence, the total downgoing wave field is the original downgoing wave field together with the upgoing wave field after reflection at z_m, yielding:

$$\vec{P}^-(z_m) = \mathbf{X}_0(z_m,z_m) \left[\vec{P}^+(z_m) + \mathbf{R}^-(z_m)\, \vec{P}^-(z_m) \right], \tag{2.2}$$

in which $\mathbf{R}^-(z_m)$ describes the angle dependent reflection against the possible inhomogeneities at depth level z_m from below (see also Appendix A and de Bruin et al. (1990) for a more elaborate discussion on reflectivity matrices). Equation (2.2) can be written explicitly for the total upgoing wave field $\vec{P}^-(z_m)$:

$$\vec{P}^-(z_m) = \left[\mathbf{I} - \mathbf{X}_0(z_m,z_m)\, \mathbf{R}^-(z_m) \right]^{-1} \mathbf{X}_0(z_m,z_m)\, \vec{P}^+(z_m) . \tag{2.3}$$

When $\mathbf{X}(z_m,z_m)$ is defined as the response of the subsurface at depth level z_m that *includes* the multiples related to depth level z_m, we arrive at (Fig. 2.2b):

$$\vec{P}^-(z_m) = \mathbf{X}(z_m,z_m)\, \vec{P}^+(z_m) , \tag{2.4}$$

matrix $\mathbf{X}(z_m,z_m)$ being given by equation (2.3):

$$\mathbf{X}(z_m,z_m) = \left[\mathbf{I} - \mathbf{X}_0(z_m,z_m)\, \mathbf{R}^-(z_m) \right]^{-1} \mathbf{X}_0(z_m,z_m) \tag{2.5a}$$

or by expanding the inverse term into a series:

$$\mathbf{X}(z_m,z_m) = \mathbf{X}_0(z_m,z_m) + \left\{ \mathbf{X}_0(z_m,z_m)\, \mathbf{R}^-(z_m) \right\} \mathbf{X}_0(z_m,z_m) + \left\{ \mathbf{X}_0(z_m,z_m)\, \mathbf{R}^-(z_m) \right\}^2 \mathbf{X}_0(z_m,z_m) + \ldots . \tag{2.5b}$$

Each term in equation (2.5b) describes one order of z_m-related multiples.

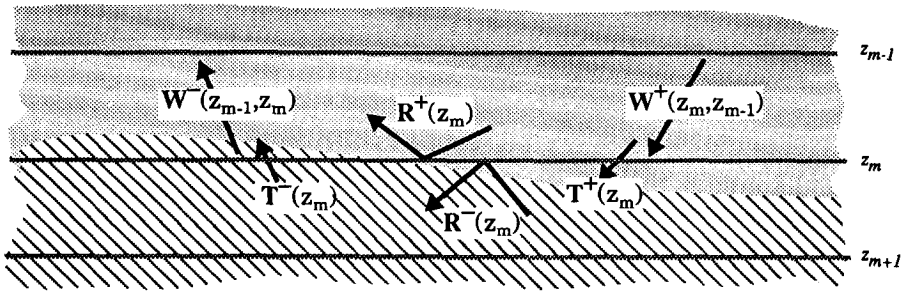

Fig. 2.3 Reflection, transmission and propagation operators related to depth level z_m.

Next, having a description for the total response with all multiples at depth level z_m, the extrapolation to depth level z_{m-1}, closer to the surface, is included. Therefore the response has to be extrapolated through the depth level (transmission effect) and through the layer between z_{m-1} and z_m (propagation effect). Also the primary reflection of depth level z_m from above has to be included. The upgoing wave field at depth level z_{m-1} without multiples related to this depth level can then be written as:

$$\vec{P}^-(z_{m-1}) = \left[\mathbf{W}^-(z_{m-1},z_m)\,\mathbf{T}^-(z_m)\,\mathbf{X}(z_m,z_m)\,\mathbf{T}^+(z_m)\,\mathbf{W}^+(z_m,z_{m-1}) \right] \vec{P}^+(z_{m-1}) + \left[\mathbf{W}^-(z_{m-1},z_m)\,\mathbf{R}^+(z_m)\,\mathbf{W}^+(z_m,z_{m-1}) \right] \vec{P}^+(z_{m-1}) \qquad (2.6)$$

or, similar to equation (2.1),

$$\vec{P}^-(z_{m-1}) = \mathbf{X}_0(z_{m-1},z_{m-1})\,\vec{P}^+(z_{m-1})\,, \qquad (2.7a)$$

where matrix $\mathbf{X}_0(z_{m-1},z_{m-1})$ is given by:

$$\mathbf{X}_0(z_{m-1},z_{m-1}) = \mathbf{W}^-(z_{m-1},z_m) \left[\mathbf{T}^-(z_m)\,\mathbf{X}(z_m,z_m)\,\mathbf{T}^+(z_m) + \mathbf{R}^+(z_m) \right] \mathbf{W}^+(z_m,z_{m-1})\,. \qquad (2.7b)$$

In equations (2.6) and (2.7b) matrix $\mathbf{W}^+(z_m,z_{m-1})$ describes the downward propagation from depth level z_{m-1} to level z_m, matrix $\mathbf{R}^+(z_m)$ describes the reflectivity for downward travelling waves at depth level z_m, matrices $\mathbf{T}^+(z_m)$ and $\mathbf{T}^-(z_m)$ describe the downward and upward transmission through depth level z_m and matrix $\mathbf{W}^-(z_{m-1},z_m)$ describes the upward propagation from depth level z_m to level z_{m-1}. In Fig. 2.3 these operators have been indicated. Each of these matrices contains discretized operators, of which the definition can be found in Berkhout (1982). A more elaborate discussion on those matrix operators can be found in Appendix A. Note again that the depth levels do not necessarily coincide with an actual geologic interface, as shown in Fig. 2.3. For example in the homogenous part at the right side of depth level z_m, the corresponding part of the reflectivity matrix is zero and the transmission matrices contain unit vectors.

At depth level z_{m-1} the multiples related to this depth level can be included in the same way as described by equation (2.3) and extrapolation to the next depth level z_{m-2} can be carried out. By applying equations (2.3) and (2.6) recursively, the total response of a medium can be calculated, starting at the deepest reflector of interest.

If we consider a model with M depth levels, we start with:

$$\mathbf{X}(z_M,z_M) = \mathbf{0} . \tag{2.8}$$

Then we apply the extrapolation to the next depth level:

$$\mathbf{X}_0(z_{M-1},z_{M-1}) = \mathbf{W}^-(z_{M-1},z_M)\, \mathbf{R}^+(z_M)\, \mathbf{W}^+(z_M,z_{M-1}) \tag{2.9}$$

and we include the multiples:

$$\mathbf{X}(z_{M-1},z_{M-1}) = [\, \mathbf{I} - \mathbf{X}_0(z_{M-1},z_{M-1})\, \mathbf{R}^-(z_{M-1}) \,]^{-1}\, \mathbf{X}_0(z_{M-1},z_{M-1}) , \tag{2.10}$$

etc.

For depth level z_m we arrive at:

$$\mathbf{X}_0(z_m,z_m) =$$

$$\mathbf{W}^-(z_m,z_{m+1}) \,[\, \mathbf{T}^-(z_{m+1})\, \mathbf{X}(z_{m+1},z_{m+1})\, \mathbf{T}^+(z_{m+1}) + \mathbf{R}^+(z_{m+1}) \,]\, \mathbf{W}^+(z_{m+1},z_m) \tag{2.11}$$

and, adding the multiples related to the depth level z_m, we obtain

$$\mathbf{X}(z_m,z_m) = [\, \mathbf{I} - \mathbf{X}_0(z_m,z_m)\, \mathbf{R}^-(z_m) \,]^{-1}\, \mathbf{X}_0(z_m,z_m) . \tag{2.12}$$

Finally the surface level is reached, yielding

$$\mathbf{X}_0(z_0,z_0) = \mathbf{W}^-(z_0,z_1) \,[\, \mathbf{T}^-(z_1)\, \mathbf{X}(z_1,z_1)\, \mathbf{T}^+(z_1) + \mathbf{R}^+(z_1) \,]\, \mathbf{W}^+(z_1,z_0) . \tag{2.13}$$

The surface-related multiples are included by

$$\mathbf{X}(z_0,z_0) = [\, \mathbf{I} - \mathbf{X}_0(z_0,z_0)\, \mathbf{R}^-(z_0) \,]^{-1}\, \mathbf{X}_0(z_0,z_0) . \tag{2.14}$$

Hence, at the surface the relation between the downgoing illuminating wave field and the upgoing reflected wave field (in a monochromatic description) is given by:

$$\vec{P}^-(z_0) = \mathbf{X}(z_0,z_0)\, \vec{S}^+(z_0) , \tag{2.15}$$

$\vec{S}^+(z_0)$ being the downgoing source wave field which has been imposed by the seismic source(s).

2.3 INCLUDING SOURCE AND RECEIVER PROPERTIES AT THE FREE SURFACE

If a seismic shot record has to be described, using the subsurface response as given by equation (2.14), the source and receiver characteristics used in the seismic acquisition have to be included. Actually, for the surface-related multiple elimination process this part of the forward model is essential. The total downgoing/upgoing wave fields that are generated/measured are influenced by the interaction of the source/receivers with the free surface. For a proper description a distinction between land and marine acquisition has to be made. In this section only the acoustic case, i.e. the marine case, is considered. Later on, the land case is discussed after introducing S-waves.

2.3.1 Including the source matrix

For a *single* seismic experiment the down- and upgoing wave fields are described by *vectors*, containing the monochromatic discretized pressure at depth level z_0: $\vec{S}^+(z_0)$ and $\vec{P}^-(z_0)$. In the *multi-experiment* situation a number of these vectors are gathered in the columns of a *matrix*, yielding $\mathbf{S}^+(z_0)$ and $\mathbf{P}^-(z_0)$. Using the matrix notation the multi-experiment forward model of equation (2.15) transforms into:

$$\mathbf{P}^-(z_0) = \mathbf{X}(z_0,z_0)\,\mathbf{S}^+(z_0)\,. \tag{2.16}$$

Each column of the source matrix $\mathbf{S}^+(z_0)$ contains the *effective* downgoing pressure wave field *at* the surface for one (monochromatic) experiment. The corresponding column of $\mathbf{P}^-(z_0)$ contains the upgoing pressure response. What does the source matrix look like?

For marine data the airgun array is still the most popular source. It is towed behind the acquisition vessel a few meters below the water surface at depth level z_s, as shown in Fig. 2.4. Each airgun behaves as a monopole. The total source wave field of the airgun array can be calculated by the superposition of the initial source wave fields of each airgun, including the ghost effect, provided non-linear effects can be neglected (which means that the airguns do not influence one another). In Appendix B this has been described.
If we write:

$$\mathbf{S}^+(z_0) = \mathbf{D}_{tot}{}^+(z_0,z_s)\,\mathbf{S}(z_s)\,, \tag{2.17}$$

then $\mathbf{S}(z_s)$ and $\mathbf{D}_{tot}{}^+(z_0,z_s)$ can be defined as follows: $\mathbf{D}_{tot}{}^+(z_0,z_s)$ describes the total airgun array response, normalized to a unit directivity for vertical angle of incidence. The frequency dependent behaviour for vertical incidence (zero wavenumber when the response is considered in the wavenumber domain) is assigned to the diagonal elements of $\mathbf{S}(z_s)$.

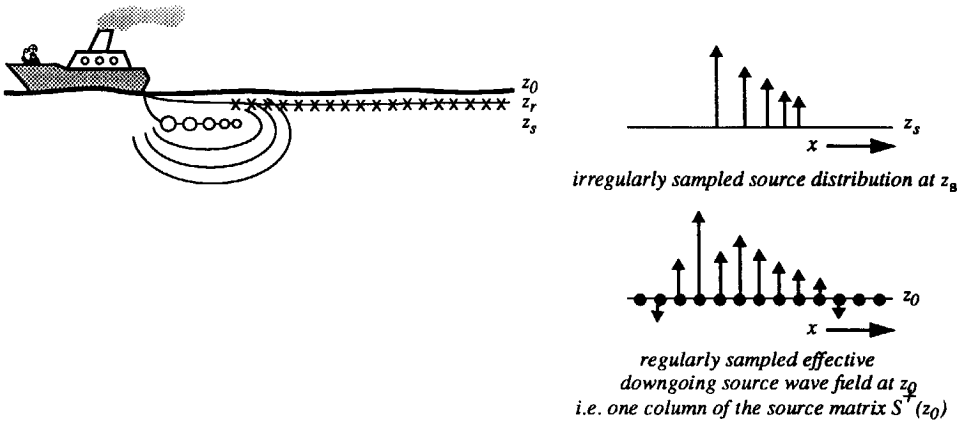

Fig. 2.4 *Airgun array towed behind the vessel for marine data acquisition. The array response can effecively be described by a spatial distribution of equidistant point sources at the surface. Note that the array description is frequency dependent.*

The matrix $\mathbf{D}_{tot}^{+}(z_0,z_s)$ can be found as follows:

- Calculate the total array response (with the ghost) in the wave number domain, taking into account the different signatures of each airgun (see Appendix B).
- Split the response in a frequency dependent basic signature $S(\omega)$ and a residual response.
- Transform the residual (normalized) response back to the space domain, and construct one column of the source matrix $\mathbf{D}_{tot}^{+}(z_0,z_s)$. The basic source signature $S(\omega)$ is put on the corresponding diagonal element of the matrix $\mathbf{S}(z_s)$.

By going back and forth to the wave number domain the transformation from the irregular airgun positions to a regular spatial sampling can be easily taken into account. A similar description of the source array can be found in Fokkema et al. (1990).

The normalized array response can be split into two responses $\mathbf{D}_s^{+}(z_0,z_s)$ and $\mathbf{D}_{array}(z_s)$, such that

$$\mathbf{S}^{+}(z_0) = \mathbf{D}_s^{+}(z_0,z_s)\,\mathbf{D}_{array}(z_s)\,\mathbf{S}(z_s)\,. \tag{2.18}$$

$\mathbf{D}_s^{+}(z_0,z_s)$ describes how the source wave field, emitted by the array at $z=z_s$, translates into a downgoing pressure wave field at the surface ($z=z_0$). This includes the monopole property, the ghost effect and the transformation from depth level z_s to z_0. $\mathbf{D}_{array}(z_s)$ contains the description (regularly sampled) of the array properties and $\mathbf{S}(z_s)$ contains the basic source signatures. Note that the airgun array $\mathbf{D}_{array}(z_s)$ is frequency dependent.

$S(z_s)$ has the basic signature $S_j(\omega)$ for each shot record on its diagonal:

$$S(z_s) = \text{diag}\,[\, S_1(\omega)\; S_2(\omega) \ldots S_j(\omega) \ldots S_N(\omega)\,]\,. \tag{2.19a}$$

When it may be assumed that the basic source signatures are equal for all shot records, then

$$S(z_s) = S(\omega)\,\mathbf{I}\,. \tag{2.19b}$$

Note that the basic source signature $S(\omega)$ can be considered as the signature of an equivalent dipole at the source position, yielding the same wavelet at vertical incidence as the airgun array.

Fig. 2.5a shows an airgun array which can be considered as typical. The directivity pattern obtained by linear superposition of the responses of the 6 guns (each considered as an omni-directional source) is shown in Fig. 2.5b for several frequencies. For simplicity, in this calculation the signatures of each airgun is considered to be a perfect pulse. In practice each gun will generate a different signature, which has its effect on the directivity pattern. As expected, the influence of the array is becoming more noticeable for higher frequencies. In practical situations the influence of the free surface should also be taken into account. Therefore in Fig. 2.5c the directivity pattern is shown including reflection against the free surface (ghost effect) if the array is positioned at 7 m depth (typical depth for airguns). Including the ghost effect makes an approximate dipole source from each individual gun. In practice a linear description is not sufficient as interaction between the airguns occurs. However, Ziolkowski et al. (1982) showed that an airgun array with interactions can be well described by a new array containing effective sources *without* interactions, the so-called notional sources. With these notional sources a linear description is again possible, and the source matrix can be constructed. In Appendix B the linear description of arrays is further discussed.

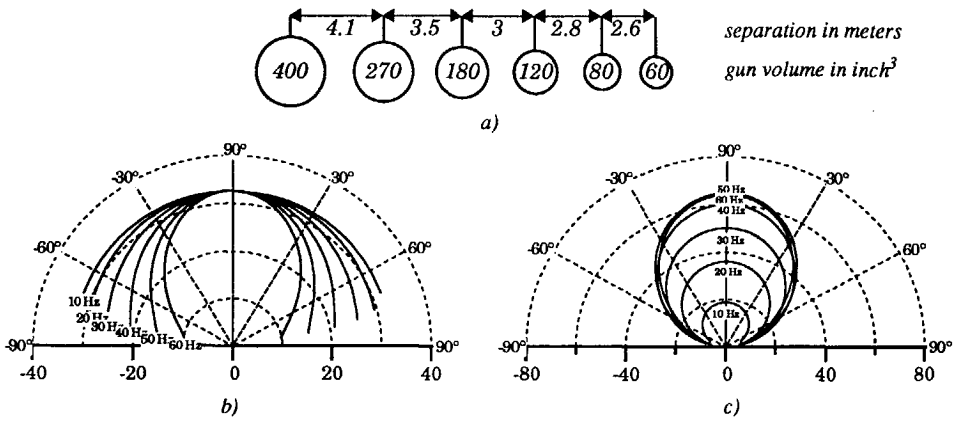

Fig. 2.5 *a) A marine source array consisting of 6 guns b) Far field directivity pattern of the source array for several frequencies c) Directivity pattern of the source array if the free surface is included and the depth of the array is 7 m. Note the dipole property after including the free surface.*

2.3.2 Including the detector matrix

The upgoing wave field $\mathbf{P}^{-}(z_0)$ does not represent the measured data, because the receiver characteristics together with the free surface have to be taken into account. For the marine situation the wave field is measured by hydrophone arrays in terms of the *total* pressure at a certain depth level z_r (as shown in Fig. 2.4). The measured wave field $\mathbf{P}(z_r)$ can be expressed in the following way:

$$\mathbf{P}(z_r) = \mathbf{D}_{array}(z_r)\, \mathbf{D}_r^{-}(z_r,z_0)\, \mathbf{P}^{-}(z_0)\,, \tag{2.20}$$

with the composition matrix $\mathbf{D}_r^{-}(z_r,z_0)$ describing the way the *upgoing* pressure wave field $\mathbf{P}^{-}(z_0)$ transforms into the actual measured *total* pressure at depth level z_r, including the ghost at the receiver side. $\mathbf{D}_{array}(z_r)$ describes the array response for each receiver station.

For both detector matrices $\mathbf{D}_{array}(z_r)$ and $\mathbf{D}_r^{-}(z_r,z_0)$ the response can be calculated in the k_x-ω domain for each receiver position (see Appendix B). After inverse Fourier transformation to the spatial domain the columns of the detector matrices are obtained. Note that when the arrays have equal responses for each receiver station, the array matrix $\mathbf{D}_{array}(z_r)$ has equal (but shifted) columns, yielding a Toeplitz structure. The same is true for the composition matrix $\mathbf{D}_r^{-}(z_r,z_0)$ if the water depth does not vary for each receiver station. In the case that both detector matrices have a Toeplitz structure, the detection in terms of matrix multiplications can be described by a scalar multiplication in the k_x-ω domain.

Fig. 2.6a shows a hydrophone array consisting of 7 identical elements with 2 m spacing. The directivity pattern of this array is shown in Fig. 2.6b.

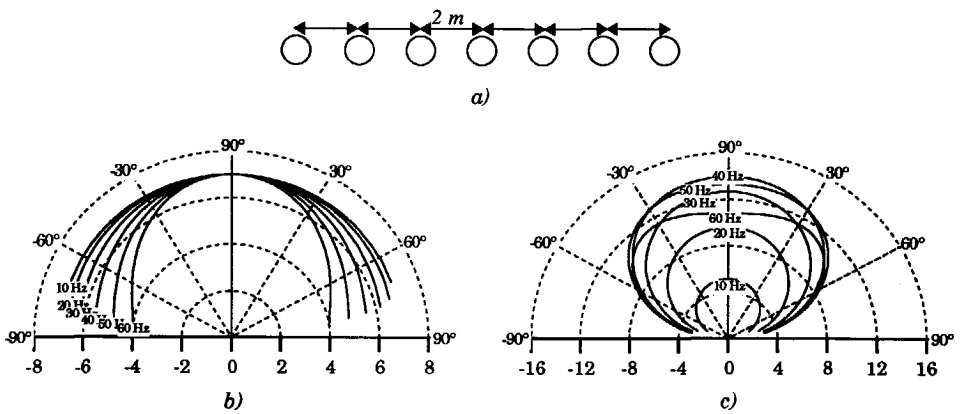

Fig. 2.6 a) Receiver array of 7 identical hydrophones with 2 m spacing b) Directivity pattern of the array for several frequencies c) Directivity pattern of the array including the free surface, taken for the array depth 9 m.

As expected, the response is frequency dependent, like the source array. Fig. 2.6c shows the array directivity if the receiver ghost is included. The array depth of 9 m is typical for marine acquisition.

Note that the array directivity tends to suppress the amplitudes at high angles. This is generally desired, as the measured waves at high incident angles are spatially aliased for the high frequencies. Both the source and receiver array act as a crude anti-alias filter. Therefore, the dimensions of the array should be carefully chosen when designing a seismic survey, see Ongkiehong and Askin (1988).

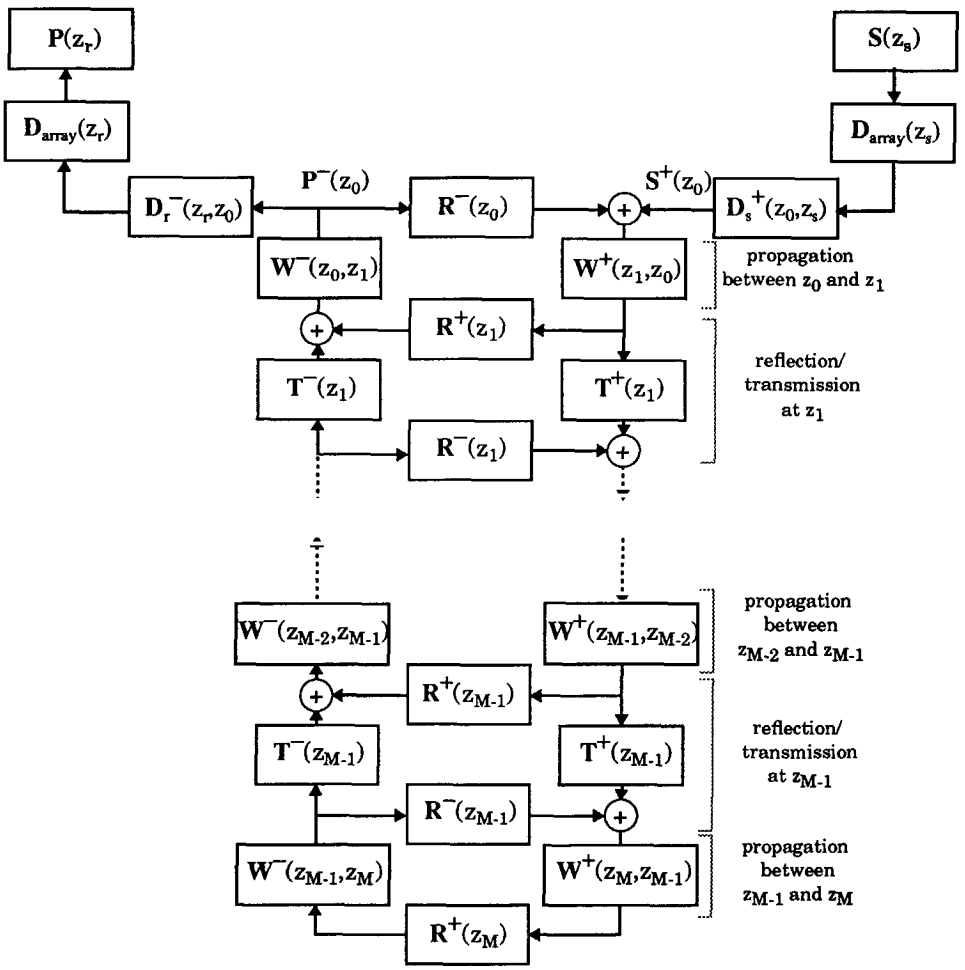

Fig. 2.7 Diagram of the response of a subsurface model with M depth levels (the direct waves are ignored). For surface-related multiple elimination only the upper part is of importance.

2.4 OVERVIEW OF THE ACOUSTIC FORWARD MODEL

Having included the source and receiver characteristics at the free surface, the forward model of seismic data in the marine case can be written as

$$\mathbf{P}(z_0) = \left[\mathbf{D}_{array}(z_r)\, \mathbf{D}_r^-(z_r,z_0) \right] \mathbf{X}(z_0,z_0) \left[\mathbf{D}_s^+(z_0,z_s)\, \mathbf{D}_{array}(z_s) \right] \mathbf{S}(z_s) . \tag{2.21}$$

Fig. 2.7 shows the total recursive forward model in a diagram, being a recursion of propagation and reflection effects. At the upper part the source and receiver properties are included.

Going back to the upgoing wave fields at the surface, as given by $\mathbf{P}^-(z_0)$, they can also be described in terms of the impulse response matrix without surface-related multiples, $\mathbf{X}_0(z_0,z_0)$, by combining equations (2.14) and (2.16):

$$\mathbf{P}^-(z_0) = \left[\mathbf{I} - \mathbf{X}_0(z_0,z_0)\, \mathbf{R}^-(z_0) \right]^{-1} \mathbf{X}_0(z_0,z_0)\, \mathbf{S}^+(z_0) . \tag{2.22}$$

In this expression the generation of the surface-related multiples is explicitly described. It is this expression that will be used as a starting point for the multiple elimination procedure.
If we introduce $\mathbf{P}_0^-(z_0)$ as the upgoing wave field at the surface without surface-related multiples:

$$\mathbf{P}_0^-(z_0) = \mathbf{X}_0(z_0,z_0)\, \mathbf{S}^+(z_0) , \tag{2.23}$$

equation (2.22) transforms into:

$$\mathbf{P}^-(z_0) = \left[\mathbf{I} - \mathbf{P}_0^-(z_0) \left\{ \mathbf{S}^+(z_0) \right\}^{-1} \mathbf{R}^-(z_0) \right]^{-1} \mathbf{P}_0^-(z_0) . \tag{2.24}$$

Fig. 2.8 shows the diagrams of equation (2.23) and equation (2.24). Note that Fig. 2.8 is equivalent to Fig. 2.2, except for the fact that Fig. 2.2 describes the situation for an arbitrary interface and Fig. 2.8 for the free surface including the seismic source characteristics. Moreover, Fig. 2.8 refers to multi-shot data.

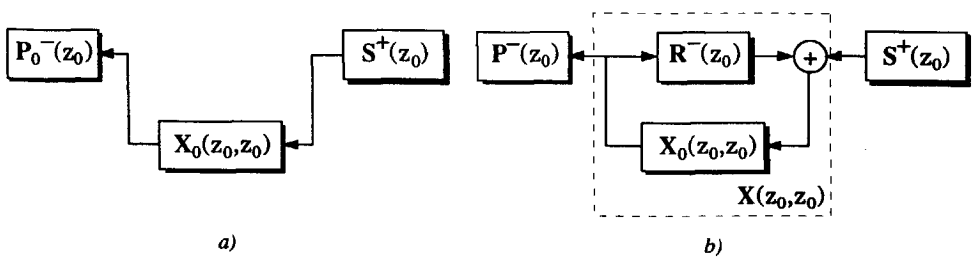

Fig. 2.8 *a) Forward model of seismic data without surface-related multiples.*
b) Forward model of seismic data with surface-related multiples.

2.5 ACOUSTIC FORWARD MODEL IN THE CASE OF A THIN SURFACE LAYER

In the case a *thin* surface layer is present, the forward model should be adapted to describe separately the thin surface layer multiples and the thin surface layer related reverberations. This description will be used in Chapter 3 to modify the surface-related multiple elimination method for the thin surface layer situation.

To be consistent with the description of the operators in the previous section, the first interface is chosen to be flat and located at depth level z_1. Furthermore, we assume that the recursive forward description until depth level z_1 has been completed, yielding $\mathbf{X}_0(z_1,z_1)$, the spatial impulse response of the medium below depth level z_1 without multiples related to this depth level.

2.5.1 Explicit description of the thin surface layer multiples and reverberations

Before extending the impulse response from depth level z_1 to the surface, the propagation through the thin surface layer is explicitly described.

When the downgoing wave field $\vec{P}^+(z_0)$ propagates from the surface through the first layer, a train of multiples is added which can be described by (see Fig. 2.9):

$$\vec{P}^+(z_1) = \mathbf{T}^+(z_1)\, \mathbf{W}_m{}^+(z_1,z_0)\, \vec{P}^+(z_0) \tag{2.25a}$$

with the downward propagation operator $\mathbf{W}_m{}^+(z_1,z_0)$ including the first layer multiples defined as:

$$\mathbf{W}_m{}^+(z_1,z_0) = \mathbf{W}^+(z_1,z_0)\, [\, \mathbf{I} - \mathbf{M}_1{}^+(z_0,z_0)\,]^{-1}\,, \tag{2.25b}$$

where the multiple operator $\mathbf{M}_1{}^+(z_0,z_0)$ is given by

$$\mathbf{M}_1{}^+(z_0,z_0) = \mathbf{R}^-(z_0)\, \mathbf{W}^-(z_0,z_1)\, \mathbf{R}^+(z_1)\, \mathbf{W}^+(z_1,z_0)\,. \tag{2.25c}$$

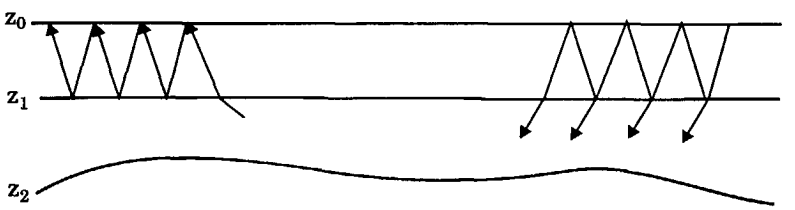

Fig. 2.9 Each propagation through the first layer adds a train of reverberations to the wave field.

Hence, $\mathbf{M}_1^+(z_0,z_0)$ describes one round trip through the first layer, starting with downward propagation from the surface to the first interface.

For the upward propagation through the first layer that includes the reverberations, equivalent expressions can be found:

$$\vec{\mathbf{P}}^-(z_0) = \mathbf{W}_m^-(z_0,z_1)\,\mathbf{T}^-(z_1)\,\vec{\mathbf{P}}^-(z_1) \tag{2.26a}$$

with the upward propagation operator including the first layer multiples defined as:

$$\mathbf{W}_m^-(z_0,z_1) = [\,\mathbf{I} - \mathbf{M}_1^-(z_0,z_0)\,]^{-1}\,\mathbf{W}^-(z_0,z_1)\,, \tag{2.26b}$$

the multiple operator $\mathbf{M}_1^-(z_0,z_0)$ being defined as

$$\mathbf{M}_1^-(z_0,z_0) = \mathbf{W}^-(z_0,z_1)\,\mathbf{R}^+(z_1)\,\mathbf{W}^+(z_1,z_0)\,\mathbf{R}^-(z_0)\,. \tag{2.26c}$$

The total transmission characteristics of this first layer system (including the reverberations) can be written as:

$$\mathbf{T}^+(z_1,z_0) = \mathbf{T}^+(z_1)\,\mathbf{W}_m^+(z_1,z_0) \tag{2.27a}$$

for the downward transmission and

$$\mathbf{T}^-(z_0,z_1) = \mathbf{W}_m^-(z_0,z_1)\,\mathbf{T}^-(z_1) \tag{2.27b}$$

for the upward transmission through this layer.

Using the generalized propagation operators for the first layer, the forward model of seismic data that includes the first layer reverberations becomes:

$$\vec{\mathbf{P}}^-(z_0) = [\;\mathbf{W}_m^-(z_0,z_1)\,\mathbf{R}^+(z_1)\,\mathbf{W}^+(z_1,z_0)\;]\,\vec{\mathbf{P}}^+(z_0) + [\;\mathbf{T}^-(z_0,z_1)\,\mathbf{X}_0(z_1,z_1)\,\mathbf{T}^+(z_1,z_0)\;]\,\vec{\mathbf{P}}^+(z_0)\,, \tag{2.28}$$

where $\mathbf{X}_0(z_1,z_1)$ is the response related to the first interface without the interface-related multiples included. The first term in equation (2.28) describes the first layer primaries and its multiples (see Fig. 2.10, left side), the second term describes the response from below the first layer including the reverberations (see Fig. 2.10, right side).

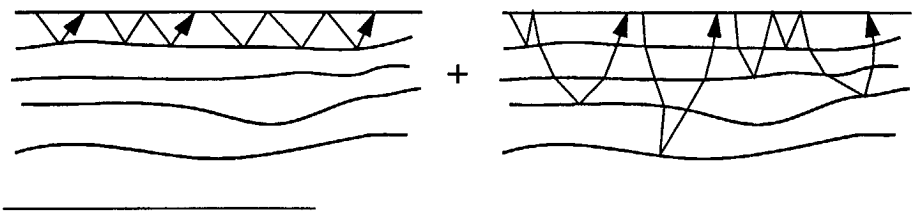

Fig. 2.10 The total response can be divided into the first layer response with its multiples and the response from below the first layer, including the reverberations in the first layer.

2.5.2 Influence of the thin surface layer on the subsurface response

In the case of a *thin* surface layer (for example shallow water) this layer can be seen as one interface with certain transmission and reflection characteristics. Therefore the description of the surface layer multiples is used to define these properties. The total transmission through a thin layer is described by the already defined operators $\mathbf{T}^-(z_0,z_1)$ and $\mathbf{T}^+(z_1,z_0)$. The total reflection of the thin layer from below can be expressed by:

$$\mathbf{R}^-_{tot}(z_1) = \mathbf{R}^-(z_1) + \mathbf{T}^+(z_1)\,\mathbf{W}^+(z_1,z_0)\,\mathbf{R}^-(z_0)\,\mathbf{T}^-(z_0,z_1)\,. \tag{2.29}$$

Note that $\mathbf{T}^+(z_1)$ describes transmission through the *interface* at z_1 and that $\mathbf{T}^-(z_0,z_1)$ describes transmission through the first *layer*, including the reverberations. In Appendix B some examples of the thin surface layer reflectivity operator are shown.

If all multiples related to the first layer are included in the way as described in the previous section we arrive at

$$\mathbf{X}_{tot}(z_1,z_1) = [\,\mathbf{I} - \mathbf{X}_0(z_1,z_1)\,\mathbf{R}^-_{tot}(z_1)\,]^{-1}\,\mathbf{X}_0(z_1,z_1)\,. \tag{2.30}$$

The influence of the thin surface layer on the surface response $\vec{\mathbf{P}}^-(z_0)$ is visualized in Fig. 2.11. Note that $\vec{\mathbf{P}}^-(z_0)$ does not contain the response of the thin layer itself. Note also the difference with the normal surface-related multiple description (as shown in Fig. 2.2b): the two transmission matrices $\mathbf{T}^-(z_0,z_1)$ and $\mathbf{T}^+(z_1,z_0)$, describing the total transmission through the thin layer including the reverberations, and the modified reflectivity operator $\mathbf{R}^-_{tot}(z_1)$. In fact, the upper multiple generation loop in the total forward model of Fig. 2.7 has been cut and split into three separate loops, used for the transmission and reflection effects of the thin layer.

To see what the influence is of a thin layer on a seismic shot record, Fig. 2.12 shows a shot record simulated in a medium with 8 horizontal reflectors and with 30 m water on top of it, including all internal and surface-related multiples. The response from the thin surface layer itself can be considered as a kind of "acoustic groundroll" (see the arrows in Fig. 2.12) and can therefore be considered as an acoustic surface wave. In Chapter 3 this example will be further investigated.

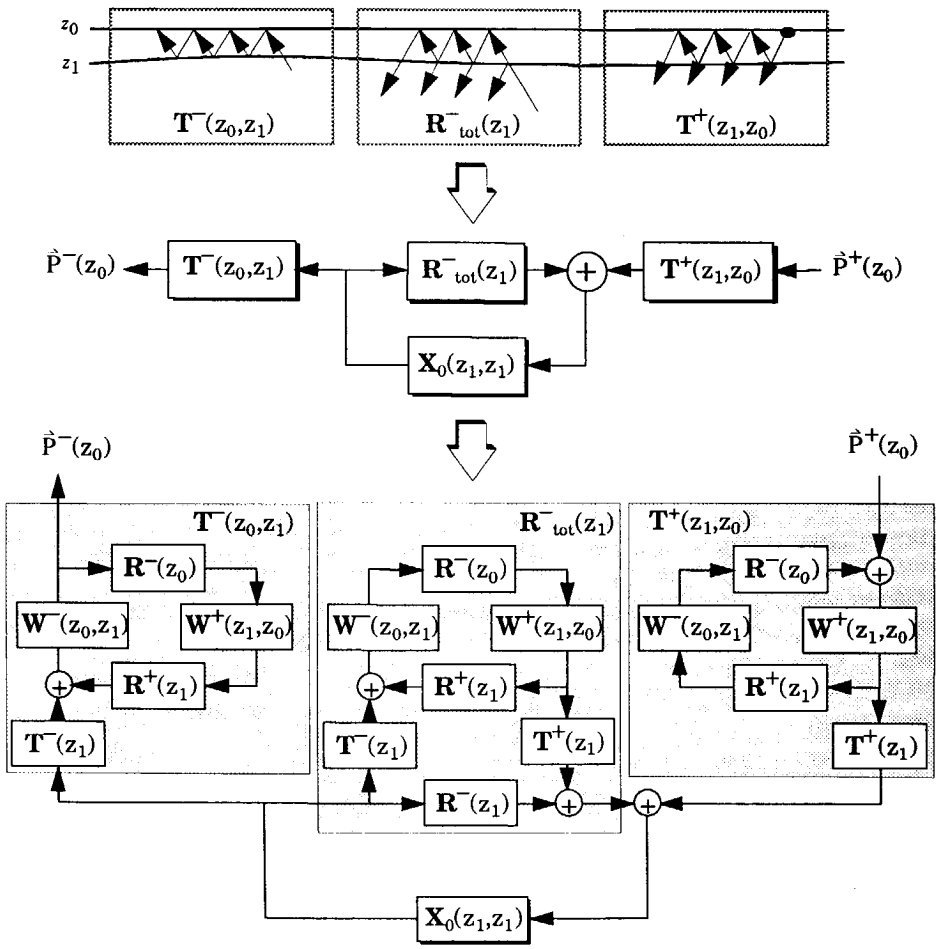

Fig. 2.11 Forward model adapted for a thin surface layer. Each propagation through or reflection against the thin surface layer adds a train of thin layer reverberations. (The response of the thin layer itself is ignored.)

In the beginning of this section we have chosen the first interface to be a flat reflector. In fact this is not a restriction of the theory. It is also correct for a tilted reflector or even for a curved reflector. However, in the latter case the curvature should obey the conditions for the validity of the Rayleigh hypothesis, as derived by van den Berg and Fokkema (1980). For larger curvatures of the reflector inaccuracies will arise in the description of the reverberations of the first layer, due to the existence of *lateral* multiples. For (locally) flat layers the procedure can be applied in the k_x-ω domain. These inaccuracies will have their effect when the influence of a thin layer influece is being corrected for as a first pre-processing step, which will be treated in Chapter 3.

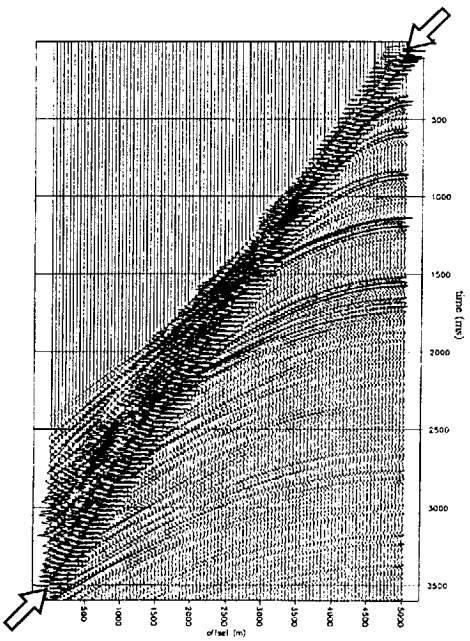

Fig. 2.12 *Shot record simulated in a 8-layer model, with a thin water layer of 30 m on top. The arrows point at the response of the thin layer.*

2.6 FORWARD MODEL OF ELASTIC SEISMIC DATA

For a description of elastic wave fields multi-component data has to be introduced. For simplicity reasons the 2D case will be discussed with two types of waves: longitudinal or P-waves and transverse or S-waves (polarized in the vertical plane), although the theory can be easily extended to the full 3D case. The P-waves are mathematically described by the potentials Φ and the S-waves are described by the potentials Ψ, as can be found in Aki and Richards (1980) and Wapenaar and Berkhout (1989). The latter describe the theoretical background of multi-component data processing. In this section the forward model is presented in terms of down- and upgoing waves; it is an extension of the foregoing acoustic model.

2.6.1 Relations between tractions, particle velocities and potentials

In the elastic case the one-way wave field at the surface should be defined by more than one quantity. For the 2D situation, two quantities are required; different quantities can be chosen. In the acoustic case we have chosen for a description in terms of pressure, although a description in terms of the vertical component of the particle velocity would also be valid.

For the elastic case we can make the following three choices:

- P- and S-wave potentials Φ and Ψ.
- The horizontal and vertical component of the traction T_{xz} and T_{zz} (the second subscript denotes that the tractions act on a plane normal to the z-axis).
- The horizontal and vertical component of the particle velocity V_x and V_z.

We define the following elastic data vectors, which describe the total traction, the particle velocity and the P-and S-wave potential of the wave field at the surface as:

$$\underset{\sim}{\vec{T}} = \begin{bmatrix} \vec{T}_{xz} \\ \vec{T}_{zz} \end{bmatrix}, \underset{\sim}{\vec{V}} = \begin{bmatrix} \vec{V}_x \\ \vec{V}_z \end{bmatrix} \text{ and } \underline{\vec{\Pi}} = \begin{bmatrix} \vec{\Phi} \\ \vec{\Psi} \end{bmatrix}. \tag{2.31}$$

Note that for simplicity reasons the indication of the depth level has been omitted in this notation. Each vector can be considered as one column of an elastic data matrix with one wave quantity in the upper part and one wave quantity in the lower part of this vector, see also Appendix A. Each of these wave quantity can be seen as the summation of the related quantities of down- and upgoing wave fields.

For the tractions this means:

$$\vec{\underline{T}} = \vec{\underline{T}}^{+} + \vec{\underline{T}}^{-}, \tag{2.32a}$$

with

$$\vec{\underline{T}}^{+} = \begin{bmatrix} \vec{T}^{+}_{xz} \\ \vec{T}^{+}_{zz} \end{bmatrix} \quad , \quad \vec{\underline{T}}^{-} = \begin{bmatrix} \vec{T}^{-}_{xz} \\ \vec{T}^{-}_{zz} \end{bmatrix}. \tag{2.32b}$$

For the particle velocity the corresponding expression is given by:

$$\vec{\underline{V}} = \vec{\underline{V}}^{+} + \vec{\underline{V}}^{-} \tag{2.33a}$$

with

$$\vec{\underline{V}}^{+} = \begin{bmatrix} \vec{V}^{+}_{x} \\ \vec{V}^{+}_{z} \end{bmatrix} \quad , \quad \vec{\underline{V}}^{-} = \begin{bmatrix} \vec{V}^{-}_{x} \\ \vec{V}^{-}_{z} \end{bmatrix}. \tag{2.33b}$$

Finally, for the P- and S-wave potentials the decomposition into down- and upgoing waves is given by:

$$\vec{\underline{\Pi}} = \vec{\underline{\Pi}}^{+} + \vec{\underline{\Pi}}^{-} \tag{2.34a}$$

with

$$\vec{\underline{\Pi}}^{+} = \begin{bmatrix} \vec{\Phi}^{+} \\ \vec{\Psi}^{+} \end{bmatrix} \quad , \quad \vec{\underline{\Pi}}^{-} = \begin{bmatrix} \vec{\Phi}^{-} \\ \vec{\Psi}^{-} \end{bmatrix}. \tag{2.34b}$$

From Wapenaar and Berkhout (1989) the following relation can be found, written in the space domain as:

$$\begin{bmatrix} \vec{\underline{T}} \\ \vec{\underline{V}} \end{bmatrix} = \begin{bmatrix} \underline{L}^{+}_{2} & \underline{L}^{-}_{2} \\ \underline{L}^{+}_{1} & \underline{L}^{-}_{1} \end{bmatrix} \begin{bmatrix} \vec{\underline{\Pi}}^{+} \\ \vec{\underline{\Pi}}^{-} \end{bmatrix}, \tag{2.35}$$

with expressions of the elastic composition matrices $\underline{L}^{+}_{2}$, $\underline{L}^{-}_{2}$, $\underline{L}^{+}_{1}$ and $\underline{L}^{-}_{1}$ in the k_x-ω domain given in Appendix B.

Also the inverse of equation (2.35) can be formulated and is defined as:

$$\begin{bmatrix} \vec{\Pi}^+ \\ \vec{\Pi}^- \end{bmatrix} = \begin{bmatrix} \underline{M}_2^+ & \underline{M}_1^+ \\ \underline{M}_2^- & \underline{M}_1^- \end{bmatrix} \begin{bmatrix} \vec{T} \\ \vec{V} \end{bmatrix}, \tag{2.36}$$

with expressions for the elastic decomposition matrices $\underline{M}_2^+$, $\underline{M}_1^+$, $\underline{M}_2^-$ and $\underline{M}_1^-$ in the k_x-ω domain given in Appendix B.

From equation (2.35) the following expressions for the down- and upgoing tractions can be extracted, using equation (2.32a) and the assumption that the down- and upgoing waves are decoupled:

$$\vec{T}^+ = \underline{L}_2^+ \vec{\Pi}^+, \tag{2.37a}$$

$$\vec{T}^- = \underline{L}_2^- \vec{\Pi}^- \tag{2.37b}$$

or, in matrix notation:

$$\begin{bmatrix} \vec{T}^+ \\ \vec{T}^- \end{bmatrix} = \begin{bmatrix} \underline{L}_2^+ & 0 \\ 0 & \underline{L}_2^- \end{bmatrix} \begin{bmatrix} \vec{\Pi}^+ \\ \vec{\Pi}^- \end{bmatrix}. \tag{2.37c}$$

Similarly, from equation (2.35) and equation (2.33a) it follows that

$$\vec{V}^+ = \underline{L}_1^+ \vec{\Pi}^+, \tag{2.38a}$$

$$\vec{V}^- = \underline{L}_1^- \vec{\Pi}^- \tag{2.38b}$$

or, in matrix notation:

$$\begin{bmatrix} \vec{V}^+ \\ \vec{V}^- \end{bmatrix} = \begin{bmatrix} \underline{L}_1^+ & 0 \\ 0 & \underline{L}_1^- \end{bmatrix} \begin{bmatrix} \vec{\Pi}^+ \\ \vec{\Pi}^- \end{bmatrix}. \tag{2.38c}$$

Therefore the relation between the down- and upgoing traction and the total traction and total particle velocity is given by:

$$\begin{bmatrix} \vec{T}^+ \\ \vec{T}^- \end{bmatrix} = \begin{bmatrix} \underline{L}_2^+ & 0 \\ 0 & \underline{L}_2^- \end{bmatrix} \begin{bmatrix} \underline{M}_2^+ & \underline{M}_1^+ \\ \underline{M}_2^- & \underline{M}_1^- \end{bmatrix} \begin{bmatrix} \vec{T} \\ \vec{V} \end{bmatrix} = \begin{bmatrix} \underline{L}_2^+\underline{M}_2^+ & \underline{L}_2^+\underline{M}_1^+ \\ \underline{L}_2^-\underline{M}_2^- & \underline{L}_2^-\underline{M}_1^- \end{bmatrix} \begin{bmatrix} \vec{T} \\ \vec{V} \end{bmatrix}, \tag{2.39}$$

and for the up-and downgoing particle velocity wave fields:

$$\begin{bmatrix} \vec{\underline{V}}^{+} \\ \vec{\underline{V}}^{-} \end{bmatrix} = \begin{bmatrix} \underline{L}_1^{+} & 0 \\ 0 & \underline{L}_1^{-} \end{bmatrix} \begin{bmatrix} \underline{M}_2^{+} & \underline{M}_1^{+} \\ \underline{M}_2^{-} & \underline{M}_1^{-} \end{bmatrix} \begin{bmatrix} \vec{\underline{T}} \\ \vec{\underline{V}} \end{bmatrix} = \begin{bmatrix} \underline{L}_1^{+}\underline{M}_2^{+} & \underline{L}_1^{+}\underline{M}_1^{+} \\ \underline{L}_1^{-}\underline{M}_2^{-} & \underline{L}_1^{-}\underline{M}_1^{-} \end{bmatrix} \begin{bmatrix} \vec{\underline{T}} \\ \vec{\underline{V}} \end{bmatrix}. \tag{2.40}$$

Of course, equations (2.40) and (2.41) can also be derived directly.

The equations given in this section are used to derive a general forward model of elastic data, which will be given in the next section. As we have given the relations between the down- and upgoing wave fields in terms of P- and S-wave potentials, tractions or particle velocities on the one hand and the total traction and particle velocity field on the other hand, we can chose for three kinds of elastic wave field descriptions at the surface

- In terms of down- and upgoing potentials $\vec{\underline{\Pi}}^{+}$ and $\vec{\underline{\Pi}}^{-}$.
- In terms of down- and upgoing tractions $\vec{\underline{T}}^{+}$ and $\vec{\underline{T}}^{-}$.
- In terms of down- and upgoing particle velocities $\vec{\underline{V}}^{+}$ and $\vec{\underline{V}}^{-}$.

2.6.2 General forward model for multi-component surface data

From the previous section it may be clear that there are three basic ways to describe elastic down- and upgoing wave fields: in terms of P- and S- wave potentials Φ and Ψ, in horizontal and vertical components of the traction T_{xz} and T_{zz}, and in terms of horizontal and vertical components of the particle velocity V_x and V_z. Let us define the elastic subsurface impulse response matrix $\underline{\mathbf{X}}(z_0,z_0)$, which consists of four submatrices, in the following way:

$$\underline{\mathbf{X}}(z_0,z_0) = \begin{bmatrix} \mathbf{X}_{\alpha\alpha}(z_0, z_0) & \mathbf{X}_{\alpha\beta}(z_0, z_0) \\ \mathbf{X}_{\beta\alpha}(z_0, z_0) & \mathbf{X}_{\beta\beta}(z_0, z_0) \end{bmatrix}, \tag{2.41}$$

with α and β standing for the quantities that have been chosen to describe the elastic one-way wave fields at the source and receiver positions:

a) Potentials
$\alpha=\phi$ and $\beta=\psi$

b) Tractions
$\alpha=\tau_{xz}$ and $\beta=\tau_{zz}$

c) Velocities
$\alpha=v_x$ and $\beta=v_z$.

Each submatrix in equation (2.41) describes the upgoing wave fields at the receiver positions in terms of α or β due to unit downgoing wave fields at the source positions in terms of α or β.

One column of the elastic impulse response matrix $\underline{\mathbf{X}}(z_0,z_0)$ contains the spatial impulse response for one source position (common source gather); the upper part consisting of the α quantity of the upgoing waves and the lower part consisting of the β quantity of the upgoing waves. The position of this column (left or right part in the matrix) determines the description of the source waves (in terms of α or β). Similarly, one row of $\underline{\mathbf{X}}(z_0,z_0)$ contains a common receiver gather with the left part consisting of the α quantity of the downgoing waves and the right part consisting of the β quantity of the downgoing waves. The position of this row (upper or lower part in the matrix) determines the description of the upgoing waves (in terms of α or β). Fig. 2.13 shows this multi-component spatial impulse response matrix, with the four sub-matrices. For a downgoing "α wave field" at source position j, as shown in Fig. 2.13, the corresponding upgoing "α and β wave fields" at receiver position i correspond to a column in the left part of the matrix $\underline{\mathbf{X}}(z_0,z_0)$. In appendix A this multi-component matrix notation is further explained.

Looking at the seismic situation, where the surface is a free surface, the downgoing source wave field at the source positions is generally described in terms of tractions ($\alpha=T_{xz}^{+}$, $\beta=T_{zz}^{+}$) and the upgoing reflected wave fields at the receiver positions are generally described in terms of particle velocities ($\alpha=V_x^{-}$,$\beta=V_z^{-}$).
Note that if the quantities α and β represent *potentials*, then α and β define also the *type* of wave field (being P- and S-waves).

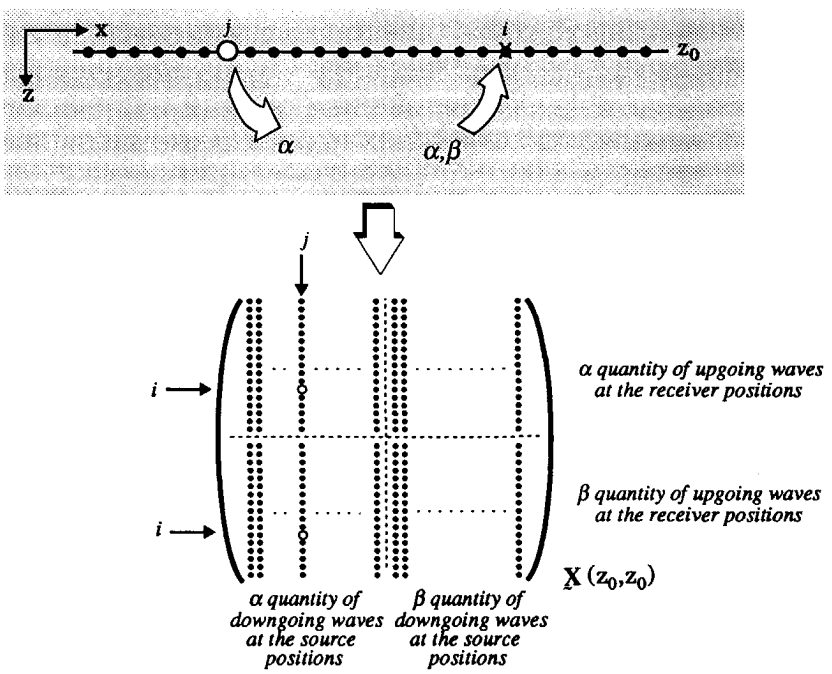

Fig. 2.13 The elastic impulse response matrix $\underline{\mathbf{X}}(z_0,z_0)$ consists of four submatrices.

Once the elastic impulse response matrix with multiples, $\underline{\mathbf{X}}(z_0,z_0)$, has been defined, the elastic impulse response matrix without multiples, $\underline{\mathbf{X}}_0(z_0,z_0)$, can be defined in the same way. The relation between the two impulse response matrices is similar as in the acoustic case (see equation (2.14)):

$$\underline{\mathbf{X}}(z_0,z_0) = [\ \underline{\mathbf{I}} - \underline{\mathbf{X}}_0(z_0,z_0)\ \underline{\mathbf{R}}^-(z_0)\ ]^{-1}\ \underline{\mathbf{X}}_0(z_0,z_0)\,, \tag{2.42}$$

with $\underline{\mathbf{R}}^-(z_0)$ describing the multi-component free surface reflectivity matrix, defined as:

$$\underline{\mathbf{R}}^-(z_0) = \begin{bmatrix} \mathbf{R}^-_{\alpha\alpha}(z_0) & \mathbf{R}^-_{\alpha\beta}(z_0) \\ \mathbf{R}^-_{\beta\alpha}(z_0) & \mathbf{R}^-_{\beta\beta}(z_0) \end{bmatrix}. \tag{2.43}$$

In equation (2.43) submatrix $\mathbf{R}^-_{\alpha\beta}$ describes the reflection at the free surface from the β quantity of upgoing waves to the α quantity of downgoing waves, etc.

2.6.3 Including source and receiver characteristics

- Including the source matrix

Similar to the acoustic case, the total upgoing elastic wave fields contained in $\underline{\mathbf{P}}^-(z_0)$ due to the downgoing elastic source wave fields $\underline{\mathbf{S}}^+(z_0)$ can be formulated as:

$$\underline{\mathbf{P}}^-(z_0) = \underline{\mathbf{X}}(z_0,z_0)\ \underline{\mathbf{S}}^+(z_0) \tag{2.44}$$

with $\underline{\mathbf{P}}^-(z_0)$ defined as:

$$\underline{\mathbf{P}}^-(z_0) = \begin{bmatrix} \mathbf{P}^-_{\alpha\alpha}(z_0) & \mathbf{P}^-_{\alpha\beta}(z_0) \\ \mathbf{P}^-_{\beta\alpha}(z_0) & \mathbf{P}^-_{\beta\beta}(z_0) \end{bmatrix} \tag{2.45}$$

and the total downgoing source wave field defined as:

$$\underline{\mathbf{S}}^+(z_0) = \begin{bmatrix} \mathbf{S}^+_{\alpha\beta}(z_0) & \mathbf{S}^+_{\alpha\beta}(z_0) \\ \mathbf{S}^+_{\beta\beta}(z_0) & \mathbf{S}^+_{\beta\beta}(z_0) \end{bmatrix}. \tag{2.46}$$

Note that in the above matrices P stands for a general wave field description (and not for P-waves); S describes a general source wave field (and not S-waves). Again α and β refer to the different quantities, depending on the way the elastic wave fields are described.

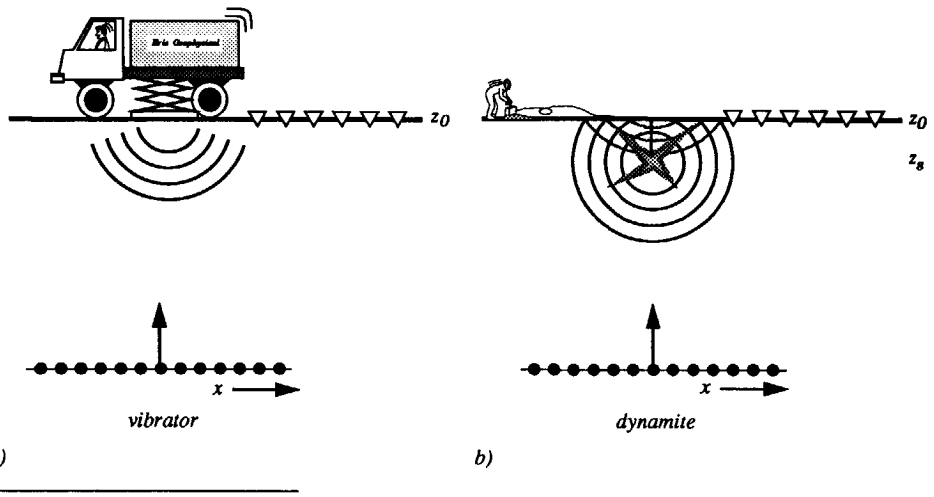

Fig. 2.14 Effective downgoing source wave field at z_0, i.e. one column of the source matrix. a) Vibrator source b) Buried dynamite source.

Land data acquisition is normally done with vibrators, as shown in Fig. 2.4a, or with buried dynamite sources (at depth level z_s), as shown in Fig. 2.4b. In the first case it is possible to use differently oriented vibrators for multi-component traction sources.

As in the acoustic situation, the downgoing source wave field can be considered as a combination of a decomposition matrix, source array matrix and the basic source matrix:

$$\underline{\mathbf{S}}^{+}(z_0) = \underline{\mathbf{D}}_s^{+}(z_0)\, \underline{\mathbf{D}}^{(s)}_{\text{array}}(z_0)\, \underline{\mathbf{S}}_T(z_0)\,, \tag{2.47}$$

with $\underline{\mathbf{S}}_T(z_0)$ the basic source matrix in terms of tractions at the free surface, $\underline{\mathbf{D}}^{(s)}_{\text{array}}(z_0)$ describing the array effects (if applicable) and $\underline{\mathbf{D}}_s^{+}(z_0)$ describing the decomposition into the downgoing wave fields. The decomposition operator $\underline{\mathbf{D}}_s^{+}(z_0)$ has a meaning which depends on the way the downgoing going wave fields $\underline{\mathbf{S}}^{+}(z_0)$ are described: in terms of P- and S-wave potentials, stresses or particle velocity components. In section 2.6.4 this will be further discussed.

- Vibrator sources

For the description of the basic source matrix we assume perfect stress sources (vibrators) oriented in the x- or z-direction. We also assume that the vibrators act as point sources, i.e. their size is small compared to the wavelengths of interest. The vibrator oriented in the x-direction imposes only horizontal stresses on the subsurface and the vertically oriented vibrator (the conventional vibrator) imposes only vertical stresses. This means that the basic source matrix $\underline{\mathbf{S}}_T(z_0)$ has only two of the four sub-matrices non-zero:

$$\underline{\mathbf{S}}_T(z_0) = \begin{bmatrix} \mathbf{S}_{xz}(z_0) & \mathbf{0} \\ \mathbf{0} & \mathbf{S}_{zz}(z_0) \end{bmatrix} . \tag{2.48}$$

At the position of the source itself stresses are present whereas at all other positions at the surface the pressure is zero because we deal with a stress free surface. This causes the source matrix to be non-zero at the diagonal elements only. The non-zero elements contain the source strength for the frequency component for which the source matrix is constructed. If the source strength for the j^{th} shot record is given as $S_{x,j}(\omega)$ for the horizontally oriented and $S_{z,j}(\omega)$ for the vertically oriented vibrator, the source sub-matrices for N (ideal) vibrators can be written as:

$$\mathbf{S}_{xz}(z_0) = \text{diag}\,[\, S_{x,1}(\omega)\, S_{x,2}(\omega) \ldots S_{x,j}(\omega) \ldots S_{x,N}(\omega)\,] \tag{2.49a}$$

and

$$\mathbf{S}_{zz}(z_0) = \text{diag}\,[\, S_{z,1}(\omega)\, S_{z,2}(\omega) \ldots S_{z,j}(\omega) \ldots S_{z,N}(\omega)\,] . \tag{2.49b}$$

If the source signatures are equal for all shot records, being $S_x(\omega)$ for the horizontally and $S_z(\omega)$ for the vertically oriented vibrator, the source sub-matrices are given by:

$$\mathbf{S}_{xz}(z_0) = S_x(\omega)\, \mathbf{I} \tag{2.50a}$$

and

$$\mathbf{S}_{zz}(z_0) = S_z(\omega)\, \mathbf{I} . \tag{2.50b}$$

Finally, if both vibrator types generate the same signature $S(\omega)$, the initial multi-component source matrix can be written as

$$\underline{\mathbf{S}}_T(z_0) = S(\omega)\, \underline{\mathbf{I}} . \tag{2.51}$$

However, in practical situations the existing generation of vibrators do not act as ideally as previously described; they have a more complex behavior. In that case a source wave field is still described by one column of the source matrix, but now also non-diagonal elements have non-zero values. For a more elaborate discussion on the behavior of vibrator sources see Baeten (1990).

- Dynamite sources

A dynamite source can be considered as a monopole source (i.e. omni-directional characteristics). Surrounded by a homogenous, isotropic medium it radiates a spherical P-wave, see for example Anstey (1981). As this source is buried close to the surface at depth level z_s, typically a few meters, we also have to deal with its mirror source. This means that the upgoing source

wave field reflects at the free surface and forms an additional downgoing wave field ("ghost" wave field). During this reflection, P-waves are partially converted to S-waves. This conversion effect is angle dependent. However, as S-wave velocities have low values close to the surface, and the angle range of the emitted source wave field that actually appears in the reflections is rather small, these conversions may be neglected. For an example of free surface reflectivity operators in the elastic case, see Appendix B. If also the depth of the dynamite source is small enough compared to the dominant wavelength in the source wave field, the two P-wave monopoles will have equal strength and opposite sign (after reflection against a perfect reflector) and can be considered as a P-wave dipole at the free surface.

It is known (Berkhout (1982)) that the downgoing wave field of a dipole measured along dipole axis can be written as a spatial delta function; see also Appendix B for a further discussion on this subject. This means that the initial source matrix in terms of P and S source wave fields has only one non-zero sub-matrix, which is a diagonal matrix if all dynamite sources are assumed to be equally strong:

$$\underline{\mathbf{S}}_{\Pi}(z_0) = \begin{bmatrix} \mathbf{S}_{\varphi\varphi}(z_0) & \mathbf{S}_{\varphi\psi}(z_0) \\ \mathbf{S}_{\psi\varphi}(z_0) & \mathbf{S}_{\psi\psi}(z_0) \end{bmatrix} = S(\omega) \begin{bmatrix} \mathbf{I} & \mathbf{0} \\ \mathbf{0} & \mathbf{0} \end{bmatrix}. \tag{2.52}$$

In terms of tractions, the source matrix $\underline{\mathbf{S}}_{\Pi}(z_0)$ should be multiplied with a composition operator $\underline{\mathbf{L}}_2^+(z_0)$ (see equation (2.35)) to arrive at the source matrix in terms of tractions $\underline{\mathbf{S}}_{T}(z_0)$:

$$\underline{\mathbf{S}}_{T}(z_0) = \underline{\mathbf{L}}_2^+(z_0)\, \underline{\mathbf{S}}_{\Pi}(z_0). \tag{2.53}$$

In the matrix $\underline{\mathbf{S}}_{T}(z_0)$ only the left half will be non-zero, meaning that only one type of source wave field is generated.

If the depth of the dynamite source is not small, the source matrix can be calculated by the superposition of the source matrices of the two monopole sources separately.

- Including the receiver matrix

For multi-component land data acquisition the data is measured by geophones that record the horizontal and vertical component of the particle velocity at the free surface (2D situation). If the detectors are also included in our forward model, the total measured wave field $\underline{\mathbf{P}}(z_0)$, i.e. the horizontal and vertical components of the particle velocity due to the source wave fields, is defined as:

$$\underline{\mathbf{P}}(z_0) = \begin{bmatrix} \mathbf{P}_{v_x\alpha}(z_0) & \mathbf{P}_{v_x\beta}(z_0) \\ \mathbf{P}_{v_z\alpha}(z_0) & \mathbf{P}_{v_z\beta}(z_0) \end{bmatrix}. \tag{2.54}$$

similar to the acoustic case the measured data can be expressed in the upgoing wave fields at the surface by:

$$\underline{P}(z_0) = \underline{D}^{(r)}_{array}(z_0)\, \underline{D}_r^{-}(z_0)\, \underline{P}^{-}(z_0)\,, \tag{2.55}$$

$\underline{D}_r^{-}(z_0)$ describing the composition of the upgoing wave fields into particle velocity components at the free surface and $\underline{D}^{(r)}_{array}(z_0)$ describing the effect of the geophone arrays. The composition operator $\underline{D}_r^{-}(z_0)$ depends on the way the upgoing wave fields $\underline{P}^{-}(z_0)$ are described: in terms of P- and S-wave potentials, stresses or particle velocity components. In section 2.6.4 this will be further discussed.

- *Total forward model for multi-component data*

Including the effect of the source and detector matrices, the total multi-component seismic data model reads:

$$\underline{P}(z_0) = \left[\, \underline{D}^{(r)}_{array}(z_0)\, \underline{D}_r^{-}(z_0) \,\right] \underline{X}(z_0,z_0) \left[\, \underline{D}_s^{+}(z_0)\, \underline{D}^{(s)}_{array}(z_0) \,\right] \underline{S}_T(z_0)\,. \tag{2.56}$$

In equation (2.56) $\underline{S}_T(z_0)$ describes the source tractions imposed by the horizontal and vertical vibrators; $\underline{D}_s^{+}(z_0)$ describes the translation of these tractions into downgoing wave fields; $\underline{D}_r^{-}(z_0)$ describes the translation from upgoing wave fields into the horizontal and vertical component of the particle velocity. $\underline{D}^{(s)}_{array}(z_0)$ and $\underline{D}^{(r)}_{array}(z_0)$ describe the source and receiver array effects.

2.6.4 Expressions for $\underline{D}_s^{+}(z_0)$, $\underline{D}_r^{-}(z_0)$ and $\underline{R}^{-}(z_0)$

In the sections 2.6.2 and 2.6.3 a general description of multi-component seismic data in terms of down- and upgoing wave fields has been given. In this section the matrices $\underline{D}_s^{+}(z_0)$, $\underline{D}_r^{-}(z_0)$ and $\underline{R}^{-}(z_0)$ will be discussed in more detail. The relations between the up-and downgoing wave fields, as described in section 2.6.1, will be used. Note that all these formulations are only exact if the medium near the surface, where the acquisition takes place, is considered to be (locally) homogeneous.

- *Description in terms of potentials*

If the wave fields are described by down- and upgoing P- and S-wave potentials Φ and Ψ, the spatial impulse response matrix reads:

$$\underline{X}(z_0,z_0) = \begin{bmatrix} X_{\varphi\varphi}(z_0, z_0) & X_{\varphi\psi}(z_0, z_0) \\ X_{\psi\varphi}(z_0, z_0) & X_{\psi\psi}(z_0, z_0) \end{bmatrix}. \tag{2.57}$$

The free surface reflectivity is defined as:

$$\underline{\vec{\Pi}}^{+}(z_0) = \underline{\mathbf{R}}_{\Pi}^{-}(z_0)\, \underline{\vec{\Pi}}^{-}(z_0)\,. \tag{2.58}$$

Substitution in equation (2.35) yields:

$$\vec{\mathrm{T}}(z_0) = \underline{\mathbf{L}}_2^{+}(z_0)\, \underline{\mathbf{R}}_{\Pi}^{-}(z_0)\, \underline{\Pi}^{-}(z_0) + \underline{\mathbf{L}}_2^{-}(z_0)\, \underline{\Pi}^{-}(z_0) = 0, \tag{2.59}$$

as we deal with a traction free surface. Equation (2.59) must be true for each upgoing wave field $\underline{\Pi}^{-}(z_0)$, so we may conclude

$$\underline{\mathbf{L}}_2^{+}(z_0)\, \underline{\mathbf{R}}_{\Pi}^{-}(z_0) + \underline{\mathbf{L}}_2^{-}(z_0) = 0 \tag{2.60a}$$

or

$$\underline{\mathbf{R}}_{\Pi}^{-}(z_0) = -[\underline{\mathbf{L}}_2^{+}(z_0)]^{-1}\, \underline{\mathbf{L}}_2^{-}(z_0)\,. \tag{2.60b}$$

The operator $\underline{\mathbf{D}}_s^{+}(z_0)$, which transforms the downgoing source traction into downgoing P- and S-wave potentials, can be directly found from equation (2.37a):

$$\underline{\mathbf{D}}_s^{+}(z_0) = [\underline{\mathbf{L}}_2^{+}(z_0)]^{-1}\,. \tag{2.61}$$

The operator $\underline{\mathbf{D}}_r^{-}(z_0)$, which transforms the upgoing P- and S-wave potentials into the total particle velocity components, can be found by setting the total traction to zero in equation (2.36):

$$\underline{\mathbf{D}}_r^{-}(z_0) = [\underline{\mathbf{M}}_1^{-}(z_0)]^{-1}\,. \tag{2.62}$$

- Description in terms of tractions

If the wave fields are described by down- and upgoing tractions τ_{xz} and τ_{zz}, the spatial impulse response matrix reads:

$$\underline{\mathbf{X}}(z_0,z_0) = \begin{bmatrix} \mathbf{X}_{\tau_{xz}\tau_{xz}}(z_0, z_0) & \mathbf{X}_{\tau_{xz}\tau_{zz}}(z_0, z_0) \\ \mathbf{X}_{\tau_{zz}\tau_{xz}}(z_0, z_0) & \mathbf{X}_{\tau_{zz}\tau_{zz}}(z_0, z_0) \end{bmatrix}. \tag{2.63}$$

The free surface reflectivity operator $\underline{\mathbf{R}}_{\mathrm{T}}^{-}(z_0)$ is defined as:

$$\underline{\mathrm{T}}^{+}(z_0) = \underline{\mathbf{R}}_{\mathrm{T}}^{-}(z_0)\, \underline{\mathrm{T}}^{-}(z_0)\,. \tag{2.64}$$

As the total traction is zero at the free surface, it follows from equation (2.64):

$$\underline{\mathbf{R}}_{\mathrm{T}}^{-}(z_0) = -\,\underline{\mathbf{I}}\,. \tag{2.65}$$

According to the definition, the operator $\underset{\sim}{\mathbf{D}}_s^+(z_0)$ is simply:

$$\underset{\sim}{\mathbf{D}}_s^+(z_0) = \underset{\sim}{\mathbf{I}} \quad . \tag{2.66}$$

The operator $\underset{\sim}{\mathbf{D}}_r^-(z_0)$, which transforms the upgoing tractions into the total particle velocity components, can be found from equation (2.39):

$$\underset{\sim}{\mathbf{D}}_r^-(z_0) = [\underset{\sim}{\mathbf{M}}_1^-(z_0)]^{-1}[\underset{\sim}{\mathbf{L}}_2^-(z_0)]^{-1} \, . \tag{2.67}$$

From the expressions for the matrices $\underset{\sim}{\mathbf{M}}_1^-(z_0)$ and $\underset{\sim}{\mathbf{L}}_2^-(z_0)$ in the k_x-ω domain (see Appendix B), one can easily verify that $\underset{\sim}{\mathbf{D}}_r^-(z_0)$ is a diagonal matrix in the k_x-ω domain.

- Description in terms of particle velocity

If the wave fields are described by down- and upgoing particle velocity V_x and V_z, the spatial impulse response matrix reads:

$$\underset{\sim}{\mathbf{X}}(z_0,z_0) = \begin{bmatrix} \mathbf{X}_{v_x v_x}(z_0, z_0) & \mathbf{X}_{v_x v_z}(z_0, z_0) \\ \mathbf{X}_{v_z v_x}(z_0, z_0) & \mathbf{X}_{v_z v_z}(z_0, z_0) \end{bmatrix} \, . \tag{2.68}$$

The free surface reflectivity operator $\underset{\sim}{\mathbf{R}}_V^-(z_0)$ is defined as:

$$\underset{\sim}{\mathbf{V}}^+(z_0) = \underset{\sim}{\mathbf{R}}_V^-(z_0) \, \underset{\sim}{\mathbf{V}}^-(z_0) \tag{2.69}$$

and can be expressed, using equations (2.37a) to (2.38c) and equations (2.64) and (2.65), as:

$$\underset{\sim}{\mathbf{R}}_V^-(z_0) = -\underset{\sim}{\mathbf{L}}_1^+(z_0) \, [\underset{\sim}{\mathbf{L}}_2^+(z_0)]^{-1} \, \underset{\sim}{\mathbf{L}}_2^-(z_0) \, [\underset{\sim}{\mathbf{L}}_1^-(z_0)]^{-1} \, . \tag{2.70}$$

The operator $\underset{\sim}{\mathbf{D}}_s^+(z_0)$, which transforms downgoing traction into downgoing particle velocity, can be found by combining equations (2.37a) and (2.38a):

$$\underset{\sim}{\mathbf{D}}_s^+(z_0) = \underset{\sim}{\mathbf{L}}_1^+(z_0) \, [\underset{\sim}{\mathbf{L}}_2^+(z_0)]^{-1} \, . \tag{2.71}$$

The operator $\underset{\sim}{\mathbf{D}}_r^-(z_0)$, which transforms the upgoing particle velocity into the total particle velocity components, can be found by setting the total traction to zero in equation (2.40):

$$\underset{\sim}{\mathbf{D}}_r^-(z_0) = [\underset{\sim}{\mathbf{M}}_1^-(z_0)]^{-1} \, [\underset{\sim}{\mathbf{L}}_1^-(z_0)]^{-1} \, . \tag{2.72}$$

As expected, for a stress free surface the wave field description at the surface is simplest in terms of down- and upgoing *traction*, see equations (2.65) to (2.67).

2.6.5 Single-component elastic data

Most present land data surveys are still single-component. Only one type of source is used, i.e. dynamite sources or vertically oriented vibrators, and one type of receiver, i.e. geophones registering the z-component of the particle velocity.

For the processing of this data the acoustic approximation is generally made, i.e. the data is considered to be true P-wave responses measured by P-wave detectors. This assumption is only acceptable for a very low velocity surface layer. In Chapter 4 we will discuss a multi-component example, in which clearly the τ_{zz}-V_z panel (Fig. 4.28d) differs from the true P-P panel (Fig. 4.29a).

However, the S-wave and P-wave responses cannot be separated in single-component data acquisition. If we concentrate on the description of the wave fields in terms of P- and S-wave potentials, as described in the previous section, we may write

$$\underline{\Pi}^{+}(z_0) = [\underline{L}_2^{+}(z_0)]^{-1}\,\underline{S}_T(z_0)\,, \tag{2.73}$$

for the transformation of the traction source wave field into the downgoing P- and S-waves (leaving out the array matrices for simplicity) and

$$\underline{V}(z_0) = [\underline{M}_1^{-}(z_0)]^{-1}\,\underline{\Pi}^{-}(z_0) \tag{2.74}$$

for the composition of the upgoing wave P- and S-wave fields into particle velocity.
If only the T_{zz}-V_z response is available and the P to P response is the desired response, then we may approximately write in the k_x-ω domain (using the expressions as given in Appendix B) for the downgoing P-waves:

$$\tilde{\Phi}^{+}(z_0) \approx -\frac{k_S^2\,(k_S^2 - 2k_x^2)}{4k_x^2 k_{z,P} k_{z,S} + (k_S^2 - 2k_x^2)^2}\;\tilde{S}_{\tau_{zz}}(z_0) \tag{2.75}$$

with $k_S=\omega/c_S$, c_S being the S-wave velocity at the surface, k_x being the horizontal wave number and $k_{z,S}$ being defined as $k_{z,S}^2=k_S^2-k_x^2$.

If the S-wave velocity is set to zero, meaning that $1/k_S=0$, equation (2.75) transforms into:

$$\tilde{\Phi}^{+}(z_0) \approx -\tilde{S}_{\tau_{zz}}\,. \tag{2.76}$$

This is indeed equivalent to the acoustic description, for which the traction is defined as the opposite of the pressure.

At the receiver side an approximate expression for composition in the k_x-ω domain yields (using the expression for $\mathbf{M}_1^-(z_0)$ in Appendix B):

$$\tilde{V}_z(z_0) \approx \frac{2}{\omega\rho} \frac{k_S^2 \, k_{z,P} (k_S^2 - 2k_x^2)}{4k_x^2 k_{z,P} k_{z,S} + (k_S^2 - 2k_x^2)^2} \tilde{\Phi}^-(z_0) \tag{2.77}$$

with ρ the medium density, $k_{z,P}$ defined as $k_{z,P}^2 = k_P^2 - k_x^2$ with $k_P = \omega/c_P$ and c_P being the P-wave velocity. For the acoustic approximation ($1/k_S = 0$) this reduces to:

$$\tilde{V}_z \approx \frac{2k_{z,P}}{\omega\rho} \tilde{\Phi}^-(z_0), \tag{2.78}$$

which can also be found in Wapenaar and Berkhout (1989). It appears that taking a guess for the S-wave velocity, yielding equations (2.75) and (2.77) gives a more accurate description than making the acoustic assumption, yielding equations (2.76) and (2.78).

For instance, if we assume a c_P/c_S ratio of 1.5 at the surface, the results for the approximate elastic and the acoustic source and receiver composition operators are shown in Fig. 2.15a and b. For a c_P/c_S ratio of 2at the surface, the results are displayed in Fig. 2.15c and d. From equations (2.75) and (2.77) and from Fig. 2.15 can be concluded that for relative small S-wave velocities at the surface (c_P/c_S ratio larger than 2) the acoustic assumption can be taken, but for smaller c_P/c_S ratios the elastic effects are better taken into account.

Note also that for the free surface reflection the elastic P to P reflectivity should be used (upper left element of equation (2.60b), see also Appendix B) in stead of the acoustic approximation of r=-1.

As a final remark, the elastic theory can be extended to 3-D wave fields, introducing two types of S-waves, with polarizations in two independent directions. In the 3-D situation the multi--component data matrices consist of 9 submatrices (9-component data). Also each multi-component operator matrix mentioned in this section consists of 9 submatrices. However, all matrix notations stay exactly the same. For a more elaborate discussion see Wapenaar et al. (1990a). Note that even for the 2-D situation a description for 3-D wave fields is useful if anisotropy effects are to be included.

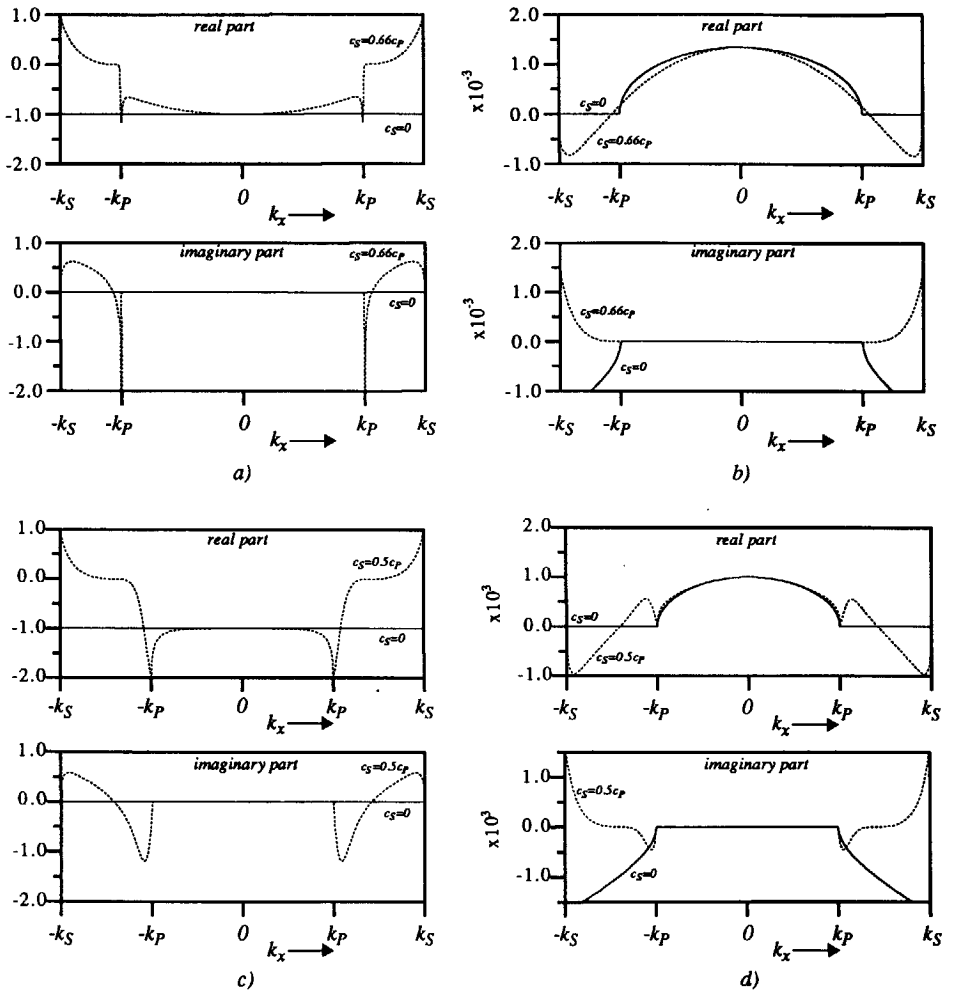

Fig. 2.15 *a) Real and imaginary part of the source decomposition operator. b) Real and imaginary part of the receiver decomposition operator. The solid line shows the acoustic assumption, the dashed line the assumption that c_P/c_S=1.5.*
c) Source decomposition operator for c_P/c_S=2. d) Receiver decomposition operator for c_P/c_S=2.

3

SURFACE-RELATED MULTIPLE ELIMINATION

In this chapter the theory of surface-related multiple elimination will be described by applying the inverse of the multiple generating operator to the data. This means that multiple elimination is formulated as an *inversion* process.

In the first part of this chapter the marine situation is considered. In the second part multi-component land data will be discussed.
In this chapter the matrix notation will be extensively used.

3.1 ACOUSTIC DECOMPOSITION INTO DOWN- AND UPGOING WAVES

For the surface-related multiple elimination method in the marine situation the forward model as described in section 2.2 has to be used. The very first step is to remove those events from the input data that have not propagated into the subsurface: i.e. the direct waves. Then, the influence of source and receiver characteristics should be removed. Next, the multiple elimination process can start.

3.1.1 Removing the direct waves

$$\mathbf{P}(z_r) = \underbrace{\left[\ \mathbf{D}_{array}(z_r)\ \mathbf{D}_r^{-}(z_r,z_0)\ \right]\ \mathbf{X}(z_0,z_0)\ \left[\ \mathbf{D}_s^{+}(z_0,z_s)\ \mathbf{D}_{array}(z_s)\ \right]\ S(\omega)}_{step\ 1}\ +\ \mathbf{N}(z_0). \qquad (3.1)$$

In equation (3.1) $\mathbf{N}(z_0)$ contains all events that are not described by the forward model, as stated by equation (2.21), i.e. direct waves and (possible) noise.

Direct waves are generally removed by a muting process in the x-t domain and/or a filtering process in the k_x-ω domain. It is important not to distort reflection events, as they are part of the multiple elimination operator.

In the special situation of a very shallow water layer, the response of the water layer itself, which may considered as an "acoustic groundroll" (see section 2.5.2), should be removed as well, again without distorting the other reflections.

3.1.2 Removing the receiver effects

$$\mathbf{P}(z_r) = \underbrace{\left[\ \mathbf{D}_{array}(z_r)\ \mathbf{D}_r^{-}(z_r,z_0)\ \right]}_{step\ 2a}\ \mathbf{X}(z_0,z_0)\ \mathbf{S}^{+}(z_0)\ . \qquad (3.2)$$

After the removal of the direct wave, the next step is to go from the *measured* data $\mathbf{P}(z_0)$ to the *upgoing* wave field just below the free surface, using equation (2.20):

$$\mathbf{P}^{-}(z_0) = [\ \mathbf{D}_{array}(z_r)\ \mathbf{D}_r^{-}(z_r,z_0)\ ]^{-1}\ \mathbf{P}(z_r)\ . \qquad (3.3a)$$

or, equivalently,

$$\mathbf{P}^{-}(z_0) = [\mathbf{D}_r^{-}(z_r,z_0)]^{-1}[\mathbf{D}_{array}(z_r)]^{-1}\ \mathbf{P}(z_r)\ . \qquad (3.3b)$$

Equation (3.1) formulates that the array effect should be eliminated first; next the ghost effect is removed and the result is transformed to reference level z_0.

The calculation of the inverse of matrices $\mathbf{D}_{array}(z_r)$ and $\mathbf{D}_r^{-}(z_r,z_0)$ can be done via the k_x-ω domain, using the receiver array configuration and the water velocity (see Appendix B). Both matrices should be inverted in a stabilized way in order to prevent instabilities at possible notches.
The result of the inversion step at the receiver side can be formulated as (see equation (2.16)):

$$\mathbf{P}^{-}(z_0) = \mathbf{X}(z_0,z_0)\ \mathbf{S}^{+}(z_0)\ . \qquad (3.4)$$

3.1.3 Removing the directional source effects

$$\mathbf{P}^{-}(z_0) = \mathbf{X}(z_0,z_0) \underbrace{\left[\ \mathbf{D}_s^{+}(z_0,z_s)\, \mathbf{D}_{array}(z_s)\ \right]}_{step\ 2b} S(\omega)\,. \tag{3.5}$$

The next step is to remove the source directional properties, ending up with true pressure dipole sources:

$$\hat{\mathbf{P}}^{-}(z_0) = \mathbf{P}^{-}(z_0)\ [\ \mathbf{D}_s^{+}(z_0,z_s)\, \mathbf{D}_{array}(z_s)\ ]^{-1}\,, \tag{3.6a}$$

or, equivalently,

$$\hat{\mathbf{P}}^{-}(z_0) = \mathbf{P}^{-}(z_0)\ [\mathbf{D}_{array}(z_s)]^{-1}[\mathbf{D}_s^{+}(z_0,z_s)]^{-1}\,. \tag{3.6b}$$

Equation (3.6a) formulates that the array effect should be eliminated first. If the source behaves as a monopole and the source array is close to the surface (less than half the minimum wave length of interest) the ghost effect at the source side simulates a dipole response. In that situation $\mathbf{D}_s^{+}(z_0,z_s)$ reduces to a unit matrix and does not need to be corrected for.

$\hat{\mathbf{P}}^{-}(z_0)$ represents the upgoing reflected wave fields in terms of pressure due to the dipole source signature $S(\omega)$. For air gun data the source signature $S(\omega)$ is difficult to measure accurately, especially in a true amplitude sense. The latter is a requirement for the surface-related multiple elimination method. Therefore, after removing both the source and receiver effects, we leave the source signature in the result.

Ziolkowski (1991) recommends to put significant effort in measuring the wavelet accurately *during acquisition*. However, further in this chapter it is shown that the source signature can be accurately estimated during the multiple elimination procedure. Of course, any information about the source signature is always helpful to constraint the optimization problem involved. Ziolkowski et al. (1982) and Parkes et al. (1984) show how the calculation of the airgun wavelet can be done, although for an initial estimate of $S(\omega)$ we certainly do not need to include the complex interaction effects.

Finally note that for an inhomogeneous array, such as an airgun array, $\mathbf{D}_{array}(z_s)$ is frequency dependent (see Fokkema et al., 1990).

3.2 REMOVING THE SURFACE-RELATED MULTIPLES

In conclusion, after removing the source and receiver effects, the resulting surface data can be represented by:

$$\hat{\mathbf{P}}^{-}(z_0) = \mathbf{X}(z_0,z_0)\, S(\omega)\,. \tag{3.7}$$

Now, the next step is to transform $\hat{\mathbf{P}}^{-}(z_0)$ to $\mathbf{X}_0(z_0,z_0)$, yielding the dipole response of the sub-surface without surface-related multiples.

3.2.1 Surface-related multiple elimination by applying the inverse of the multiple generating operator

The relation between $\mathbf{X}(z_0,z_0)$ and $\mathbf{X}_0(z_0,z_0)$ is given by equation (2.14):

$$\mathbf{X}(z_0,z_0) = [\,\mathbf{I} - \mathbf{X}_0(z_0,z_0)\,\mathbf{R}^{-}(z_0)\,]^{-1}\,\mathbf{X}_0(z_0,z_0)\,. \tag{3.8}$$

After inverting this expression, we arrive at:

$$\mathbf{X}_0(z_0,z_0) = \mathbf{X}(z_0,z_0)\,[\,\mathbf{I} + \mathbf{R}^{-}(z_0)\,\mathbf{X}(z_0,z_0)\,]^{-1}\,, \tag{3.9a}$$

or, equivalently,

$$\mathbf{X}_0(z_0,z_0) = [\,\mathbf{I} + \mathbf{X}(z_0,z_0)\,\mathbf{R}^{-}(z_0)\,]^{-1}\,\mathbf{X}(z_0,z_0)\,. \tag{3.9b}$$

Using equation (3.4) we may write

$$\mathbf{X}_0(z_0,z_0) = [\,\mathbf{I} + \mathbf{P}^{-}(z_0)\,\{\mathbf{S}^{+}(z_0)\}^{-1}\,\mathbf{R}^{-}(z_0)\,]^{-1}\,\mathbf{P}^{-}(z_0)\,\{\mathbf{S}^{+}(z_0)\}^{-1}\,. \tag{3.10a}$$

or:

$$\begin{aligned}\mathbf{P}_0^{-}(z_0) &= \mathbf{X}_0(z_0,z_0)\,\mathbf{S}^{+}(z_0)\\ &= [\,\mathbf{I} + \mathbf{P}^{-}(z_0)\,[\{\mathbf{S}^{+}(z_0)\}^{-1}\,\mathbf{R}^{-}(z_0)]\,]^{-1}\,\mathbf{P}^{-}(z_0)\,,\end{aligned} \tag{3.11}$$

which has an equivalent structure as the forward model in equation (2.24).

If also the directional source effects have been removed,equation (3.11) simplifies to:

$$\begin{aligned}\hat{\mathbf{P}}_0^{-}(z_0) &= \mathbf{X}_0(z_0,z_0)\,S(\omega)\\ &= [\,\mathbf{I} + \hat{\mathbf{P}}^{-}(z_0)\,[S^{-1}(\omega)\,\mathbf{R}^{-}(z_0)]\,]^{-1}\,\hat{\mathbf{P}}^{-}(z_0)\,,\end{aligned} \tag{3.12}$$

with $\hat{\mathbf{P}}_0^-(z_0)$ defined as the upgoing wave field at the surface after directional deconvolution and without surface-related multiples.
From equations (3.9a) to (3.11) it can be seen that only the free surface reflectivity and the source wave field have to be known. *Any information about the subsurface is not needed!* In fact the data itself is used as extrapolation operator to predict all surface-related multiples. This becomes even more clear if the inversion term in equation (3.11) is expanded into a Taylor series:

$$\mathbf{P}_0^-(z_0) = \mathbf{P}^-(z_0) - \{\mathbf{P}^-(z_0)\,\mathbf{A}(z_0)\}\,\mathbf{P}^-(z_0) + \{\mathbf{P}^-(z_0)\,\mathbf{A}(z_0)\}^2\,\mathbf{P}^-(z_0) - \{\mathbf{P}^-(z_0)\,\mathbf{A}(z_0)\}^3\,\mathbf{P}^-(z_0) + \ldots . \tag{3.13}$$

with the surface matrix $\mathbf{A}(z_0)$ being defined as

$$\mathbf{A}(z_0) = \{\mathbf{S}^+(z_0)\}^{-1}\,\mathbf{R}^-(z_0) \tag{3.14a}$$

or, if the directional source effects have been removed already,

$$\mathbf{A}(z_0) = \mathbf{S}^{-1}(\omega)\,\mathbf{R}^-(z_0)\,. \tag{3.14b}$$

Each term in equation (3.13) predicts one order of surface-related multiples. As there will be only a limited order of multiples present in the data, only a limited number of terms have to be taken into account in equation (3.13). A direct inversion, as described by equation (3.11), will cause instability problems in a large number of seismic situations. Hence, our multiple elimination scheme is based on equation (3.13).

To simplify the notation, the symbol $\hat{\mathbf{P}}^-(z_0)$ will be replaced by $\mathbf{P}^-(z_0)$. Hence, in the following $\mathbf{P}^-(z_0)$ may or may not be corrected for the directional source characteristics.

Fig. 3.1 shows the application of our multiple elimination scheme for a simple 1D example, with a model consisting of 20 reflectors. Fig. 3.1a to d show the first four terms of the Taylor series, the first one of which is the data with multiples. For this 1D example, the matrix multiplications reduce to simple scalar multiplications in the frequency domain (1D convolutions in the time domain). If the results for 10 Taylor terms are added, Fig. 3.1e is the result. All surface-related multiples have been removed and the 20 primaries with the (much weaker) internal multiples are left. Also direct inversion has been applied on the input data (Fig. 3.1a), the result of which is shown in Fig. 3.1f. Wrap around effects can be observed in the data after multiple elimination, which are caused by predicted higher order multiples, that have not been captured within the registration time of the data. As for a horizontal plane wave no critical reflections occur in a 1D medium, no instability problems are present.

In the marine situation we may assume a reflection coefficient in stead of a reflectivity operator, which means that surface operator (3.14a) reduces to a surface *factor* (depending on frequency only):

$$\mathbf{A}(z_0) = A(\omega)\,\mathbf{I} = S^{-1}(\omega)\,r_0\,\mathbf{I}\,, \tag{3.15}$$

which transforms equation (3.13) into

$$\mathbf{P}_0^{-}(z_0) = \mathbf{P}^{-}(z_0) - A(\omega)\,\{\mathbf{P}^{-}(z_0)\}^2 + A^2(\omega)\,\{\mathbf{P}^{-}(z_0)\}^3 - \ldots\,. \tag{3.16}$$

The multiple elimination process can be carried out as a weighted summation of the auto convolution terms of the seismic data. The weighting function $A(\omega)$ is needed to deconvolve each Taylor term for the source signature $S(\omega)$.

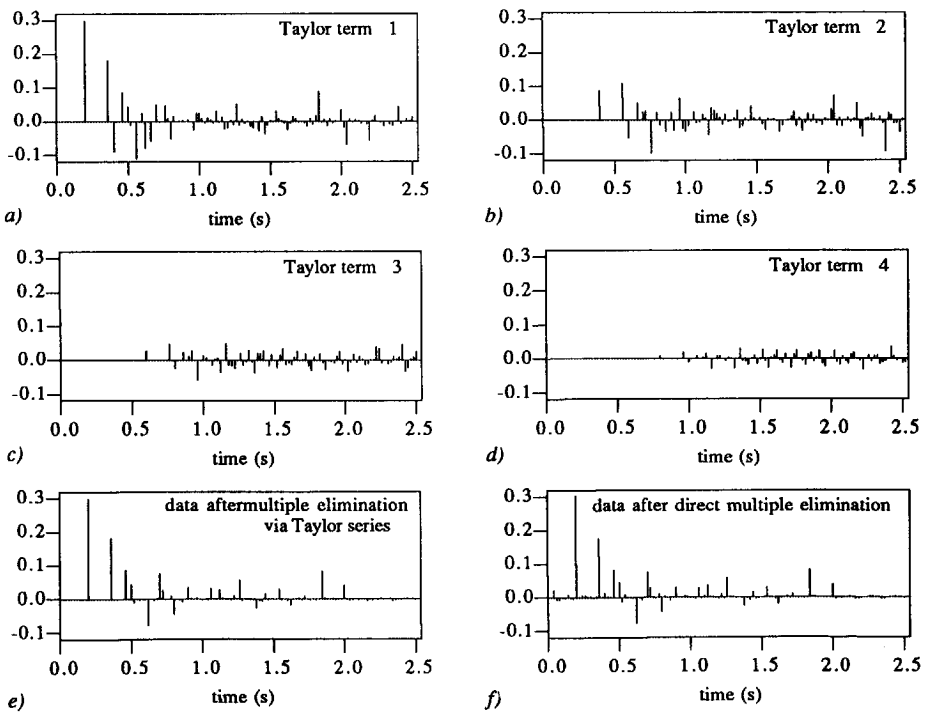

Fig. 3.1 *a) Horizontal plane wave response in a 1D medium consisting of 20 reflectors, which is the first term of the Taylor series expansion. b) Second term of the Taylor series expansion. c) Third term of the Taylor series expansion. d) Fourth term of the Taylor series expansion. e) Summation of the first 10 terms of the Taylor series expansion, yielding the response without surface-related multiples. f) Result of applying a direct inversion on the response of a), yielding wrap around effects of high order Taylor series terms in the time domain.*

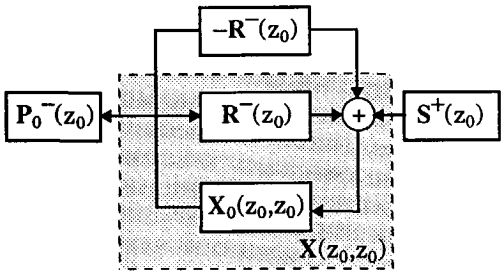

Fig. 3.2 *Seismic data after surface-related multiple elimination; the data is fed back into the earth with an opposite free surface reflectivity.*

3.2.2 Surface-related multiple elimination and Huygens' principle

- Direct feedback of the upgoing wave field into the subsurface

Looking at equation (3.11) we observe that the multiple elimination process can be described with a similar diagram as in Fig. 2.8; this diagram is shown in Fig. 3.2. As can be seen from Fig. 3.2 the surface-related multiple elimination acts as if the upgoing wave field at the free surface is instantaneously put back into the subsurface with an *opposite* free surface reflectivity. In that way the reflecting effect of the free surface is neutralized.

Theoretically, if at each receiver position a source would be placed that emits the received upgoing wave field instantaneously back into the subsurface, weighted with $-r_0$, all surface-related multiples would vanish.

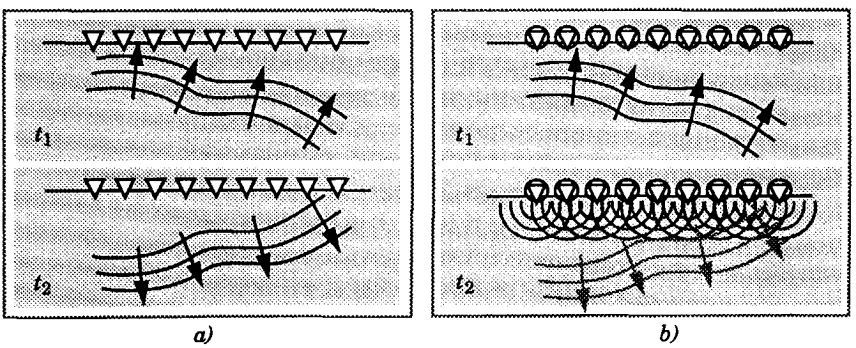

Fig. 3.3 *a) At the free surface any upgoing wave field is transformed into a downgoing wave field.*
b) Theoretically, surface-related multiple elimination could be applied during acquisition. At each receiver position a source should instantaneously emit the upgoing wave field back into the subsurface with an opposite free surface reflectivity. As a result the total downgoing wave field will be zero.

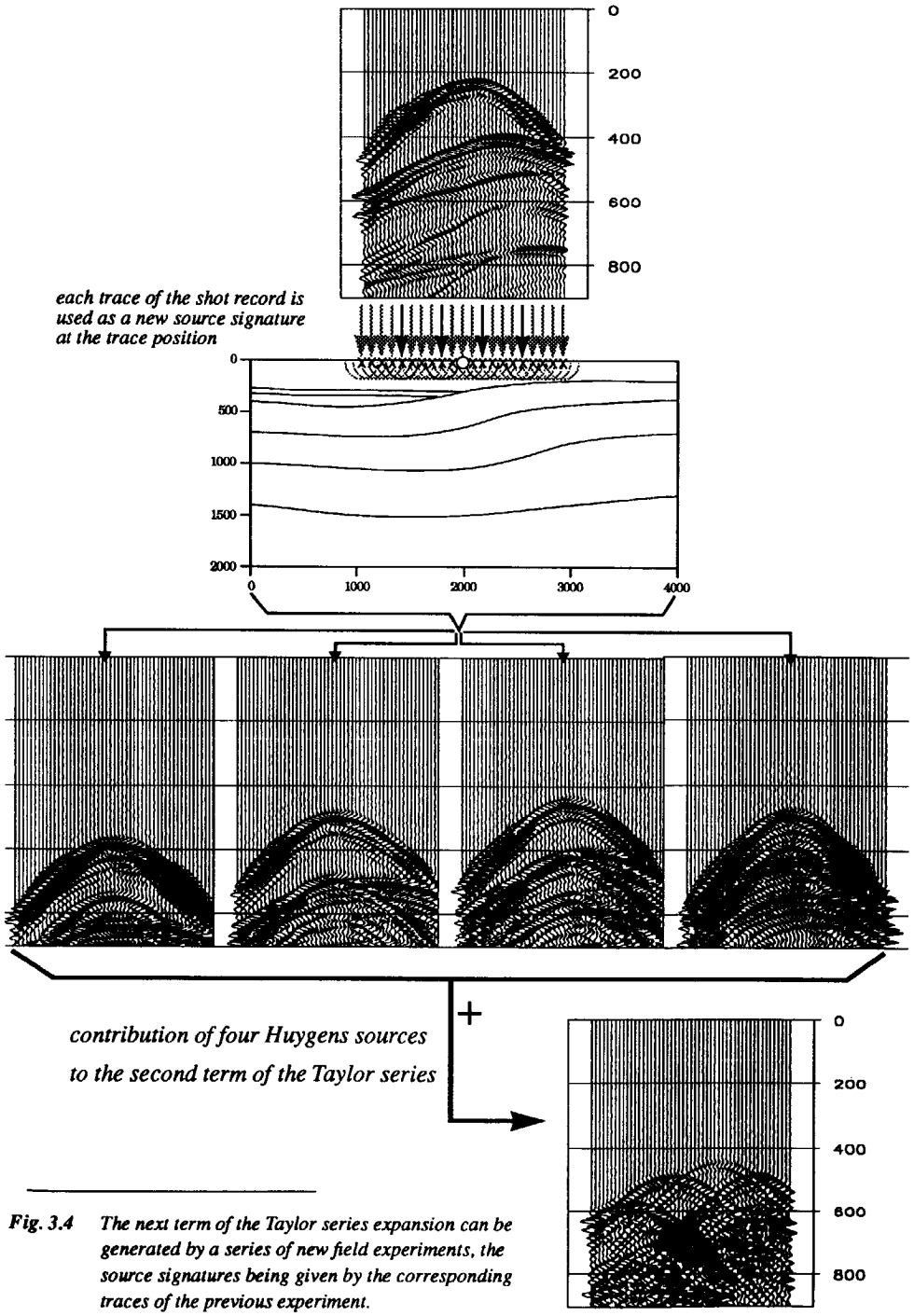

Fig. 3.4 *The next term of the Taylor series expansion can be generated by a series of new field experiments, the source signatures being given by the corresponding traces of the previous experiment.*

This concept is illustrated in Fig. 3.3a, where a wave front is shown for two time instants t_1 and t_2, just before and after reflection against the free surface. In Fig. 3.3b the same situation is sketched, but with the "active" receiver situation. Each receiver emits the received upgoing wave field weighted with $-r_0$. In this way equation (3.11) is applied instantaneously in the field and the data without surface-related multiples, $\mathbf{P}_0^-(z_0)$, is the final registration result.

- Recursive feedback of the upgoing wave field into the subsurface

A more practical way of looking at the feedback principle is based on the Taylor series expansion, as stated in equation (3.16). Each term of this series expansion is separately measured in the field and finally a (weighted) summation yields the multiple free data. Each term is the result of a series of new field experiments, the source signatures being given by the corresponding traces of the previous experiment.

The Taylor series feedback method is examined by considering the same simulated data set as in Chapter 1, section 1.1. Fig. 3.4 shows how the feedback procedure of the data into the subsurface can be accomplished.

Note that if one shot record of the dataset is considered (corresponding with one column of the datamatrix $\mathbf{P}^-(z_0)$ in equation (3.16)), to generate the next Taylor term $\{\mathbf{P}^-(z_0)\}^2$ each trace is used as a new source signature. This means that at each trace position a new shot record experiment is carried out with the measured trace used as source signature. This results in as many new shot records as there are traces in the shot record under consideration. These shot records are added and the resulting "shot record" is the time domain representation of the corresponding column in the second term, $\{\mathbf{P}^-(z_0)\}^2$, of the Taylor series in equation (3.16).

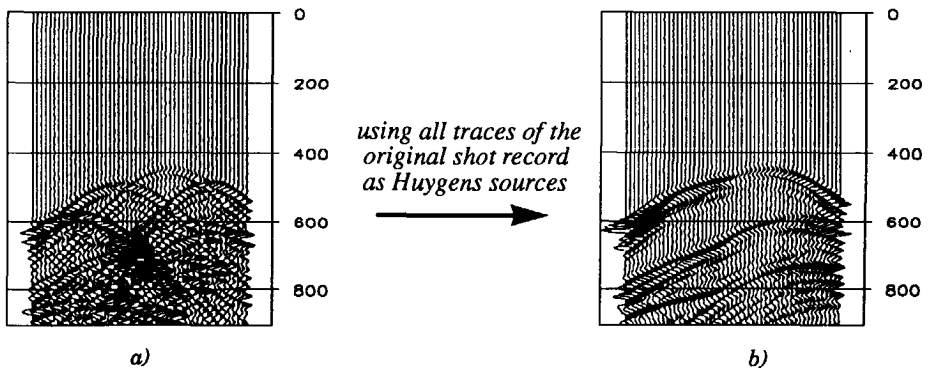

Fig. 3.5 *a) The contribution of four Huygens sources to the second term of the Taylor series. b) The second term of the Taylor series if all Huygens sources have been taken into account*

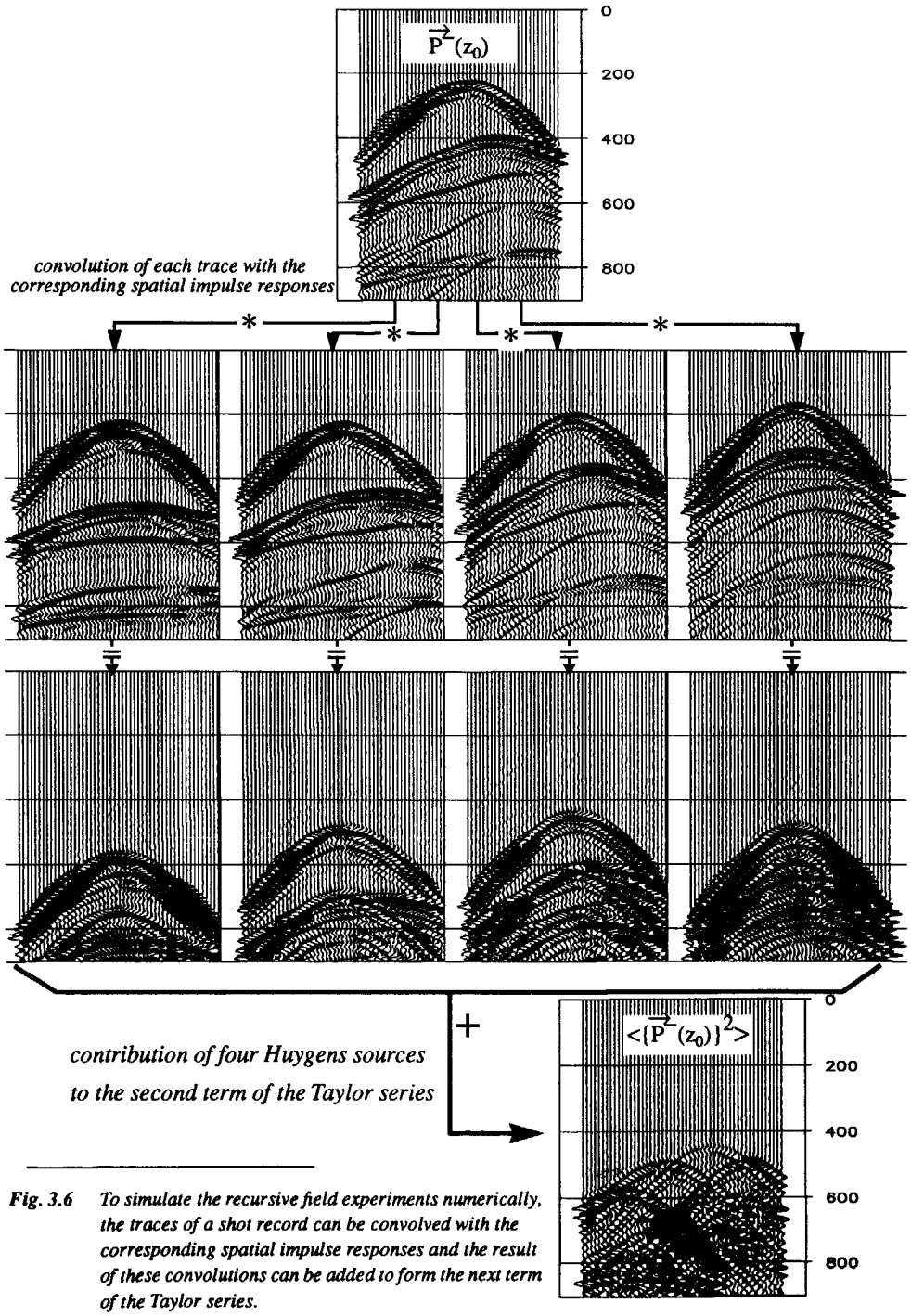

Fig. 3.6 *To simulate the recursive field experiments numerically, the traces of a shot record can be convolved with the corresponding spatial impulse responses and the result of these convolutions can be added to form the next term of the Taylor series.*

In other words, each receiver acts as a Huygens point source. The result of all Huygens source responses is exactly the same as the extrapolation result of the upgoing wave field $\vec{P}^{-}(z_0)$ (one column of $\mathbf{P}^{-}(z_0)$) for an extra round trip through the *whole* subsurface. In Fig. 3.4 this is shown for only four of the receiver positions, yielding a severely aliased result in the lower right corner. If all traces of the original shot record are used as Huygens source signatures, the result is given separately in Fig. 3.5. Fig. 3.5a shows again the combination of the 4 considered Huygens sources from Fig. 3.4; Fig. 3.5b is the result if all traces are used, yielding the correct version of the second Taylor term.

For the third term of the Taylor series, the second term should be used as input of the feed-back procedure, i.e. each trace of the data in Fig. 3.5b is again used as a Huygens source signature, yielding the data which has traveled two extra round trips through the whole subsurface. This procedure is repeated until enough terms have been generated to cover all orders of surface-related multiples present in the data. Finally, a (weighted) addition of these terms yields the multiple free data.

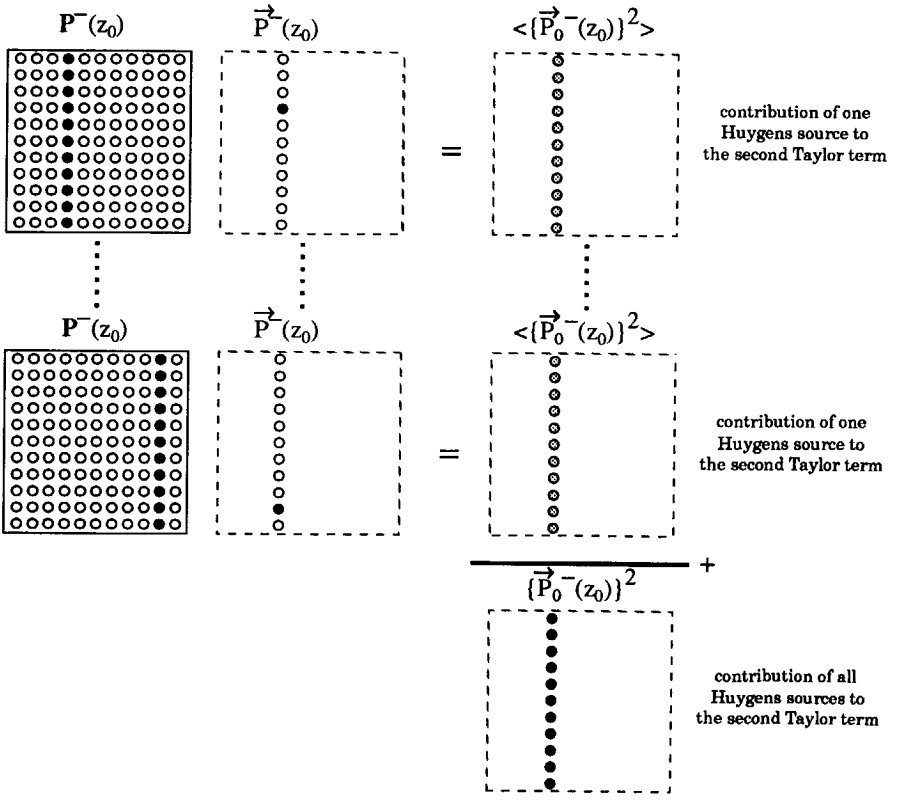

Fig. 3.7 *The matrix multiplication result for one column can be subdivided into contributions from one element in that column (one Huygens source) to the corresponding output column (response of one Huygens source). The black dots indicate the trace positions involved in the multiplications.*

- Numerical recursive feedback of the upgoing wave field into the subsurface

The feedback procedure in the field is not practical and has only be introduced to explain the method. However, the same result can be obtained *numerically*. In stead of using each trace of a shot record as a Huygens source signature for a new field experiment, this trace is *convolved* with the spatial impulse response related to that receiver position. If this convolution procedure is applied for all traces of the shot record, and the results are added, the next term of the Taylor series expansion is calculated. This procedure is visualized in Fig. 3.6. The result is only displayed for *four* of the traces, yielding exactly the same aliased Taylor series term as in Fig. 3.4. Fig. 3.5 already showed the result if all traces are used. It is important to realize that the shot records, when correctly deconvolved for the source and receiver characteristics, are identical to the required spatial impulse responses. Thus the multiples can be predicted by convolving each trace of one shot record with the shot record corresponding to that trace position. Hence, the data is convolved with itself. This is exactly what equation (3.16) tells us.

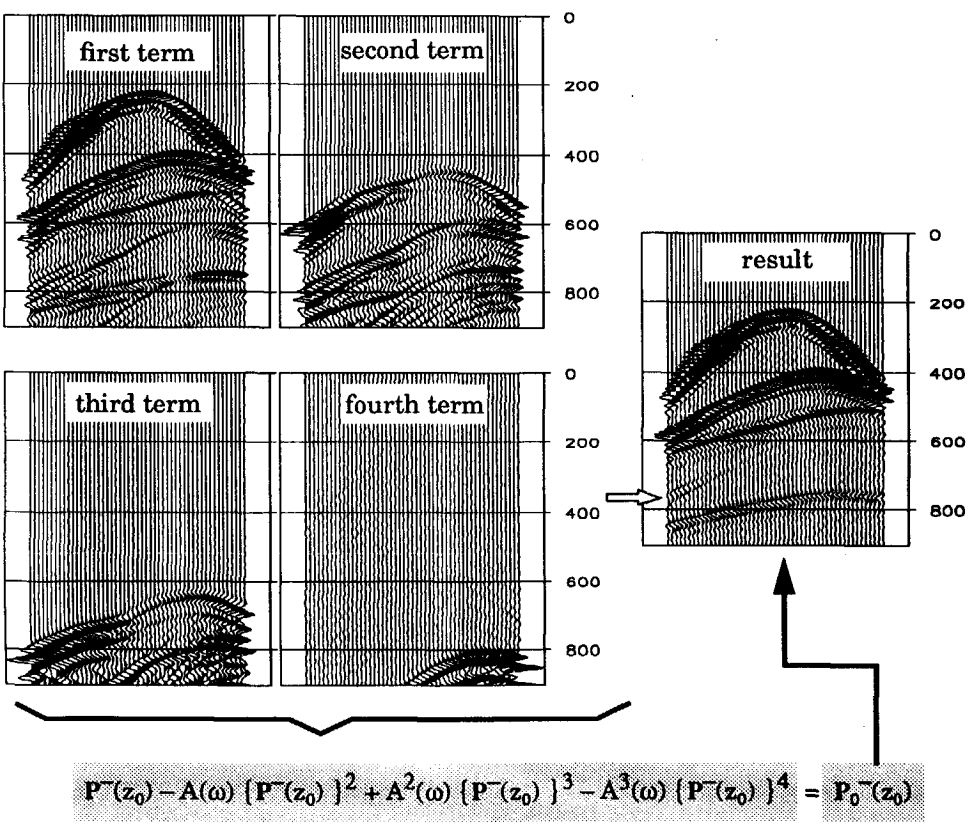

Fig. 3.8 Time domain versions of the first four terms of the Taylor series for one shot record. A weighted addition of these four terms yields the shot record without multiples.

The convolution of each trace of the input shot record with all traces of the corresponding shot records can be carried out in the frequency domain as multiplications. If all multiplications of each trace with a complete shot record are combined, the result is exactly a multiplication of the data matrix with itself. This has been indicated in Fig. 3.7, where the matrix multiplication for one column (corresponding to one shot record) is subdivided in contributions for each element of that column (corresponding to each trace position in the shot record). Of course, this matrix multiplication should be applied for all frequencies.

After the second term has been calculated, this result can be used as input for a similar multiplication sequence, generating the third term of the Taylor series expansion, etc. In this way all terms of the Taylor series can be calculated for one shot record. After a weighted addition according to equation (3.16) the shot record without surface- related multiples is the result. Fig. 3.8 shows the first four terms of the Taylor series for the same shot record which has been considered in the previous figures. After the weighted addition of these terms, the resulting shot record without surface-multiples is shown. The surface-related multiples have been perfectly eliminated indeed, restoring the primaries from the interference with the multiples. Note that this result has already been shown in Chapter 1. Apart from the primaries, also one internal multiple is visible in the output data; it is indicated with an arrow.

3.2.3 Iterative interface-related multiple elimination

On principle the inversion can be extended to other interfaces by a combination of downward extrapolation (redatuming) and interface-related multiple elimination (removing of multiples related to that specific interface).

After removing the surface-related multiples we can assume that we have acquired $\mathbf{X}_0(z_0,z_0)$. With this equation (2.13) can be inverted, starting with redatuming to the first interface:

$$\mathbf{X}(z_1,z_1) = \{\mathbf{T}^-(z_1)\}^{-1}\,\{\mathbf{W}^-(z_0,z_1)\}^{-1}\,\mathbf{X}_0(z_0,z_0)\,\{\mathbf{W}^+(z_1,z_0)\}^{-1}\,\{\mathbf{T}^+(z_1)\}^{-1}\,. \qquad (3.17)$$

The pre-stack redatuming procedure has been extensively treated by Kinneging et al (1989).

The redatuming step results in $\mathbf{X}(z_1,z_1)$, which is the spatial impulse response matrix of the subsurface related to the first interface including all multiples related to this interface (next surface). Redatuming can be followed by an interface-related multiple elimination step:

$$\mathbf{X}_0(z_1,z_1) = [\,\mathbf{I} + \mathbf{X}(z_1,z_1)\,\mathbf{R}^-(z_1)\,]^{-1}\,\mathbf{X}(z_1,z_1)\,. \qquad (3.18)$$

Note that after the redatuming step, as described by equation (3.17), the primary of the first interface has to be removed from the data. It can be found at zero time (the reflectivity operator) and even moves to negative times after further redatuming to other depth levels (see de Bruin et al. (1990)).

This iterative multiple elimination procedure can be extended to each depth level z_m removing the propagation and multiple effects iteratively for each depth level. However, its application will only be useful for the main interfaces s_m in the subsurface, and not for each depth level z_m. Taking this into account, the iterative multiple elimination procedure related to the interface s_m reads:

a. Redatuming

$$\mathbf{X}(s_m,s_m) = \{\mathbf{T}^-(s_m)\}^{-1}\{\mathbf{W}^-(s_{m-1},s_m)\}^{-1}\mathbf{X}_0(s_{m-1},s_{m-1})\{\mathbf{W}^+(s_m,s_{m-1})\}^{-1}\{\mathbf{T}^+(s_m)\}^{-1}\,, \quad (3.19)$$

b. Interface-related multiple elimination

$$\mathbf{X}_0(s_m,s_m) = [\,\mathbf{I} + \mathbf{X}(s_m,s_m)\,\mathbf{R}^-(s_m)\,]^{-1}\,\mathbf{X}(s_m,s_m)\,. \quad (3.20)$$

The multi-boundary multiple elimination procedure is visualized in Fig. 3.9. For the iterative multiple elimination the reflection, transmission and propagation matrices of the current interface c.q. layer have to be known in order to apply equations (3.19) and (3.20) correctly. In other words, the position and reflectivity characteristics of the multiple generating interface have to be known. An interesting feature to consider is the fact that the multiples that have been eliminated in the previous step might provide that information. For example, the eliminated surface-related multiples will contain a lot of information about the first layer and its bottom, because they contain events that have been traveling many times within this layer.

In practical situations the process described by equations (3.19) and (3.20) will not be applied. We may expect that only a few very strong reflectors, such as the sea bottom, may be considered for interface-related multiple elimination.

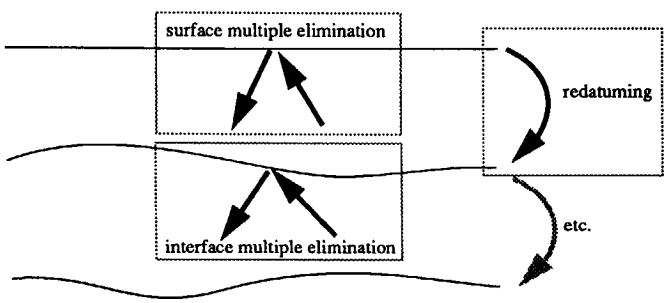

Fig. 3.9 *Multi-boundary multiple elimination: recursive application of surface-related multiple elimination followed by redatuming to the next multiple generating interface.*

To demonstrate the iterative interface-related multiple elimination method, the example with the four primaries of Chapter 1 is considered again. The shot record with all multiples is shown in Fig. 3.11a, with the four primaries indicated. After surface-related multiple elimination, the result is Fig. 3.11b; it has already been shown in Chapter 1. The vast majority of multiples has been removed, but internal multiples can be observed in the data (see the arrows in Fig. 3.11b). Therefore interface-related multiple elimination is applied to this data. First a redatuming step to the first interface has been done, after removing its primary reflection. The result of this downward continuation step is shown in Fig. 3.10a. On this data the surface-related multiple elimination procedure has been applied, the first interface now acting as the new "surface". Note the fact that the angle dependent upward reflection coefficient of this interface has to be taken into account. The result is shown in Fig. 3.10b. An internal multiple, generated between the second and third interface, remains in the data (see the arrow in Fig. 3.10b). The result of the first interface-related multiple elimination can be extrapolated back to the surface, if surface data is the desired output. The result of this extrapolation step is shown in Fig. 3.11c. Note that the first primary has been removed from the data before redatuming to the first interface. The multiples related to the first interface, indicated with the arrows in Fig. 3.11b have been removed indeed. Fig. 3.11d shows the two types of multiples that have been removed. The arrows indicate the first interface-related multiples. The other events in Fig. 3.11d are surface-related multiples.

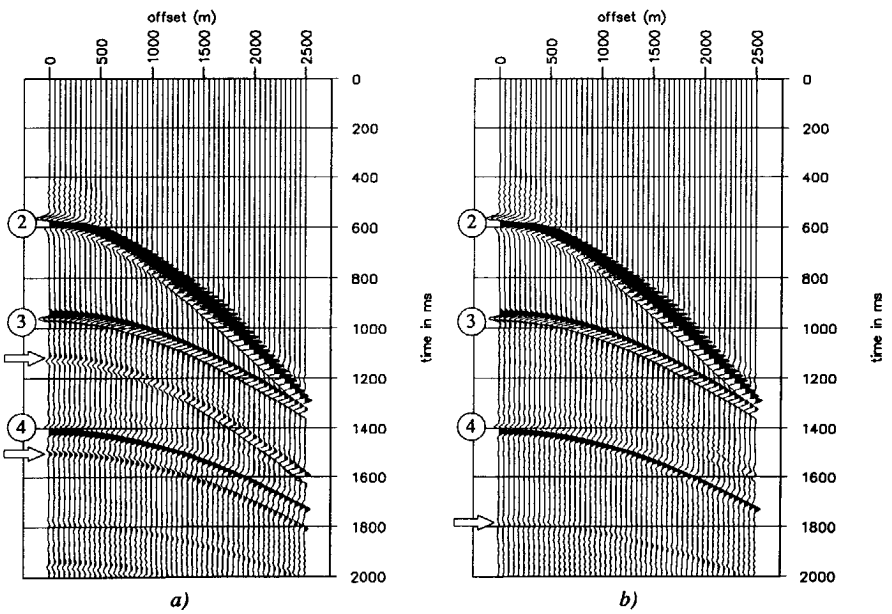

Fig. 3.10 *a) Shot record after surface-related multiple elimination and redatuming to the first interface. b) Shot record after first interface-related multiple elimination as well.*

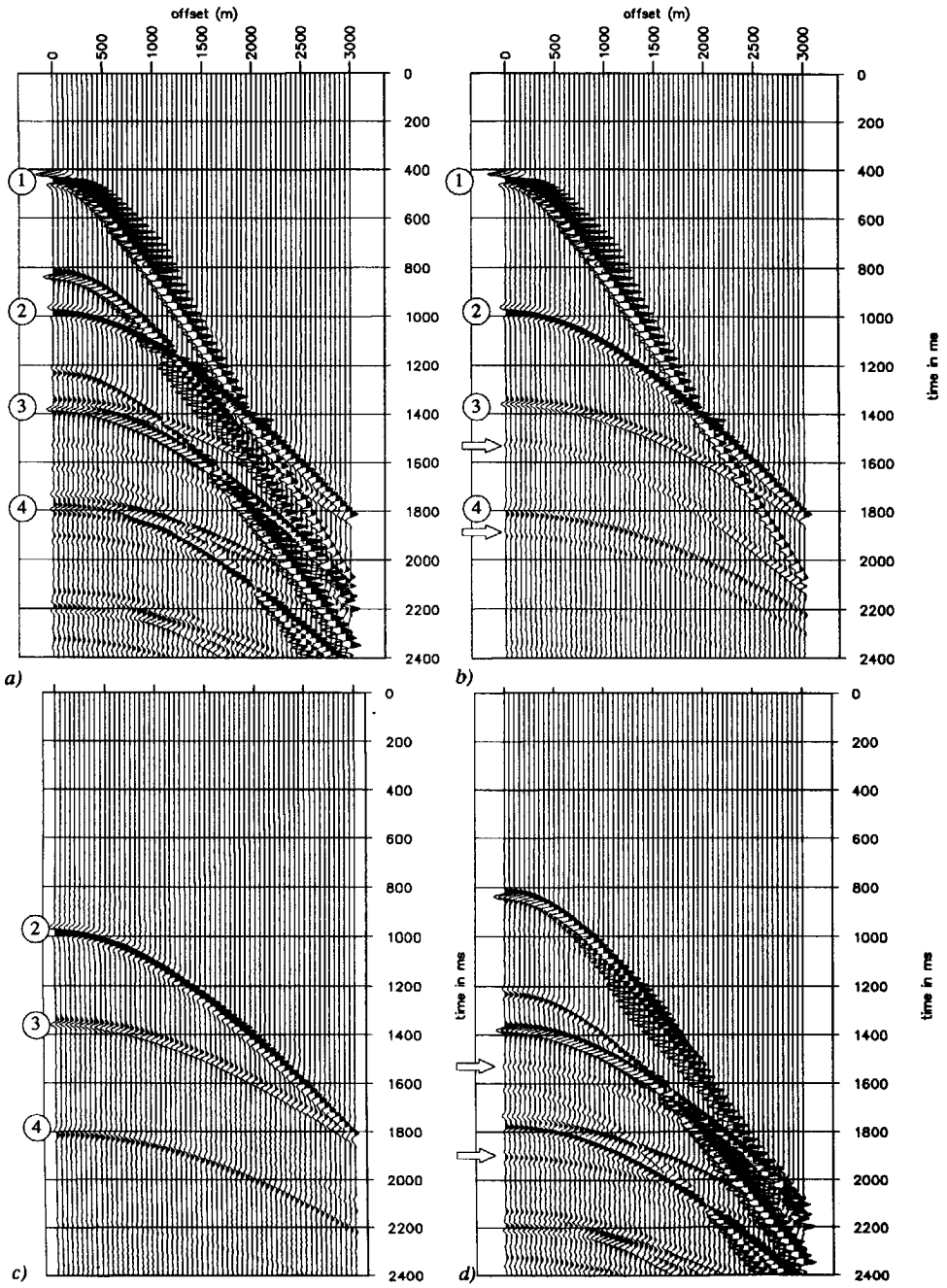

Fig. 3.11 *a) Shot record with 4 primaries and multiples b) Shot record after surface-related multiple elimination c) Shot record after both surface-related and first interface-related multiple elimination, including extrapolation back to the surface d) All removed surface and first interface multiples.*

3.3 ADAPTIVE MULTIPLE ELIMINATION

3.3.1 Estimation of the inverse source signature using multiple elimination

As pointed out in section 3.2 the multiple elimination process only depends on the seismic data itself, the inverse source signature and the free surface reflectivity properties. Generally the source signature is an unknown quantity, especially concerning the absolute amplitude of the source (the scaling factor of the data).

If we take an estimate of the inverse source signature this yields an estimate of the surface operator $<A(\omega)>$, as defined in equation (3.15). When used in the multiple elimination procedure (equation (3.16)) an estimate of the multiple free data $<\mathbf{P}_0^-(z_0)>$ is acquired:

$$<\mathbf{P}_0^-(z_0)> = \mathbf{P}^-(z_0) - <A(\omega)> \{\mathbf{P}^-(z_0)\}^2 + <A(\omega)>^2 \{\mathbf{P}^-(z_0)\}^3 - \ldots . \tag{3.21}$$

A erroneous estimate of the surface operator yields a erroneous estimate of the multiple free data. In the worst case multiples may be overcorrected, which means the generation of new events. Therefore the multiple removal procedure can only be successful on field data when applied in an *adaptive* way: find the best surface operator $<A(\omega)>$ that removes the multiples in an optimum way.

3.3.2 Minimum energy criterion

The question that arises is which criterium to use in deciding whether the optimum surface factor $A(\omega)$ has been found or not. A very useful and robust criterion appears to be the total energy $\mathcal{E}$ in the seismic data after multiple elimination, measured by the sum of the squares of the samples in the traces in the time domain:

$$\mathcal{E} = \sum_{k=1}^{N_t} \sum_{j=1}^{N_s} \sum_{i=1}^{N_r} <p_0^-(i\Delta x_r, j\Delta x_s, k\Delta t; z_0)>^2 , \tag{3.22}$$

with Δx_r, Δx_s and Δt the sample distances in the receiver, shot and time direction respectively and N_r, N_s and N_t the number of receivers per shot, the number of sources and the number of time samples per trace respectively. Being in the time domain has the advantage that a certain time window can be selected.

Although it cannot be proven that the minimum energy *always* coincides with the optimum removal of the multiples, it can be intuitively understood that it is a robust criterium. To understand this, consider the fact that doing a perfect multiple elimination job means making the free surface completely transparent, which means that all upgoing energy will disappear.

Going back to the *forward* model, the subsurface response with multiples can be thought of being constructed from a number of recursive Huygens experiments:

$$\mathbf{P}^{-}(z_0) = \mathbf{P}_0^{-}(z_0) + \mathbf{P}_1^{-}(z_0) + \mathbf{P}_2^{-}(z_0) + \ldots . \tag{3.23a}$$

each term $\mathbf{P}_n^{-}(z_0)$ being defined as

$$\mathbf{P}_n^{-}(z_0) = \mathbf{P}_0^{-}(z_0) \left[\{\mathbf{S}^{+}(z_0)\}^{-1} \mathbf{R}^{-}(z_0) \mathbf{P}_0^{-}(z_0) \right]^{n-1} . \tag{3.23b}$$

The first term, $\mathbf{P}_0^{-}(z_0)$, contains the subsurface response with a transparent surface (no surface-related multiples). The terms $\mathbf{P}_1^{-}(z_0)$, $\mathbf{P}_2^{-}(z_0)$ etc. contain the first, second etc. order of surface-related multiples. If the total energy is calculated in the time domain, we arrive at:

$$\mathcal{E}\{p^{-}(x_r,x_s,t;z_0)\} = \sum_{k=1}^{N_t} \sum_{j=1}^{N_s} \sum_{i=1}^{N_r} [\, p_0^{-}(i\Delta x_r, j\Delta x_s, k\Delta t; z_0) + p_1^{-}(i\Delta x_r, j\Delta x_s, k\Delta t; z_0) + p_2^{-}(i\Delta x_r, j\Delta x_s, k\Delta t; z_0) + \ldots \,]^2 \tag{3.24a}$$

or

$$\mathcal{E}\{p^{-}(x_r,x_s,t;z_0)\} = \mathcal{E}\{p_0^{-}(i\Delta x_r, j\Delta x_s, k\Delta t; z_0)\} + \mathcal{E}\{p_1^{-}(i\Delta x_r, j\Delta x_s, k\Delta t; z_0)\}^2 + \mathcal{E}\{p_2^{-}(i\Delta x_r, j\Delta x_s, k\Delta t; z_0)\} + \ldots + \text{cross-terms} . \tag{3.24b}$$

If the cross-terms are small enough compared to the other terms in equation (3.24b), the total energy will be minimum if the higher order terms in equation (3.23a) are zero, i.e. when the surface is transparent. This can be achieved by taking the time window not too small (at least one second) and the number of traces not too small (at least 100). This was fully confirmed by all our experiments (simulated data as well as field data).

Fig. 3.12 shows the flow diagram for the optimization procedure. Note that the weighted summation of the terms, according to equation (3.16), has to be recalculated for each new guess of $\langle A(\omega) \rangle$. The matrix multiplications $\{\mathbf{P}^{-}(z_0)\}^2, \{\mathbf{P}^{-}(z_0)\}^3$ etc. have to be done only once, and the results can be stored. The optimization of the parameters can be done by a standard optimization procedure, like steepest descent.

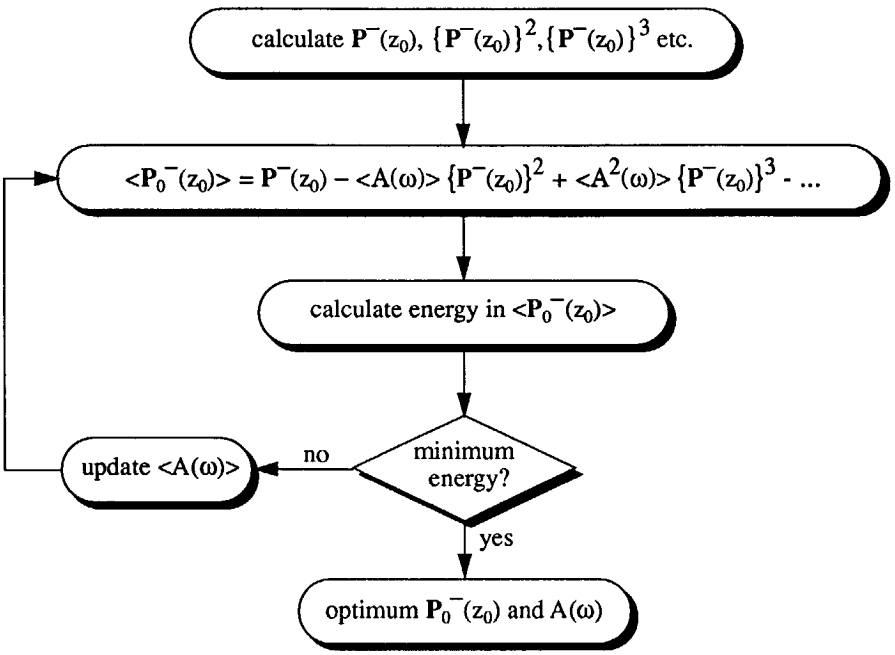

Fig. 3.12 Flow diagram for adaptive multiple elimination.

3.3.3 Source signature parametrization

The unknown surface function $A(\omega)$ is a function of frequency only, which considerably reduces the number of parameters to be optimized. Moreover, due to the limited length of $a(t)=FT^{-1}\{A(\omega)\}$, we do not need to estimate $A(\omega)$ for each frequency component in the data but only for a limited number of frequencies. If we have defined a parameter at every Δf Hz, the corresponding time length will be $L_t=1/\Delta f$ s. Typically a length of 0.2 s, in contrast to the 6 s full trace length, requires one frequency parameter every 5 Hz only.

A restriction on the length of a(t) is also necessary as the maximum length that can be estimated should not exceed the shortest multiple periodicity (e.g. the water bottom multiple in marine data). This can be understood by considering the fact that application of a(t) means deconvolution. If the deconvolution filter is too long it is possible that primaries are removed as well; the latter will falsify our forward model. In situations where the length of a(t) is larger than the smallest multiple periodicity (in the case of shallow water), wavelet deconvolution should be applied on the data first (pre-decon) to shorten the wavelet sufficiently.

If the frequency sampling of the signature to be estimated has been decided on, for each definition point a complex valued parameter is defined. These complex valued parameters can either consist of a real and imaginary part or an amplitude and a phase, as shown in Fig. 3.13. The values of the surface operator $A(\omega)$ for all other frequency points can be calculated by interpolation. For our purpose two methods have been used: interpolation by cubic splines or by applying an inverse Fourier transform of the sparsely defined surface function to the time domain, padding zeroes until the full trace length is reached, and then applying a forward Fourier transform to the frequency domain using the full trace length. The spline interpolation method allows an arbitrary positioning of the frequency definition points (Fig. 3.13a), the Fourier transform method is restricted to an equidistant distribution along the frequency axis (Fig. 3.13b). If desired, a band-limited stabilized inversion of the surface operator $A(\omega)$ (assuming r_0=-1) yields an estimate for the signature $S(\omega)$.

For an example the data of Fig. 3.4 to Fig. 3.8 is considered again. For simulating this data the mixed phase wavelet of Fig. 3.14a has been used. For the estimation of this wavelet 5 shot records and 4 terms of the Taylor series have been used. The source signature has been parametrized with 5 definition points at 10, 20, 30, 40 and 50 Hz. Through these points the amplitude and phase has been interpolated using the cubic spline method to get the wavelet for all frequencies. The spacing of 10 Hz in the frequency domain implied an approximate length of about 100 ms in the time domain, which appeared to be correct. In the band from 0 to 10 Hz and from 50 to 60Hz a smooth tapering to zero has been imposed on the amplitude and phase spectrum of the wavelet. In these regions accurate estimation is impossible.

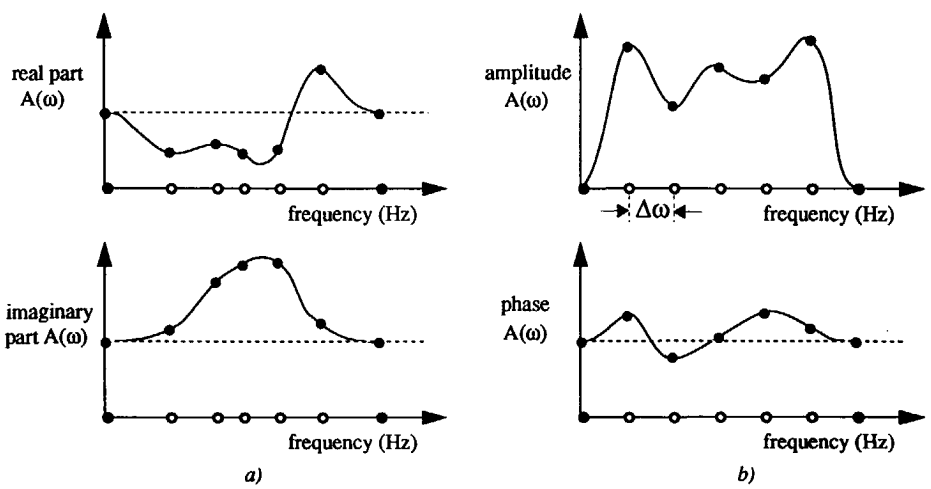

Fig. 3.13 Definition of A(ω) by interpolating a few definition points in the frequency domain of either real and imaginary parts (a) or amplitudes and phase (b). The interpolation can be done by a cubic spline.

The resulting wavelet after optimization is shown in Fig. 3.14b. Indeed a very accurate estimation of the original wavelet could be accomplished. Note that the excellent results confirm our believe in the energy criterion indeed.

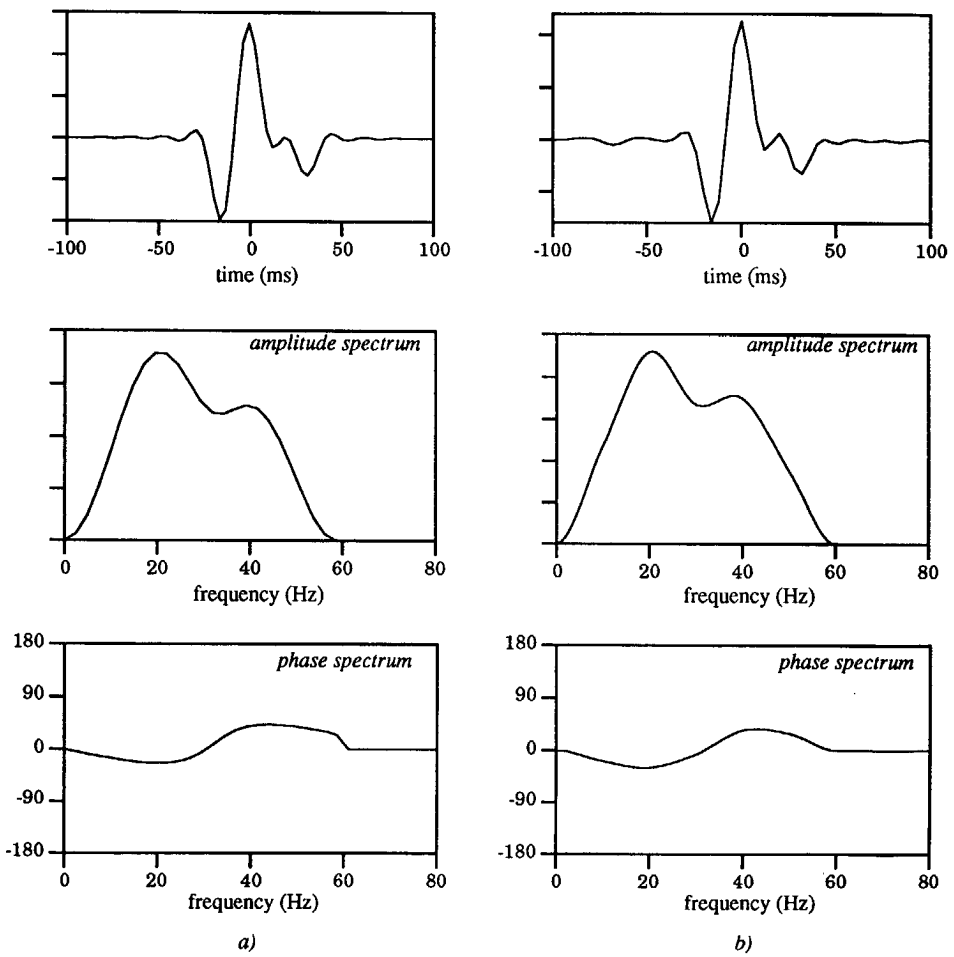

Fig. 3.14 *a) Mixed phase wavelet used for modeling the data in Fig. 3.4. b) Wavelet estimated with the adaptive surface-related multiple elimination using 5 definition points at 10, 20, 30, 40 and 50 Hz. Note the excellent estimation result.*

3.4 MULTIPLE ELIMINATION IN THE PRESENCE OF A THIN SURFACE LAYER

3.4.1 Problems due to the presence of a thin surface layer

In the situation where the first interface is very close to the surface (in the order of one wavelength or less) the multiple elimination procedure as described in section 3.2 will not work satisfactory, because of the following reasons:

- The periodicity of the thin layer multiples is so small that they interfere with each other. In this way there is no room to estimate a good source signature, as the smallest periodicity should be larger than the inverse signature length, see section 3.3.3.
- Because of the missing near offsets in any real data set, too much information is missing to predict the multiples correctly (see also Chapter 5). For example, in the case of a 30m water layer with 150m near offsets missing, the primary water bottom reflection is missing until 68°, first order multiple data is missing until 51°, second order multiple data until 40°, etc.
- As the periodicity of the water bottom multiples is small, a large number of terms in the Taylor series expansion has to be taken into account, which slows down the application.

In the thin surface layer situation it is better to make use of a different approach: the surface in combination with the first interface is considered as one complex reflector.

In section 2.5 this situation has already been described in a forward way: the first layer multiples are included explicitly. In Fig. 2.11 we showed the reverberations within the thin surface layer on each propagation through this layer. The forward model as described in section 2.5 reads:

$$\mathbf{P}^{-}(z_0) = \mathbf{T}^{-}(z_0,z_1)\,\mathbf{X}_{tot}(z_1,z_1)\,\mathbf{T}^{+}(z_1,z_0)\,\mathbf{S}^{+}(z_0), \tag{3.25}$$

with the matrices $\mathbf{T}^{+}(z_1,z_0)$, $\mathbf{T}^{-}(z_0,z_1)$ and $\mathbf{X}_{tot}(z_1,z_1)$ being defined by equations (2.27a), (2.27b) and (2.30) respectively. Note that the primary response of the thin layer with its multiples (the waves that do not travel below the thin layer) are not included in the description of section 2.5 and in equation (3.25).

The surface-related multiple elimination method should be modified for this specific situation, and consists of the following steps:

1. Remove the direct wave and the thin layer response (primary and its multiples).
2. Remove the source and receiver directivity, and transform the data in upgoing waves due to a downgoing source wave field (decomposition).

3. Remove the thin layer reverberations at the source and receiver side.

4. Remove the "surface-related multiples", considering the thin layer as one complex surface reflector.

3.4.2 Removal of the thin surface layer response

The first step is to remove all events from the data that do not propagate below the thin layer, i.e. the direct wave, the thin layer primary and its multiples. This can be done by muting and/or fk-filtering. Note that the thin layer primary and multiples almost travel at 90° within the first layer, and show up as a "kind of groundroll" (see also the example in Fig. 3.16a).

After the decomposition process, as described in the beginning of this chapter, we obtain:

$$\mathbf{P}^{-}(z_0) = [\, \mathbf{D}_{\text{array}}(z_r)\, \mathbf{D}_r^{-}(z_r,z_0)\,]^{-1}\, \mathbf{P}(z_r)\, [\, \mathbf{D}_s^{+}(z_0,z_s)\, \mathbf{D}_{\text{array}}(z_s)\,]^{-1}\,, \tag{3.26}$$

in which $\mathbf{P}(z_r)$ is now defined as the data after the removal of the thin layer response.

3.4.3 Removal of the thin surface layer reverberations

After removing the direct wave with the thin layer primary and multiples and applying the decomposition procedure, the two thin layer transmission matrices $\mathbf{T}^{+}(z_1,z_0)$ and $\mathbf{T}^{-}(z_1,z_0)$, as defined in equations (2.27a) and (2.27b), have to be removed. This means the application of a dereverberation process, yielding:

$$\mathbf{P}^{-}_{\text{derev}}(z_0) = [\, \mathbf{I} - \mathbf{W}^{-}(z_0,z_1)\mathbf{R}^{+}(z_1)\mathbf{W}^{+}(z_1,z_0)\mathbf{R}^{-}(z_0)\,]\, \mathbf{P}^{-}(z_0)$$

$$[\, \mathbf{I} - \mathbf{R}^{-}(z_0)\mathbf{W}^{-}(z_0,z_1)\mathbf{R}^{+}(z_1)\mathbf{W}^{+}(z_1,z_0)\,]\,. \tag{3.27a}$$

After applying a redatuming step to the bottom of the first interface, we obtain

$$\mathbf{P}^{-}_{\text{derev}}(z_1) = \{\mathbf{W}^{-}(z_0,z_1)\mathbf{T}^{-}(z_1)\}^{-1}\, \mathbf{P}^{-}_{\text{derev}}(z_0)\, \{\mathbf{T}^{+}(z_1)\mathbf{W}^{+}(z_1,z_0)\}^{-1}\,. \tag{3.27b}$$

The result of the dereverberation and extrapolation procedure can also be written in terms of the subsurface impulse response related to the thin layer bottom:

$$\mathbf{P}^{-}_{\text{derev}}(z_1) = [\, \mathbf{I} - \mathbf{X}_0(z_1,z_1)\, \mathbf{R}^{-}_{\text{tot}}(z_1)\,]^{-1}\, \mathbf{X}_0(z_1,z_1)S(\omega)\,, \tag{3.27c}$$

with the total reflectivity of the thin layer defined as (see also equation (2.29)):

$$\mathbf{R}^{-}_{\text{tot}}(z_1) = \mathbf{R}^{-}(z_1) + \mathbf{T}^{+}(z_1)\, \mathbf{W}^{+}(z_1,z_0)\, \mathbf{R}^{-}(z_0)\, \mathbf{T}^{-}(z_0,z_1)\,. \tag{3.28}$$

The dereverberation process at the receiver side (left part of the right hand side in equation (3.27a)) can be applied per shot gather: the operator acts on the columns of the data matrix $\mathbf{P}^{-}(z_0)$. For the dereverberation process at the source side the data has to be reordered into common receiver gathers, because the operator at the right part of the right hand side in equation (3.27a) acts on the rows of the data matrix. The dereverberation process is a very neat way to do an angle dependent deconvolution of the data to get rid of the signature-elongating thin layer reverberations.

Note that the removal of the first layer reverberations is conceptually the same as the multiple prediction and subtraction technique as described in section 1.2.3. However, here it is used as a dereverberation process for small period reverberations and, therefore, it is more robust.

3.4.4 Removal of the thin surface layer related multiples

In the fourth step, the remaining thin surface layer related multiples have to be removed from the data. This can be done by inverting equation (3.27c):

$$\begin{aligned} \mathbf{P}_0^{-}(z_1) &= \mathbf{X}_0(z_1,z_1)\, S(\omega) \\ &= \mathbf{P}^{-}_{derev}(z_0)\, [\, \mathbf{I} + S^{-1}(\omega)\, \mathbf{R}^{-}_{tot}(z_1)\, \mathbf{P}^{-}_{derev}(z_0)\,]^{-1} . \end{aligned} \tag{3.29}$$

This is comparable to the normal surface-related multiple elimination, as described by equation (3.11), the only difference being the modified free surface reflectivity operator. Hence, *adaptive* multiple elimination, including this modified reflectivity operator, can be applied again.

To show the effect of a thin surface layer on the seismic data the subsurface model of Fig. 3.15 is considered, containing 8 horizontal layers with a 30 m water layer on top of it. The influence of this small water layer on the seismic data is significant, as can be observed in Fig. 3.16a, where a shot record is shown that has been simulated with an acoustic finite difference algorithm. The source is at x=0, with receivers from 0 to 5000 m offset. Both source and receivers were located 5 m below the free surface. The response of the water layer itself, primary and water layer multiples, interfere to a kind of guided wave, being trapped in the water layer for emergence angles above the critical angle of the water bottom reflectivity.

As a first processing step we remove the water layer response by filtering in the k_x-ω domain and muting in the x-t domain, without distorting the other events. Next, decomposition into upgoing waves is applied at the receiver positions, which is in fact an angle dependent deghosting procedure.

Fig. 3.16b shows the shot record after removing the thin layer response and the decomposition process. The events in the data of Fig. 3.16b have all traveled below the water bottom.

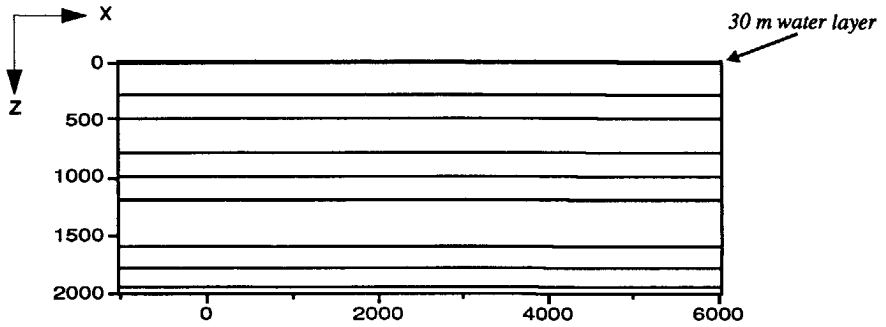

Fig. 3.15 Subsurface model with a 30 m water layer on top.

At this stage the third step of the modified thin surface layer related multiple elimination, as described by equation (3.27a), can be applied: removing the thin layer reverberations at source and receiver side. As we deal with a horizontal thin layer, this dereverberation procedure can be applied in the k_x-ω domain. Note that if the reflectors *below* the thin layer are non-horizontal, the dereverberation process can still be applied in the k_x-ω domain.

The result is given in Fig. 3.16c. Comparing Fig. 3.16b with Fig. 3.16c shows that a significant wavelet sharpening has been achieved. Note that this dereverberation process is not simple prediction-error filtering but a wave field based inversion using the thickness and contrasts of the thin layer.

The fourth step is the multiple elimination itself, as described by equation (3.29), using the total reflectivity of the thin layer for upgoing waves.

Fig. 3.16d shows the shot record after the modified multiple elimination procedure. Indeed all surface-related multiples have been removed and the 8 primaries can be easily distinguished. The other remaining events are internal multiples which have much lower amplitudes (especially at the small offsets) compared to the surface-related multiples. Also the wavelet has been estimated. Fig. 3.17 shows the Gaussian wavelet that has been used to model the data (solid line) and the wavelet estimated with the adaptive multiple elimination process (dashed line). The wavelet has been parametrized with 4 definition points at 10, 20, 30 and 40 Hz. Taken in to account the pre-processing steps, the wavelet could be estimated surprisingly well, especially the phase spectrum.

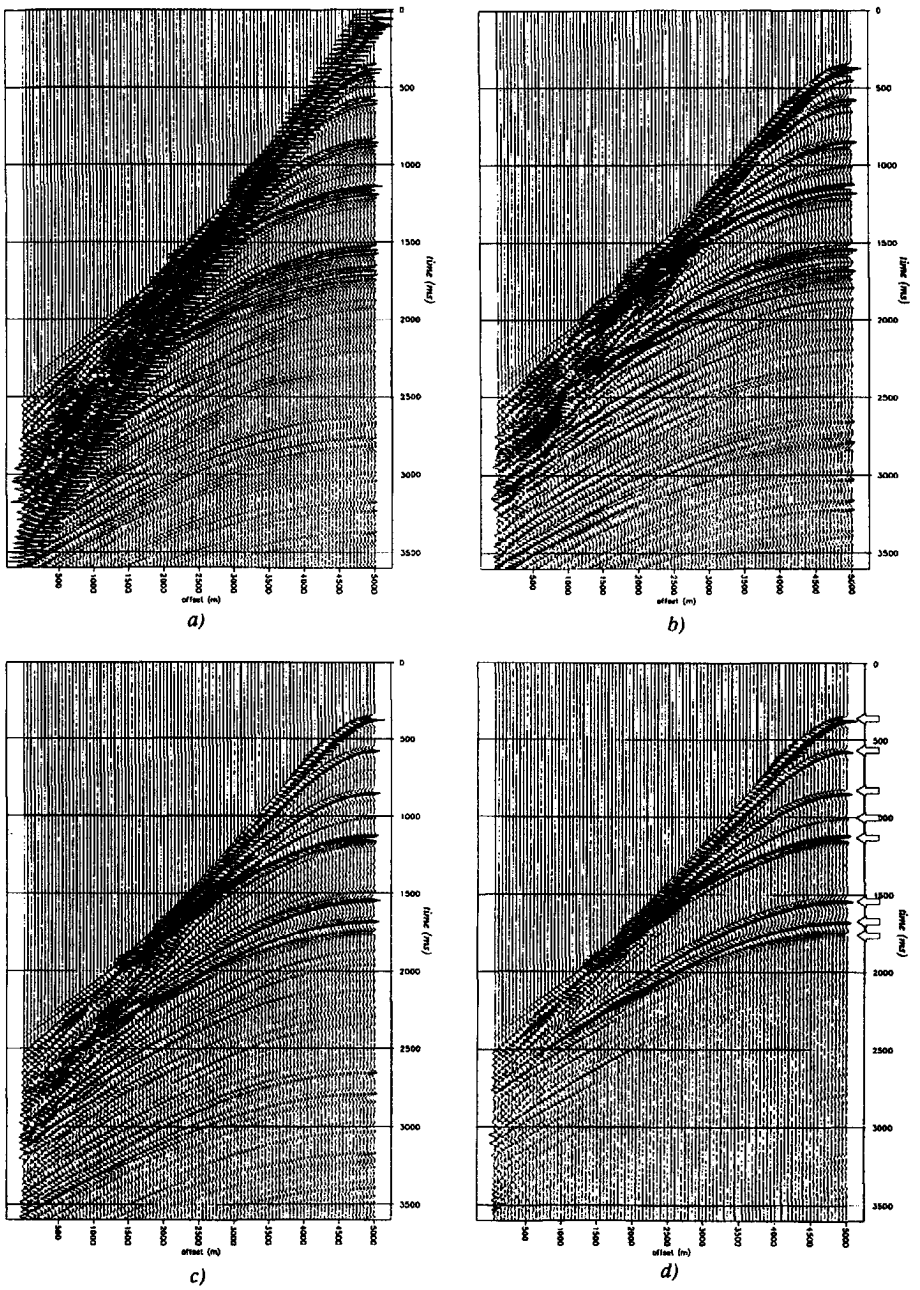

Fig. 3.16 *a) Shot record simulated for the subsurface model of Fig. 3.15 b) Shot record after removing the thin layer response and after applying the decomposition process c) Shot record after removing the thin layer reverberations as well d) Shot record after modified surface related multiple elimination as well. Note the remaining internal multiples, particularly at the far offsets.*

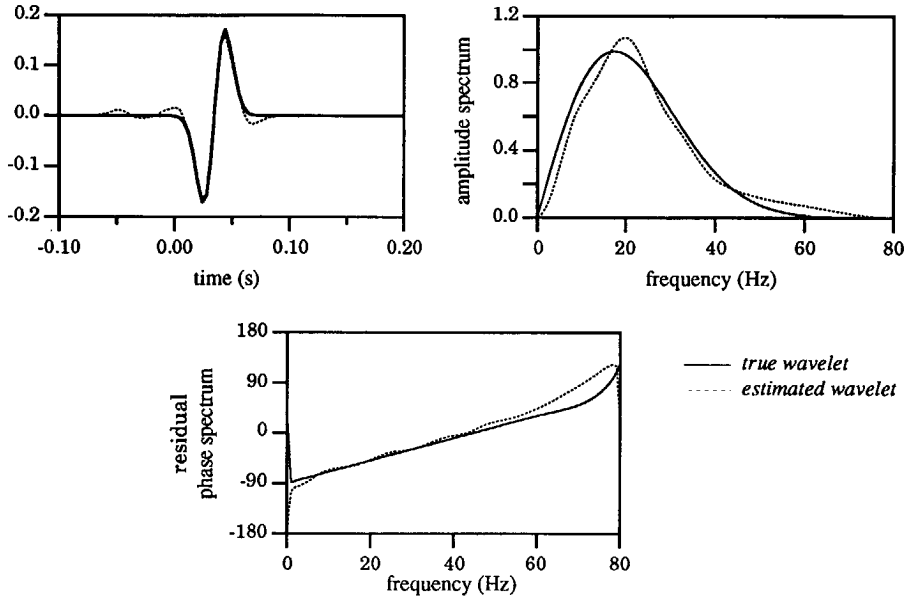

Fig. 3.17 Gaussian wavelet used for simulating the shot record of Fig. 3.16a (solid line) and the wavelet estimated by the adaptive multiple elimination process (dashed line).

3.5 MULTIPLE ELIMINATION FOR ELASTIC DATA

As in the acoustic case, a description of the multiple elimination procedure for multi-component data is obtained by applying the inverse of the multiple operator, as described by the forward multi-component model in section 2.6. In section 2.6 a general forward model has been given for down- and upgoing elastic wave fields, without being specific about the actual type of wave field description that has been used. In the decomposition process a choice must be made of either potentials, tractions or particle velocity components. In this section this general model is used to describe the elastic surface-related multiple elimination procedure, starting with the elastic decomposition.

To start the multiple elimination process, direct waves and ground roll should be removed. For this process the reader is referred to Beresford-Smith and Rango (1989).

3.5.1 Decomposition of multi-component data

For the elastic multiple elimination procedure, i.e. using equation (2.42), upgoing elastic wave responses due to downgoing elastic source wave fields are needed. Therefore first a pre-processing has to be done, transforming the measured data as described by equation (2.56) into data containing pure upgoing reflected waves due to pure downgoing source waves, i.e. retrieve the elastic impulse response matrix $\underline{\mathbf{X}}(z_0,z_0)$ from the measured data $\underline{\mathbf{P}}(z_0)$, using equation (2.56):

$$\underline{\mathbf{P}}(z_0) = \left[\underline{\mathbf{D}}^{(r)}_{array}(z_0)\, \underline{\mathbf{D}}_r^{-}(z_0) \right] \underline{\mathbf{X}}(z_0,z_0) \left[\underline{\mathbf{D}}_s^{+}(z_0)\, \underline{\mathbf{D}}^{(s)}_{array}(z_0) \right] \underline{\mathbf{S}}_T(z_0)\,. \tag{3.30}$$

This so-called *decomposition* procedure consists of two main steps:

– Decomposition at the receiver side

The decomposition at the receiver side transforms the V_x and V_z registrations into upgoing elastic waves at the surface. The upgoing waves can be described in terms of potentials, tractions or particle velocities. The receiver decomposition is done by inverting the left part of equation (3.30):

$$\underline{\mathbf{P}}^{-}(z_0) = [\underline{\mathbf{D}}_r^{-}(z_0)]^{-1}\, [\underline{\mathbf{D}}^{(r)}_{array}(z_0)]^{-1}\, \underline{\mathbf{P}}(z_0)\,, \tag{3.31a}$$

or

$$\underline{\mathbf{P}}^{-}(z_0) = \underline{\mathbf{X}}(z_0,z_0)\, \underline{\mathbf{D}}_s^{+}(z_0)\, \underline{\mathbf{D}}^{(s)}_{array}(z_0)\, \underline{\mathbf{S}}_T(z_0)\,, \tag{3.31b}$$

with $\underline{\mathbf{P}}^{-}(z_0)$ containing upgoing multi-component wave fields due to the traction sources.

– Decomposition at the source side

The decomposition at the source side transforms the tractions T_{xz} and T_{zz} of the sources into downgoing waves at the surface. This can be achieved by inverting equation (3.31b):

$$\underline{\mathbf{X}}(z_0,z_0) = \underline{\mathbf{P}}^{-}(z_0)\, [\underline{\mathbf{S}}_T(z_0)]^{-1}\, [\underline{\mathbf{D}}^{(s)}_{array}(z_0)]^{-1}\, [\underline{\mathbf{D}}_s^{+}(z_0)]^{-1}. \tag{3.32}$$

We assume that the signatures of the horizontally and vertically oriented vibrators $S_x(\omega)$ and $S_z(\omega)$, are equal to $S(\omega)$. Similar to the acoustic case the first inversion step will be omitted. In that case the source wavelet is kept in the data, yielding only a *directional* deconvolution at the source side:

$$\hat{\underline{\mathbf{P}}}^{-}(z_0,z_0) = \underline{\mathbf{P}}^{-}(z_0)\, [\underline{\mathbf{D}}^{(s)}_{array}(z_0)]^{-1}\, [\underline{\mathbf{D}}_s^{+}(z_0)]^{-1}\,. \tag{3.33}$$

For notational simplicity decomposition results $\underline{\mathbf{P}}^{-}(z_0)$ and $\hat{\underline{\mathbf{P}}}^{-}(z_0)$ will be both indicated by $\underline{\mathbf{P}}^{-}(z_0)$. This was also done in the acoustic case.

3.5.2 Elimination of surface-related multiples and conversions

After removing the source and receiver effects, the resulting elastic surface data can be represented by:

$$\underline{\mathbf{P}}^{-}(z_0) = \underline{\mathbf{X}}(z_0,z_0)\, S(\omega)\,. \tag{3.34}$$

Now, elastic surface-related multiple elimination is described by:

$$\underline{\mathbf{X}}_0(z_0,z_0) = \underline{\mathbf{X}}(z_0,z_0)\,[\ \underline{\mathbf{I}} + \underline{\mathbf{R}}^{-}(z_0)\,\underline{\mathbf{X}}_0(z_0,z_0)\ ]^{-1}\,, \tag{3.35}$$

or by defining the decomposed seismic data without the influence of the free surface as

$$\underline{\mathbf{P}}_0^{-}(z_0) = \underline{\mathbf{X}}_0(z_0,z_0)\, S(\omega)\,, \tag{3.36a}$$

we arrive at

$$\underline{\mathbf{P}}_0^{-}(z_0) = \underline{\mathbf{P}}^{-}(z_0)\,[\ \underline{\mathbf{I}} + \underline{\mathbf{R}}^{-}(z_0)\,\underline{\mathbf{P}}^{-}(z_0)\,\{S(\omega)\}^{-1}\ ]^{-1}\,, \tag{3.36b}$$

and after expanding the inversion term into a series expansion

$$\underline{\mathbf{P}}_0^{-}(z_0) = \underline{\mathbf{P}}^{-}(z_0) - \{\underline{\mathbf{P}}^{-}(z_0)\underline{\mathbf{A}}(z_0)\}\underline{\mathbf{P}}^{-}(z_0) + \{\underline{\mathbf{P}}^{-}(z_0)\underline{\mathbf{A}}(z_0)\}^2\underline{\mathbf{P}}^{-}(z_0) - \ldots\,, \tag{3.37a}$$

with the elastic surface operator

$$\underline{\mathbf{A}}(z_0) = \{S(\omega)\}^{-1}\,\underline{\mathbf{R}}^{-}(z_0)\,. \tag{3.37b}$$

As the full elastic reflectivity matrix $\underline{\mathbf{R}}^{-}(z_0)$ is used, also surface related *conversions* are properly eliminated by this scheme. Of course, this is only possible if the full multi-component dataset is available. Note that the exact meaning of the multi-component free surface reflectivity matrix $\underline{\mathbf{R}}^{-}(z_0)$ depends on the choice of wave field description, as discussed in section 2.6.4. We prefer a description in terms of down- and upgoing traction, yielding a reflectivity matrix that reduces to a simple unit matrix with negative sign, which is the exact counterpart of the acoustic free surface reflectivity coefficient of -1. Also the source decomposition is a simple one in this case: $[\underline{\mathbf{D}}_s^{+}(z_0)]^{-1} = \mathbf{I}$ and $[\underline{\mathbf{D}}_r^{-}(z_0)]^{-1}$ is a diagonal matrix in the k_x-ω domain.

3.5.3 Adaptive multi-component multiple elimination

Similar to the acoustic case, the multiple elimination as defined by equation (3.37a) will only work if the frequency dependent source signatures are known and if the data has true amplitudes. Therefore, elastic surface-related multiple elimination is also applied adaptively, minimizing the energy of the output. If we assume that the medium parameters just below the free surface are known, the reflectivity matrix $\underline{\mathbf{R}}^{-}(z_0)$ can be determined. Then equation (3.37a) can be rewritten as

$$\underline{\mathbf{P}}_0^{-}(z_0) = \underline{\mathbf{P}}^{-}(z_0) - \{S(\omega)\}^{-1}\,\{\underline{\mathbf{P}}^{-}(z_0)\,\underline{\mathbf{R}}^{-}(z_0)\}\,\underline{\mathbf{P}}^{-}(z_0) + \{S(\omega)\}^{-2}\,\{\underline{\mathbf{P}}^{-}(z_0)\,\underline{\mathbf{R}}^{-}(z_0)\}^2\,\underline{\mathbf{P}}^{-}(z_0) - \ldots\,, \tag{3.38}$$

In case of down- and upgoing tractions this expression simplifies to:

$$\underline{\mathbf{P}}_0^{-}(z_0) = \underline{\mathbf{P}}^{-}(z_0) - A(\omega)\{\underline{\mathbf{P}}^{-}(z_0)\}^2 + A^2(\omega)\{\underline{\mathbf{P}}^{-}(z_0)\}^3 - \ldots\,, \tag{3.39}$$

the surface factor $A(\omega)$ being again defined as

$$A(\omega) = r_0\{S(\omega)\}^{-1}\,. \tag{3.40}$$

Each term of equation (3.39) can be split into 4 different components of the wave fields. On these data subsets the optimization can be done separately yielding 4 estimated source signatures. In the formulation of equation (3.38) and (3.39) they are taken to be equal.

3.5.4 Multiple elimination for single-component land data

For the single -component land data only the T_{zz} to V_z response is available. In this case no proper decomposition into the down- and upgoing components of the elastic wave field can be made. Therefore, the data is treated as a P-wave field response, neglecting the S-waves in the data. However, for the decomposition of this data the existence of S-waves in the medium is taken into account as much as possible.

– Decomposition at source and receiver side

For the decomposition the relation between the upgoing pressure and the vertical component of the particle velocity at the surface in the k_x-ω domain has been given by equation (2.77). To extract the upgoing pressure (due to a down going traction wave field) $\tilde{\Phi}_{\tau_z}^{-}(z_0)$ from the measured particle velocity, equation (2.77) has to be inverted, reading:

$$\tilde{\Phi}_{\tau_z}^{-}(z_0) \approx \frac{\omega\rho}{2}\,\frac{4k_x^2 k_{z,P} k_{z,S} + (k_S^2 - 2k_x^2)^2}{k_S^2\,k_{z,P}\,(k_S^2 - 2k_x^2)}\,\tilde{V}_z(z_0)\,. \tag{3.41}$$

Of course, this process will only restore the amplitudes for the P-waves as much as possible; S-wave reflections are not removed by this operation.

For the source decomposition equation (2.75) has to be inverted, yielding an estimate of the upgoing P-wave field due to downgoing P-wave sources:

$$\tilde{\Phi}^{-}(z_0) \approx -\frac{4k_x^2 k_{z,P} k_{z,S} + (k_S^2 - 2k_x^2)^2}{k_S^2 (k_S^2 - 2k_x^2)} \tilde{\Phi}^{-}_{\tau_z}(z_0) . \tag{3.42}$$

Again S-waves emitted by the vertical vibrators are not removed and the amplitudes of the P-waves are only partly recovered.

Array effects of the sources and receivers can be removed from the single-component data in the same way as can be done in the acoustic case. Leaving the source wavelet $S_z(\omega)$ in the data after decomposition, the resulting forward description is given by:

$$\mathbf{P}^{-}(z_0) \approx \mathbf{X}_{\phi\phi}(z_0,z_0)\, S_z(\omega). \tag{3.43}$$

– Surface-related multiple elimination

The multiple elimination on this approximated P to P-wave dataset can be done in a way similar way to the acoustic case. However, the free surface reflectivity operator for elastic P to P-wave reflection, $\mathbf{R}_{\phi\phi}^{-}(z_0)$, should be taken into account:

$$\mathbf{P}_0^{-}(z_0) \approx \left[\mathbf{I} + \mathbf{P}^{-}(z_0) \{S_z(\omega)\}^{-1} \mathbf{R}_{\phi\phi}^{-}(z_0) \right]^{-1} \mathbf{P}^{-}(z_0) , \tag{3.44}$$

with $\mathbf{P}_0^{-}(z_0)$ the PP data without surface-related multiples, including the source signature. Note that by this procedure no surface-related *conversions* can be eliminated, and that the surface-related multiples can only be partly reduced (especially for the smaller angles). However, in the example in Chapter 4 we will see that, even with the assumptions that have to be made for single-component elastic data, a satisfactory multiple elimination result can be achieved.

As a last remark, note that the multi-component theory also holds for 3D wave fields, introducing two types of S-waves with polarizations in two independent directions. In the 3-D situation, the multi-component data matrices consist of 9 submatrices (9-component data). For a more elaborate discussion see Wapenaar et al. (1990a).

3.6 OVERVIEW OF SURFACE-RELATED PROCESSING

To summarize this chapter, an overview is given of all processes involved. Basically, three main processing steps can be recognized:

1) Removal of waves that are not described by the forward model.

2) Removal of array effects and application of decomposition into upgoing wave fields at the surface due to downgoing source wave fields at the surface.

3) Apply surface-related multiple elimination in an adaptive mode. The output consists of three parts:

   - Primary data

   - Multiple data

   - Source signature

The total surface-related processing sequence is visualized in Fig. 3.18. The matrices can either represent single- or multi-component data and operators in either 2D or 3D.

With respect to the *source* related pre-processing, note that for land data (a traction source at the surface or a volume injection source just below the surface) $\mathbf{D}_s^+(z_0,z_s)=\mathbf{I}$. For marine data, being shot with airgun arrays, the two operators $\mathbf{D}_{array}(z_s)$ and $\mathbf{D}_s^+(z_0,z_s)$ need be combined.

With respect to the *receiver* related pre-processing, note that for land data $z_r=z_0$ and $[\mathbf{D}_r^+(z_r,z_0)]^{-1}$ transforms the particle velocity measurements to upgoing traction data. For marine data application of $[\mathbf{D}_r^+(z_r,z_0)]^{-1}$ means wave field based "deghosting".

Finally, note that surface matrix $\mathbf{A}(z_0)$ is determined adaptively during the actual multiple elimination process.

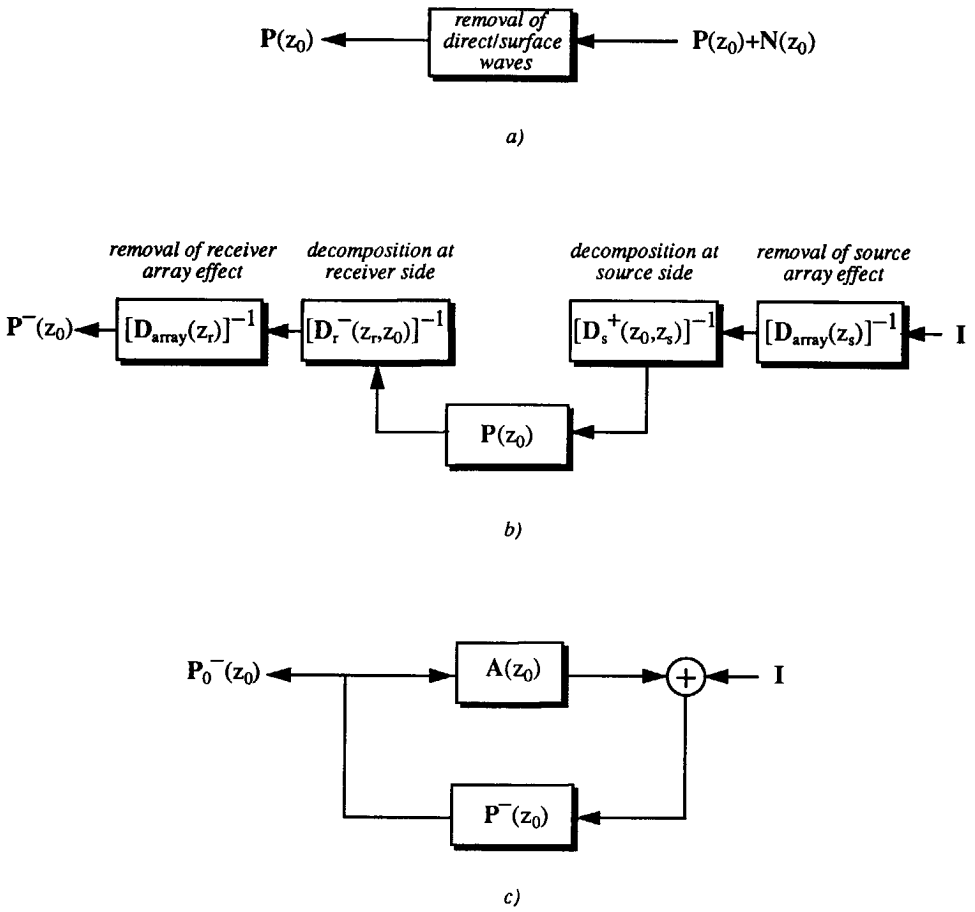

Fig. 3.18 Overview of surface-related processing. a) Removal of events that are not described by the forward model b) Removal of source and receiver array effects and decomposition c) Surface-related multiple elimination.

4

SIMULATED DATA EXAMPLES

In this chapter the surface-related multiple elimination process will be illustrated on simulated data, generated by a 2nd order finite difference technique. We start with a horizontally layered acoustic medium. Next, simulated acoustic data of a laterally varying subsurface model will be discussed. Finally, an example on simulated multi-component data will be given.

4.1 ACOUSTIC 1D MODEL BASED ON A WELL LOG

4.1.1 Simulation and decomposition

For the first example we consider a 1D subsurface model. In Chapter 1 already a simple example has been shown on a 1D subsurface model with 4 reflectors. Therefore we make the model more complicated by considering a 1D model based on a true velocity and density field log. The modeling procedure is as follows:

- Apply to the velocity and density log a high cut filter, in order to increase the sampling interval from 0.15 m to 6.25 m (which will be the finite difference grid interval).
- Add a water layer of 300 m to introduce a marine data experiment.
- Extend the model in the lateral direction to a laterally homogeneous velocity and density grid, representing a 1D subsurface model.
- Apply acoustic finite difference modeling to simulate a shot record.

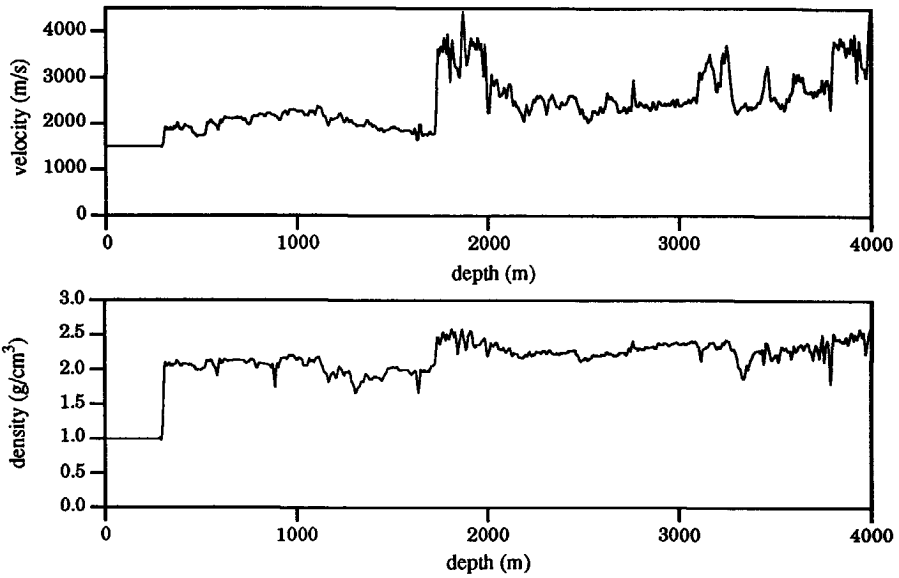

Fig. 4.1 Low-pass filtered velocity and density log. The filtered logs are used to define a 1D subsurface.

Fig. 4.1 shows the filtered velocity and density log, used to simulate a shot record with the aid of an acoustic finite difference modeling algorithm. The simulated shot record is shown in Fig. 4.2. It has been modeled with a monopole and omni-directional receivers at 6.25 m depth. The receiver spacing is 12.5 m. Fig. 4.2 shows the total pressure at 6.25 m depth. Note that for plotting purposes every fourth trace of the data has been shown in Fig. 4.2; this introduces visual aliasing which is not present in the original data. The shot record shows a lot of events (primaries and multiples), which give a complex interference pattern in the lower part of the shot record. The strong reflections between 1800 and 2000 ms produce well visible water layer related multiples below 2200 ms.

Before multiple elimination is applied, 2 pre-processing steps have to be carried out:

- *Direct wave removal*
  The direct wave should be removed from the data, as described in Chapter 2. In this example it can be done by a careful mute, as the direct wave does not interfere with the first primary reflection.

- *Decomposition into upgoing waves*
  The surface-related multiple elimination requires *upgoing* waves *at* the free surface. As the recording has been done *below* the free surface, measuring the *total* pressure wave field, an acoustic decomposition at the receiver positions, as described in Chapter 3, should be applied.

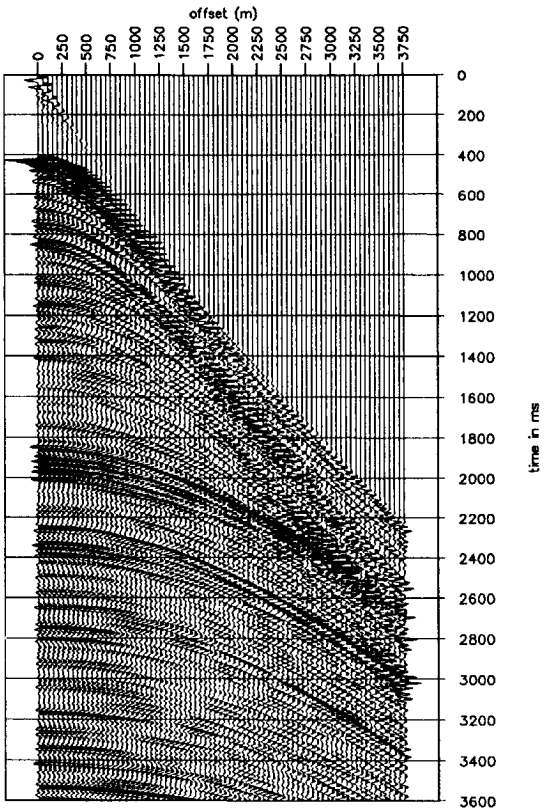

Fig. 4.2 *Shot record simulated with an acoustic finite difference modeling algorithm for a subsurface model based on the velocity and density log of Fig. 4.1.*

The result of the two pre-processing steps is shown in Fig. 4.3. The result of the decomposition on the data is two-fold: the wavelet is changed and the amplitude at large angles of incidence is increased. In fact, the decomposition process transforms the *total* measured pressure at 6.25 m depth to the *upgoing* pressure wave field at z=0 m.

Note that the decomposition at the source need not be carried out, as the monopole together with the free surface acts as a dipole.

4.1.2 Adaptive multiple elimination

As the medium is horizontally layered, all shot records are equal. This means that all columns of the data matrix are equal (with respect to the diagonal), or in other words, the data matrix has a Toeplitz structure. In that case, the matrix multiplications of the data with itself (see equation (3.16)) can be carried out in the k_x-domain as straightforward multiplications. To do this, only one shot record has to be transformed to the k_x-ω domain, reducing the calculation and the IO time considerably.

Fig. 4.3 shows the first term of the Taylor series expansion (equation (3.16)), i.e. the data itself. The second and third term of the Taylor series for this dataset (without the application of the surface operator $A(\omega)$) are shown in Fig. 4.4. The second term (Fig. 4.4a) contains the first order surface-related multiples and higher order terms. The third Taylor term (Fig. 4.4b) contains second and higher order surface-related multiples. All sections have been displayed with the same amplitude scale.

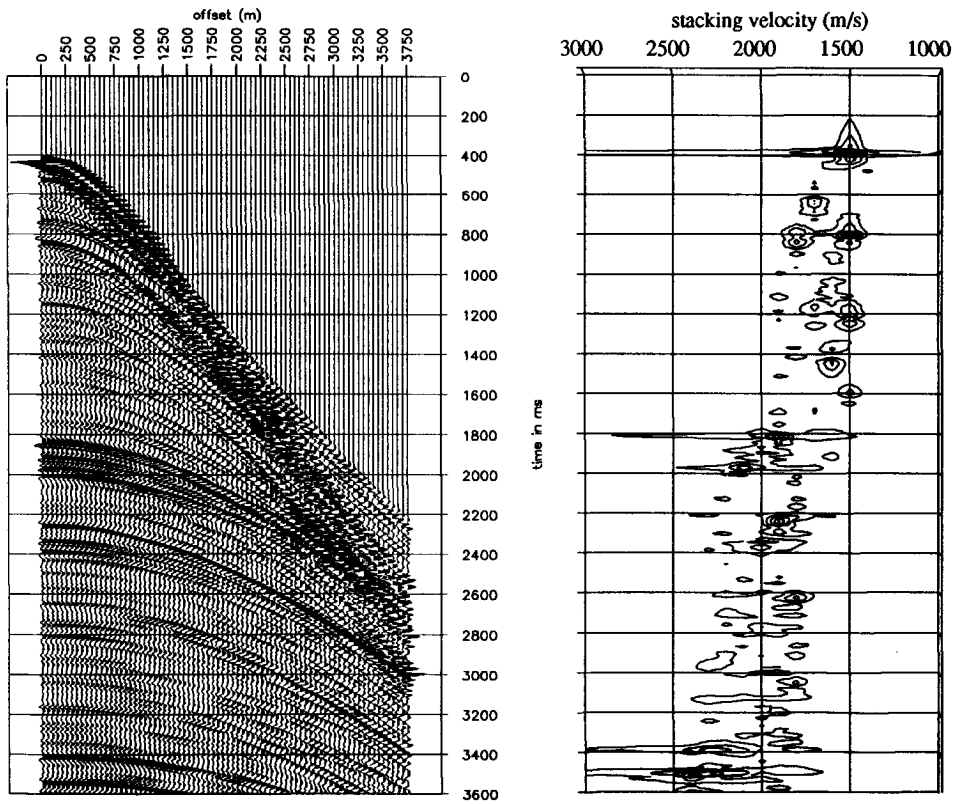

Fig. 4.3 Shot record of Fig. 4.2 after removing the direct wave and applying decomposition into upgoing waves. On the right hand side the corresponding velocity panel has been displayed.

Note that the second order term contains not only the first-order multiples but also *partly* the higher-order multiples. On principle as much terms are needed in order to predict the highest order of surface-related multiples present in the data. Fortunately, in practice less terms are needed, as the amplitudes generally decay for each higher order term (except at critical reflections, as visible in the right hand side of the sections in Fig. 4.4).

For this example 6 terms were needed to correctly predict all multiples within the considered time range of 3600 ms. To retrieve the surface function $A(\omega)$, these Taylor terms are adaptively combined according to equation (3.16) until the minimum energy has been reached.

Let us consider the adaptive process in more detail for this example.

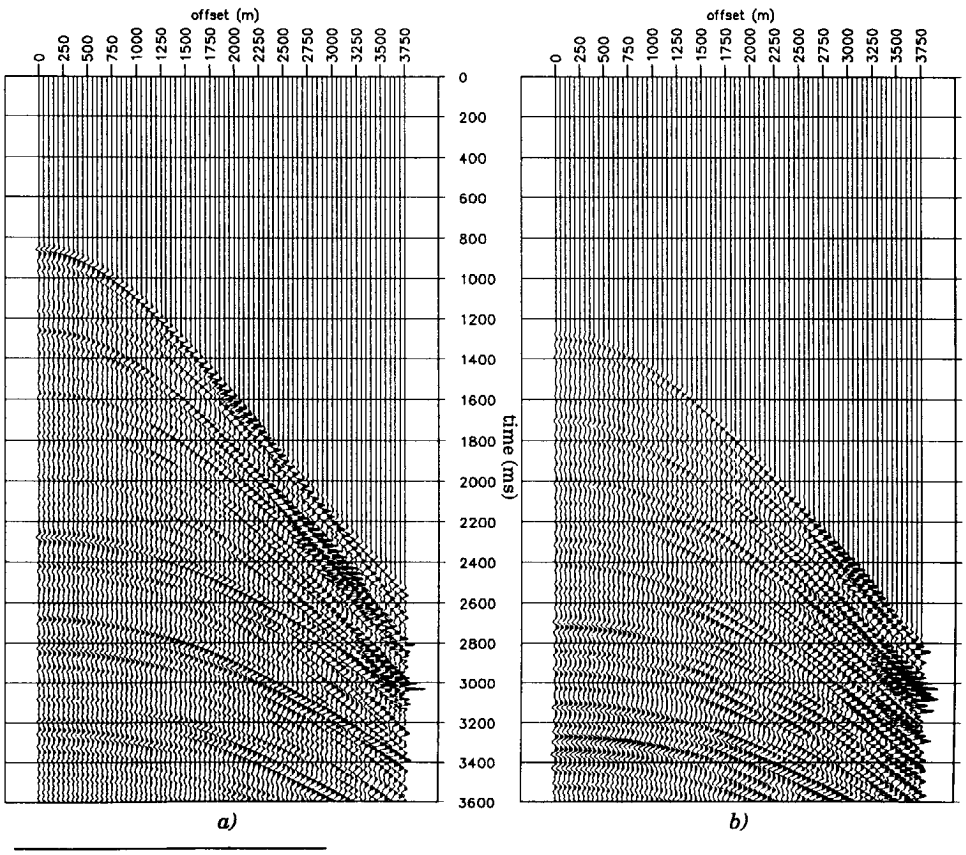

Fig. 4.4 *a) Second term of the Taylor series related to the shot record of Fig. 4.3. b) Third term of the Taylor series related to the shot record of Fig. 4.3.*

The first stage is to balance the terms of the Taylor series, i.e. to find a rough estimate of the scale factor in the data. This is done by comparing the amplitudes of the events in the second Taylor term with those of the original data (first Taylor term). In our case a scaling factor of about 10 was found, due to the finite difference modeling software. Then the data is corrected with this factor. In this way we are sure that the surface operator $A(\omega)$ has amplitude values in the order of unity roughly. This amplitude correction was already made in the display of Fig. 4.4.

The next step in the adaptive process is to get an initial estimate of the source wavelet. This can be done with a parametrization of $A(\omega)$ with 2 parameters: an amplitude and a time shift: $A(\omega)=r_0 e^{-j\omega\Delta t_0}$. With these two parameters a fast optimization can be done. If the optimum values of r_0 and Δt_0 have been found, this means that the position and the amplitude of the main peak of the inverse wavelet has been found. For these two parameters there are also a lot of local minima that can be found, one for each lobe in the source wavelet. Fig. 4.5 shows the wavelet that has been used to simulate the data of Fig. 4.2. It is a non-minimum phase wavelet, consisting of two main peaks with a number of smaller side lobes. To show how the energy in the data after multiple elimination varies as a function of the two parameters r_0 and Δt_0, this energy has been calculated for a grid of r_0 and Δt_0 values and is shown in Fig. 4.6. In Fig. 4.6a the energy is shown in a 3D plot, and in Fig. 4.6b as a contour plot. Especially from the contour plot the two minima, corresponding to the two main peaks in the wavelet are clearly visible. Of course this function is not known in reality, and an optimization is done for r_0 and Δt_0 starting at different initial values (multi-trial approach).

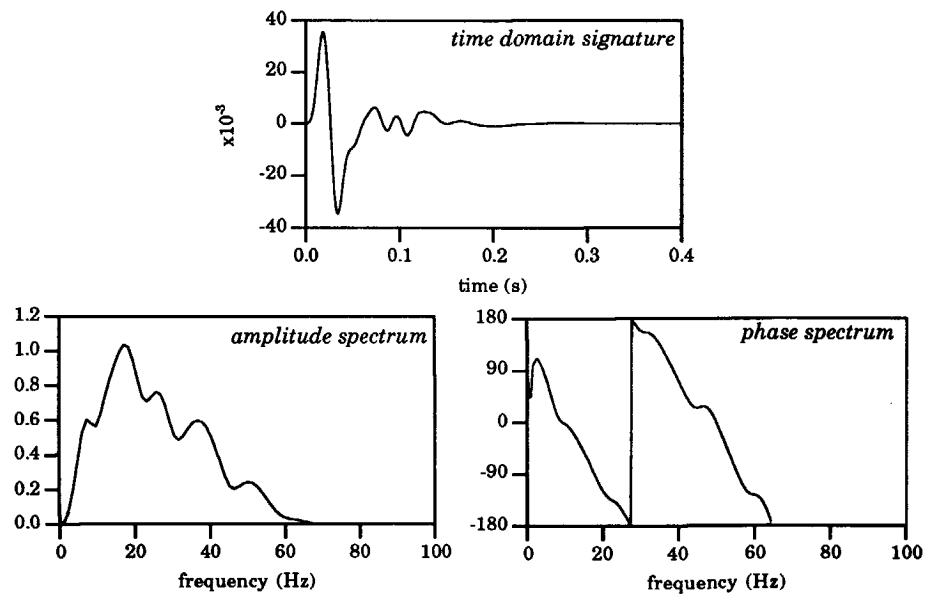

Fig. 4.5 Non-minimum phase wavelet that was used in the simulation of the data of Fig. 4.2

In Fig. 4.6b three optimization trajectories are displayed (steepest descent optimization) using one initial amplitude value (r_0=-1) and three initial phase values: Δt_0=0,-20 and -40 ms. All these three initial values yield different minima. The first one is a local minimum (r_0 close to zero) and the other two yield two almost equivalent minima, corresponding to the two main peaks in the wavelet. The third minimum has been chosen, being defined by r_0=0.55 and Δt_0=-35 ms. These values are used as deconvolution parameters, to transform the wavelet into a wavelet that is more close to a zero phase, unit valued pulse.

With other words, the surface function $A(\omega)$ is split into two parts, $A(\omega)=A'(\omega)r_0e^{-j\omega\Delta t_0}$. The time shift transforms the phase spectrum to a more flat one which is easier to estimate. The value r_0 is used to be sure that the amplitude spectrum is close to 1. Since $A(\omega)$ is defined as the multiplication of the free surface reflectivity with the inverse source wavelet, and the free surface reflectivity is -1, this means that for this example the wavelet corresponding to $A'(\omega)$ is shifted with -35 ms and multiplied with -1/0.55.

The result of adaptive multiple elimination with only two parameters is shown in Fig. 4.7. Even with this poor parametrization, a considerable reduction of the multiples could be achieved, comparing Fig. 4.3 with Fig. 4.7. Note especially that the interferences of primaries with multiples in the lower part has been reduced, making primary energy visible.

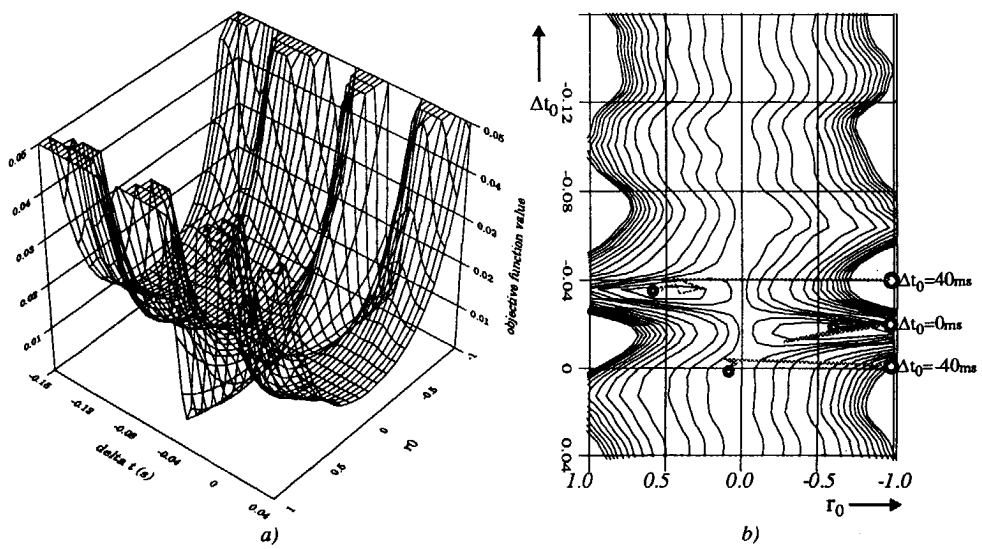

Fig. 4.6 *Energy after multiple elimination as a function of two parameters r_0 and Δt_0. a) 3D plot (clipped at the upper side). b) Contour plot. In the contour plot three trajectories of the optimization for three starting positions of r_0 and Δt_0 are shown.*

The wavelet corresponding to the residual surface factor A'(ω) is plotted in Fig. 4.8, using Δt_0=-32ms (a multiple of the sample rate of 4ms) and r_0=-0.5. Note that the wavelet has changed sign and that the average of the amplitude spectrum is unity, as desired. In fact by making use of multi-trial two-parameter wavelet deconvolution, the optimization is guided in the right direction, and local minima are avoided. The residual wavelet of Fig. 4.8 is the one that is to be estimated for all frequencies, starting the optimization process with a unit valued, zero phase spectrum as initial estimate.

The parametrization of the residual inverse wavelet was done with 13 complex valued (amplitude and phase) definition points from 8 Hz to 56 Hz with steps of 4 Hz. The interpolation for all other frequencies was done by the Fourier method (see section 3.3.3). As the original wavelet, which is plotted in Fig. 4.5, is a causal one, the estimated wavelet was also forced to be one-sided, starting at -32ms. The optimization has been applied with a steepest descent optimization scheme, which used 110 iterations to reach the minimum (for a specific accuracy).

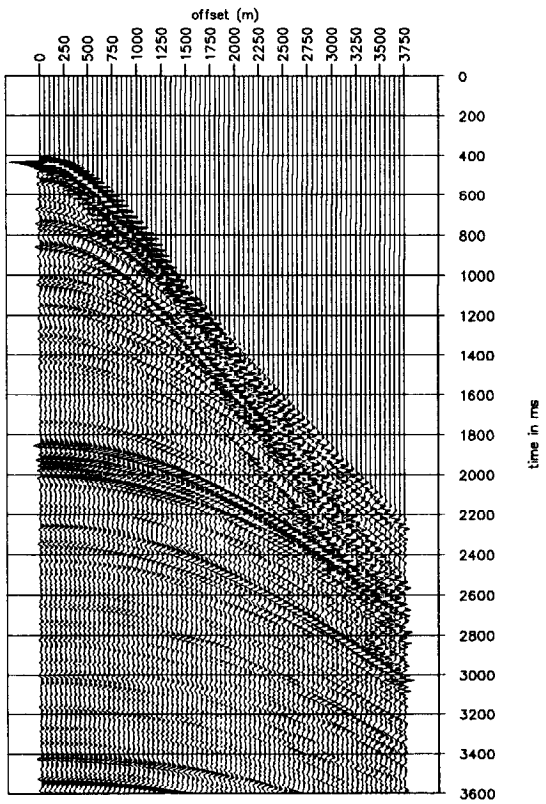

Fig. 4.7 Shot record of Fig. 4.3 after adaptive multiple elimination using only two parameters for describing the wavelet.

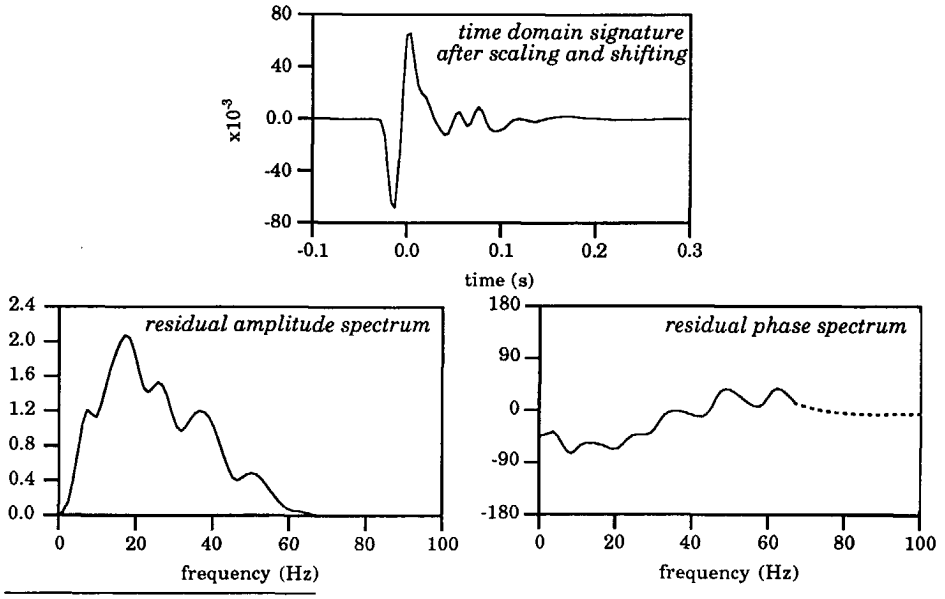

Fig. 4.8 *Residual wavelet to estimate, which is the original wavelet after a time shift of -32ms and a scaling factor of -2.0.*

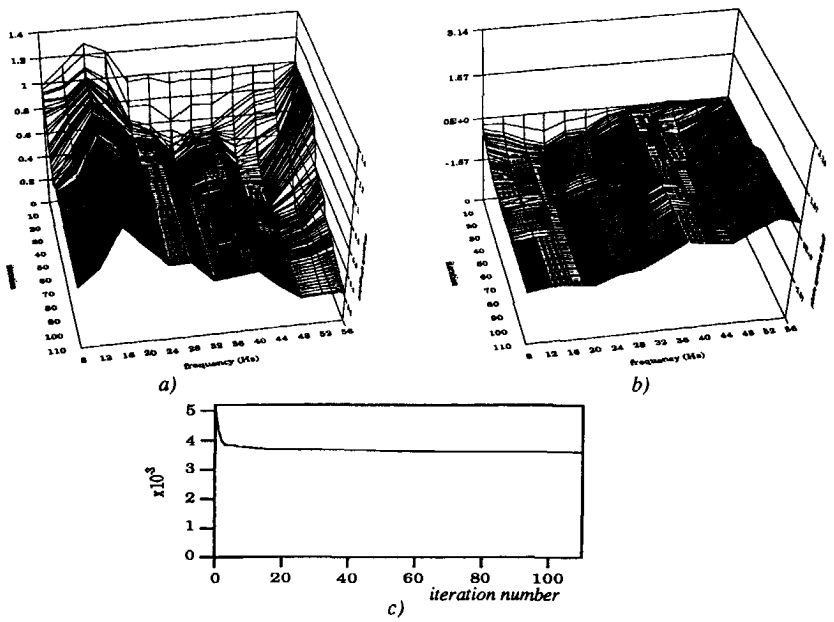

Fig. 4.9 *a) Amplitude spectrum (13 parameter values) for each iteration during the optimization procedure.*
b) Phase spectrum (13 parameter values) for each iteration during the optimization procedure.
c) Energy of the data after multiple elimination as a function of the iteration number.

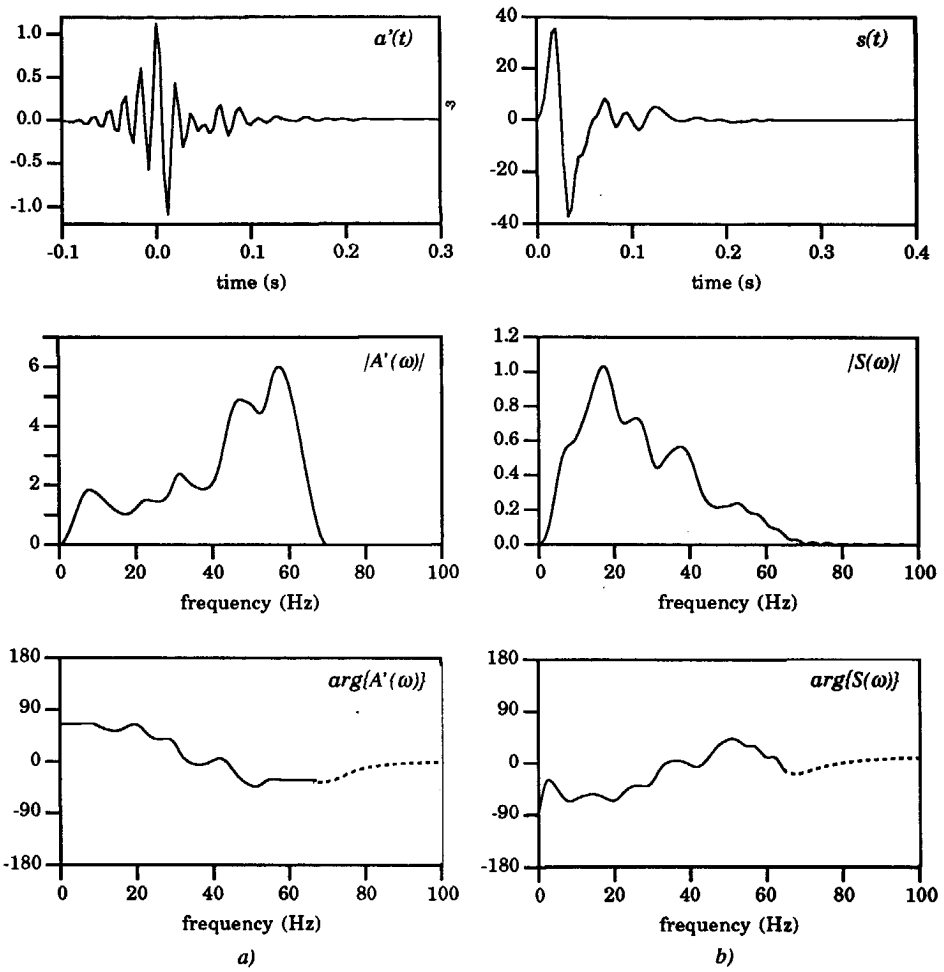

Fig. 4.10 *a) The inverse source wavelet as defined by A'(ω). b) The source wavelet as defined by $S(\omega)=[A'(\omega)]^{-1}$. The time domain representation of the source wavelet s(t) is shown after shifting it back to its original position.*

Fig. 4.9 shows the optimization process in a 3D plot. Fig. 4.9a displays the values of the amplitude spectrum as a function of the iteration number for the 13 parameters. Fig. 4.9b gives a similar plot for the phase spectrum.It can be observed that in the beginning the optimization goes very fast, but the final convergence is slow. This is well known from steepest descent methods, and other methods may be more effective. The optimization could have been stopped much earlier, as the energy reduction in the last part of the iteration is very small. This can also be judged from Fig. 4.9c, which shows the energy of the data after each multiple elimination iteration.

Note that the surface factor A'(ω) contains the inverse wavelet or deconvolution filter. So this is actually the function that is used in the weighting factors for the Taylor terms.

Fig. 4.10a shows the result of the estimation process. If the free surface reflection coefficient is assumed to be -1, and the estimated surface operator is inverted (within the band of 8 to 56 Hz), the result is the estimated wavelet as shown in Fig. 4.10b. For this figure the time shift of -32ms has been removed from the time domain representation. In fact a very good match can be observed with the original wavelet of Fig. 4.5, and with the phase spectrum of Fig. 4.8.

Using the estimated surface operator, the shot record without multiples can be calculated and is shown in Fig. 4.11. Note the enormous reduction of events, when compared to Fig. 4.3. Also from the velocity panel in Fig. 4.11 the reduction of events can be clearly observed. The primaries (and internal multiples) have been fully recovered, despite the serious interference with the surface-related multiples.

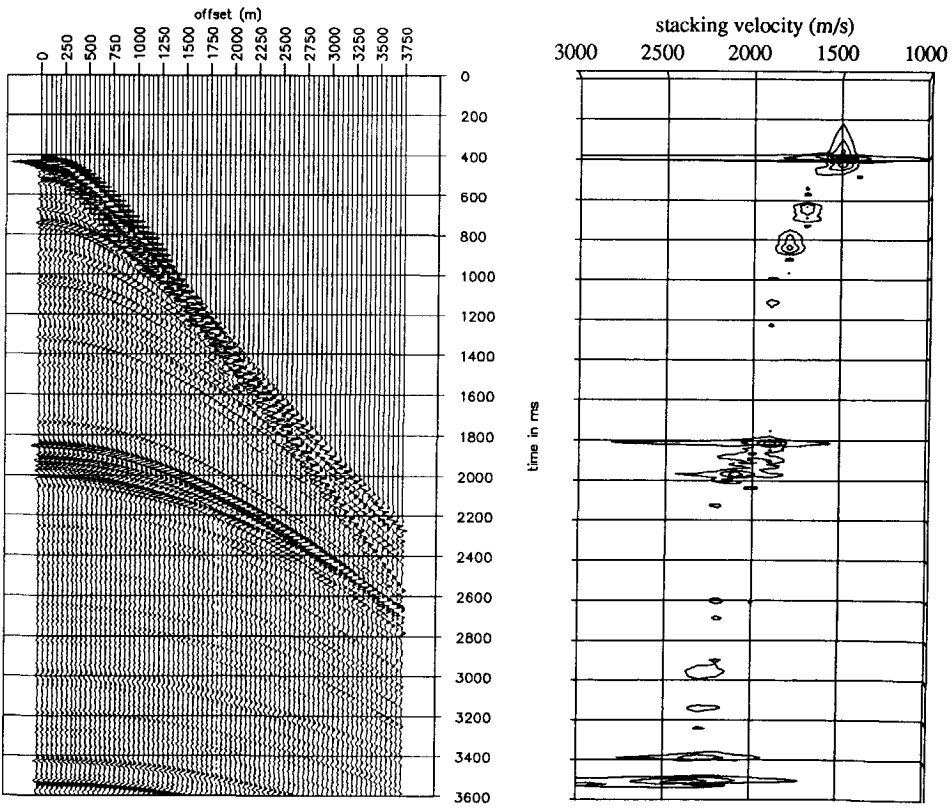

Fig. 4.11 Shot record of Fig. 4.3 after surface-related multiple elimination, together with its velocity panel.

To illustrate this, Fig. 4.12 shows the difference plot of the data before and after multiple elimination, with the corresponding velocity panel. For this display the same amplitude scaling has been used in order to make a good comparison.

For a further analysis of the multiple elimination result, the shot record has been simulated again with the finite difference program but without surface-related multiples. The result of this modeling exercise is shown in Fig. 4.13a. The resemblance with Fig. 4.11 is very good. This can be judged from Fig. 4.13b, which displays the difference between the simulated data without surface-related multiples (Fig. 4.13a) and the data after surface-related multiple elimination (Fig. 4.11), plotted on the same scale.

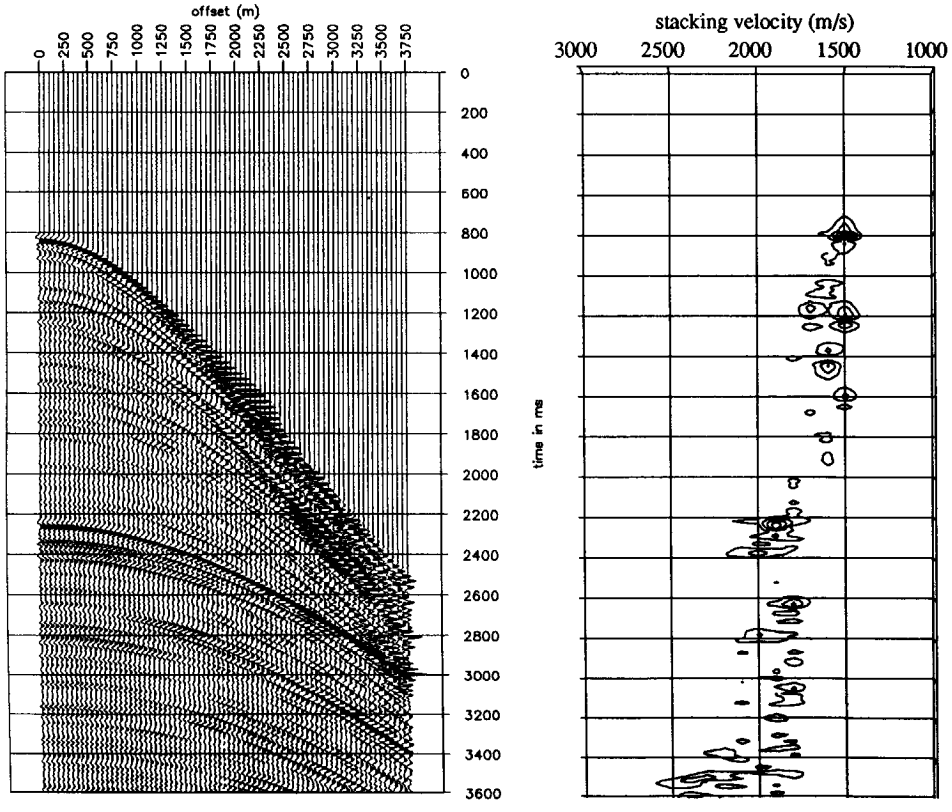

Fig. 4.12 Difference between the data before (Fig. 4.3) and after (Fig. 4.11) surface-related multiple elimination with the corresponding velocity panel.

The small remainings are differences due to the processing on the data with multiples, i.e. the decomposition into upgoing waves is done in a stabilized way, sacrificing a little on the exact amplitude recovery, especially at the large offsets. Note that the direct wave field in the simulated shot record without multiples (Fig. 4.13a) has not been removed. Therefore it turns up in the difference plot.

To make a comparison with another multiple elimination method, the velocity filtering procedure (as described in Chapter 1) has also been applied to this data. To do this, the primary stacking velocity curve has been picked and all events with a stacking velocity lower than 90% of this curve have been removed by filtering in the k_x-ω plane, using NMO correction (see section 1.2.2).

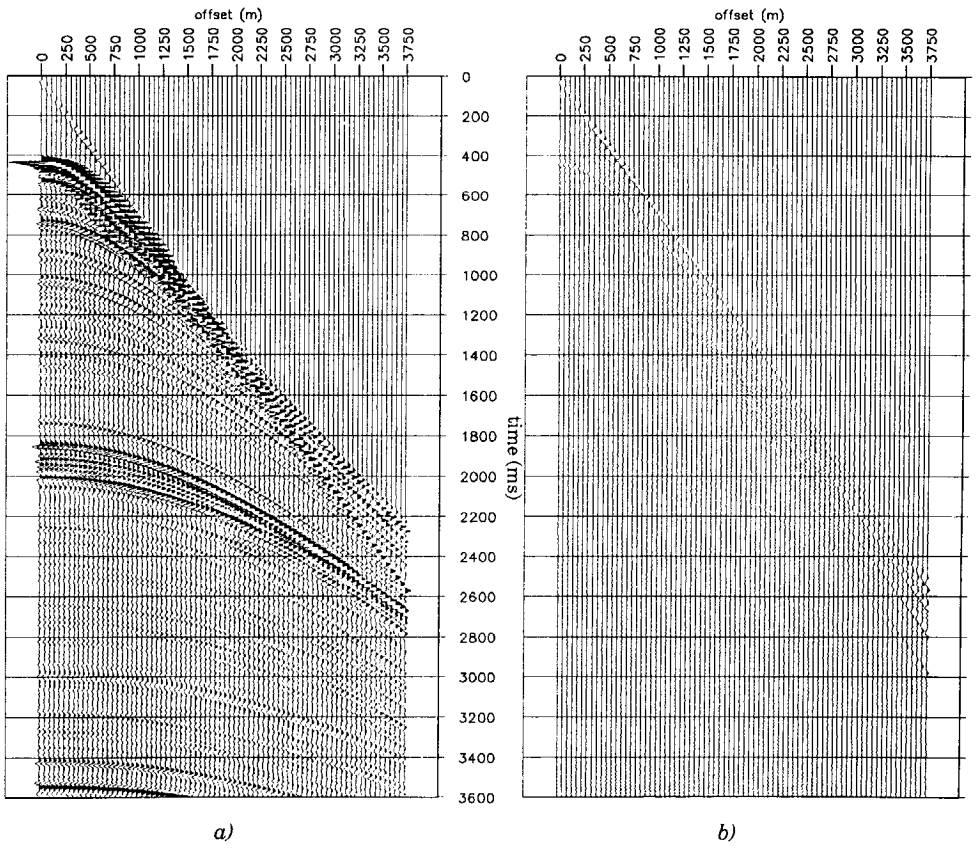

Fig. 4.13 *a) Shot record corresponding to the subsurface model of Fig. 4.1 without surface-related multiples. b) Difference between shot record a) and the shot record after surface-related multiple elimination (Fig. 4.11), plotted on the same scale.*

The result is shown in Fig. 4.14a, together with the difference between Fig. 4.13a and Fig. 4.14a. As can be seen, for this example the filtering process has been reasonably effective. However, considerable remainings are left in the data. Note that primary events have been partly destroyed, as the difference plot shows some primary energy as well. Especially in the region around 2s primary and multiple energy could not be separated well. The remainings of the water layer multiples at the arrow in Fig. 4.14b are due to the (inverse) NMO correction, which becomes non-unique when move-out curves are crossing at the larger offsets.

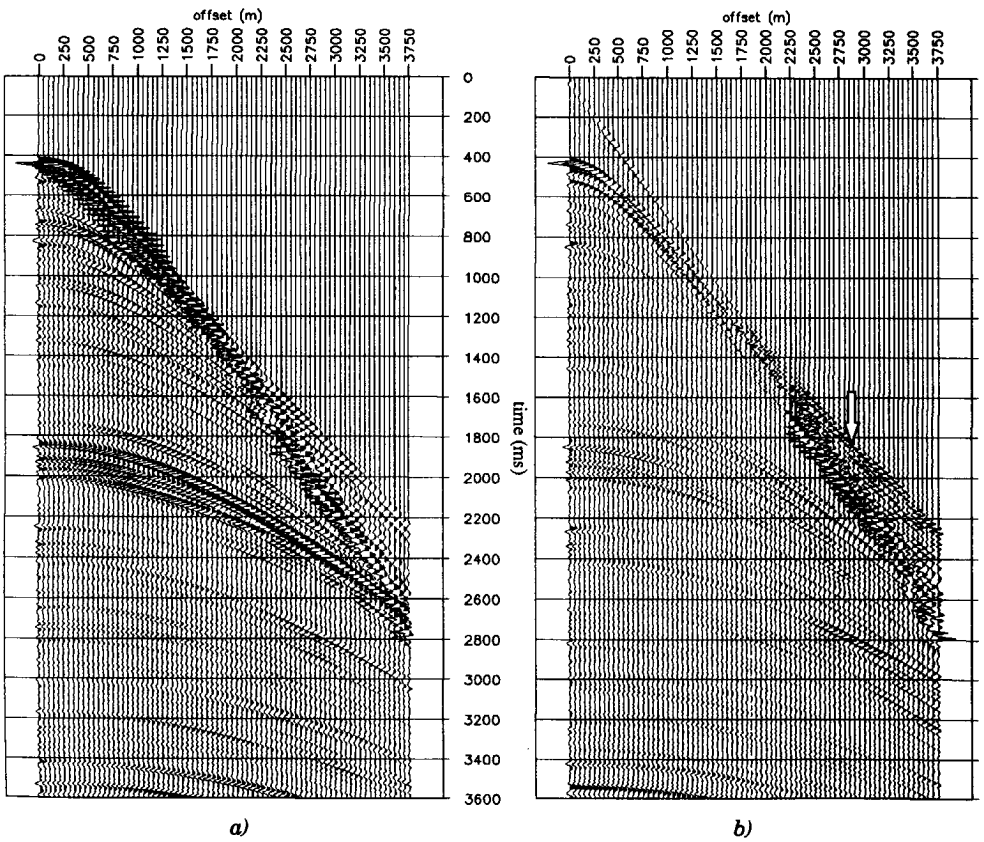

Fig. 4.14 a) Shot record of Fig. 4.3 after velocity filtering, removing all events with stacking velocities lower than 90% of the primary velocities. b) Difference between shot record a) and the shot record simulated without multiples (Fig. 4.13a), plotted on the same scale. Note the difference between Fig. 4.13b and Fig. 4.14b.

4.2 ACOUSTIC DOME MODEL

For data simulated in a laterally inhomogeneous medium, consider the subsurface model of Fig. 4.15. The velocity variations have been chosen to be significant to show that surface-related multiple elimination works for each subsurface model, as no information about the subsurface is required.

Hundred shot records, with one hundred receivers each, were simulated with acoustic finite difference. Shot and receiver spacing were chosen to be 20 m; shots and receivers were positioned at a depth of 5 m.

Three shot records are displayed in Fig. 4.16 with the source at 700, 1100 and 1500 m respectively. These shot positions have been indicated by arrows in Fig. 4.15. Before the multiple elimination process can start, decomposition into upgoing waves has to be applied. Fig. 4.17 shows the shot records after this decomposition process. Notice the different wavelet shape (for example at the left side arrow in Fig. 4.17) and the amplitude increase at the large offsets (for example at the right side arrow in Fig. 4.17).

To all shot records the adaptive multiple elimination procedure has been applied, which results into Fig. 4.17. The very strong multiples, with non-hyperbolic offset behavior, have been removed from the data and the weak primaries have been restored from the interference with the multiples (see for example the primary reflections indicated with the arrows in Fig. 4.17). To show what has been removed, Fig. 4.17 shows the difference plot of the data before (Fig. 4.17) and the data after multiple elimination (Fig. 4.17), i.e. the eliminated surface-related multiples. The arrows in Fig. 4.17 point at artifacts caused by the decomposition procedure due to the limited offset range (edge effects).

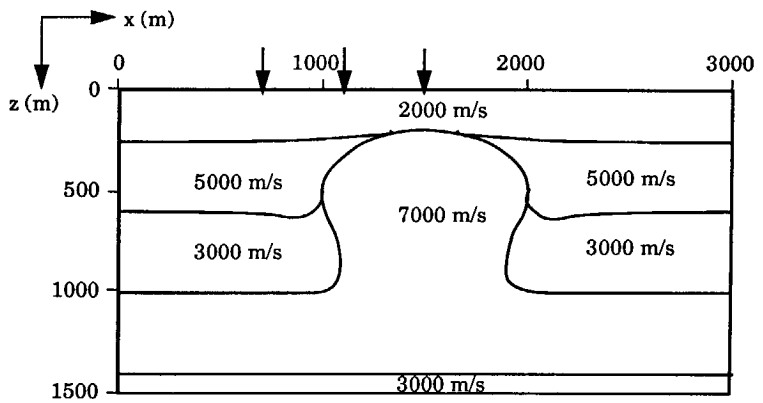

Fig. 4.15 Subsurface model with significant lateral velocity variations

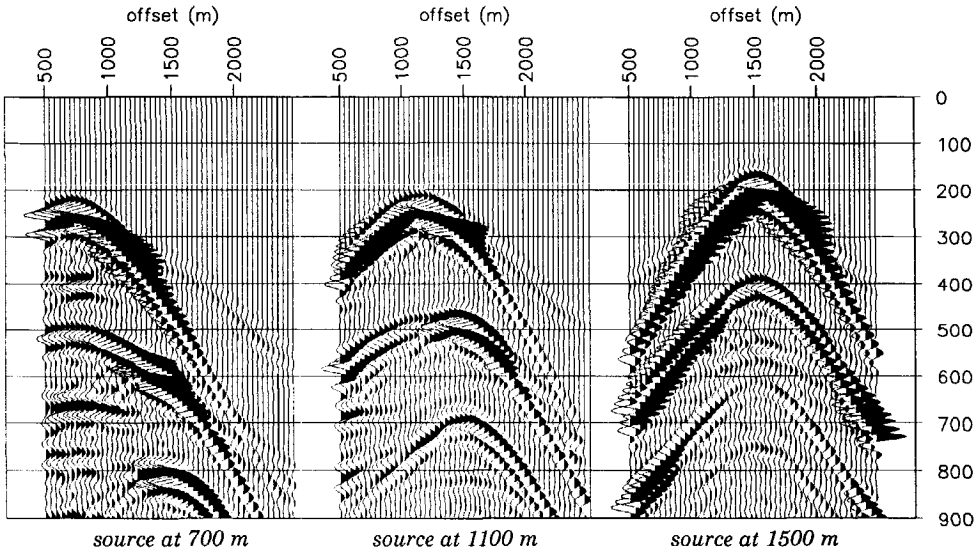

Fig. 4.16 *Three shot records corresponding to the subsurface model of Fig. 4.15 with the source at position x=700, 1100, and 1500 m respectively.*

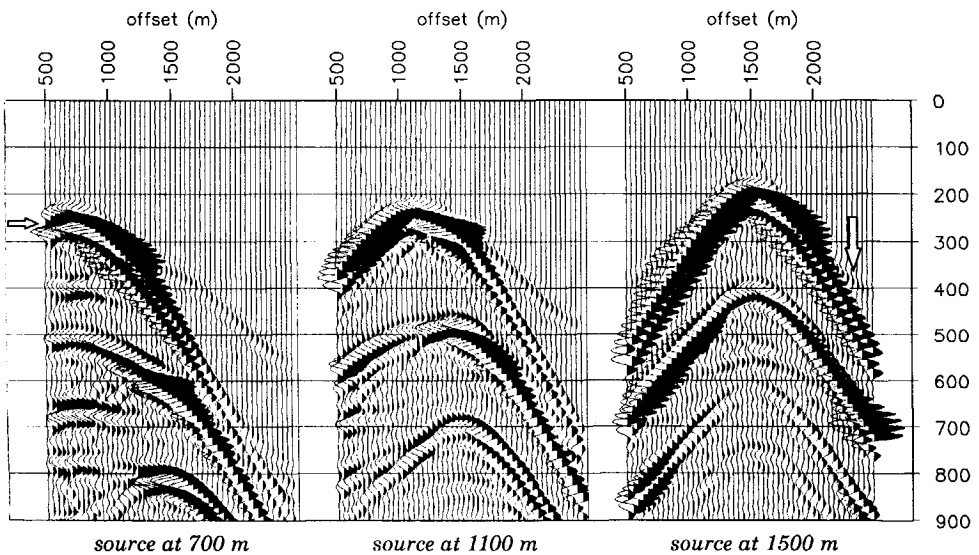

Fig. 4.17 *Shot records of Fig. 4.16 after decomposition into upgoing waves, i.e. decomposition at the receiver side.*

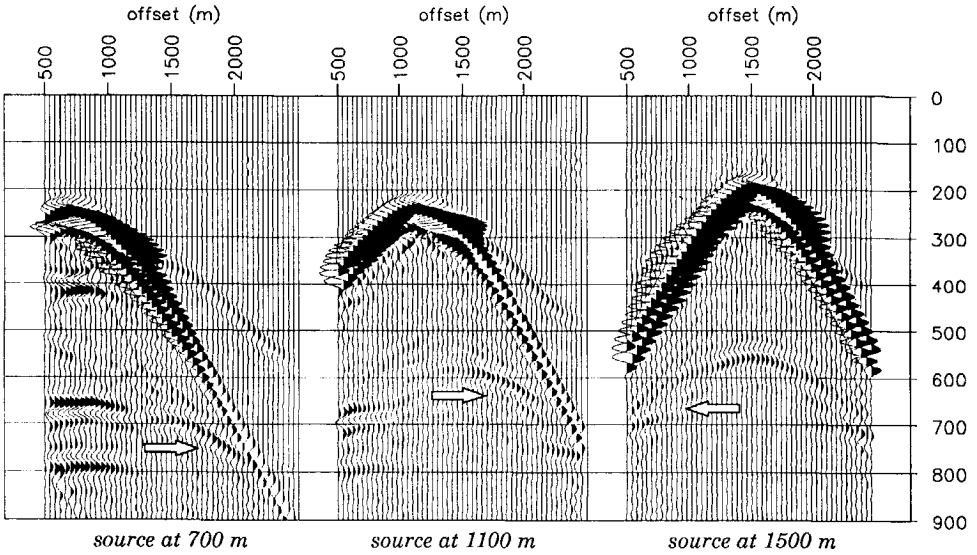

Fig. 4.18 *Shot records of Fig. 4.17 after the adaptive surface-related multiple elimination process.*

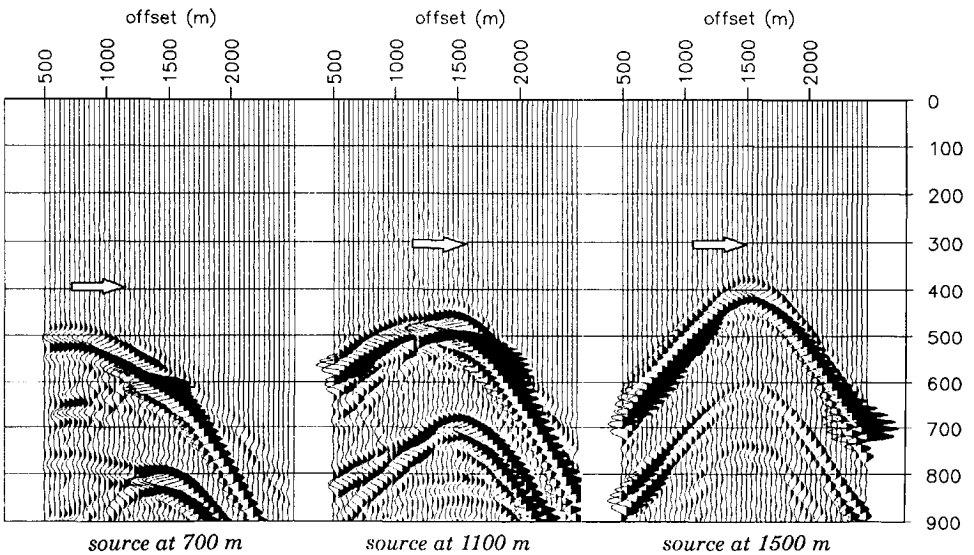

Fig. 4.19 *Difference between the shot records before (Fig. 4.17) and after (Fig. 4.17) surface-related multiple elimination, showing the multiples that have been eliminated.*

As the multiple elimination process has been carried out adaptively, the source wavelet has been estimated as well. Fig. 4.20a shows the zero phase cosine square wavelet from 0 to 40 Hz that was used to simulate the data of Fig. 4.16. For the estimation of the wavelet, 5 definition points have been used at 10, 15, 20, 25 and 30 Hz. Within this band the surface operator $A(\omega)$ has been estimated and, assuming a surface reflectivity of -1, this estimate yields also the inverse source wavelet. After band-limited inversion of this wavelet, and adding a smooth extension from 0 to 10 Hz and from 30 to 40 Hz, Fig. 4.20b shows the result. The wavelet has been recovered very well. The different amplitude values are due to the fact that the finite difference modeling introduces a scale factor. When wavelet deconvolution is applied, the result represents a band-limited true amplitude impulse response. Note that the zero phase property of the wavelet has not been put in the optimization as a constraint.

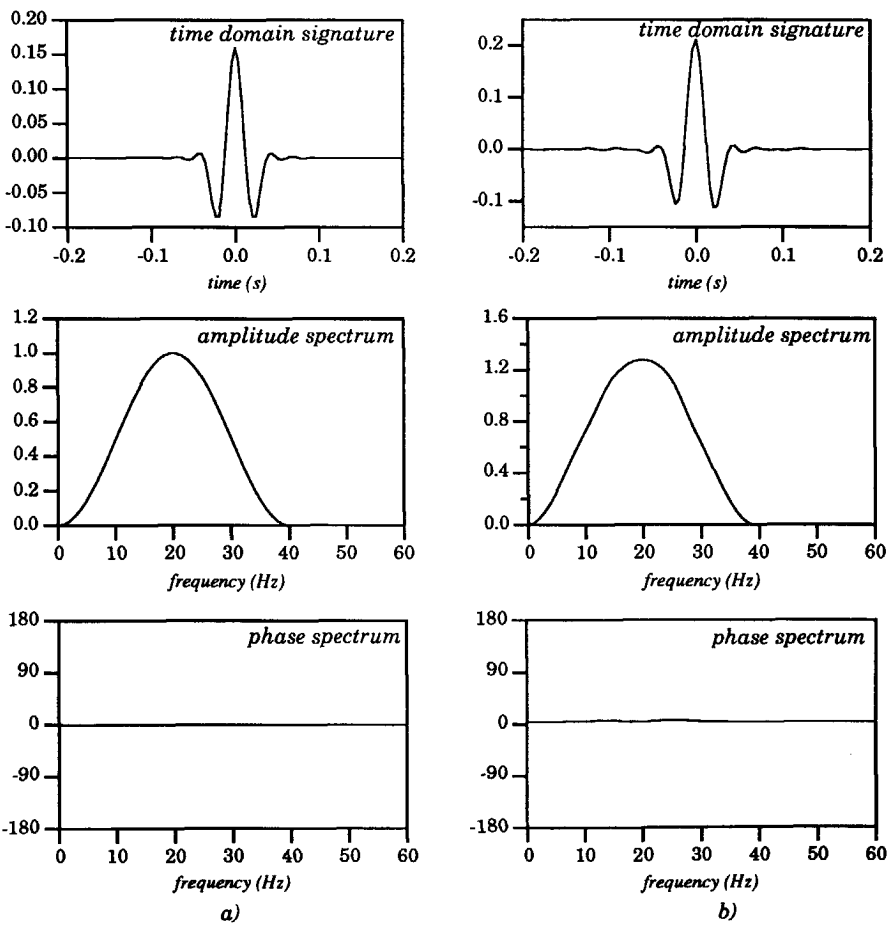

Fig. 4.20 a) Wavelet that was used to model the data of Fig. 4.16 b) Wavelet estimated by the adaptive multiple elimination procedure.

4.3 ELASTIC MODEL

4.3.1 The subsurface model and the acquisition parameters

In this section we consider a subsurface model (Fig. 4.21) for which both acoustic and elastic finite difference modeling has been applied. For the acoustic modeling the S-wave velocities are set to zero and the density is taken constant. On these simulated data sets single- and multi-component multiple elimination has been applied.

At the free surface 128 shot records with a spacing of 16 meters have been simulated. The seismic wavelet is a zero phase Ricker wavelet and is shown in Fig. 4.22. For the acoustic simulation the receiver sampling has been chosen to be 16 m. The pressure sources and pressure receivers are at a depth of 4m. For the elastic simulation 8 m receiver spacing has been used, to be able to remove the groundroll in the k_x-ω domain without aliasing. The stress sources and velocity receivers are located at the surface.

layer	P-wave velocity (m/s)	S-wave velocity (m/s)	Density (kg/m^3)
1	2400	1400	1000
2	3000	2000	1600
3	3000	2000	2100
4	4100	2200	2200
5	3700	2000	2300
6	4200	2400	2000
7	3500	2100	1800

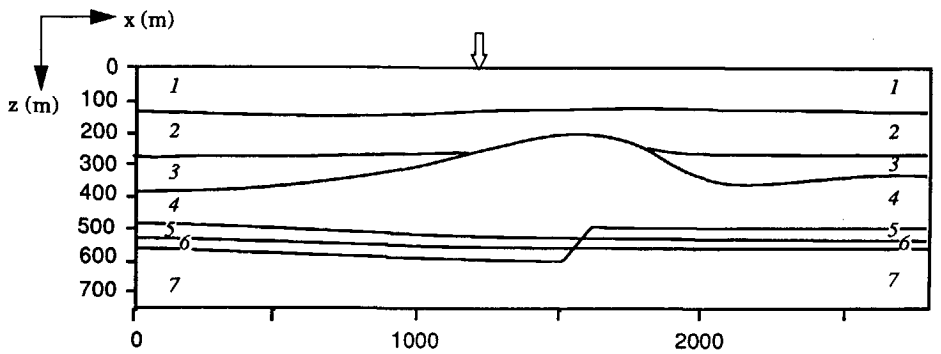

Fig. 4.21 Lateral inhomogeneous subsurface model used for acoustic and elastic finite difference simulations. The arrow indicates the shot position for which the results are shown.

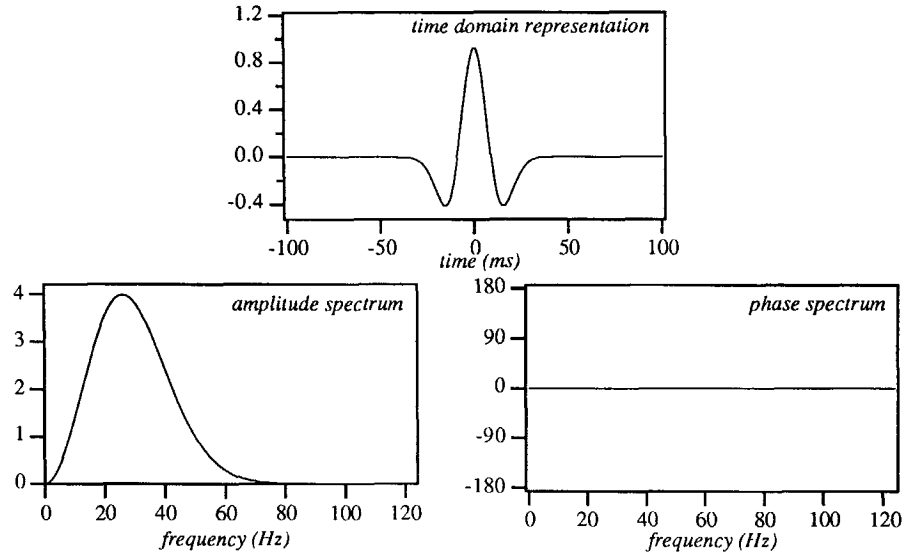

Fig. 4.22 *Zero phase Ricker wavelet used for simulating the acoustic and elastic data in the model of Fig. 4.21.*

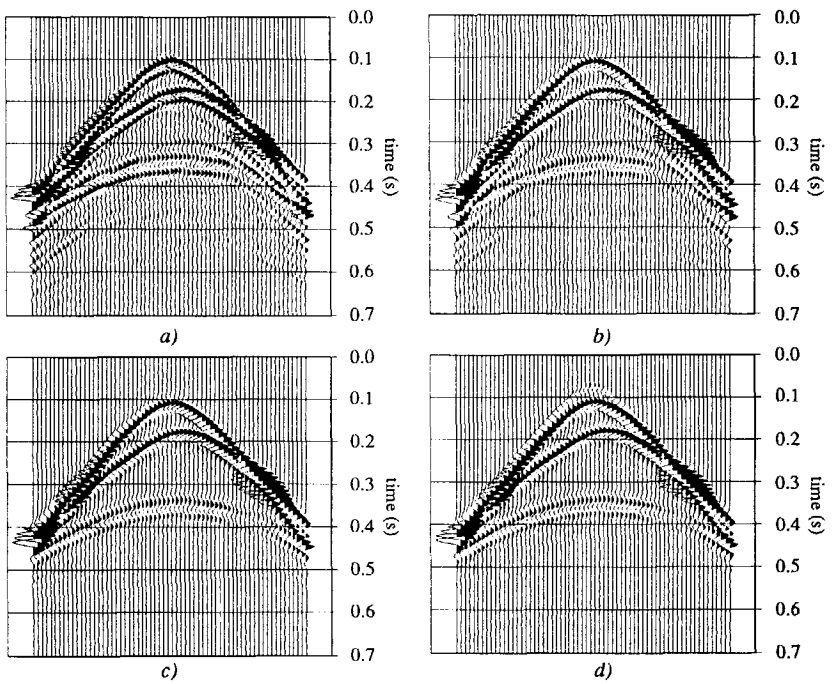

Fig. 4.23 *a) Acoustic shot record simulated for the subsurface model of Fig. 4.21 with the source positioned at the arrow b) Shot record after decomposition into upgoing waves c) Shot record after adaptive multiple elimination d) Shot record simulated without surface-related multiples.*

4.3.2 Processing of acoustic single-component data.

Fig. 4.23a shows the acoustic shot record with the source at the position indicated with the arrow in Fig. 4.21. Before applying adaptive multiple elimination we have to transform the total pressure at 4 m depth into the upgoing pressure wave field at the free surface. This is done with the acoustic decomposition procedure as described in section 3.2. After the decomposition the wavelet and the amplitude versus offset have changed as can be seen in Fig. 4.23b. For the source a monopole positioned just below the surface was used, which yields a dipole at the free surface. Therefore no decomposition has been applied at the source side. Next, the acoustic adaptive multiple elimination process has been applied. Fig. 4.23c shows the result. To check whether the output corresponds to a shot record without the influence of the free surface, the same shot record has been simulated without surface-related multiples. The result is displayed in Fig. 4.23d, which shows a very good agreement with Fig. 4.23c. The surface-related multiples are not strong as the acoustic subsurface reflectivity is small. For the *adaptive* multiple elimination process 4 definition points at 10, 20, 30, 40 Hz have been used to estimate the wavelet. Via a spline interpolation the estimated real and imaginary part has been computed for all frequencies. Fig. 4.24 shows the estimated source wavelet, which is in good agreement with the original wavelet of Fig. 4.22. Note that the zero phase property of the original wavelet has not been used as a constraint in the optimization.

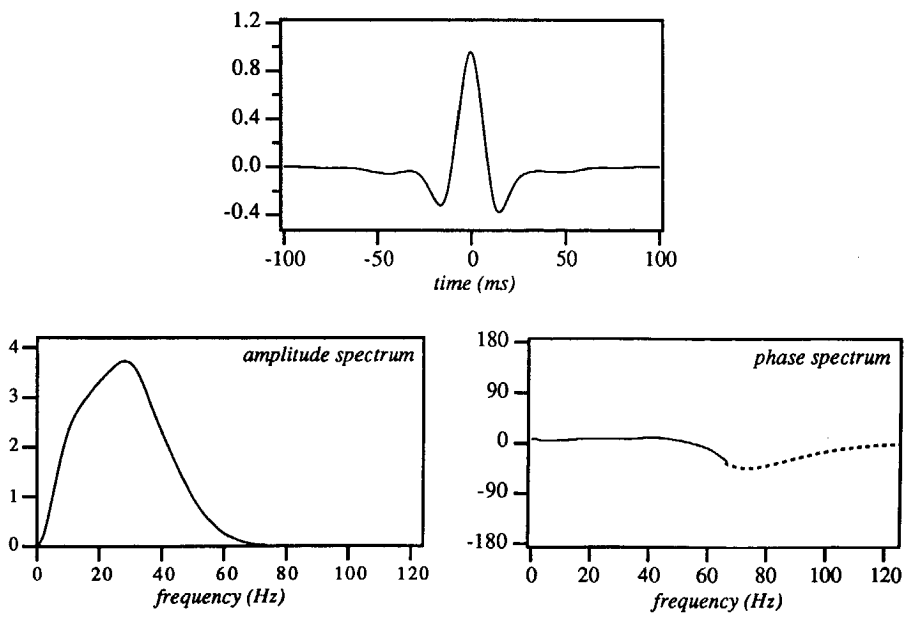

Fig. 4.24 Estimated wavelet after acoustic multiple elimination.

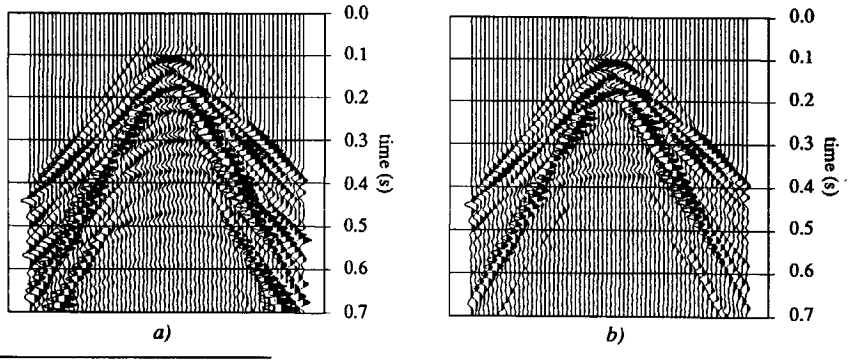

Fig. 4.25 a) Elastic single-component shot record (V_z) simulated with a vertical vibrator at the position indicated in Fig. 4.21 b) Single-component shot record after adaptive acoustic multiple elimination.

4.3.3 Processing of elastic single-component data

The subsurface model of Fig. 4.21 (including the S wave velocities) has also been used to model a multi-component seismic dataset with an *elastic* finite difference modeling scheme. At each source position two types of sources were modeled: one vibrator oriented in the x- and one in the z- direction. For each source type the x- and z-component of the particle velocity at the free surface has been recorded, yielding four datasets.

Before applying full elastic multiple elimination, we consider the conventional single-component land data set: the shot records with the z-component of the particle velocity due to a vertically oriented vibrator. For the source position indicated in Fig. 4.21 the single-component elastic shot record is shown in Fig. 4.25a. The groundroll has already been removed from this shot record. As expected, by introducing elastic effects the shot records looks far more complicated compared to the acoustic situation (Fig. 4.23a). The multiples are stronger and a lot of converted events can be seen.

Application of the *acoustic* adaptive multiple elimination procedure yields the shot record of Fig. 4.25b. Note again that in order to achieve the result for one shot record, all other shot records have to be taken into account. Note also that even with *acoustic* multiple elimination, surface-related multiples of *both* P- and S-wave events have been reduced. They are not removed completely due to the fact that with acoustic multiple elimination the data is considered to have amplitudes for an acoustic medium with a free surface reflectivity that is equal for all wave types. This means that the surface-related multiples cannot be perfectly eliminated and surface related conversions cannot be taken into account at all. The estimated wavelet is shown in Fig. 4.26 and, as a pleasant surprise, it agrees very good with the original wavelet (Fig. 4.22), except for an overall scaling factor. This means that the source wavelet can still be estimated with an *adaptive* acoustic multiple elimination procedure applied on single-component land data.

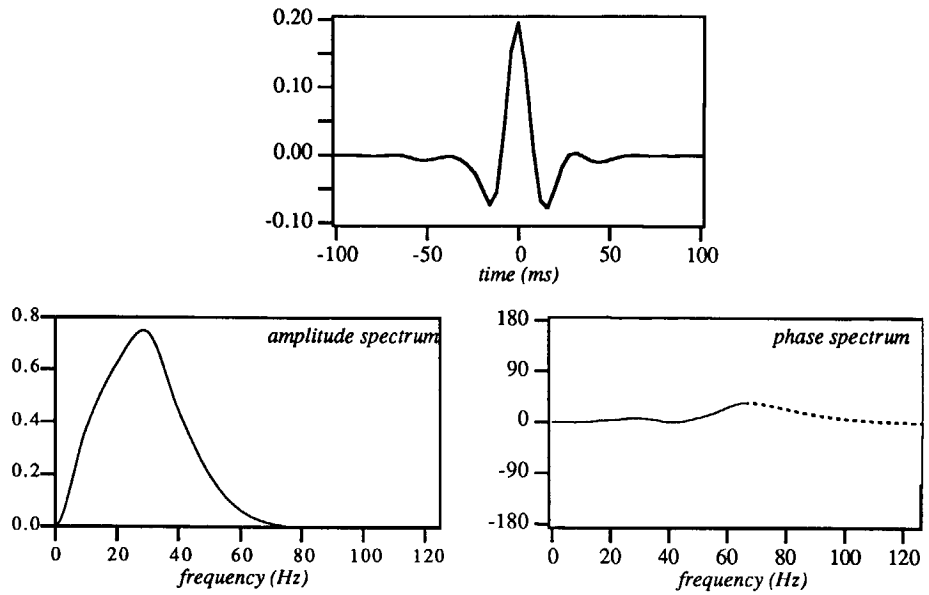

Fig. 4.26 Estimated wavelet after acoustic multiple elimination of T_{zz}-V_z data.

4.3.4 Processing of elastic multi-component data

Finally, the multi-component data set as described in section 4.3.3 is used to apply the *multi-component* adaptive surface-related multiple elimination procedure. Fig. 4.27 shows a multi-component shot record (4 shot records) at the source position that has been indicated in Fig. 4.21. The two sources generate the horizontal and vertical traction, T_{xz} and T_{zz}, at the surface. The responses of these two source types are registered with multi-component geophones, measuring the horizontal and vertical component of the particle velocity field, V_x and V_z, at the surface.

In those shot records the groundroll is clearly visible. It should be removed in a first processing step. In this example, the spatial sampling allows elimination in the k_x-ω domain; Fig. 4.28 shows the result. As expected, the groundroll has been well removed and the other events have not been destroyed.

Before applying the multiple elimination process the multi-component data has to be transformed into upgoing wave fields. According to Chapter 2 and 3 several descriptions for the upgoing wave fields can be chosen. For this example, a description in terms of upgoing P- and S-wave potentials has been used.

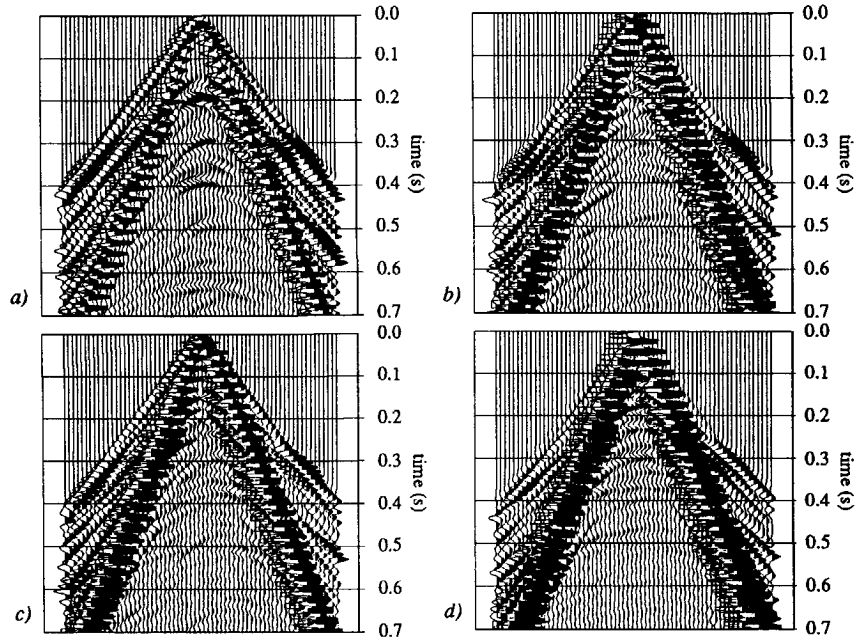

Fig. 4.27 Multi-component shot record with groundroll at the position indicated in Fig. 4.21. a) T_{xx}-V_x data b) T_{zz}-V_x data c) T_{xz}-V_z data d) T_{zz}-V_z data.

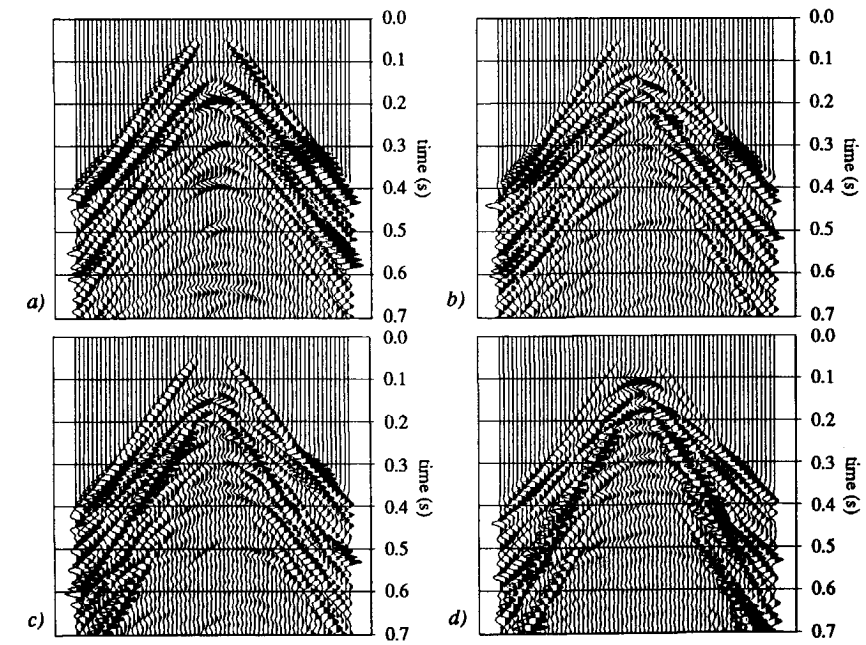

Fig. 4.28 Multi-component shot record of Fig. 4.27 after groundroll removal. a) T_{xx}-V_x data b) T_{zz}-V_x data c) T_{xz}-V_z data d) T_{zz}-V_z data.

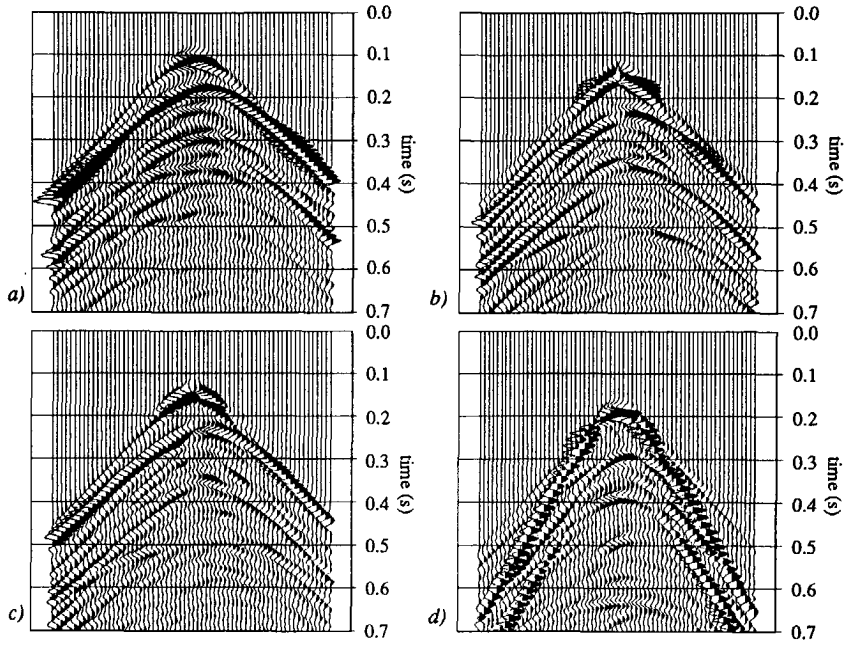

Fig. 4.29 *Multi-component shot record of Fig. 4.28 after decomposition into one-way P- and S-waves. a) P-P data b) S-P data c) P-S data d) S-S data.*

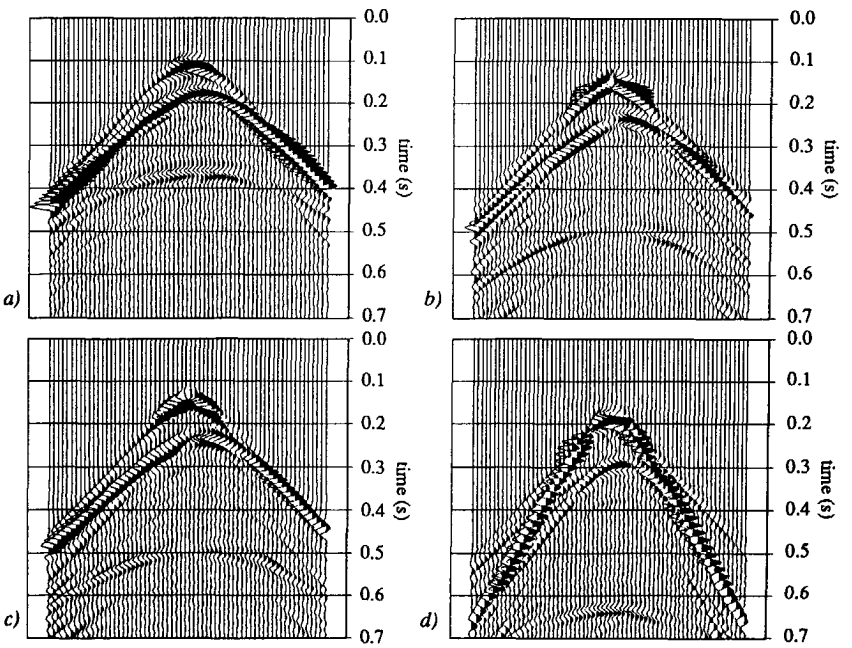

Fig. 4.30 *Multi-component shot record of Fig. 4.29 after elastic surface-related multiple elimination. a) P-P data b) S-P data c) P-S data d) S-S data.*

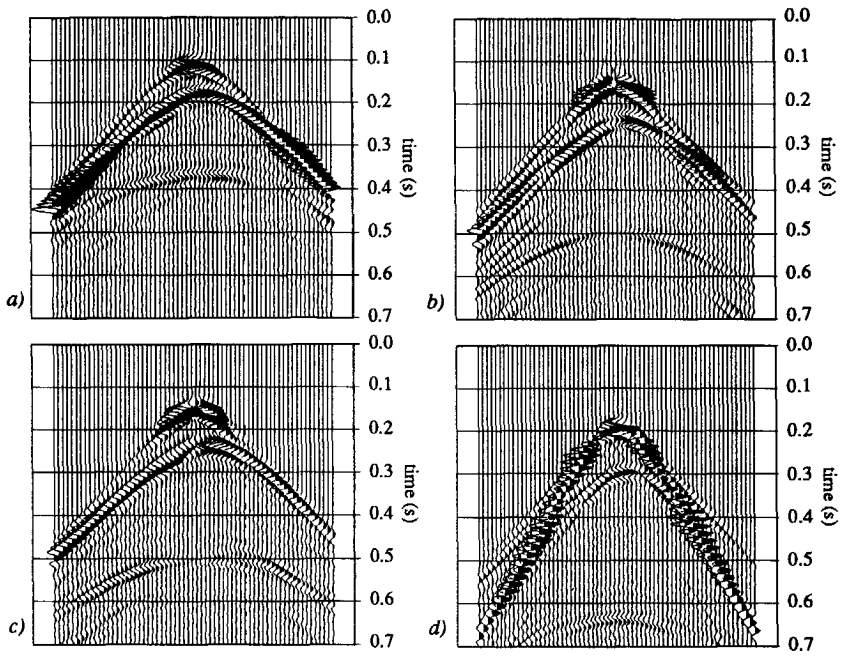

Fig. 4.31 Multi-component shot record related to the subsurface model of Fig. 4.21, simulated with an absorbing surface. a) P-P data b) S-P data c) P-S data d) S-S data.

This choice means that at the receiver positions decomposition from the total particle velocity components into pure upgoing P- and S-wave responses should be accomplished. In addition, at the source side the downgoing traction wave fields should be transformed in downgoing P- and S-wave source wave fields. The receiver decomposition can be applied in common shot gathers. For the decomposition at the source positions the shot records have to be reordered into common receiver gathers. For both decomposition operations, all single-component sub records are needed to do the decomposition. In fact, looking to decomposition in the k_x-ω domain, decomposition is a weighted addition of the single-component terms (see also Wapenaar et al. (1990) or Appendix B). Fig. 4.29 shows the multi-component shot record after decomposition into upgoing P- and S-wave responses due to downgoing P and S source wave fields.

Next, the elastic adaptive surface-related multiple elimination process is applied, taking into account the elastic reflectivity matrix of the free surface. The multi-component shot record after adaptive multiple elimination is shown in Fig. 4.30. Note that also surface related *conversions* have been eliminated. For comparison, the multi-component shot record at the same source position has been simulated with a fully absorbing surface and with pure P and S wave sources. The result of this modeling exercise is shown in Fig. 4.31. The differences between the multi-component data after surface-related multiple elimination and the simulated data

with the absorbing surface are very small. It proves that both the decomposition process and the elastic multiple elimination process have performed very well.

The multiple elimination process has been applied in an adaptive way, meaning that the source wavelet in the data is estimated as well. The wavelet optimization has been done in two steps: firstly doing the optimization for the data related to the P wave sources and secondly doing the optimization for the data related to the S wave sources. This yields two estimated source wavelets, one for the P wave source and one for the S wave source. Both source wavelets have been chosen identically in the modeling (Fig. 4.22). The result of the estimation process is given in Fig. 4.32. Both estimated wavelets show a good agreement with the true wavelet, although the S source wavelet has a small amplitude mismatch.

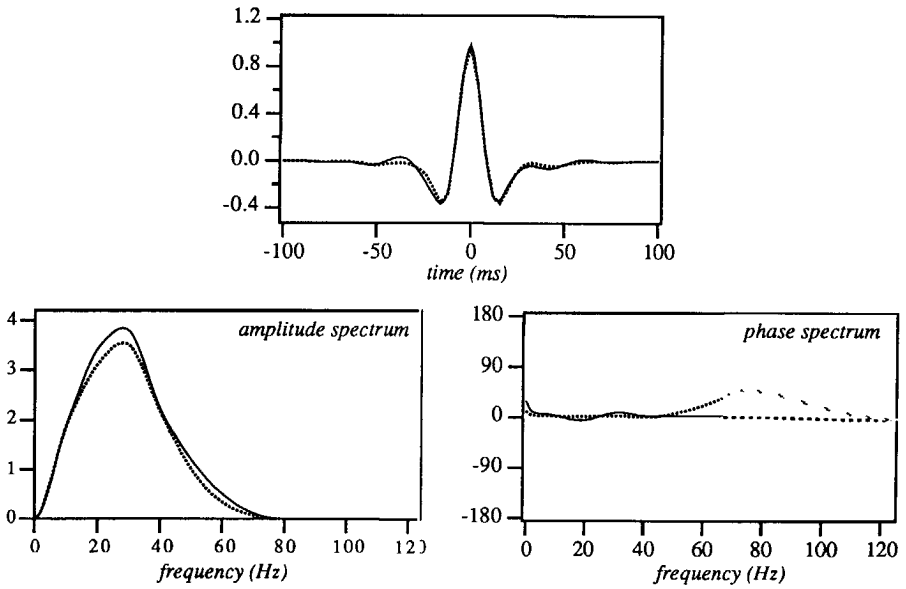

Fig. 4.32 Estimated wavelet after elastic multiple elimination of multi-component data. The solid line is the P-wave estimated wavelet, the dashed line the S-wave estimated wavelet.

5

FROM SIMULATED DATA TO FIELD DATA, PRACTICAL CONSIDERATIONS

Going from simulated data to field data is not a trivial step. When applying the multiple elimination method on field data, several problems are encountered, which are not present in the simulated examples. Most of them are caused by the way seismic acquisition takes place; however, also important is the fact that we live in a 3D world in stead of a 2D finite difference grid.

In this chapter problems are addressed that may be encountered when working on field data.

5.1 MISSING OFFSETS

The theory of the surface-related multiple elimination method has been set up for infinite offsets in order to perfectly predict the multiples from the measured primary and multiple information.

The "infinite" offset range is never met in reality, as measurements are only done for a limited number of offsets. Typically, 100 to 250 offsets in one lateral direction are used per shot record experiment.

In Chapter 3 it has been discussed that each trace in the data acts as a Huygens source signature, which generates a Huygens contribution to the multiple field in the next Taylor term. For any trace missing in the input data, a Huygens source response is missing in the next Taylor

term.The range of offsets that is influenced by the missing traces will increase for each higher order Taylor term.

For the influence of missing offsets three cases will be distinguished (Fig. 5.1):

- Missing near offsets, i.e. the offset gap between the source and the first receiver position.
- Missing or bad traces within a shot.
- Missing far offsets, i.e. the "gap" between the last receiver position and infinity.

In the next sections the influence of each of these missing offsets on the multiple elimination result are further evaluated.

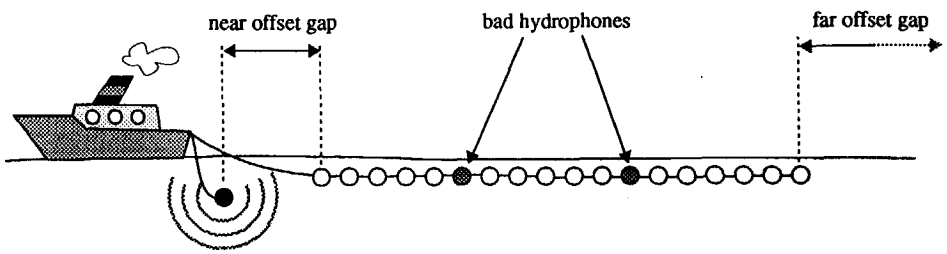

Fig. 5.1 Three situations for missing offsets can be distinguished: missing near offsets, missing intermediate offsets and missing far offsets.

5.1.1 Missing near offsets

The near offset gap has the largest influence on the multiple elimination procedure. For marine acquisition it is typically in the order of 50 to 200 m; for land data a typical number is 200 to 400 m. Missing near offsets are due to practical considerations. In marine acquisition it is difficult to keep the streamer down in the water close to the vessel when it is moving. Also hydrophones close to the source and vessel suffer from a lot of noise, resulting in bad traces. In land acquisition the geophones near the source suffer from a lot of shot generated noise.

Missing near offset information will harm the multiple prediction severely for a much larger offset range than the missing offset gap itself. This is because the missing offset problem is actually a missing angle problem. To show this, let us consider the configuration of Fig. 5.2, where a flat reflector situation is sketched. All primary information until angle α is missing.

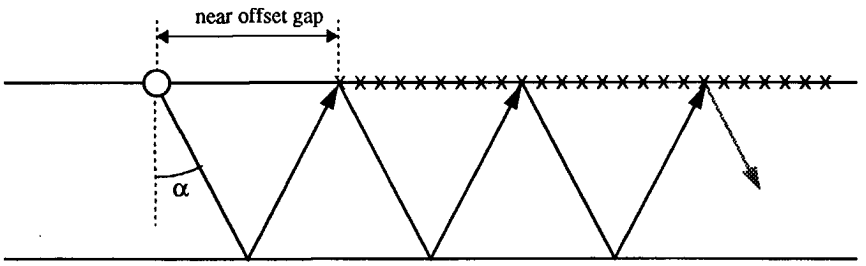

Fig. 5.2 Energy emitted under the same angle moves to the far offsets for each multiple event.

This means that multiple information until angle α can not be predicted. For the first order multiple, this means that an offset range of roughly twice the near offset gap cannot be predicted, for the second order multiple three times the offset gap etc. So with the measured primary information, only part of the measured multiples can be predicted. From Fig. 5.2 it is clear that angle α increases when the first reflector is shallower. For example, a reflector depth of 150 m and an offset gap of 150 m yields 27° of missing primary information. If the depth is only 50 m, the primary data is missing until 56°. This problem has already been mentioned in Chapter 2 and 3 when describing the thin surface layer situation.

Apart from the missing predicted multiples for the small offsets, edge effects will occur when predicting the recoverable part of the multiple events. These edge effects can be easily understood if we consider the missing Huygens source responses for the near offsets.

The above limitations are illustrated with a simple example. Consider the shot record of Fig. 5.3a, where for one reflector at a depth of 150 m data has been simulated. In Fig. 5.3a the primary and 3 multiples are visible. As there are 3 multiples present, 4 terms of the Taylor series have been generated, the shot record itself being the first term. Fig. 5.3b and c show the second and third Taylor term respectively. The Taylor terms are used the adaptive surface-related multiple elimination procedure, which results in the multiple free gather of Fig. 5.3d. The multiple elimination process has been very successful; all multiple energy has been removed. With the adaptive multiple elimination procedure the original (0-60 Hz cosine square) wavelet could be fully recovered, as shown in Fig. 5.3e and f. Note that the zero phase property has not been used in the optimization process.

On this shot record a 150 m near offset gap (to both sides of the gather) has been imposed. The shot record with the gap is shown in Fig. 5.4a. For this modified shot gather (and using the fact that all other shot records of this medium have the same gap) the terms of the Taylor series have been generate. Fig. 5.4b shows the second order term, in which two effects can be observed.

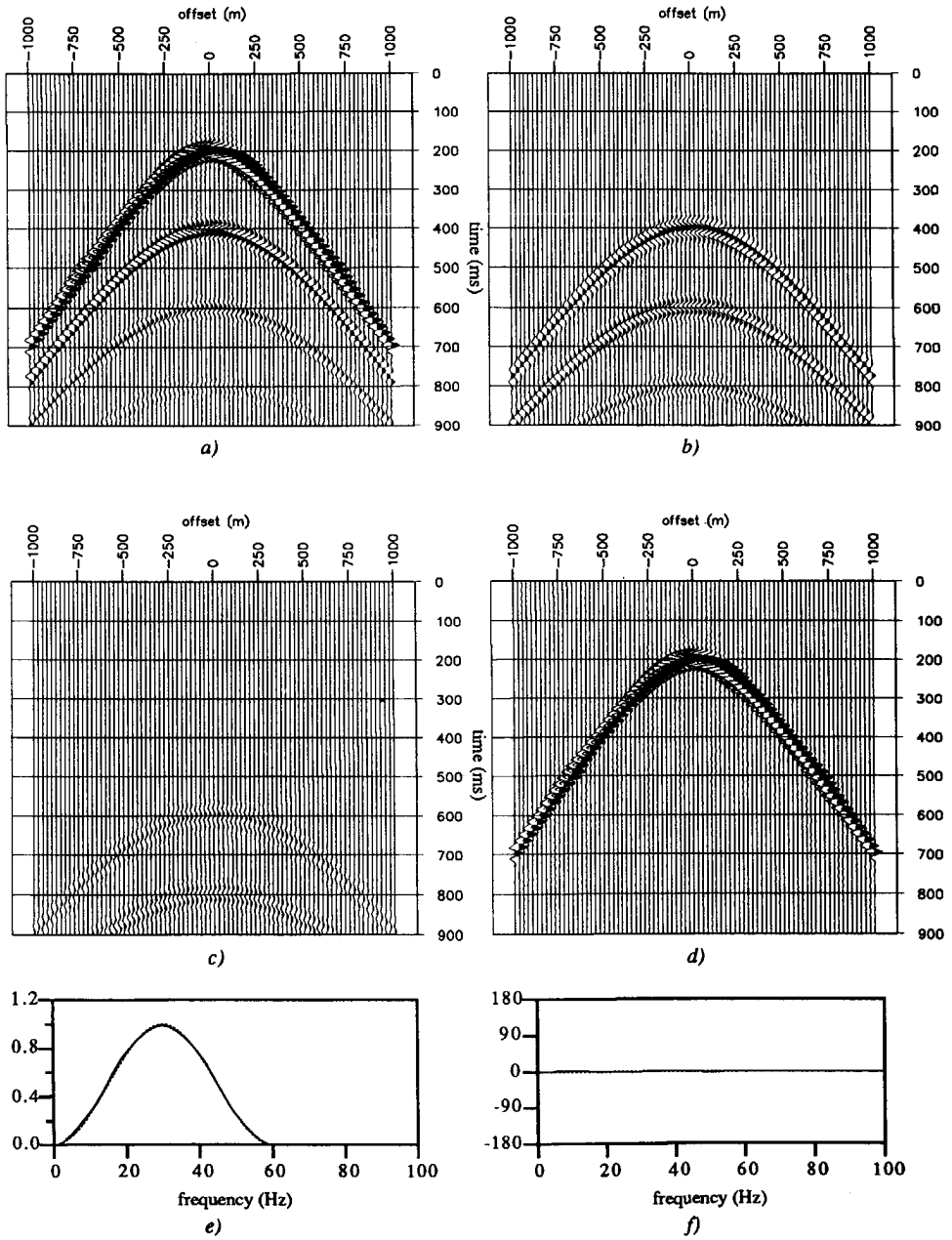

Fig. 5.3 *a) Shot record of a one-reflector model (150 m depth) containing a primary and 3 multiples b) Second term of the Taylor series c) Third term of the Taylor series d) Shot record after adaptive multiple elimination e) Amplitude spectrum of the original (dashed line) and estimated wavelet (solid line) f) Phase spectrum of the original (dashed line) and estimated wavelet (solid line).*

Firstly, for the predicted multiples the near offset gap has grown to about twice the original gap. Secondly, edge effects can be observed due to the sudden stop of data in the gap, see the arrow in Fig. 5.4b. These effects can be explained if we consider the part that is missing in the second term, i.e. the Huygens responses of the near offset traces. These missing responses are shown in Fig. 5.4c. The summation of Fig. 5.4b and Fig. 5.4c will yield the perfect second Taylor term (Fig. 5.3b). Fig. 5.4d shows the third order term of the Taylor series. It can be clearly observed from the Taylor terms that the higher the order of the predicted multiples, the larger the detrimental effect. In other words, the near offset gap propagates to the larger offsets. Apart from this growing gap, truncation effects can be observed (indicated with arrows in Fig. 5.4b,c,d).

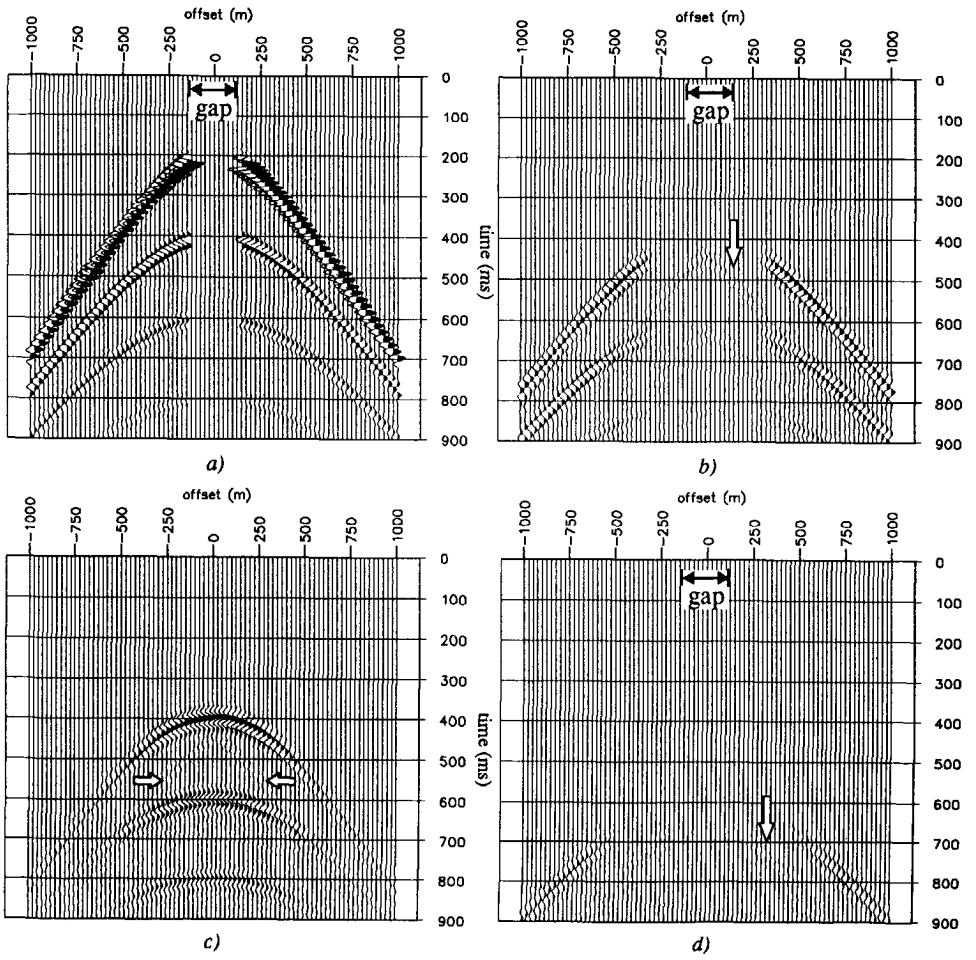

Fig. 5.4 *a) Shot record of Fig. 5.3a with a near offset gap of 150 m b) Second term of the Taylor series c) Huygens responses of the missing near offset traces in the second Taylor term d) Third term of the Taylor series. The arrows point at edge effects due to the sudden stop of data in the near offset gap (rectangular truncation window).*

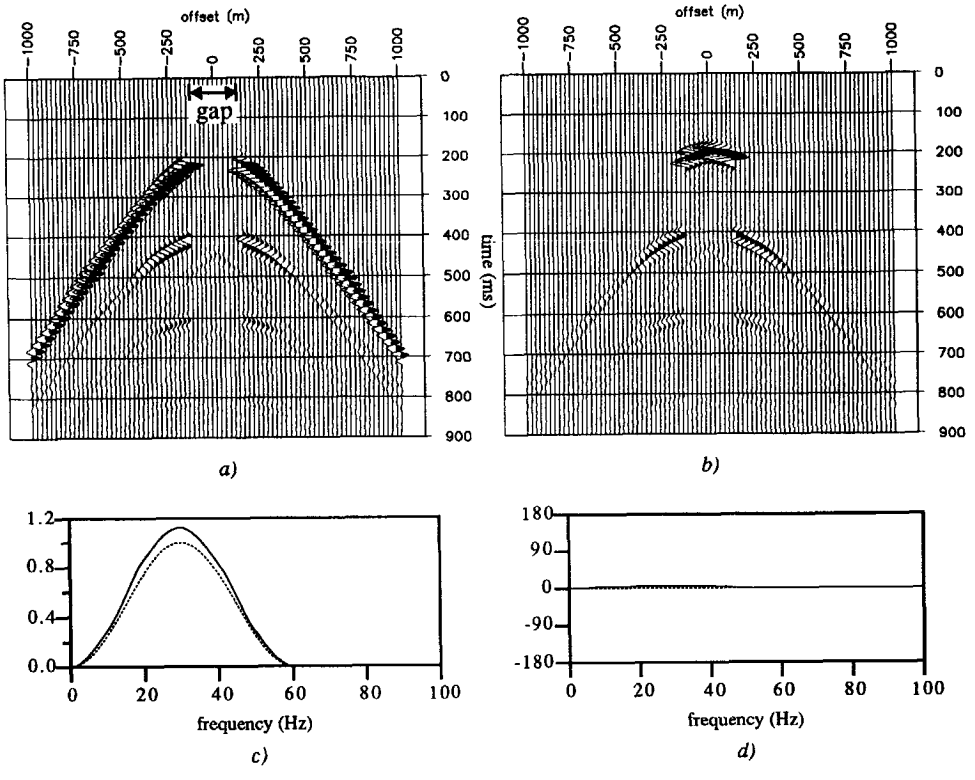

Fig. 5.5 *a) Shot record after adaptive multiple elimination b) Difference between result a) and the perfect multiple elimination result (Fig. 5.3b) c) Amplitude spectrum of the original (dashed line) and estimated wavelet (solid line) d) Phase spectrum of the original (dashed line) and estimated wavelet (solid line).*

When the Taylor terms are used in the adaptive multiple elimination process, Fig. 5.5a is the result. As expected, the multiples have been removed at the larger offsets, but at the small offset range they have not been suppressed at all. In addition, extra events due to the edge effects have been introduced there. For comparison Fig. 5.5b shows the difference between the perfect result without missing near offsets (Fig. 5.3d) and the result with the missing near offsets (Fig. 5.5a), i.e. the contribution of the Huygens sources of the near offsets only. All edge effects in the result of Fig. 5.5a can be indicated in those Huygens source responses. Looking at the wavelet estimation result, shown in Fig. 5.5c and d, the original wavelet could be surprisingly well recovered. Only an overall scaling factor in the amplitude spectrum is left in the wavelet.

The way to overcome the near offset problem is to apply interpolation. For the field data examples used in Chapter 7, the following procedure for interpolating the near offset traces has been used (see also Fig. 5.6):

- Reorder the data into common midpoint gathers and apply the reciprocity principle.
- Apply NMO correction using the stacking velocities of the *strongest* events (not necessarily primaries).
- Smooth the data in the offset direction to remove fast amplitude variations.
- Fill the data in the gap using a cubic spline interpolation from the nearest offset traces per time sample. For the derivatives of the splines the amplitude trend of the smoothed traces in the offset direction at both sides of the gap is extracted by finite difference derivatives. The interpolation might also be applied in the frequency domain.
- Place the interpolated traces in the unsmoothed, NMO corrected CMP gather and repeat the smoothing and interpolation procedure until the result is stable.
- Apply inverse NMO correction to the final interpolation outcome, and insert the result in the original CMP gather.
- Reorder the interpolated CMP gathers into shot records (if desired).

To the data of Fig. 5.4 the interpolation procedure has been applied. Fig. 5.7a shows the CMP gather (which is for a 1D medium identical to the shot record) after NMO correction. Fig. 5.7b gives the final result after three smoothing and interpolation steps. Those traces are inverse NMO corrected and inserted in the gap of the original CMP gather, see Fig. 5.7c. On this interpolated CMP gather the adaptive multiple elimination is applied, yielding a multiple free result of Fig. 5.7d. The result is as good as the result without the gap (Fig. 5.3b), except for very small remainings in the (interpolated) near offset traces. The wavelet, that could be recovered with this interpolated data, is equal to the actual wavelet.

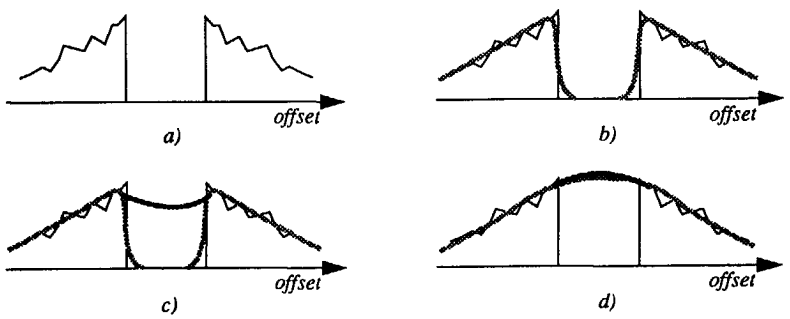

Fig. 5.6 *a) Amplitudes of the NMO corrected CMP data for one time sample. b) Data after lateral smoothing. c) Data after smoothing and first interpolation step. d) Data after smoothing and interpolation after 3 iterations. The gray line shows the smoothed result, the solid line the interpolated result.*

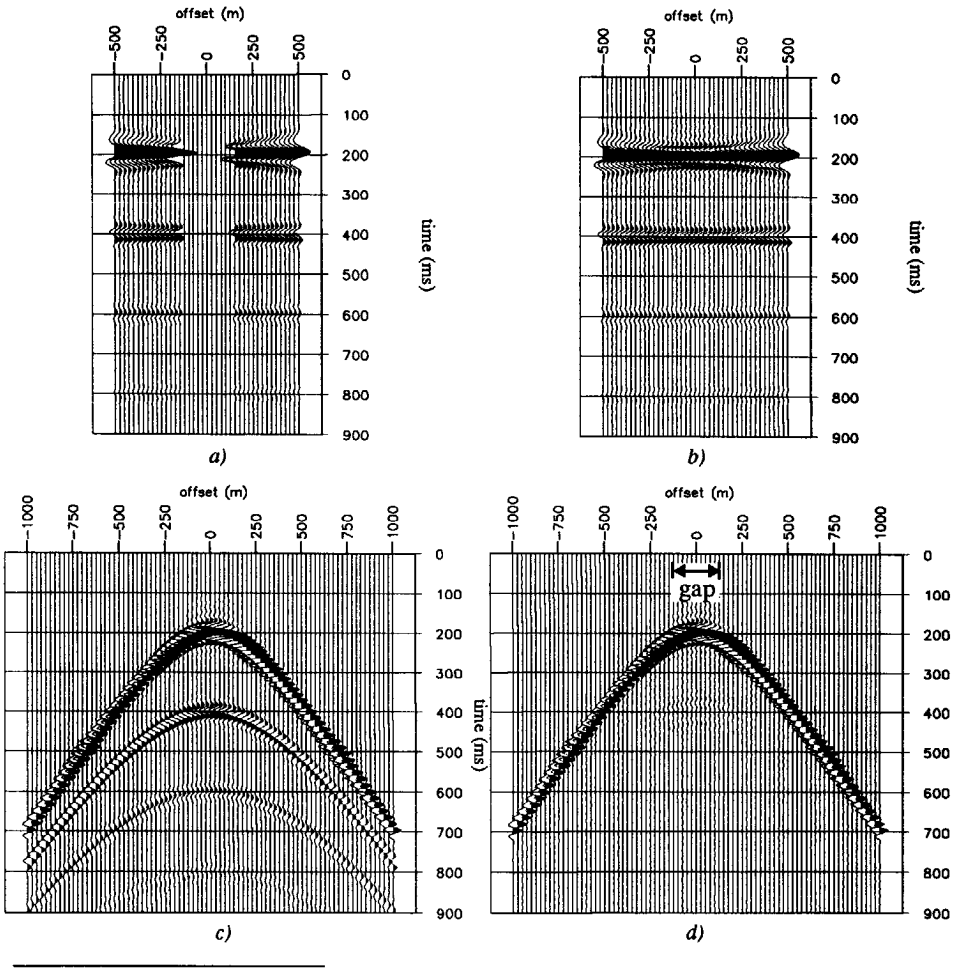

Fig. 5.7 *a) NMO corrected CMP gather related to the shot record of Fig. 5.4 b) NMO corrected CMP gather after interpolation c) Shot record after interpolation of the near offsets d) Interpolated shot record after adaptive multiple elimination.*

Note that the interpolation procedure uses small offsets to predict the missing near offsets. Its application yields therefore satisfactory results if the hyperbolic assumption is valid for the small offset traces (say the first 20 traces) only. This means that in most seismic situations this method can be applied.

For a more complicated example we consider again the subsurface model of Fig. 5.8a, which has already been shown in Fig. 1.2 of Chapter 1. Fig. 5.8b shows the zero offset data corresponding to this model. As can be observed, the subsurface is clearly not one-dimensional and

the reflections are laterally varying due to the pinch out. From all simulated shot gathers, a near offset gap of 150 m has been introduced and the interpolation procedure has been applied. This results in the interpolated zero offset section, which is shown in Fig. 5.8c. The result is very good. Even the grid diffractions could be well interpolated. Also the crossing primary and multiple events could be well handled.

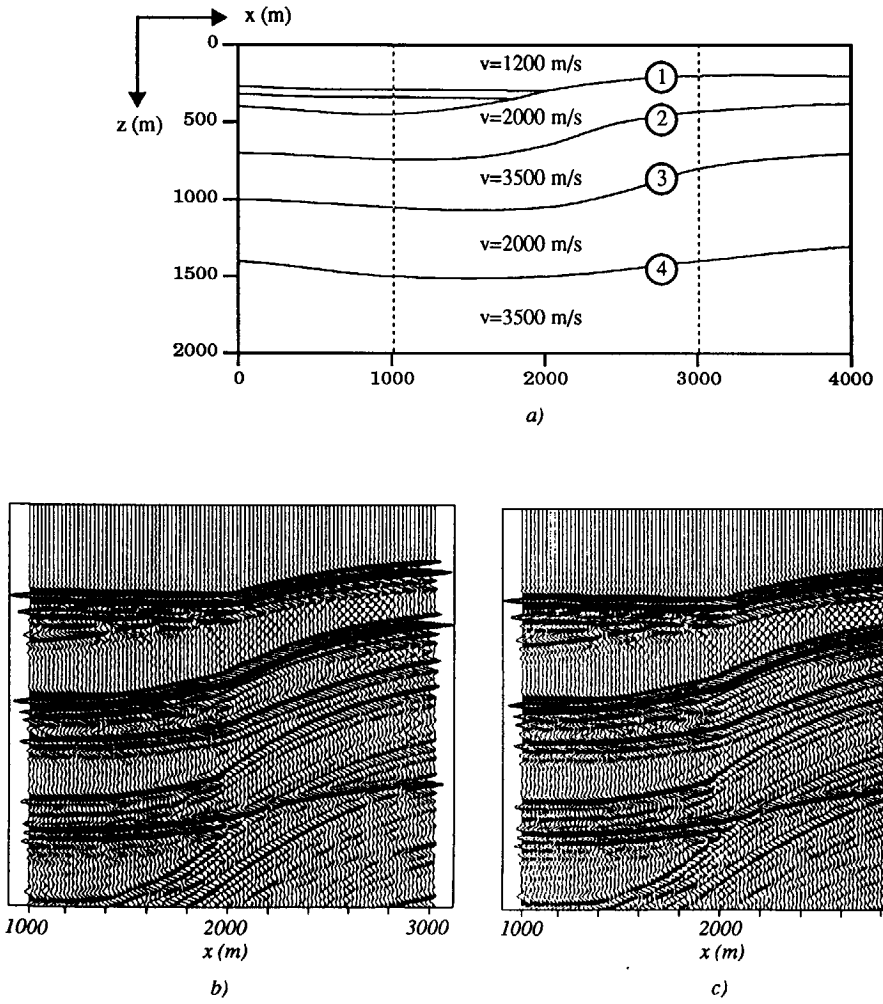

Fig. 5.8 *a) Subsurface model for the simulation of seismic surface data*
b) Zero offset section corresponding to the model of a)
c) Interpolated zero offset section after introducing a 150 m near offset gap in the shot records.

5.1.2 Missing intermediate offsets

During acquisition some channels may produce bad or "dead" traces. Each missing trace within a data gather will produce artifacts in the multiple elimination result. These artifacts are easily explained again if we consider the influence of any missing trace on the multiple elimination result as a missing Huygens source contribution. This is shown in Fig. 5.9, where for the shot record of Fig. 5.3a a trace has been zeroed (at 500 m offset). Fig. 5.9b shows the second term of the Taylor series, assuming that all other shot records have a dead trace at 500 m as well.

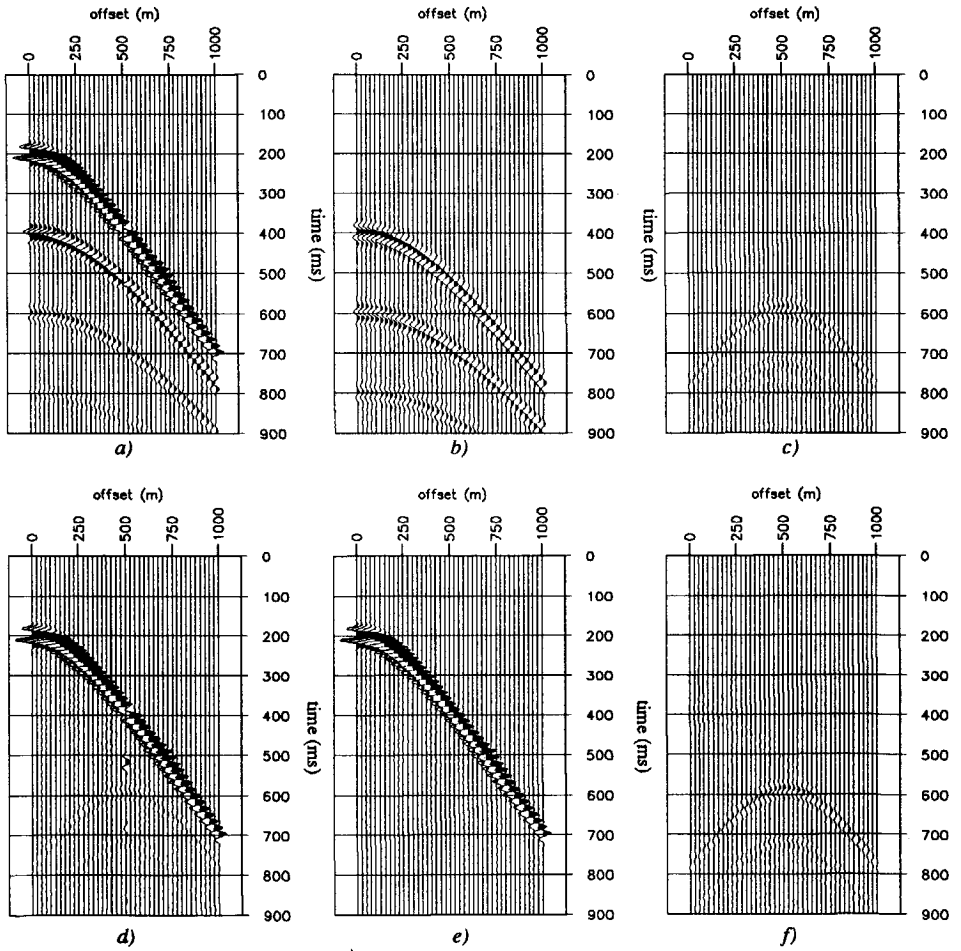

Fig. 5.9 *a) Shot record with a zero trace at 500 m offset b) Second term of the Taylor series c) Missing Huygens source response of second Taylor term d) Result of adaptive multiple elimination e) Perfect result of data without zero trace (identical to Fig. 5.3d) f) Difference between perfect result and result with the missing intermediate trace. c) and f) are scaled with a factor 2 for plotting.*

The second term contains one extra hyperbolic event for each multiple with the apex at the missing offset position. In fact this is one missing Huygens source response due to the missing trace in the shot gather. This is visible in Fig. 5.9c, where the Huygens contribution of the missing trace for the second Taylor term has been displayed. For this shot record the adaptive multiple elimination procedure is applied. The result after adaptive multiple elimination (Fig. 5.9d) looks good, although the missing Huygens source response can be found back in this shot record after multiple elimination. For field data each zero trace will produce such a Huygens response in the data for each order of multiples that is removed. The wavelet estimation did not suffer from the missing offset and the wavelet was recovered perfectly. Note that at the missing trace itself, the multiples are now predicted with a negative sign. For comparison the perfect multiple elimination result (identical to Fig. 5.3d) is shown in Fig. 5.9e, with the difference in Fig. 5.9f. It shows the influence of the missing trace on the total multiple elimination result.

In conclusion, missing intermediate traces should be preferably filled prior to multiple elimination. The interpolation need not be as sophisticated as in the missing near offset situation. Normally a (rough) NMO correction and a linear interpolation of the missing trace from both sides of the "gap" will do well.

For larger gaps methods based on the previously discussed near offset interpolation, or based on correlation at both sides of the gap (see Martinson and Hopper (1990)), or based on the Radon transform (see Darche (1990)) can be used.

5.1.3 Missing large offsets

Missing large offsets are normally not a problem for the multiple elimination procedure. This is due to the fact that the multiple energy tends to move from small to large offsets (as already mentioned in 5.1.1) and, therefore, the measured multiples at the some offset can be predicted with the information at smaller offsets, without using information at larger offsets.
However, the sudden stop of data at large offsets (rectangular truncation window) may introduce edge effects similar to those of the "dead" traces. For the same example under consideration, Fig. 5.10a shows the (right side) of the shot record with an offset limitation of 500 m. On this data the adaptive multiple elimination procedure is applied. The second term of the Taylor series is shown in Fig. 5.10b and the final multiple elimination result is given by Fig. 5.10c. Both in Fig. 5.10b and Fig. 5.10c the edge effect of the limited offset range can be observed (see the arrows). However, the multiples are well suppressed. If these edge effects are severe, due to high amplitudes at the large offsets, a tapering procedure is preferred. For the example under consideration a taper of 15 traces has been applied before multiple elimination. Fig. 5.10d displays the result, showing that the edge effect has been suppressed indeed; small remainings of the multiples are visible at the largest offsets only. It depends on what the user prefers: the edge effects or the small multiple remainings. As expected, the original wavelet could be estimated without noticeable amplitude or phase discrepancies.

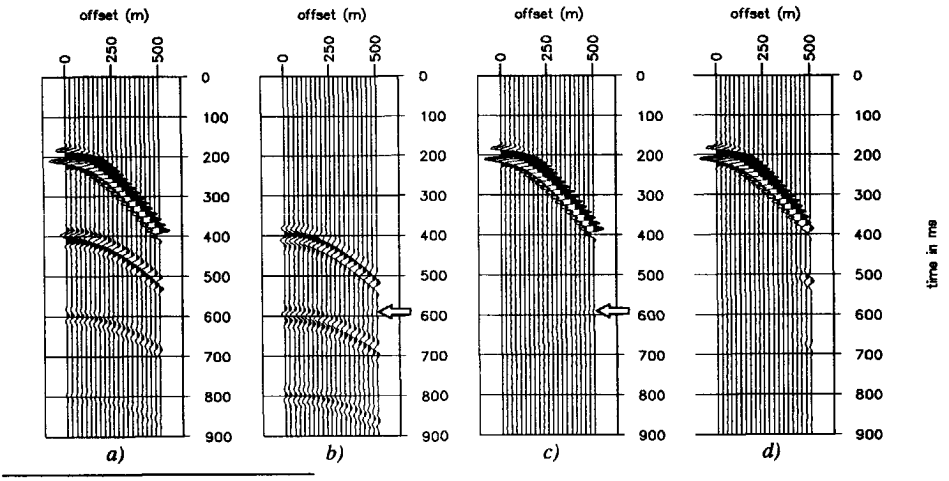

Fig. 5.10 a) Shot record with 500 m maximum offset b) Second term of the Taylor series c) Adaptive multiple elimination result d) Adaptive multiple elimination result after using a 15 trace taper.

In situations with strong dipping subsurface structures, missing large offset data may become a serious problem, similar to missing near offset data. For a geometric explanation see Fig. 5.11, where for a horizontal reflector the multiple at the far offsets can be predicted by the measured primary information at smaller offsets. However, for strongly dipping interfaces there is a turning point. Beyond that point primary energy occurs at larger offset than the corresponding multiple. This can be easily seen by bearing in mind that each reflection against the dipping reflector decreases the angle of propagation with twice the interface dip angle. This means that multiple energy can be measured, although the corresponding primary is not captured within the offset range. If those type of multiples are to be correctly predicted and eliminated, a trace *extrapolation* technique should be used.

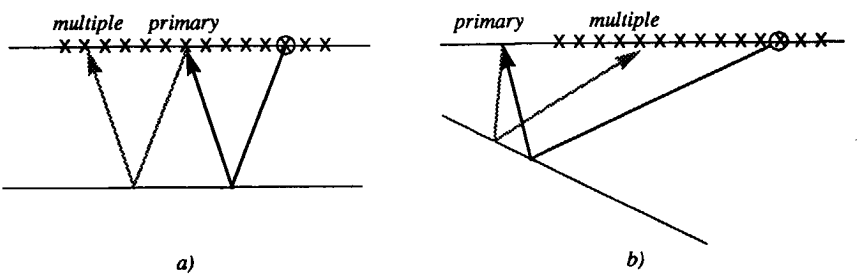

Fig. 5.11 a) For reflectors with small dips, multiple energy is predicted from primary energy at smaller offsets. b) For reflectors with steep dips, some of the multiple energy must be predicted from primary energy at larger offsets.

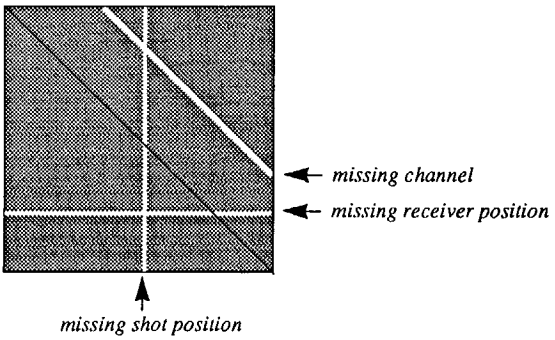

Fig. 5.12 *The problem of missing data should be looked at in terms of the data matrix. It shows that missing receiver and missing shot positions give rise to similar problems.*

5.1.4 Missing shot and receiver positions

In practical situations complete shot records may be of unacceptable quality or totally missing. However, for surface-related multiple elimination the problem of missing a shot position is similar to the problem of missing a receiver position. To explain this, consider the data matrix as shown in Fig. 5.12. A missing shot position or a missing receiver position has a comparable influence on the matrix multiplication result, as the data is multiplied with itself, yielding combinations of rows with columns. In fact there will be a missing Huygens source response in the next Taylor term if an input Huygens source trace is missing at a certain offset, or if the corresponding shot record at that position is missing. Actually, if the missing shot position is identical to the missing receiver position the effects are identical. Note that the already discussed missing intermediate offsets is in fact a missing channel problem (Fig. 5.12).

5.1.5 Aliasing effects

Like most of the pre-stack processing methods, also the surface-related multiple elimination method is sensitive to aliasing. The data used to do the multiple elimination procedure should satisfy the temporal and spatial aliasing criteria *in both shot and receiver direction!* As the data matrix is multiplied with itself, this is only possible if the shot and receivers have the same spatial sampling interval. This requirement can also be seen with the Huygens source principle: a shot record is needed at each trace position, which is not satisfied in situations with unequal source and receiver spacing. Therefore, shot records should be interpolated to arrive at the same sampling density of sources and receivers. This can be easily achieved on NMO corrected CMP gathers (see Berkhout (1984)).

The procedure is as following:

- Reorder the shot records into CMP-gathers and apply a (rough) NMO correction, reducing the curvature in the events. This results in a larger allowable spatial sampling interval.
- Apply a double Fourier transform and pad zeroes in the wave number domain, resulting in a spatial interpolation.
- Apply an inverse double Fourier transform and remove the NMO correction from the interpolated CMP-gathers; the interpolated shot records can be acquired after reordering of the CMP-gathers.

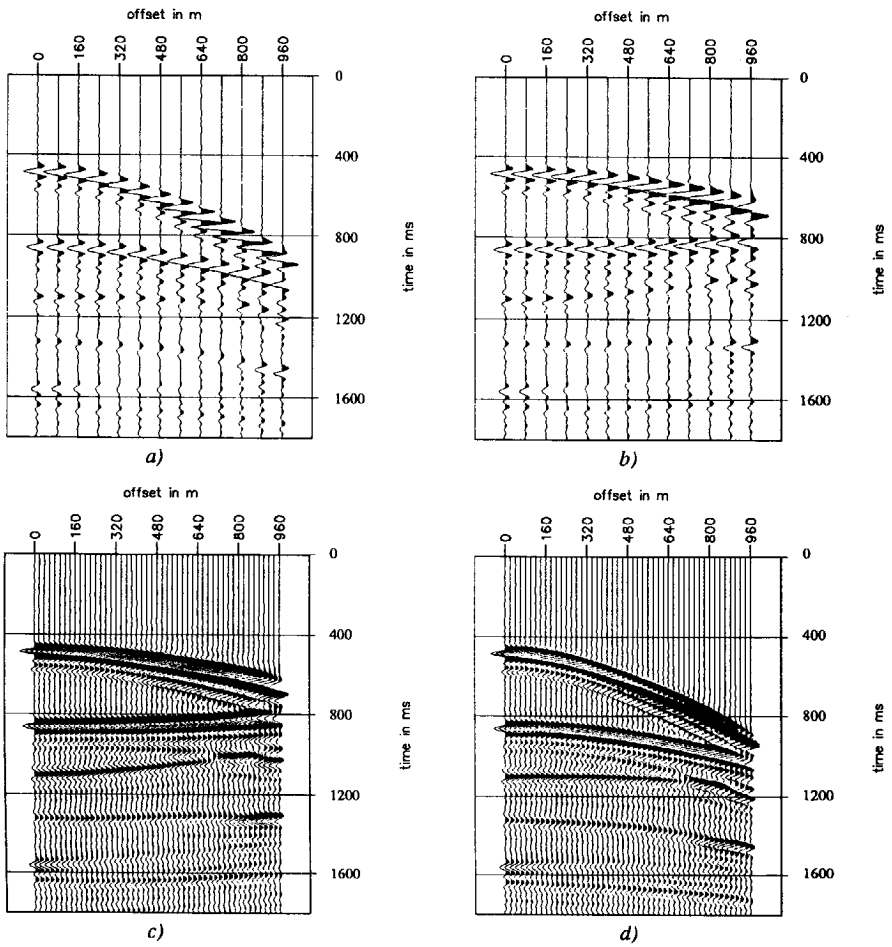

Fig. 5.13 *a) CMP-gather related to the model of Fig. 5.8a b) CMP-gather after approximate NMO correction c) CMP-gather after NMO and interpolation via the wave number domain d) Interpolated CMP-gather after removing the NMO correction.*

This procedure is illustrated on a CMP-gather extracted from the dataset which is also shown in Fig. 5.8 and in Chapter 1. Fig. 5.13a shows a CMP-gather extracted from this dataset after removing every other shot record, giving a reduced spatial sampling of 80 m (note that a CMP-gather already has a twice as sparse spatial sampling as a shot record). First a rough NMO correction is applied (using a single stacking velocity) to reduce the maximum angle in the wave number domain, as shown in Fig. 5.13b. After padding zero samples in the wave number domain Fig. 5.13c shows the interpolated CMP-gather. The final step is to undo the NMO correction, resulting in the interpolated CMP-gather (Fig. 5.13d) with 20m spacing. If this procedure is repeated for all CMP gathers, interpolated shot records can be acquired after reordering. Following Berkhout (1984), aliasing can only be removed by interpolation if extra information is provided. Here, the extra information consists of the NMO model.

5.2 INFLUENCE OF NOISE

A low signal to noise ratio will have a negative effect on the multiple elimination result, noise being defined as events that are not given by the forward model equation (2.20).
Each event in the data, whether it is part of the model or not, will be converted to multiple energy and will be subtracted from the data. This means that correlated noise events which are present in all shot records, like vessel and cable noise, will create artificial multiples which are not actually present in the data. Therefore, correlated noise should be removed from the data as much as possible. This can be seen as follows. Consider the formulation of the surface-related multiple elimination procedure, as given by equation (3.11):

$$\mathbf{P}_0^-(z_0) = \left[\mathbf{I} + \mathbf{P}^-(z_0)\mathbf{A}(z_0) \right]^{-1} \mathbf{P}^-(z_0) \tag{5.1}$$

with

$$\mathbf{A}(z_0) = \{\mathbf{S}^+(z_0)\}^{-1} \mathbf{R}^-(z_0) . \tag{5.2}$$

If the data $\mathbf{P}^-(z_0)$ is contaminated with noise $\mathbf{N}(z_0)$, the estimate of the multiple free data becomes:

$$\begin{aligned} <\mathbf{P}_0^-(z_0)> &= \left[\mathbf{I} + \{\mathbf{P}^-(z_0) + \mathbf{N}(z_0)\} \mathbf{A}(z_0) \right]^{-1} \{\mathbf{P}^-(z_0) + \mathbf{N}(z_0)\} \\ &= \mathbf{P}_0^-(z_0) - \{\mathbf{P}^-(z_0) + \mathbf{N}(z_0)\} \mathbf{A}(z_0) \mathbf{N}(z_0) + \ldots\ldots . \end{aligned} \tag{5.3}$$

Apart from the true multiple elimination result, $\mathbf{P}_0^-(z_0)$, as given by equation (5.1), the output also consists of terms which contain "auto convolutions" of the noise and "cross convolutions" of signal and noise.

Uncorrelated noise will be less harmful, as the multiple elimination procedure has a dispersing effect, only enhancing correlating events (similar to stacking). From the examples, that will be shown, it may be concluded that uncorrelated noise is not noticeably increased. Another interesting noise property is that the adaptive multiple elimination procedure will stop when the multiples are suppressed until the noise level. A distinction between uncorrelated noise and correlated events cannot be made with the minimum energy criterion.

To illustrate the effect of noise, the data of Fig. 5.3 is considered again to which different noise levels are added before multiple elimination is applied.

First -20 dB noise (defined as the ratio of the average of absolute values of the noise amplitudes to the maximum amplitude in the data) is added, resulting in the shot record of Fig. 5.14a. If the second term of the Taylor series is calculated (Fig. 5.14b) it can be observed that the noise is reduced considerably. This means that the noise level after multiple elimination will be hardly increased!

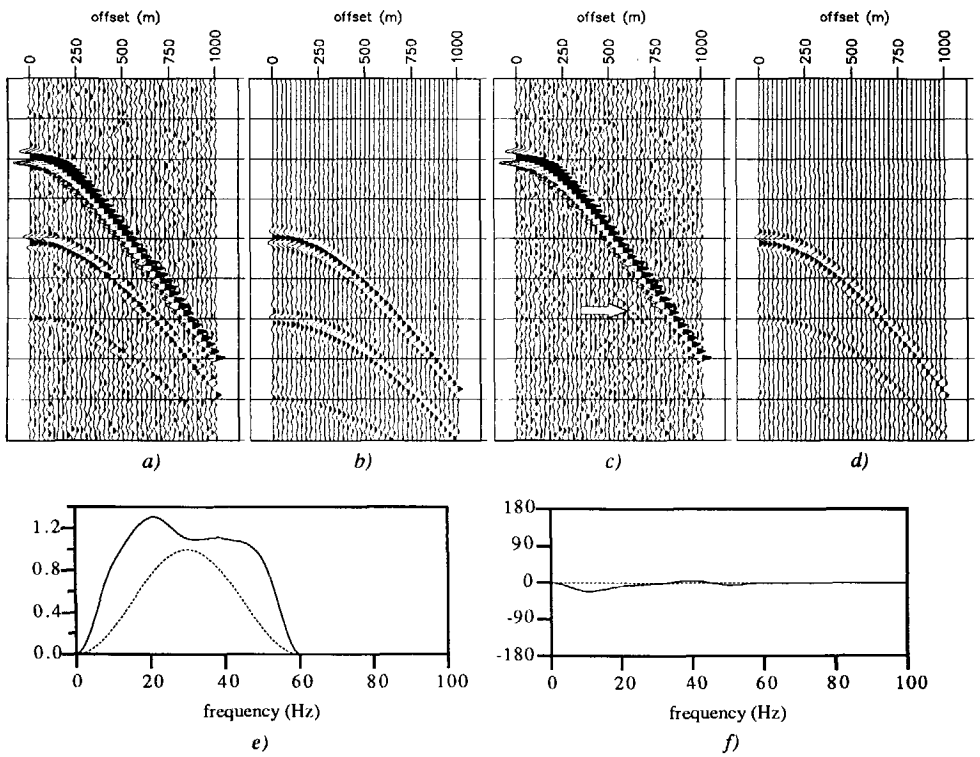

Fig. 5.14 a) Shot record of Fig. 5.3 with -20 dB noise added b) Second term of the Taylor series c) Adaptive multiple elimination result d) Difference before and after multiple elimination, i.e. the eliminated multiples only e) Estimated amplitude spectrum f) Estimated phase spectrum. The dashed line shows the original wavelet spectra.

When applying adaptive multiple elimination Fig. 5.14c is the result, which shows that the multiples have been reduced until the noise level. The remaining of the first order multiple can just be seen through the noise (see the arrow in Fig. 5.14c). However, its amplitude level is the same as the noise amplitude level. Fig. 5.14d shows the difference between the data before and after multiple elimination, i.e. the eliminated multiples. It shows that the multiple section has a much lower noise level (uncorrelated noise) than the original section, approximately 6 dB lower. This explains that the signal to uncorrelated-noise ratio of the output is virtually unchanged.

The fact that the adaptive multiple elimination stops when the multiple amplitudes have been reduced until the noise level can be observed in the amplitude spectrum of the estimated wavelet in Fig. 5.14d. The amplitude spectrum is over-estimated, which means that the *inverse* wavelet has smaller amplitudes at those frequencies. This is exactly what we want.

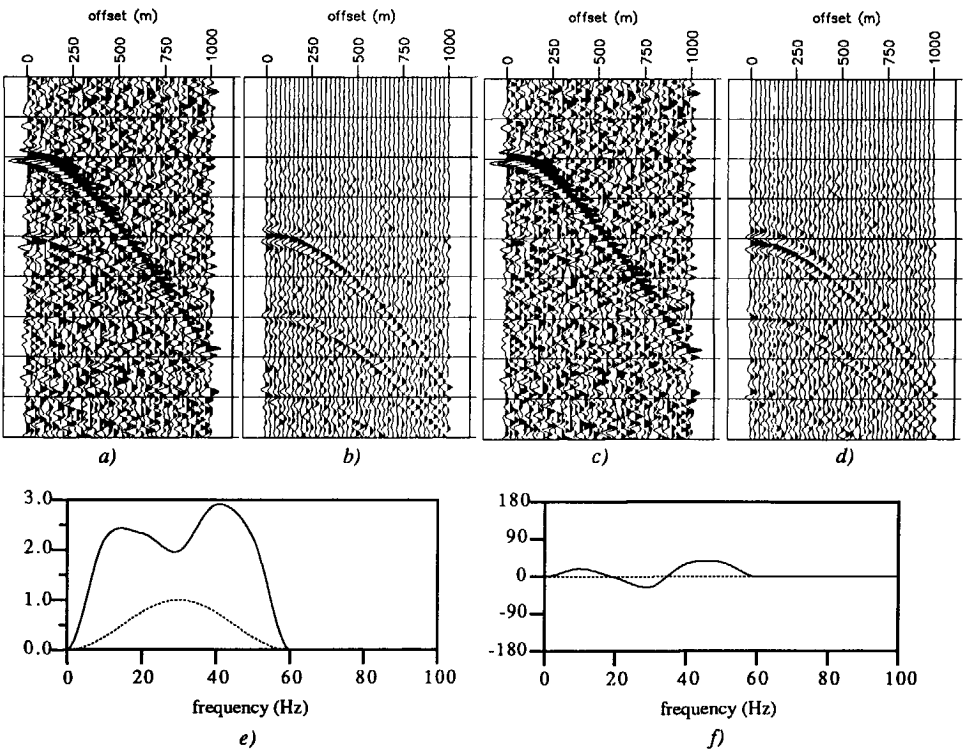

Fig. 5.15 *a) Shot record of Fig. 5.3 with -10 dB noise added b) Second term of the Taylor series c) Adaptive multiple elimination result d) Difference before and after multiple elimination, i.e. the eliminated multiples only e) Estimated amplitude spectrum f) Estimated phase spectrum. The dashed line shows the original wavelet spectra.*

Especially the edges of the wavelet are less well estimated. This is because the added noise had a flat spectrum and the data has a cosine shaped spectrum, yielding that the signal to noise ratio to be frequency dependent, being highest at 30 Hz. Using the *inverse* of this wavelet as a weighting factor for the Taylor terms means that the multiples are *less* suppressed. Generally it can be said that the higher the noise level, the smaller the amplitudes of the estimated *inverse* wavelet spectrum, the less the multiples are suppressed. As the noise is uncorrelated, the estimated phase spectrum should suffer less from the added noise. This is indeed true, as Fig. 5.14e shows still a remarkably good estimate of the original zero phase spectrum!

The same experiment is repeated for -10 dB noise added to the data, as shown in Fig. 5.15. The noise level is rather high, as the first order multiple is almost drowned in the noise (Fig. 5.15a). Calculating the second order term of the Taylor series results in Fig. 5.15b. This again shows the reduction of noise due to the dispersion effect of the matrix multiplications for uncorrelated signals. It is important to realize the fact that for this noisy data still a surprisingly good estimate for the multiples can be acquired. The signal to noise ratio of the data after adaptive multiple elimination is slightly less then in the input data; the difference is approximately 0.1 dB only.

As the multiples have the same amplitudes as the noise in the original data, hardly any *visual* improvement of the multiple elimination process can be expected, as can be seen in Fig. 5.15c. The difference before and after multiple elimination is shown in Fig. 5.15d, which shows that the *multiple* signal to noise ratio has been increased significantly, with approximately 6 dB. The phase spectrum in Fig. 5.15f is still a surprisingly good estimate for the wavelet spectrum.

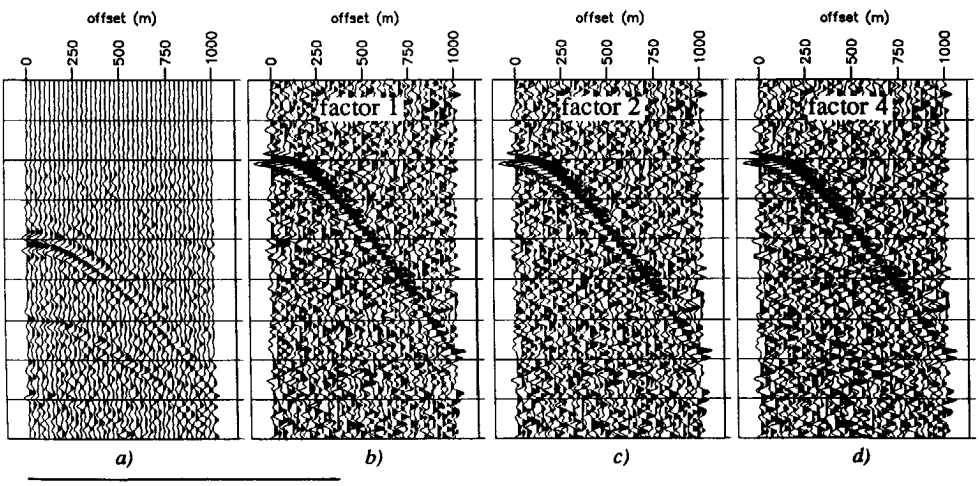

Fig. 5.16 *a) Eliminated multiples for shot record of Fig. 5.15a, i.e. the difference of Fig. 5.15a and Fig. 5.15c*
b) Shot record of Fig. 5.15a after adaptive multiple elimination
c) Shot record of Fig. 5.15a after adaptive multiple elimination with an oversubtraction of 2
d) Shot record of Fig. 5.15a after adaptive multiple elimination with an oversubtraction of 4.

If the multiples are insufficiently reduced due to the high noise level, two remedies can be considered:

1 Use another criterion that takes also correlation into account.

2 Apply an oversubtraction of the predicted multiples. From the examples it is clear that the amplitude spectrum of the estimated wavelet suffers mostly from the noise, and the phase can still be recovered reasonably well. Therefore only an amplitude correction is needed.

The oversubtraction has been used on the example of Fig. 5.15, using a factor of 1, 2 and 4. Fig. 5.16a shows the multiples that have been eliminated from Fig. 5.15a by the adaptive multiple elimination procedure (difference between Fig. 5.15a and Fig. 5.15c). The multiple elimination results are displayed in Fig. 5.16b to d. From a visual inspection it appears that Fig. 5.16c, with the oversubtraction of 2, gives the best result. Using more oversubtraction increases the noise level.

5.3 SOURCE AND RECEIVER PERTURBATIONS

In Chapter 3 we assumed that before the multiple elimination procedure is applied, the remaining source and receiver matrices have been reduced to unity matrices by a source and receiver decomposition procedure (see section 3.1.2 and 3.1.3). It means that after decomposition the wavelet is the same for each shot record, i.e. each column of the data matrix. This assumes that all sources have equal strength and equal signature shape and that each receiver has the same sensitivity. For marine data this assumption may be largely valid in most cases but for land data this is generally not true, as the wavelet repeatability highly depends on the near surface effects.

In this section the influence of varying source strength and receiver sensitivity are investigated with a few simple examples, which may be used as a rule of thumb.

Suppose that each source has a variation in amplitude only, which is represented by the scalar a_i for shot record i. For the next Taylor term corresponding to shot record i each trace of this shot record is convolved with the shot record corresponding to the receiver position (using the Huygens principle, as explained in section 3.2.2). This means that each convolution result of one trace of shot i with a shot record j yields a scaling factor if $a_i a_j$, as shown in Fig. 5.17. The addition of these sub-results yields the next Taylor term corresponding to shot record i, i.e. a scaling factor of $a_i \frac{1}{N} \sum_j a_j \approx a_i$. Thus each higher order term of the Taylor series has similar amplitude perturbations as the first term (=input data).

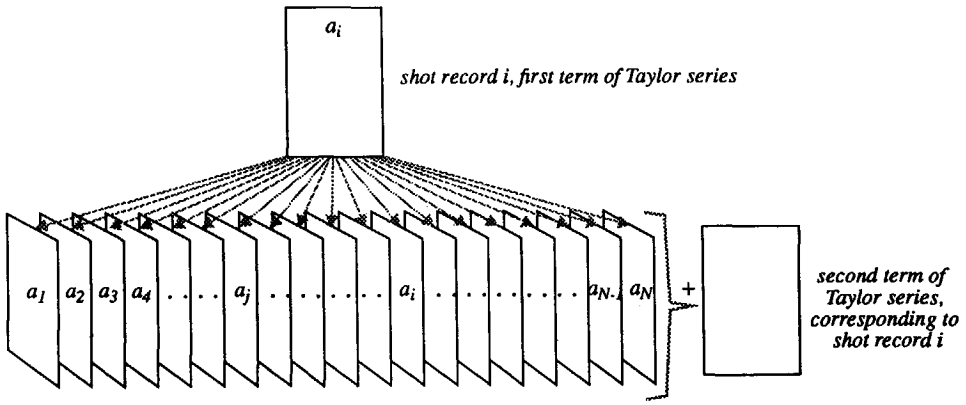

Fig. 5.17 The next term of the Taylor series is calculated by convolving each trace of a shot record with the shot record corresponding to the trace position. Next, these sub-convolution results are added.

This means that the amplitude variations will be averaged for the predicted multiples (similar to the averaging effect on uncorrelated noise), and will therefore have little effect on the multiple elimination result.

This is shown for the same shot record as in Fig. 5.3. The perfect result without source variations is repeated in Fig. 5.18b. Next source variations of maximum 20% are introduced along the seismic line, as shown in Fig. 5.18c. After adaptive multiple elimination the result of Fig. 5.18d hardly deviates from the optimal result (Fig. 5.18b). If the random source strength variations are increased to maximal 50% deviations, as shown in Fig. 5.18e, and the adaptive multiple elimination procedure is applied for this line, still the result is very good, as shown in Fig. 5.18f. In both cases the wavelet could be perfectly recovered. It can be concluded that the adaptive multiple elimination process is very insensitive to random source and receiver variations with respect to amplitudes.

If the sources have variations in timing only, which means that each source signature is equal except for a time shift Δt_i in shot record i, the result is different from the situation with amplitude variations only. Each Huygens source contribution for the second Taylor term will have a total time shift of $\Delta t_i + \Delta t_j$ for each trace j in shot record i. Hence, the interference effect is no longer correct, as the signals of the Huygens source contributions are no longer added with the correct phase. This applies to the constructive as well as the destructive interference.

To illustrate this effect the same dataset is considered again, but now time shifts are introduced. Fig. 5.19b shows the perfect result without any time shifts incorporated (identical to Fig. 5.18b). Next, uncorrelated source time shifts are introduced per shot record with a maximum of 2 ms, as shown in Fig. 5.19c. After adaptive multiple elimination for one shot record selected from these perturbed shot records, the result (Fig. 5.19d) shows already some remainings, due to the improper addition of all Huygens source responses. Increasing the maximum source time shifts to 4 ms (Fig. 5.19e) the result after adaptive multiple elimination for this selected shot record is shown in Fig. 5.19f. A further increasing of the timing errors will lead to unacceptable results. Nevertheless, the estimated source wavelet hardly suffered from those time shift deviations!

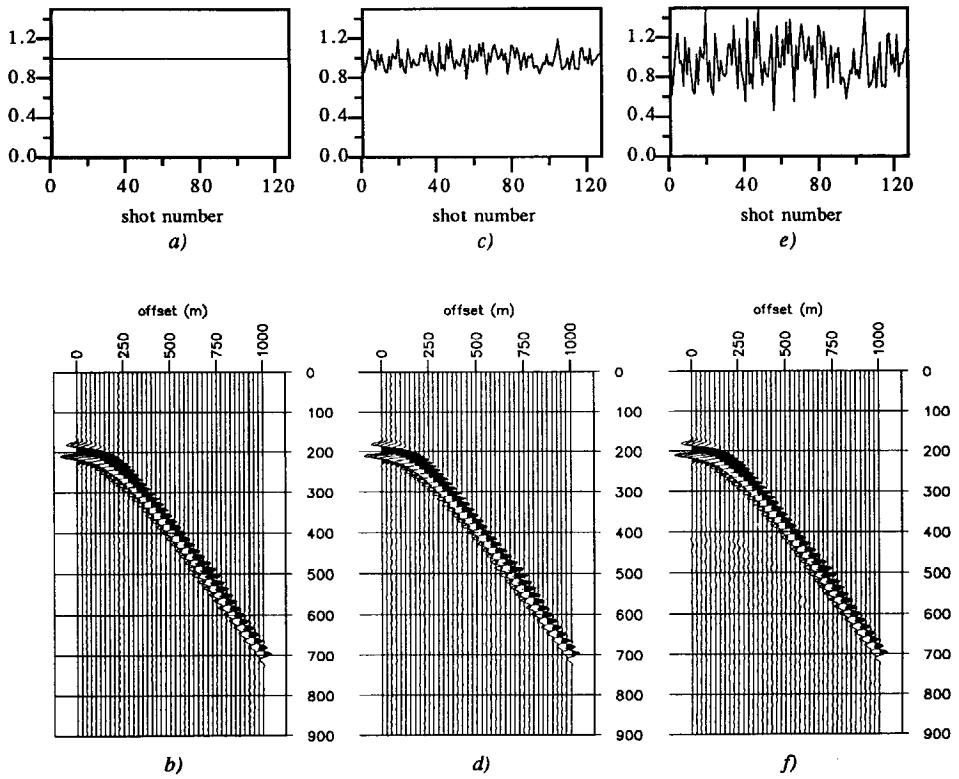

Fig. 5.18 *a) Source strength as a function of the shot number without variations*
b) Shot record after surface-related multiple elimination without source strength variations
c) Source strength variations as a function of the shot numbers, with a maximum variation of 20%
d) One shot record out of this set of shots after adaptive multiple elimination
e) Source strength variations as a function of the shot number, with a maximum variation of 50%
f) Shot record out of this set of shots after adaptive multiple elimination.

In general any shot to shot wavelet deviation can be considered as a combination of amplitude and phase deviations. The amplitude deviations are not very harmful for the multiple elimination result. However, phase deviations will have a more significant influence on the output of the multiple elimination process. If on land data serious shot to shot wavelet deviations do occur, wavelet balancing of the shot records prior to multiple elimination is desired.

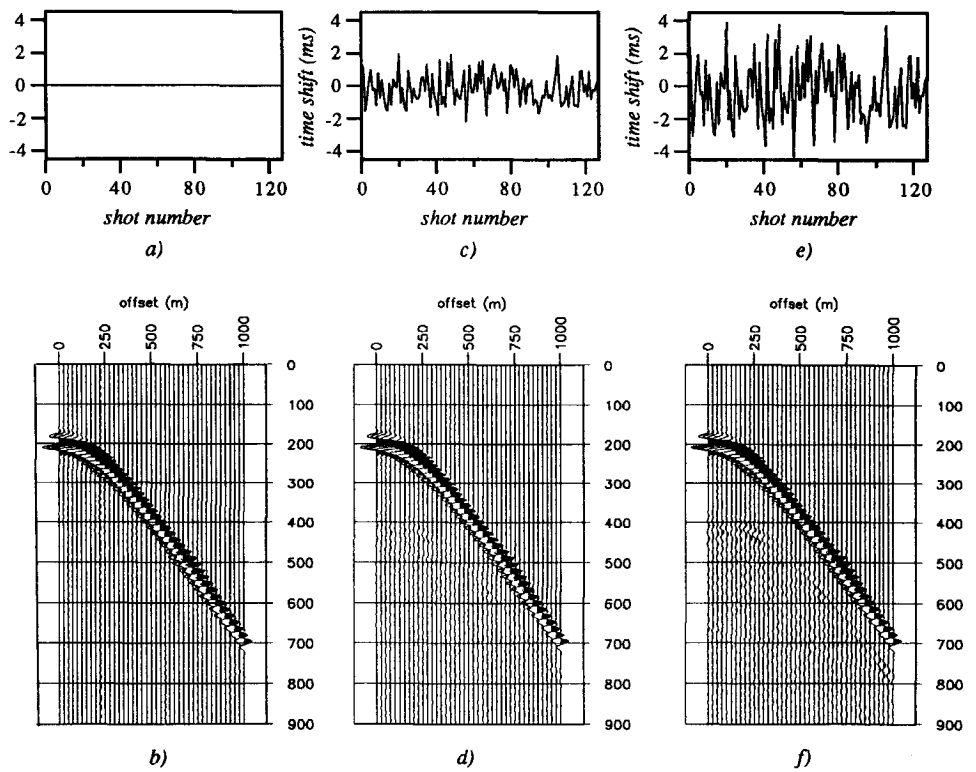

Fig. 5.19 *a) Source time shifts as a function of the shot number without variations*
b) Shot record after surface-related multiple elimination without source variations
c) Source time shifts as a function of the shot numbers, with a maximum variation of 2 ms
d) One shot record after adaptive multiple elimination
e) Source time shifts as a function of the shot number, with a maximum variation of 4 ms
f) Shot record after adaptive multiple elimination

5.4 STATICS

For land data, statics is generally a severe problem in almost all seismic processing stages and is therefore removed in advance. Two different types of statics can be indicated:

- *Elevation statics*
  The statics caused by traveltime differences due to the non-flatness of the surface.

- *Weathered layer statics*
  The statics caused by traveltime differences due to one or more irregularly shaped low velocity layers near the surface.

The two types of static causes are visualized in Fig. 5.20. The irregular (near) surface can influence the upcoming wave front shapes considerably. Generally these influences are approximated by one delay parameter per source position (source static) and one delay parameters per receiver position (receiver static). Statics should be removed ("static correction") if a process assumes a homogeneous flat surface.

The *weathered layer* statics are generally not a problem for the multiple elimination method, as the weathered layer is part of the *sub*surface. The surface-related multiple elimination procedure does not need any subsurface information. The traveltime and amplitude influence on the events by the weathered layer will be doubled for the first order multiples etc. The multiples will be perfectly predicted by their primaries. However, discrepancies may arise by coupling problems (treated in the previous section on receiver variations) and by the *reflecting* properties of the weathered layer.

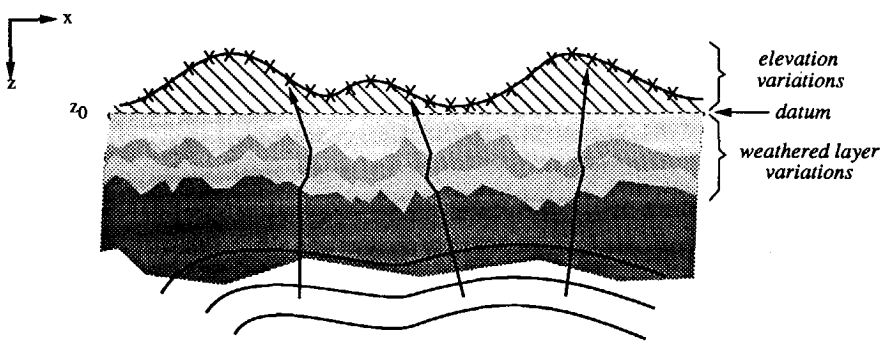

Fig. 5.20 Statics can be divided into elevation statics and weathered layer statics. The first type is due to the elevation changes of the surface, the second type is due to the irregularly shaped low velocity layers below the surface.

If the weathered layer acts as a thin layer reflector, the "thin surface layer" variant should be used, as described in Chapter 3. In this variant, information of the weathered layer is needed to eliminate the multiples related to the free surface in combination with the weathered layer interfaces.

If the weathered layer acts mainly as a *propagation* layer, the surface-related multiple elimination method can be applied without modification. Note that for a *buried* dynamite source the source position should be corrected to the datum during decomposition.

For the *elevation* statics the situation may be different. The multiple elimination theory assumes that at the free surface decomposition into upgoing and downgoing wave fields can be carried out. At the receiver side the upgoing wave fields are assumed to be reflections from the *subsurface*, the downgoing wave fields are assumed to be wave fields after reflection against the free *surface*. This is not true anymore for very large surface curvatures, in which internal reflections exist. For these situations, the surface-related multiple elimination method does not work perfectly anymore, although acceptable results may still be expected.

To show this in an example, we consider the subsurface model of Fig. 5.21a. In this model elevation statics have been introduced varying from left to right with a maximum local dip angle ranging from 5° at the left to about 25° at the right. Shot records have been simulated with a finite difference modeling algorithm, the shot positions ranging from x=1000 m to x=5000 m (see Fig. 5.21a). Fig. 5.21b shows the zero offset section that has been extracted from the simulated shot records. As the reflector is flat, the irregularities of the primary and the multiples are due to the elevation statics.

Note also the fact that as the data has been simulated in a *gridded* model, the curved surface has a "stair case" shape, which produces a number of small diffractions in the primary and the multiples (see the arrows in Fig. 5.21b). After applying the surface-related multiple elimination procedure on all shot records, the zero offset section is extracted. The result has been displayed in Fig. 5.21c. Indeed the multiples could not be eliminated perfectly, but the reduction for this complex problem is still significant. The second and higher order multiples around x=2500 m are completely removed. The first order multiple is reduced to an acceptable level.

The problems related to the existence of statics and its influence on the multiple elimination is not fully discussed in this section. However, a thorough description of statics is beyond the scope of this thesis. It is a thesis on its own.

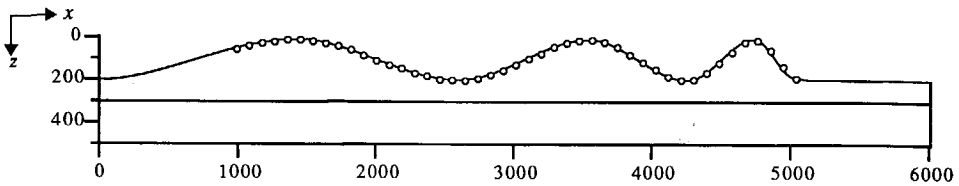

a)

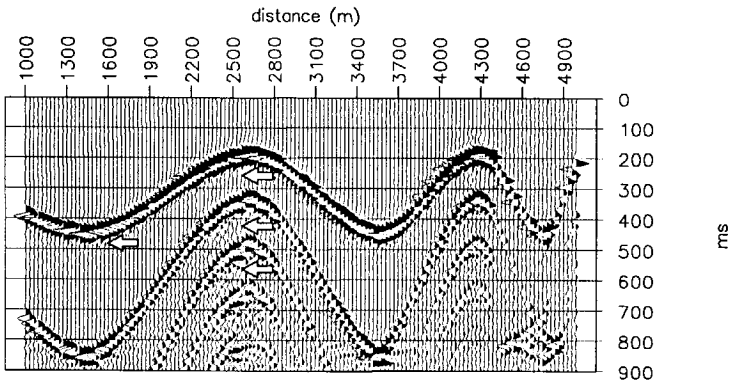

b)

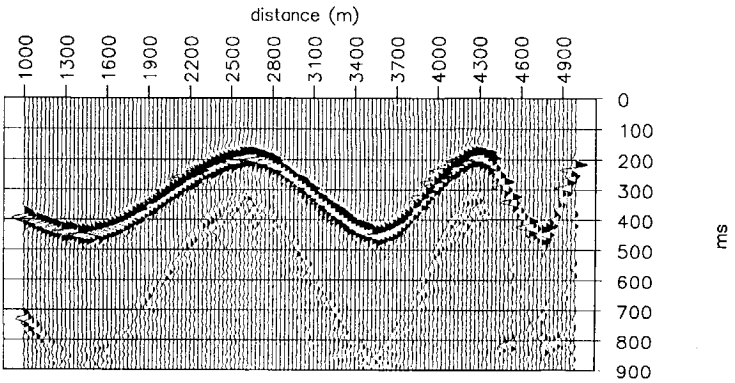

c)

Fig. 5.21 *a) Subsurface model with a varying surface level and a reflector at 300 m depth*
b) Zero offset section related to the subsurface model of a), with all multiples included
c) Zero offset section extracted from the shot record after multiple elimination.
The arrows point at diffractions due to the gridded velocity field.

5.5 3D VERSUS 2D EFFECTS

5.5.1 Introduction

The multiple elimination method as described in Chapter 3 is applied as a 2D procedure. This means that the assumption has been made that the data is considered to be gathered in a 2D world. This has two consequences:

1. The subsurface model is assumed to be invariant in the cross-line direction. Hence, out of plane events are not properly treated.

2. The sources are considered to be line sources in the cross-line direction. The resulting amplitudes are thus considered to be 2D.

Both assumptions are not met in practice and therefore we have to look at the effects of these assumptions in situations were they are not valid.

5.5.2 3D geometry aspects

In theory the multiple elimination procedure can be applied in a full 3D sense. The matrix notation is also suited to contain 3D data, which leaves the formulations exactly the way they are (see Appendix A). However, this requires an enormous amount of data to be gathered during the acquisition, as both source and receivers should be moved along a dense sampled grid along the surface. In stead of matrices of the size $N_s * N_r$, with N_s the number of shot records and N_r the number of receivers per shot for a 2D line, full 3D matrices have $N_s^2 * N_r^2$ elements (assuming the same geometry in the x and y direction). This huge amount of data is never recorded in practical 3D surveys. Normally the source and receivers are densely sampled in one direction and coarsely in the perpendicular direction, see Fig. 5.22. If a courser sampling of a factor 10 is used, the total amount of data reduces with a factor of 100. Even in this case the amount of data is still extremely large.

Present 3D seismic surveys prohibit *full* 3D multiple elimination; we should have a source at each receiver position to make a proper prediction of the multiples, as explained in section 3.2.2. For practical acquisition geometries the full 3D multiple elimination result will be severely aliased, and a proper interpolation to a dense grid source/receiver positions is needed. In addition, the application of the full 3D multiple elimination will take too much calculation time to be feasible at current super computers. Therefore *full* 3D multiple elimination will be saved for a future generation.

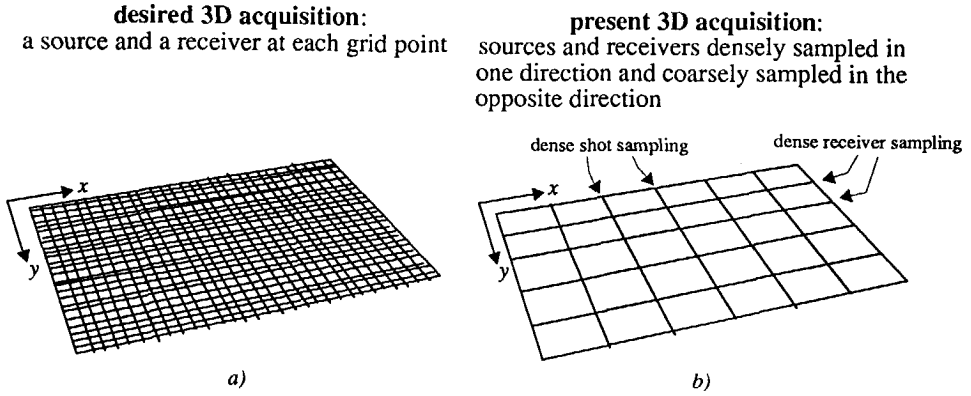

Fig. 5.22 *a) For the desired 3D acquisition the receivers are densely distributed in both x and y direction, and a shot record is generated for a source at each grid position b) In present 3D acquisition the source and receivers are densely sampled in one direction only.*

To show the principle that the method can be applied to 3D data that is measured on an ideal dense grid at the surface in both x and y direction, the 3D subsurface model is considered which is shown in Fig. 5.23. At the surface a 2D grid with a spacing of 25 m is used to simulate a *full* 3D seismic survey. In the x-direction 33 receivers are positioned and in the y-direction 17 receivers, resulting in a 2D spread of 561 receivers. For the simulation each grid point is also used as source position once, resulting in 561 shot records of each 561 traces in a fixed spread configuration. A data matrix, generated in a quasi 3D way as described in Appendix A, consists of 561*561 points. For each Fourier component there exists such a data matrix.

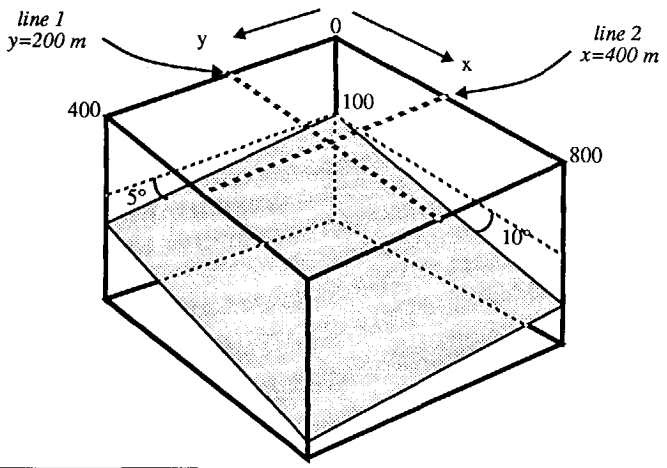

Fig. 5.23 *3D subsurface model containing one dipping reflector with an in-line dip of 10° and a cross-line dip of 5°. The smallest depth of the reflector with respect to the seismic area is 100m.*

In Fig. 5.24 the 3D data matrices are shown for the example under consideration for 3 Fourier components, corresponding to 5, 15 and 25 Hz respectively. Each 3D matrix consists of a number of submatrices, in this example 17x17 submatrices. One such a submatrix contains a complete 2D acquisition with the receiver varying in the x-direction (for a fixed y-coordinate) and the sources also varying in the x-direction (for another fixed y-coordinate). In the highlighted submatrix of Fig. 5.24, the source is positioned in the 5th grid line in the y-direction and the receivers are positioned in the 2nd grid line in the y-direction. Each column of this submatrix corresponds with a 2D shot record with the receivers in the x-direction, as shown at the top of Fig. 5.24. However, the source is located at a different y-position than the receiver line. One column of the full 3D matrix corresponds to a 3D shot record, with the source at one position and the receiver varying along the full grid in the x- and y-direction.

For the subsurface model of Fig. 5.23 one such a 3D shot record is shown in Fig. 5.25a. All 561 3D shot records have been used to do the multiple elimination with exactly the same algorithm as the 2D multiple elimination.

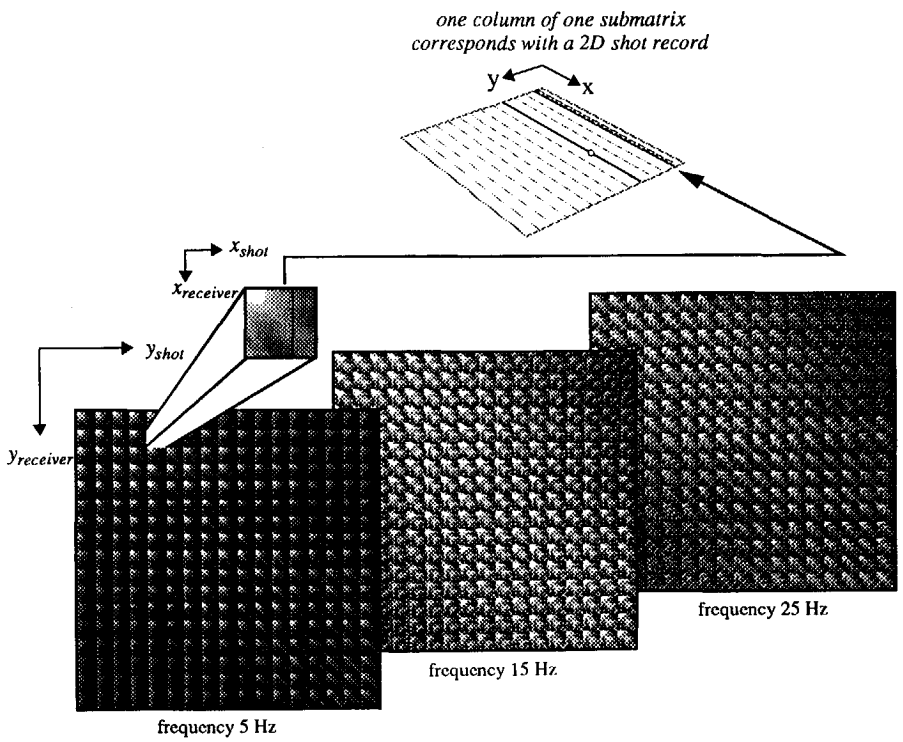

Fig. 5.24 *3 Data matrices of the full 3D data set simulated in the subsurface model of Fig. 5.23. The horizontal axis contains the shot coordinate, the vertical axis contains the receiver coordinate. Each submatrix contains a complete 2D seismic experiment.*

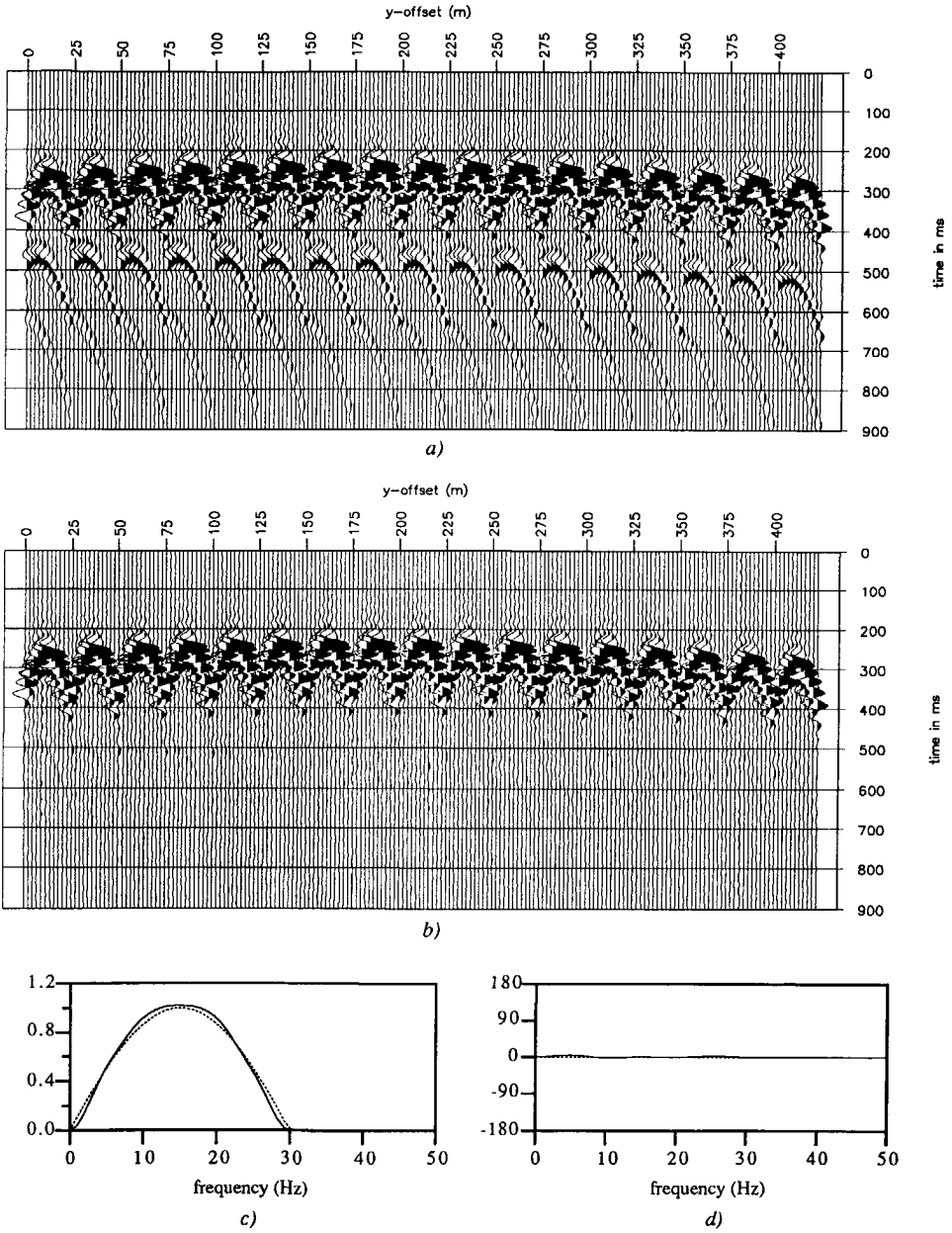

Fig. 5.25 *a) 3D shot record simulated in the subsurface model of Fig. 5.23. It contains 17 parallel receiver lines in the y-direction for the source in the middle of the acquisition grid b) Shot record after full 3D surface-related multiple elimination c) Estimated amplitude spectrum d) Estimated phase spectrum. The dashed line shows the true wavelet spectra.*

The only difference is the way the matrices are filled. Applying matrix multiplications with these 3D matrices, automatically describes the desired convolutions. The resulting shot records after adaptive multiple elimination are displayed in Fig. 5.25b, which shows that indeed all multiples have been eliminated well. Also the original 0-30 Hz cosine wavelet could be fully recovered, as is shown in Fig. 5.25c and d.

The same data set has been used to do some 2D experiments. We start with line 1 in Fig. 5.23 (y=200m), yielding a fixed spread seismic line of 33 shot records with each 33 receivers in the x-direction. Fig. 5.26a shows 9 shot records of this line. A 2D adaptive multiple elimination procedure is applied on this data, yielding the shot records of Fig. 5.26b, with the estimated wavelet shown in Fig. 5.26c and d. The results are still reasonably good, as the out of plane dip is 5° for this example. The wavelet does not correspond with the original wavelet for several reasons.
Firstly, using 3D data in a 2D multiple elimination, there will be an overall amplitude mismatch (scaling factor). In this example a scaling factor of about 10 has been found. In addition, for 3D data the amplitude decays faster (spherical spreading) than 2D data (cylindrical spreading). Therefore there will also be a discrepancy between the amplitude balance for different orders of the predicted multiples and the corresponding multiples in the data.

Secondly, the shape of the amplitude spectrum has been deformed, because of 3D-2D amplitude discrepancies. The 2D multiple elimination assumes line sources (see next section) in stead of point sources. This has also its influence on the wavelet. Going from 3D to 2D there is an amplitude scaling proportional to $\sqrt{f}$ and a phase shift of 45°. The factor $\sqrt{f}$ can be found back in Fig. 5.25c (increasing effect of high frequencies).

Thirdly, there is a phase spectrum deformation, due to the already mentioned 45° phase difference between 3D and 2D data.

Last but not least the fact that the multiples are not exactly periodic anymore according to a 2D world (out of plane effects) yields that with the wavelet estimation these out of plane effects are tried to be corrected. This mainly results in a phase spectrum deformation.

Also for line 2 in Fig. 5.23 (x=400 m) the adaptive 2D multiple elimination procedure has been applied. Fig. 5.27a shows 9 shot records of this line containing 17 shot records with each 17 receivers in the y-direction. After adaptive multiple elimination, the resulting shot records are displayed in Fig. 5.27b with the estimated amplitude and phase spectrum shown in Fig. 5.27c and d. The result is worse compared to the in-line result, as the out of plane dip is now 10°, yielding the multiple periodicity to be less correct. The first order multiple could still be well suppressed, but the second order multiple could only be very slightly reduced, due to both the 3D/2D amplitude discrepancies as well as the out of plane timing errors.

From the geometrical point of view it may be concluded that small out of plane dips (smaller than 5°for multiple generating interfaces) may be accepted for a reasonable 2D multiple elimination result.

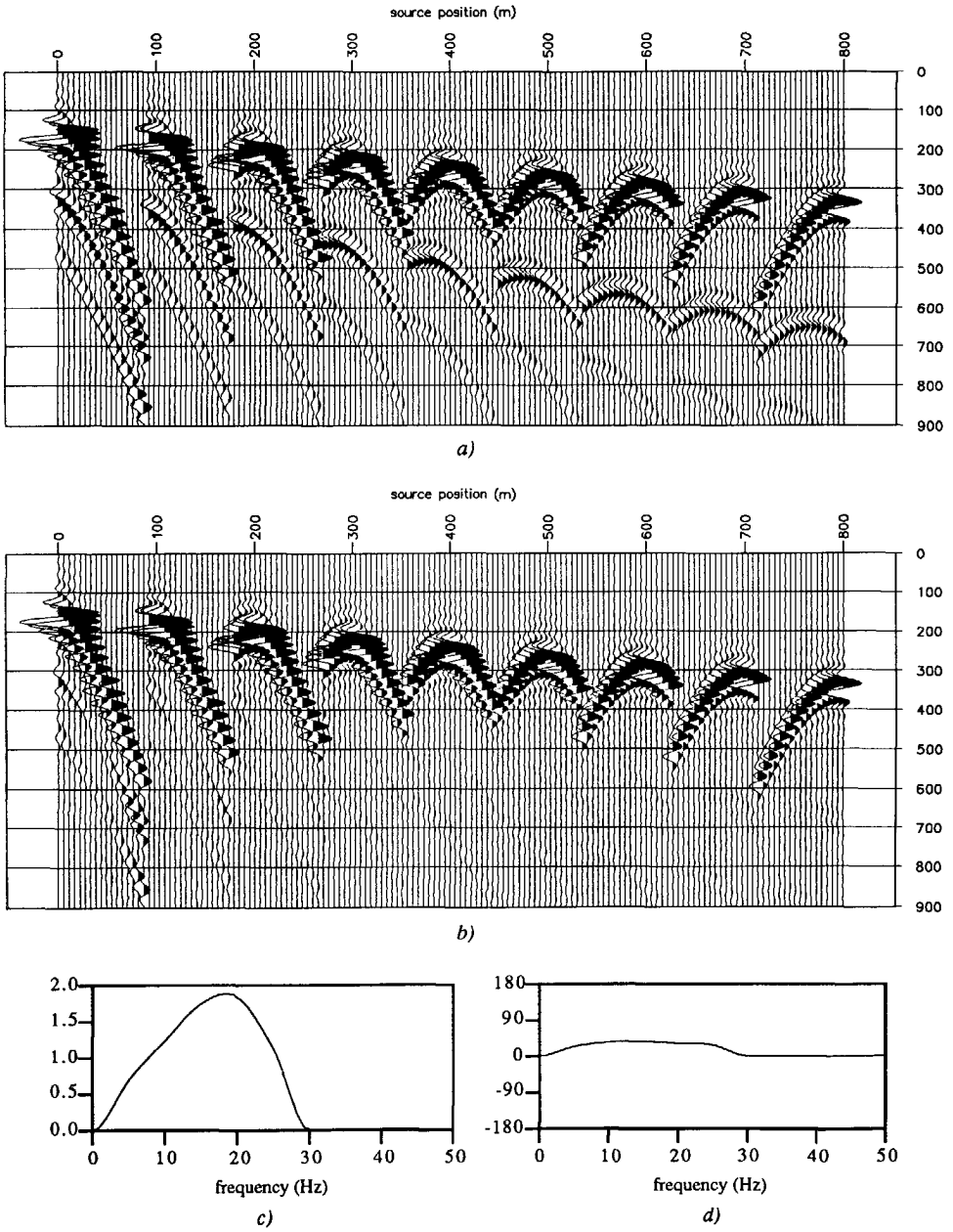

Fig. 5.26 *a) 9 shot records of line 1 in Fig. 5.23 b) Shot records after 2D surface-related multiple elimination c) Estimated amplitude spectrum d) Estimated phase spectrum.*

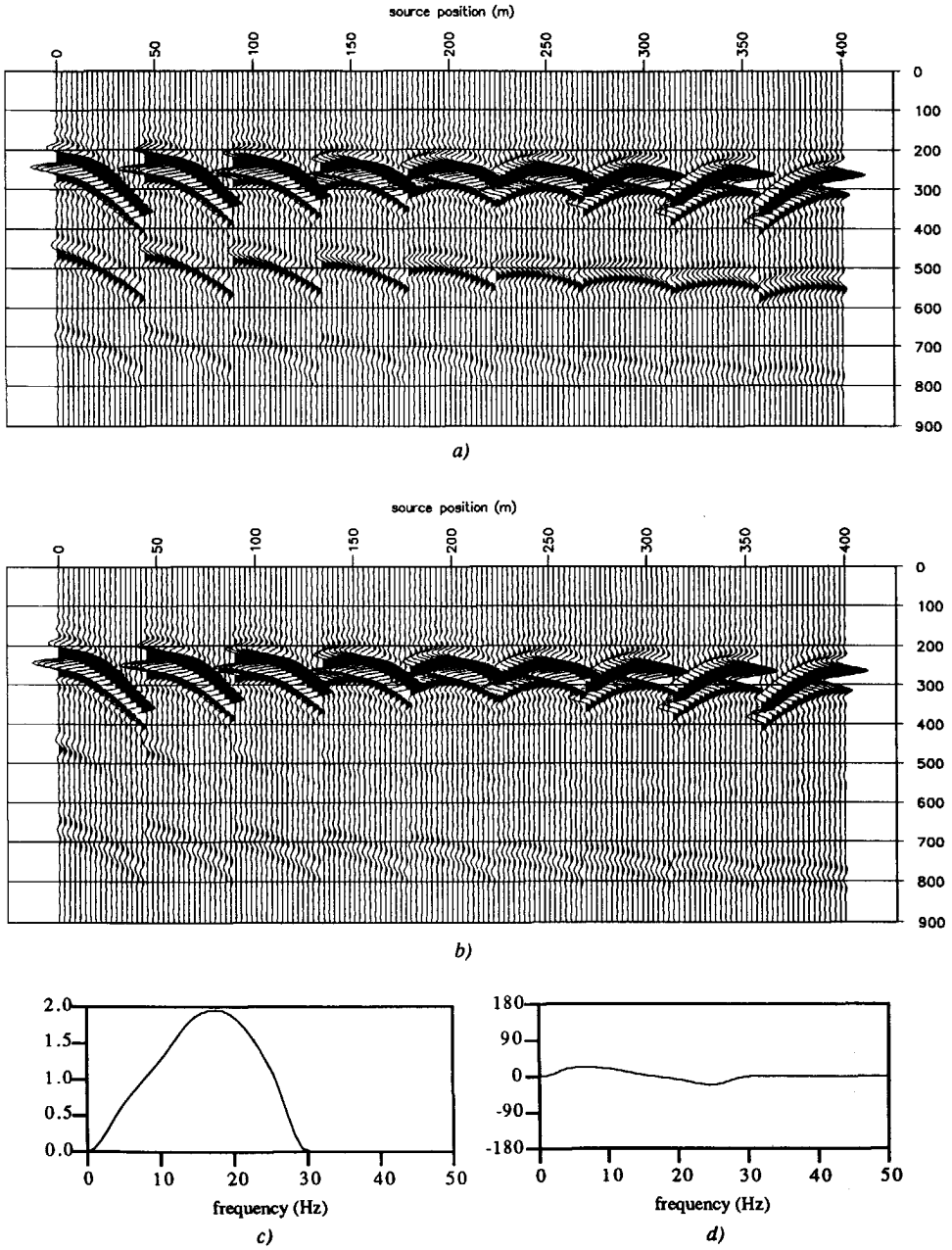

Fig. 5.27 a) 9 shot records of line 2 in Fig. 5.23 b) Shot records of after 2D surface-related multiple elimination c) Estimated amplitude spectrum d) Estimated phase spectrum.

5.5.3 3D amplitude aspects

Even in the case of 3D wave propagation in a 2D medium, i.e. a medium which is constant in the y-direction, the 2D multiple elimination will not yield optimal results. Although the position of the multiples can be exactly predicted with the 2D multiple elimination method, still amplitude discrepancies will be present. This has already been mentioned in the previous section, considering 2D cross-sections of 3D data.

The amplitude discrepancies arise from the fact that 2D multiple elimination assumes that the waves only expand in 2 dimensions. For 3D media, this can be acquired by considering line--sources in stead of point sources. So, if a 2D seismic line with 3D amplitudes is to be treated with the 2D multiple elimination, an amplitude pre-processing step should be applied, transforming point source responses into line source responses.

The most simple way to do this is a simple time scaling with a factor of $\sqrt{t}$, or a time gain which is dependent on the velocities in the media, see Yilmaz (1987). However, these are only rough corrections, which do not take into account the offset (or with better words: angle) dependent differences between 3D and 2D data.

Wapenaar et al. (1990b) suggest a method that is exact for horizontally layered media, and approximate for lateral inhomogeneous media if the not too high dips are present. This method makes use of a combination of a forward Hankel and an inverse spatial Fourier transform. However, it can be applied by a so called "square root" filter in the offset direction only, which makes the method very fast. The procedure consists of a weighted summation of the traces with larger offsets than the one under consideration, as shown in Fig. 5.28. If lateral inhomogeneities are present, the amplitude transformation is best applied on CMP gathers, as the CMP gather simulates the 1D assumption better than shot records.

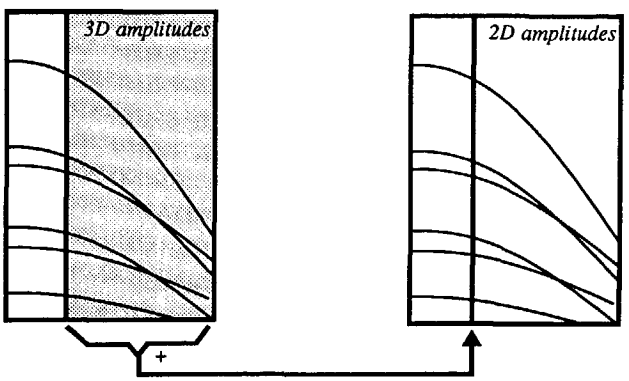

Fig. 5.28 For the amplitude transformation from point source to line source responses, per output trace a weighted summation of all input traces with larger offsets is involved.

The examples of sections 5.1 to 5.3 have all been simulated with line source responses. If the shot record of Fig. 5.3a is simulated as a point source response with 3D amplitudes, the result is Fig. 5.29a. On this shot record the amplitude transformation as described by Wapenaar et al (1990b) is applied, yielding Fig. 5.29b. For comparison the original 2D shot record is displayed in Fig. 5.29c. Comparing the point source (Fig. 5.29a) with the line source (Fig. 5.29c) response, there are three differences to be observed. For the point source response the amplitude decays faster as a function of time (3rd order multiple is hardly visible). Secondly it decays faster as a function of offset. Thirdly the wavelet is different. The first two differences are due to the geometrical spreading. The wavelet changes are due to the fact the a line source response is in fact a summation of point source responses along a line in the y-direction. This summation tends to increase lower frequencies more than higher ones, giving a difference proportional to $\sqrt{f}$. However, the phase spectrum is shifted by 45°.

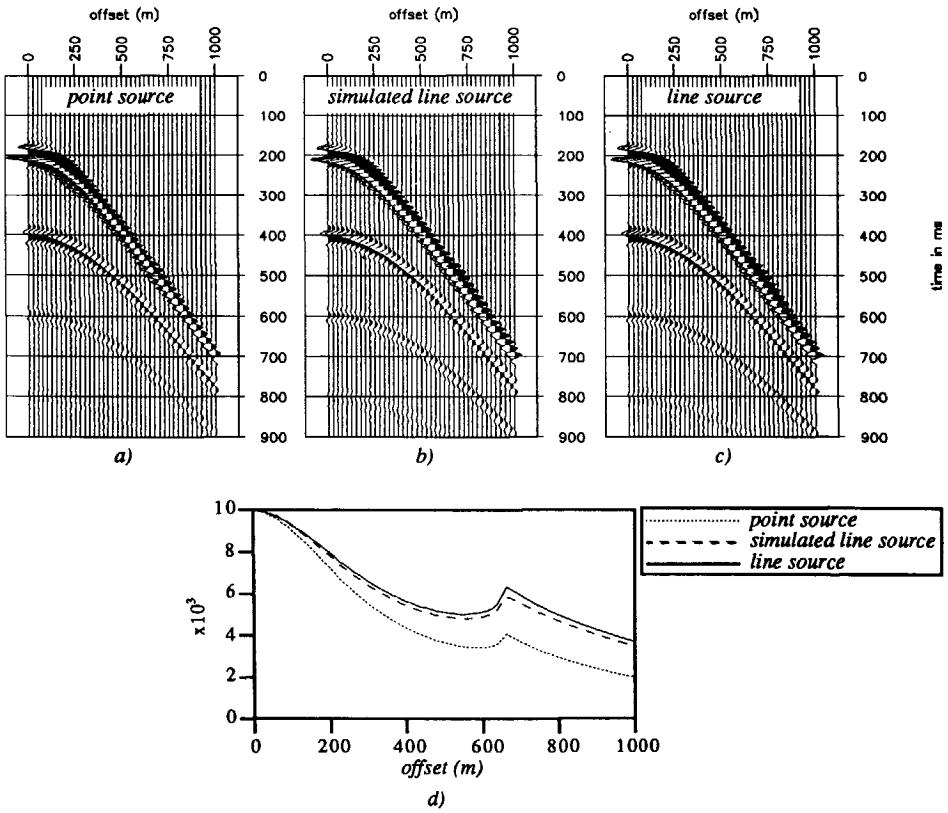

Fig. 5.29 a) Shot record with 3D amplitudes (point source response) b) Shot record with 3D amplitudes after amplitude transformation to 2D amplitudes (simulated line source response) c) Shot record with true 2D amplitudes (line source response) d) Maximum amplitude section picked for the shot records of a), b) and c). The 3D shot record has been normalized to 2D amplitudes at zero offset.

For the exact difference between point and line source responses, see the analytical expressions in Berkhout (1982) or Appendix B. Note that by the amplitude transformation the 2D amplitudes can be (almost exactly) recovered, see Fig. 5.29b. Also the wavelet changes are properly taken into account. The small deviations between the true 2D amplitudes and the simulated 2D amplitudes are due to the discretization of the amplitude transformation formula's.

The amplitude and phase differences between point and line sources can be observed when the wavelet is estimated using a 2D multiple elimination procedure on the 3D point source data. The resulting shot record is shown in Fig. 5.30a, which shows that although the amplitudes are not correct, a good multiple elimination result can be acquired. Fig. 5.30b shows the estimated amplitude spectrum, which shows that indeed the amplitudes at the higher frequencies range are estimated. Also the 45° phase shift is recovered in Fig. 5.30c.

The conclusion may be that the amplitude correction is not that important for marine seismic data, to get an acceptable multiple elimination result. However, Wapenaar et al (1990b) show that for multi-component elastic data the amplitude differences between 3D and 2D wave field expansion are of much more importance. For land data the amplitude correction will be a necessary pre-processing step.

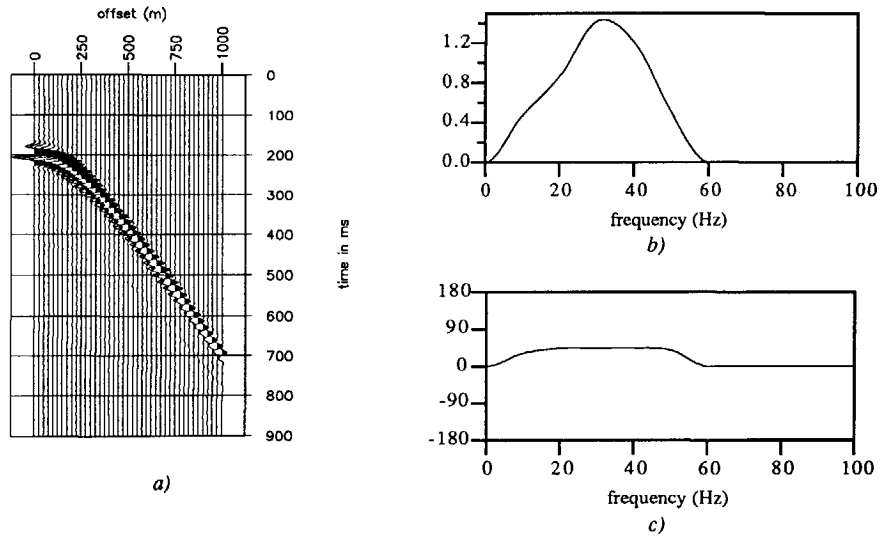

Fig. 5.30 *a) Shot record of Fig. 5.29a with 3D amplitudes after 2D adaptive multiple elimination. b) Amplitude spectrum estimated with 2D multiple elimination. c) Phase spectrum estimated with the 2D multiple elimination.*

6

IMPLEMENTATION AND APPLICATION ASPECTS

In this chapter, the implementation aspects of the surface-related multiple elimination method as described in Chapter 3 will be discussed. Additionally, a strategy how to apply adaptive multiple elimination on *field* data will be given.

6.1 IMPLEMENTATION ASPECTS OF SURFACE-RELATED MULTIPLE ELIMINATION

6.1.1 Wrap around effects in the multiple elimination procedure

The theory of the surface-related multiple elimination procedure has been formulated in the x-ω domain for monochromatic data matrices, which means that the multiple elimination process can be carried out completely independently for all frequency components. The multiple elimination process in its simplest form (after removing the source and receiver directivity) has been formulated as:

$$\mathbf{P}_0^-(z_0) = \mathbf{P}^-(z_0) - A(\omega)\{\mathbf{P}^-(z_0)\}^2 + A^2(\omega)\{\mathbf{P}^-(z_0)\}^3 - A^3(\omega)\{\mathbf{P}^-(z_0)\}^4 + \dots , \qquad (6.1)$$

with $\mathbf{P}^-(z_0)$ the matrix of the data with multiples, $A(\omega)$ the surface factor containing the free surface reflectivity and the inverse source signature, and $\mathbf{P}_0^-(z_0)$ the matrix with the data after multiple elimination.

The matrix multiplications in the x-ω domain, as described by equation (6.1), correspond to generalized 2-dimensional convolutions in the space-time domain, along the lateral and the time coordinate. Generally, each convolution elongates the signal to the sum of the length of the original signal and the convolution operator. As in our case the input data is used as the convolution operator, it means that the output of each convolution operation has been lengthened with the length of the input data.

As far as the *lateral* convolution is concerned, it is actually applied as a convolution in the space domain. Therefore, no wrap around in the spatial direction is involved. In fact, by writing the convolutions as matrix multiplications this spatial wrap around is automatically avoided.

As far as the *temporal* convolution is concerned it is applied as a multiplication in the frequency domain and the wrap around effect will occur if the frequency sampling interval is related to the length of the input traces. The wrap around in the time domain can be avoided by padding zeroes in the time direction *before* going to the frequency domain. However, this would mean that for eliminating N^{th} order multiples the trace length should be N+1 times as long as the original length. Of course this is not an efficient way to work. For this problem two solutions are considered.

6.1.2 Using the Laplace transform in stead of the Fourier transform

The most elegant solution is provided by Rosenbaum (1974) and reviewed by Thybo (1989). They suggest to taper the data in the time direction with an exponential taper e^{-qt} before going to the frequency domain. In this way implicitly a complex frequency axis ω-jq is introduced. The combination of this taper and a Fourier transform results effectively in a Laplace transform. With this taper applied to the data, matrix multiplications still describe the correct convolutions, because data in the Laplace domain has the same convolutional properties as in the Fourier domain. The advantage of such a tapering is that the signal for larger time values is suppressed and that the corresponding wrapped events after convolutions are very small in amplitude, and can be neglected. After the multiple elimination process has been applied the exponential taper is removed from the data.

Using tapering, the total procedure for multiple elimination is as follows:

1. Apply an exponential taper to all traces of the data in the time domain.
2. Apply a forward Fourier transform to the frequency domain for each trace.
3. Construct monochromatic data matrices as described in Appendix A, yielding $\mathbf{P}^{-}(z_0)$.
4. Perform a matrix multiplication and subtraction step recursively for each order of multiples to be eliminated:

$$\mathbf{P}_{i+1}^{-}(z_0) = \mathbf{P}^{-}(z_0)\,[\,\mathbf{I} - A(\omega - jq)\mathbf{P}_i^{-}(z_0)\,] \qquad i=1,2,\ldots . \tag{6.2}$$

The result of this recursive application is identical to equation (6.1), starting the recursion with $\mathbf{P}_1^{-}(z_0)=\mathbf{0}$.

5. Apply an inverse Fourier transform to the resulting data matrices ($\omega \rightarrow t$), and reorder to shot records.

6. Apply an inverse exponential taper on the traces.

For a good suppresion of the wrapped events, q is to be chosen as large as possible. On the other hand, there is a limit given by the computational noise. We recommend $q \approx 1$.

6.1.3 Using padded zeroes in the time domain

We have also investigated an alternative by padding zeroes on the input traces to twice the signal length before going to the frequency domain. This empty part of the trace can contain the convolution products that would have been wrapped otherwise. However, this will only be helpful for one convolution. Therefore, after each recursion according to equation (6.2), the data has to be transformed to the time domain for removing the second half of the traces, and replacing it by zeroes.

The recursive procedure in this situation is as follows:

1. Double the trace length in the time direction by padding zeroes to all traces of all shot records.

2. Apply a forward Fourier transform to the frequency domain for each trace.

3. Construct monochromatic data matrices as described in Appendix A, yielding $\mathbf{P}_i^{-}(z_0)$, $i=1,2,\ldots .$

4. Perform *one* matrix multiplication and subtraction step, thus eliminating one order of multiples:

$$\mathbf{P}_{i+1}^{-}(z_0) = \mathbf{P}^{-}(z_0)\,[\,\mathbf{I} - A(\omega)\mathbf{P}_i^{-}(z_0)\,] \qquad i=1,2,\ldots . \tag{6.3}$$

5. Apply an inverse Fourier transform to the time domain.

6. Replace the second half of each trace by zeroes.

7. Go back to step 2 to include the next Taylor term ($i \rightarrow i+1$).

The procedure has been visualized in Fig. 6.1, with the numbered steps indicated. Note that the matrix multiplication at point 4 in Fig. 6.1 is repeated for each Fourier component. For one output matrix element the inner product of one row of the original data matrix with one column of the current matrix is involved. For each term in the Taylor series one recursion is done, until no further improvement of the multiple elimination result is expected.

In conclusion we can say that the "padding zeroes" method gives the exact solution (no wrap around) and that the "Laplace" method is the most efficient one, as the total multiple elimination procedure can be carried out per frequency component independently.

Additionally, as in the "Laplace" method no zeroes need to be padded, yielding less Fourier components, this method will be at least twice as fast as the "padding zeroes" method. Therefore, the "Laplace" method is to be preferred, unless problems with the computational noise occur.
If the "Laplace" method cannot be used because of this computational noise problems, one could consider an intermediate solution: pad zeroes in the time domain, but still use the exponential taper, allowing a smaller factor q to be chosen.

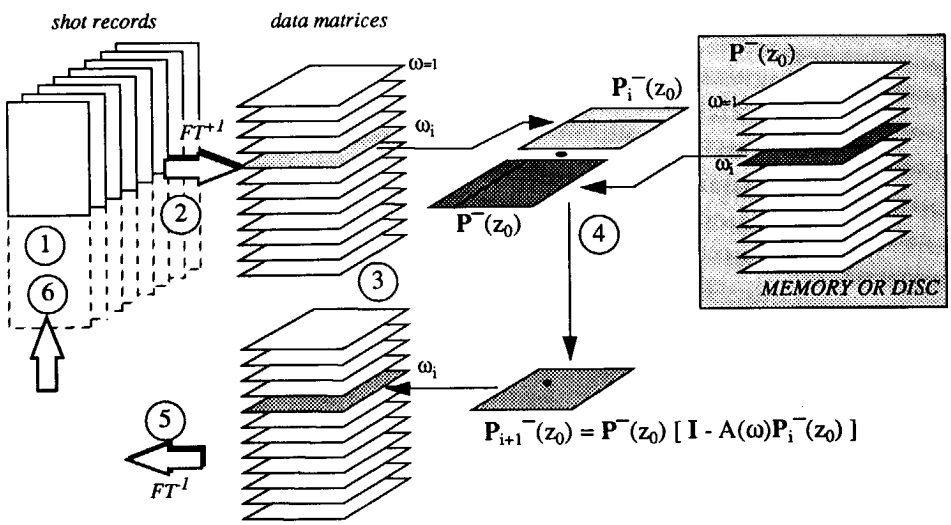

Fig. 6.1 *A practical implementation of surface-related multiple elimination. In the time domain zeroes are padded to the traces (step 1) and data matrices are constructed in the frequency domain (step 2 and 3). Per frequency the matrix multiplication with the original data is applied (step 4) after which the new data matrices are combined and Fourier transformed to the time domain (step 5). In the time domain the second half of each trace is zeroed again (step 6) and the next recursion can be carried out, starting at step 2.*

6.2 SURFACE-RELATED MULTIPLE ELIMINATION STRATEGY

For application of the surface-related multiple elimination procedure to field data, the following strategy has been designed:

1 Remove direct and surface waves.

2 Apply interpolation for the missing traces (in particular the near offsets). For the near offset interpolation a reordering into CMP gathers is preferred.

3 Apply a 3D to 2D amplitude transformation, to satisfy the 2D geometrical divergence as much as possible. For the square root filtering procedure (as described in section 5.5.3), this should be applied in the CMP domain. As the multiple elimination process is applied adaptively, in many situations a simple scaling by $\sqrt{t}$ may be applied without loosing quality.

4 Apply anti-alias filtering in the f-k domain.

5 Apply a correction for the receiver patterns and the receiver ghost. Also apply a correction for the source directivity. Optionally apply wavelet deconvolution to pre-shorten the wavelet.

6 Construct data matrices from the pre-processed shot records for a desired frequency range of the *multiples*.

7 Generate Taylor terms for a number of shot records along the line, to do the source wavelet analysis on. For example, once every 25 shot records. If the estimated wavelet along the line for these shot records does not vary much, it means that we can be rather confident in the result. However, if there are *considerable* wavelet variations along the line, which cannot be assigned to source variations, the data may be suffering from out of plane multiples. The application of the multiple elimination process will be questionable in that situation.
The actual estimation of the wavelet can be best applied in two stages:

   * Apply a multi-trial optimization for only 2 parameters: a global amplitude and a global time shift. This process solves the local minima problem and yields the position and strength of the main peak in the wavelet. Fix these values for further optimization.

   * Apply optimization for all frequencies for the residual wavelet (after removing the time shift and amplitude scaling found in the previous step). The optimization can be done by starting with a band-limited zero phase wavelet, or with an initial estimate of the wavelet (when available).

8 If the results for the few shot records in the previous step are satisfactory, apply the adaptive multiple elimination process to all shot records. The wavelet is not *estimated*, but *used* in this stage. Note that not the wavelet itself but the *inverse* of the wavelet (i.e. a deconvolution filter) is used in the multiple elimination process.

It is important to realize that the estimated inverse wavelet (or deconvolution filter) has been applied *only* to the multiple prediction terms, not to the seismic data itself. Hence, the output data will contain exactly the same wavelet as the input data. However, if desired, a separate deconvolution of the data with the estimated deconvolution filter will transform the seismic data into a true amplitude impulse response. Next, the deconvolved data can be used as input for a pre-stack inversion procedure, estimating the reflectivity of the subsurface in a true amplitude sense.

7

FIELD DATA EXAMPLES

In this chapter the full surface-related multiple elimination procedure is demonstrated on two marine field data examples, using the strategy discussed in the previous chapter.

7.1 MARINE DATA EXAMPLE 1

From a seismic line 201 shot records were used each consisting of 96 receivers with 25 m receiver and shot spacing. The nearest offset is 80 m, so about 3 traces are missing (including the zero offset trace). The area where the acquisition has been done is known for its tough multiple problem. The subbottom velocities are increasing slowly with depth, which makes it very difficult for move-out based methods to do a proper multiple elimination job. The water bottom depth is rather shallow, about 70 m. This makes that the smallest surface-related multiple periodicity is less than 100 ms. With a relatively strong sea bottom and several strong sub-bottom reflectors, a lot of surface-related multiple energy is present in the data, obscuring weaker primary reflections. The water bottom depth of 70 m is still sufficient to use the regular version of the surface-related multiple elimination method. For water layers shallower than about 50 m the thin layer version is preferred.

The first raw shot record of this line is shown in Fig. 7.1a. Apart from the (not shown) missing near offsets, 2 intermediate traces are missing. All shot records have the same missing trace pattern. The large amplitudes at the right hand side of the shot record are the post-critical water layer multiples and reverberations.

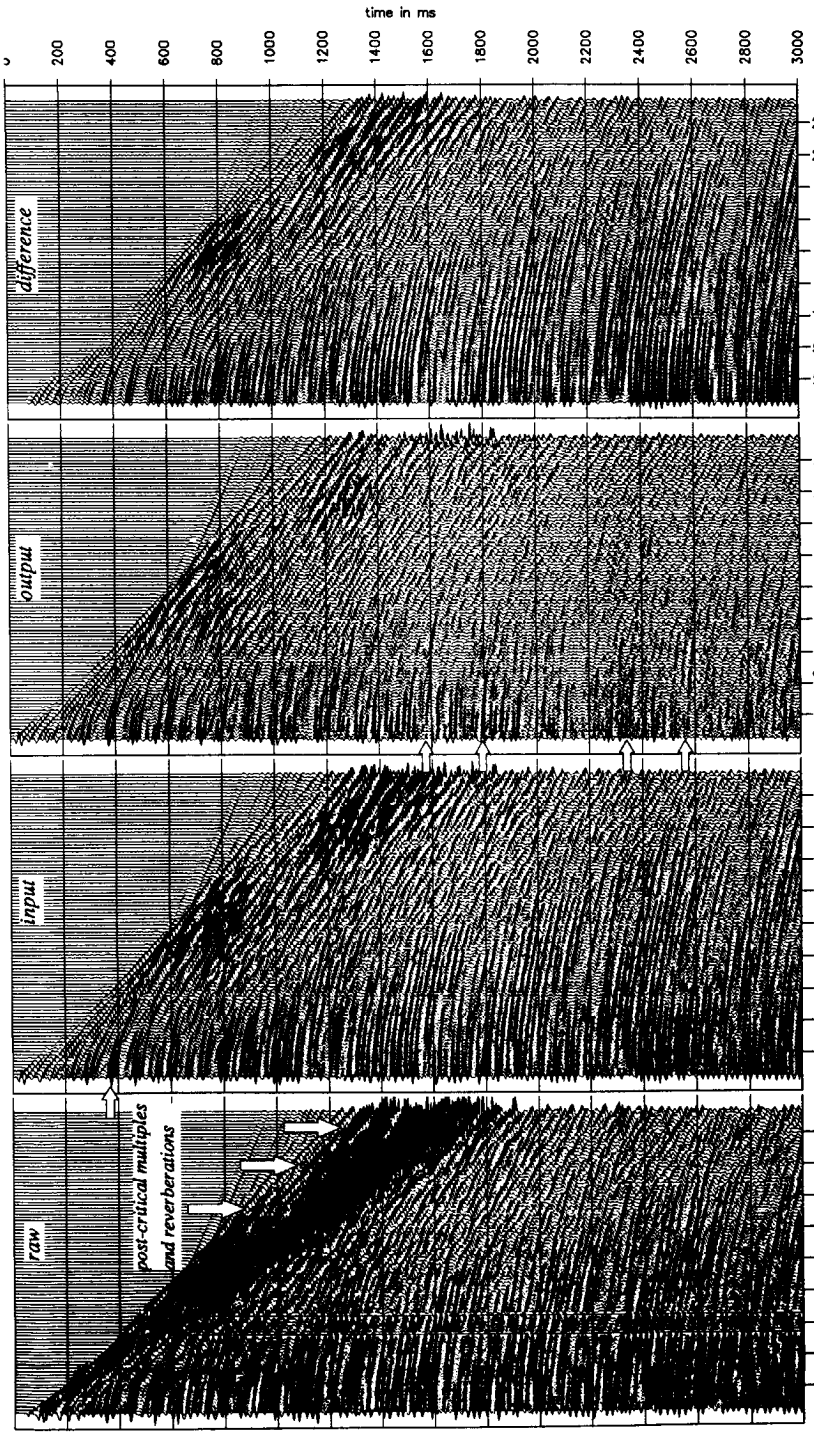

Fig. 7.1 a) Shot record 1 before pre-processing. b) Shot record 1 after anti-alias filtering and trace interpolation. c) Shot record 1 after adaptive surface-related multiple elimination. d) Difference before and after multiple elimination, i.e. the eliminated multiples.

The following pre-processing has been applied on the data:

- For the estimation of the missing near offset traces, NMO correction on the data has been applied, followed by the spline near offset interpolation, as described in Chapter 5. Also the intermediate missing offsets have been interpolated in the NMO corrected data, using a linear interpolation between the two nearest traces.

- To avoid aliasing in the multiple elimination process the spatial sampling has been transformed from 25 to 12.5 m by padding zeroes to the (NMO-corrected) shot records in the k_x-ω domain, yielding twice as many traces per shot record.

- In the k_x-ω domain also a window has been applied to reduce the high amplitudes of the post-critical events.

- Finally, the direct wave has been muted in the x-t domain.

Fig. 7.1b shows the pre-processing result on the first shot record. The result of adaptive multiple elimination is displayed in Fig. 7.1c. The difference before and after multiple elimination (so the eliminated multiples only) has been plotted in Fig. 7.1d. Note that all shot records have been displayed with the same amplitude scaling. Looking at the results of Fig. 7.1b, c and d it can be observed that not only water layer reverberations are eliminated but also surface-related multiples due to some strong sub-bottom primary reflections; see for example at 0.4 seconds (see arrow in Fig. 7.1b). They belong to the group of what we called the "remaining" surface-related multiples in Chapter 1. Note that some primary events are remarkably well restored from interference with multiples (see at the arrows in Fig. 7.1c). Comparing Fig. 7.1c and Fig. 7.1d one can conclude that most energy in the data, especially at the larger travel times, is multiple energy!

For the sections of Fig. 7.1b, c and d (shot record before and after multiple elimination and the difference) a velocity panel has been generated. These velocity panels are displayed in Fig. 7.2a, b and c. Also from the velocity panels the enormous reduction of events going from Fig. 7.2a to b is clearly visible. Fig. 7.2b also shows that primary events are left in the data after multiple elimination.

Fig. 7.3 gives the estimated wavelet. As the smallest periodicity of the surface-related multiples is less than 100 ms, the inverse wavelet that is estimated should not have a longer duration than 100 ms.

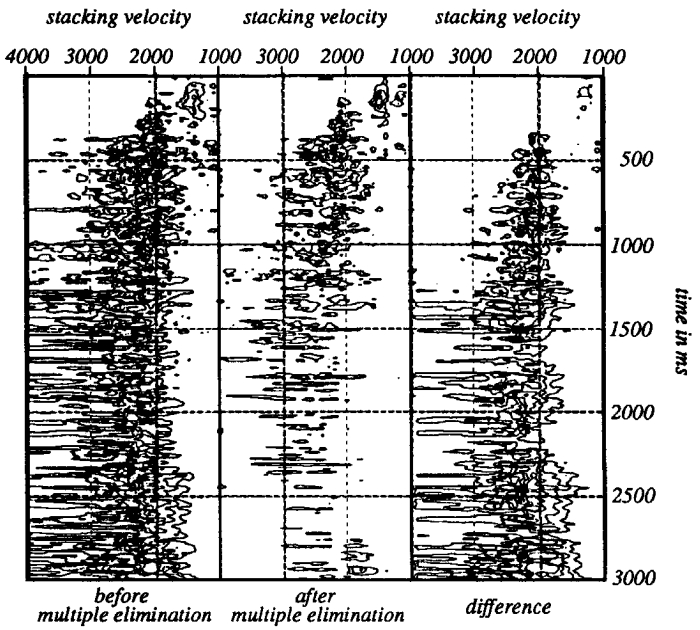

Fig. 7.2 *Velocity panels corresponding to the sections of Fig. 7.1b, c and d.*

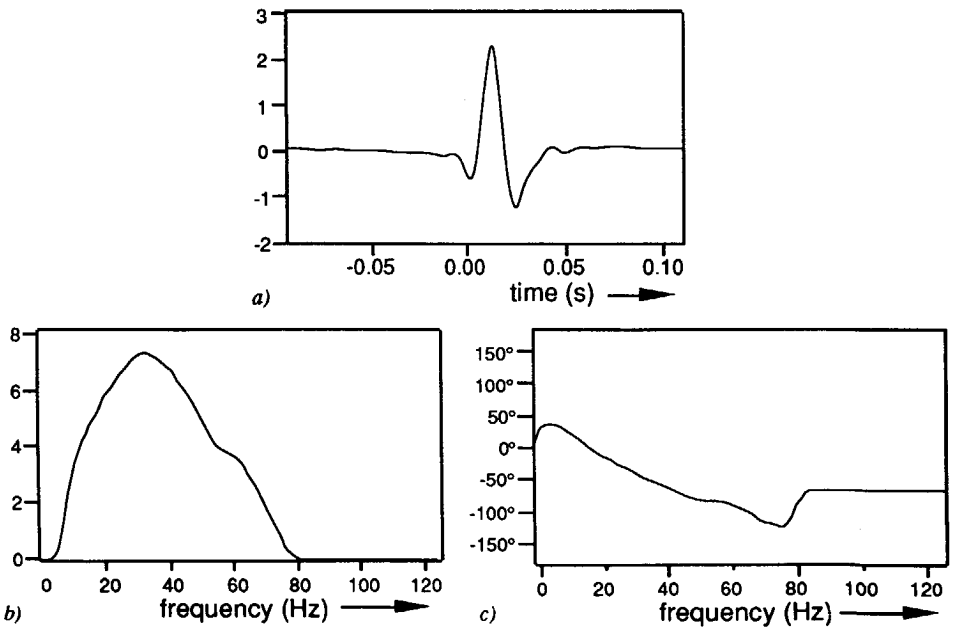

Fig. 7.3 *a) Wavelet estimated with the adaptive multiple elimination procedure b) Amplitude spectrum of the estimated wavelet c) Residual phase spectrum of the estimated wavelet.*

The results of two other shot records (shot 101 and shot 151) are displayed in Fig. 7.4, with the shot record after surface-related multiple elimination and the removed multiples being shown. Indeed the multiple elimination process for shot record 101 and 151 has been very effective. Note that the behavior of the multiples is rather different for these 3 records. Note also that the multiple problem seems to be most severe for the smaller offsets.

A common offset section (at offset 200m) is extracted from the shot records before and after multiple elimination and has been displayed in Fig. 7.5. From Fig. 7.5a, the common offset section with multiples, and Fig. 7.5c, the removed multiples, it is clear that the multiple behavior varies significantly from shot to shot. The multiple generating part of the subsurface (upper part of the sections) looks rather horizontally layered. However, small variations in the structure and/or reflectivity has a large influence on the multiple behavior. This is because with each order of multiples the influence of those variations is increased. The surface-related multiple elimination procedure is capable of following these variations perfectly as no information about the subsurface is needed. The data itself contains all the necessary information for perfect multiple elimination.

The same conclusions can be drawn from the stacked section, as shown in Fig. 7.6. Even for the stack the difference before and after multiple elimination (Fig. 7.6a and b) is large. Apparently the stacking velocities of primaries and multiples are very close which results in the fact that stacking does not lead to a considerable reduction of multiples. In the multiple free stack (Fig. 7.6b) continuous events are restored from behind the strong multiples in the lower half of the section, indicated with arrows. This makes interpretation a lot more easy. Note again from Fig. 7.6c the remarkable amount of multiples that has been removed.

Although the stacked section shows a good improvement after multiple elimination, the strong point of the surface-related multiple elimination lies in the fact that the output consists of multiple-free shot records, which allows further processing on *pre-stack* data.

For this data set, after resampling in both source and receiver direction, yielding a line of 401 shot records of 397 traces of each 1024 time samples, eliminating multiples up to the 10th order took about 30 minutes CPU time per shot record on a Convex C1. No effort was made to optimize the code for efficiency. For example, the "padding zeroes" method (see Chapter 6) has been used for the field data examples, to prevent wrap around effects. With the "Laplace" method being used a factor 2 in CPU time could be gained.

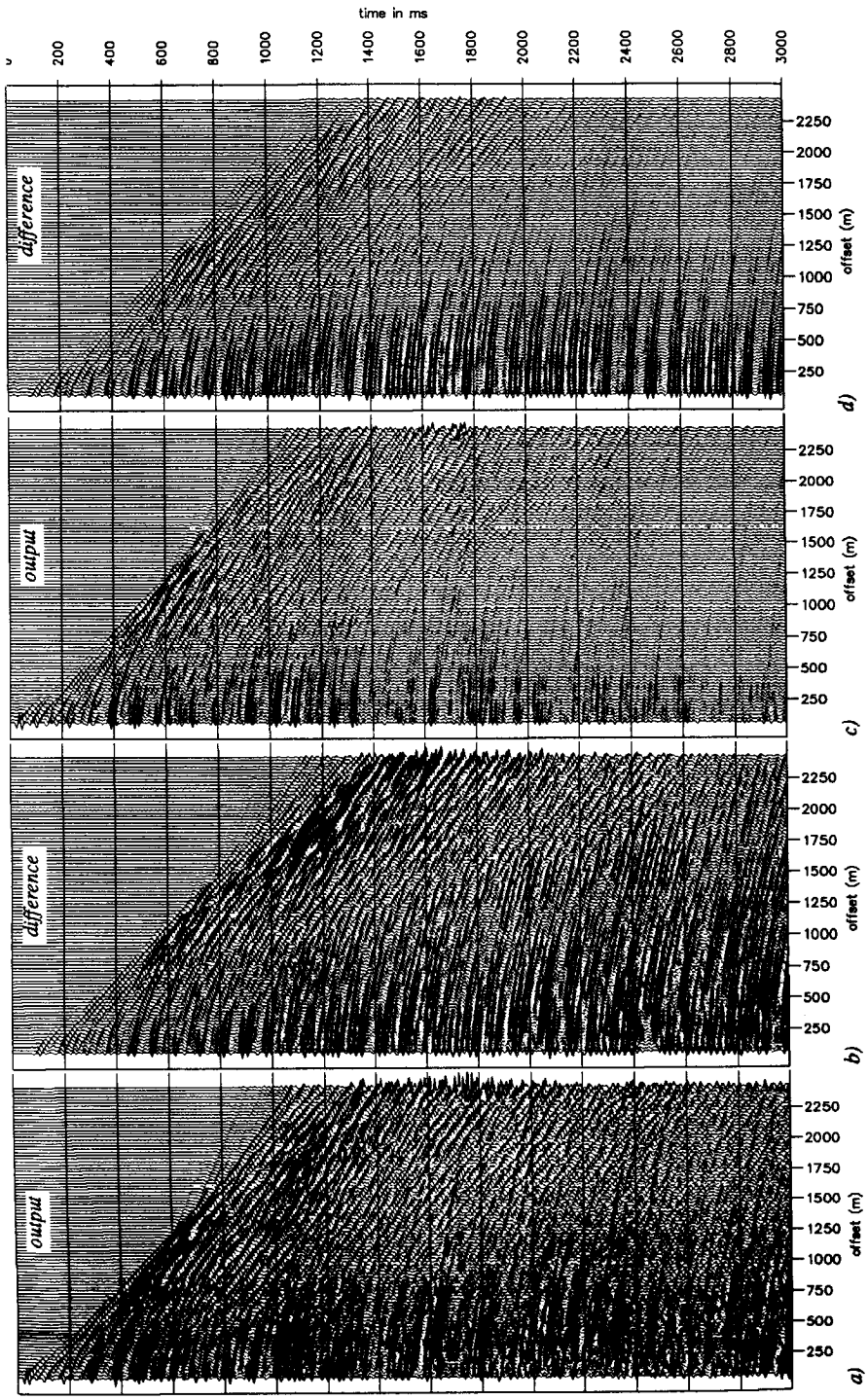

Fig. 7.4 a) Shot record 101 after adaptive surface-related multiple elimination b) Difference with input data, i.e. the eliminated multiples c) Shot record 151 after adaptive surface-related multiple elimination d) Difference with input data, i.e. the eliminated multiples

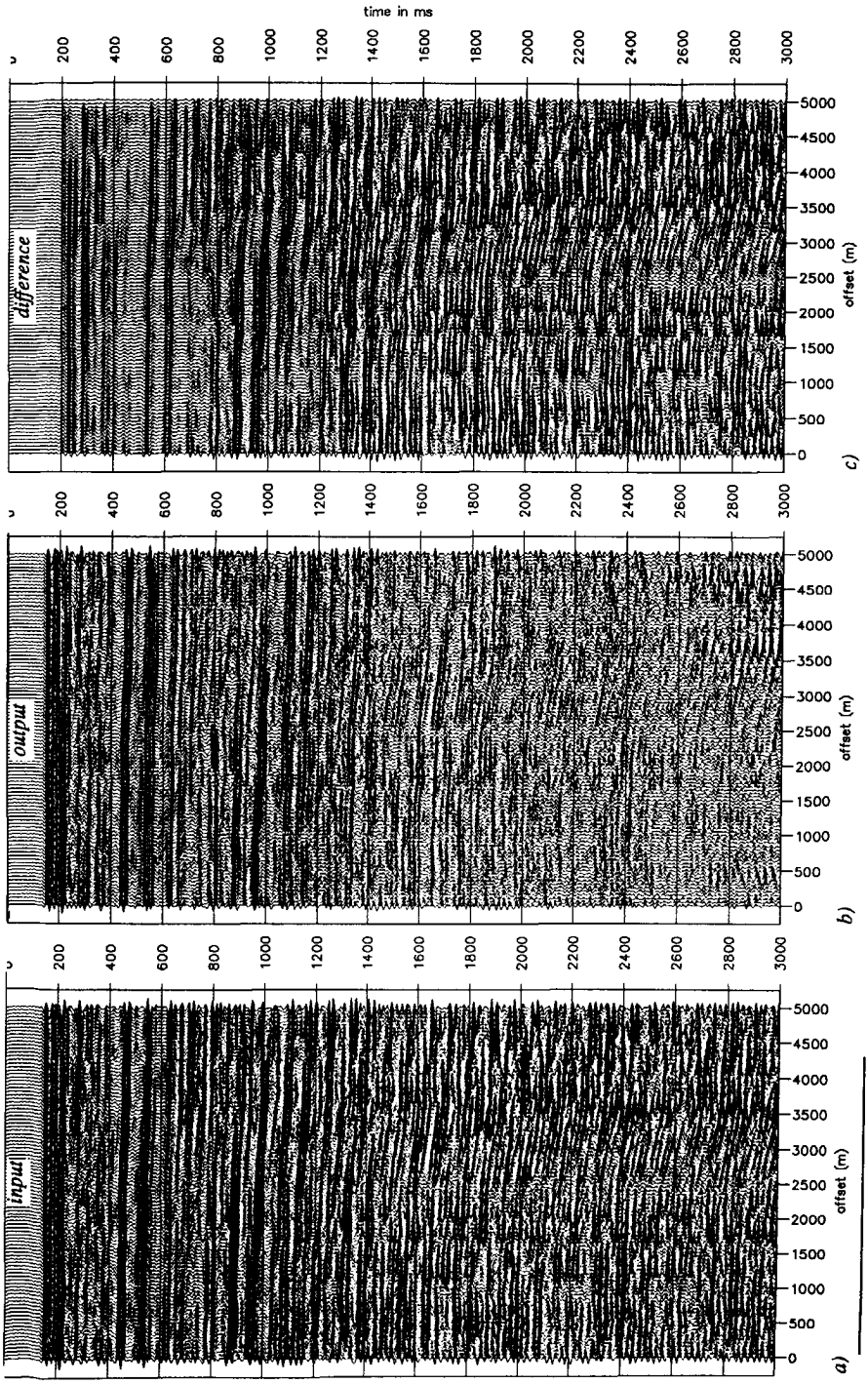

Fig. 7.5 a) *Common offset section before multiple elimination b) Common offset section after multiple elimination c) Difference before and after multiple elimination, i.e. the eliminated multiples. Note the significant lateral changes in the multiple system.*

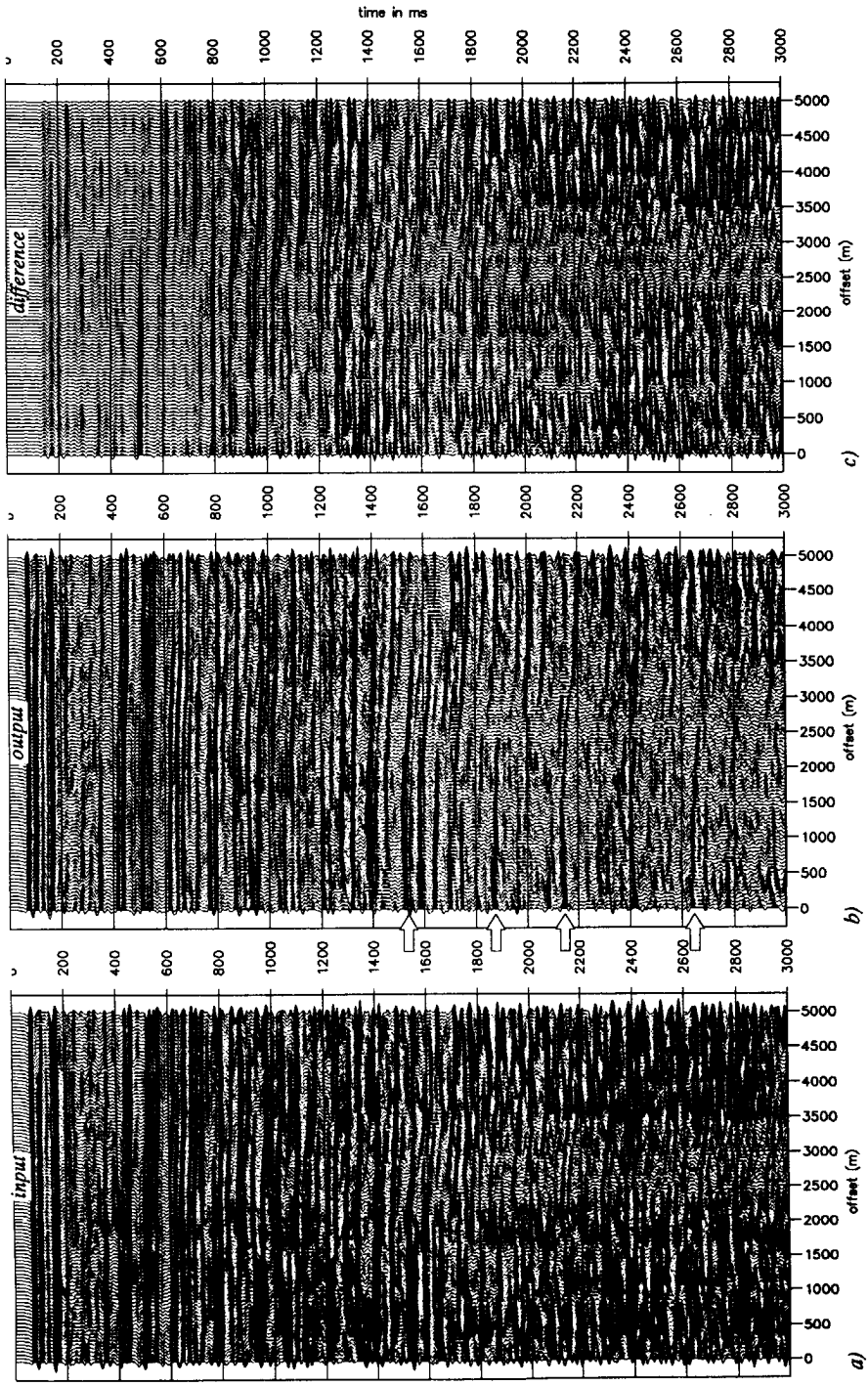

Fig. 7.6 a) Stacked section without multiple elimination b) Stacked section including multiple elimination c) Difference before and after adaptive surface-related multiple elimination, i.e. the eliminated multiples. Note that for this situation the stack is not an effective multiple remover.

7.2 MARINE DATA EXAMPLE 2

The second field data set is from the North Sea with a local water depth of almost 300 m. This means that the water layer reverberations have a period of about 400 ms. A line of 350 shot records has been treated, each shot record consisting of 120 traces with 25 m shot and receiver spacing. The missing near offset is 150 m or 6 traces. The processing sequence for the surface related multiple elimination is similar to the previous example, except the shot and receiver resampling could be skipped, as the data could be easily anti-alias filtered. The adaptive surface-related multiple elimination procedure has been applied for all shot gathers. The pre-stack multiple elimination process itself took about 15 CPU minutes per shot gather on a Convex C1.

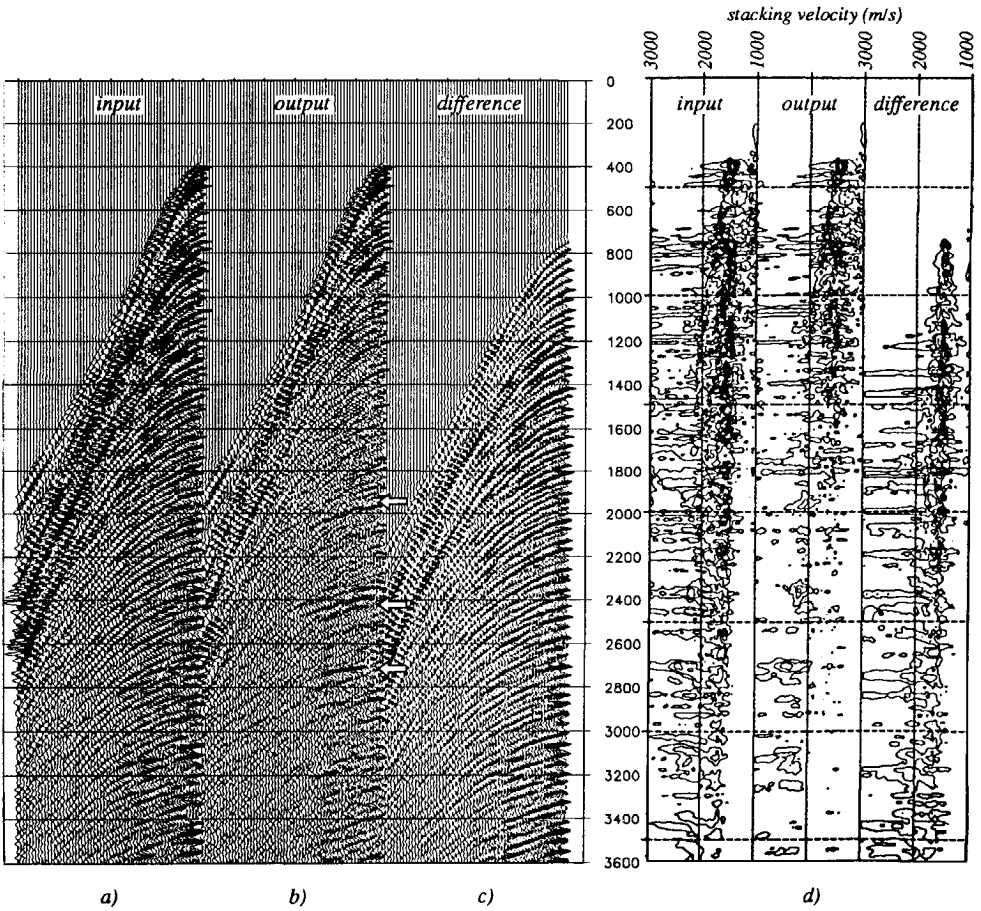

Fig. 7.7 *a) Shot record 180 with multiples b) Shot record 180 after adaptive surface-related multiple elimination c) Difference between a) and b), i.e. the eliminated multiples d) Velocity panels corresponding to a) b) and c).*

Fig. 7.7 shows shot record 180 before and after surface-related multiple elimination and the difference of these two, all displayed with the same scaling. To see the effect on the velocity panel, Fig. 7.7d shows the velocity panels of the CMP-gather before and after multiple elimination, and the velocity panel of the difference (Fig. 7.7c). Clearly a reduction of multiples is visible in Fig. 7.7, especially in the lower part of the section. Also the velocity panels show the enormous reduction in multiple energy. The shot record with the eliminated multiples only, Fig. 7.7c, together with the corresponding velocity panel, show that all eliminated events are highly correlated events indeed. The arrows in Fig. 7.7b point at recovered primaries, which can also be identified in the corresponding velocity panel.

The source signature that has been estimated is shown in Fig. 7.8, with in Fig. 7.8c the actual estimated phase spectrum (after applying a -24 ms time shift on the wavelet) and in Fig. 7.8d the phase spectrum after restoring this time shift. As a limited frequency band has been used for multiple prediction only (10-60Hz) , the estimated wavelet is a band pass filtered version of the original wavelet. As the decomposition procedure in upgoing wave fields has been omitted in the processing sequence, the receiver ghost is part of the estimated wavelet. Although the wavelet has been estimated for different source positions, no noticeable deviations have been found.

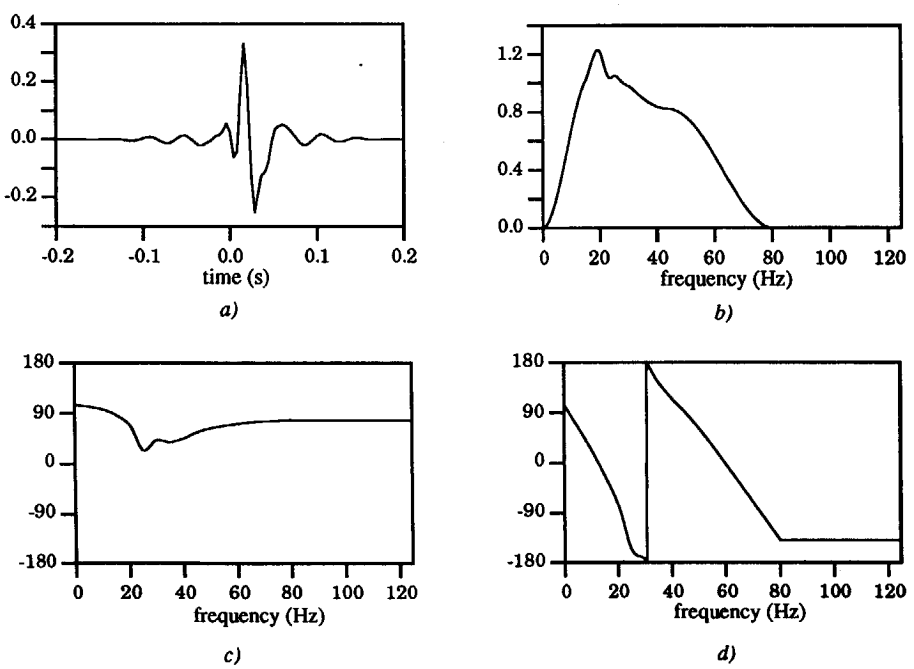

Fig. 7.8 Estimated wavelet from the real dataset. a) Time domain representation b) Residual amplitude spectrum c) Residual phase spectrum d) Full phase spectrum.

Fig. 7.9 shows a common offset section (600 m offset) of the data before and after multiple elimination, together with a plot of the difference. The reduction of multiples is clear. Note the small synclinal structure around shot position 70, which produces a focussing of multiple energy. Also around shot 170 a focussing of multiple energy can be observed. This is probably due to small variations in the structure of the water bottom; it yields a remarkable variation of multiple energy density going from left to right in the section. The surface-related multiple elimination method can fully cope with those lateral changes.

Also the stack is shown before and after multiple elimination; the velocity analysis was done on the data after multiple elimination. Fig. 7.9a shows the stacking result with multiples. As expected, the removal of multiple energy is not so spectacular on the stacked sections as for this situation the velocity differences between primary and multiple events is sufficient to remove a significant amount of multiple energy by stacking. But still there are many multiples that appear on the stack before multiple elimination (Fig. 7.9a) which have been nicely removed by the surface-related multiple elimination method (Fig. 7.9b). In Fig. 7.9a some of these events and areas have been pointed at by arrows. As a matter of fact, these are the multiples that have small move-out differences with the primaries and belong to the category "remaining surface-related multiples". To judge the value of the stack after multiple elimination the difference plot of the stacked section before and after surface-related multiple elimination is shown in Fig. 7.9c. The difference plot shows correlated events, especially in the lower part of the section. In the target zone, which is between 2200 and 2400 ms, a stacked multiple at 2300 ms is visible at the left side of Fig. 7.9c (see the arrow); it is masking the primary reflection that occurs at the same time in Fig. 7.9b. Note again the band of focussed multiples under the small synclinal structure around CMP positions 70 and 170 in Fig. 7.9c.

As a last remark it should be mentioned that the improvement of *pre-stack* data (restoring the primaries over the full offset range, see Fig. 7.7) is more interesting than the improvement of the stack.

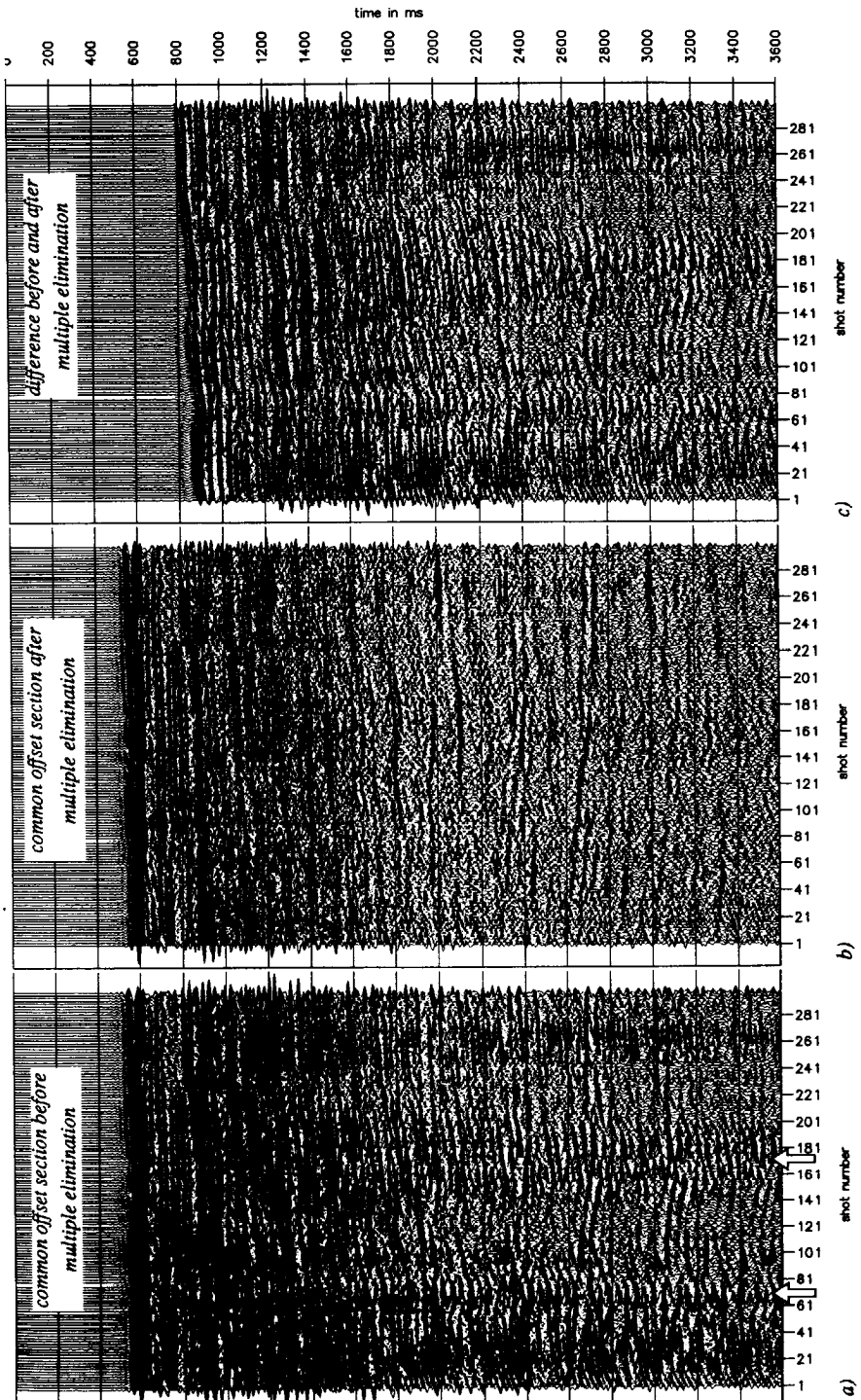

Fig. 7.9 *a) Common offset section with multiples. b) Common offset section after surface-related multiple elimination. c) Difference before and after surface-related multiple elimination, i.e. the surface-related multiples only. Note the large lateral differences in multiple energy.*

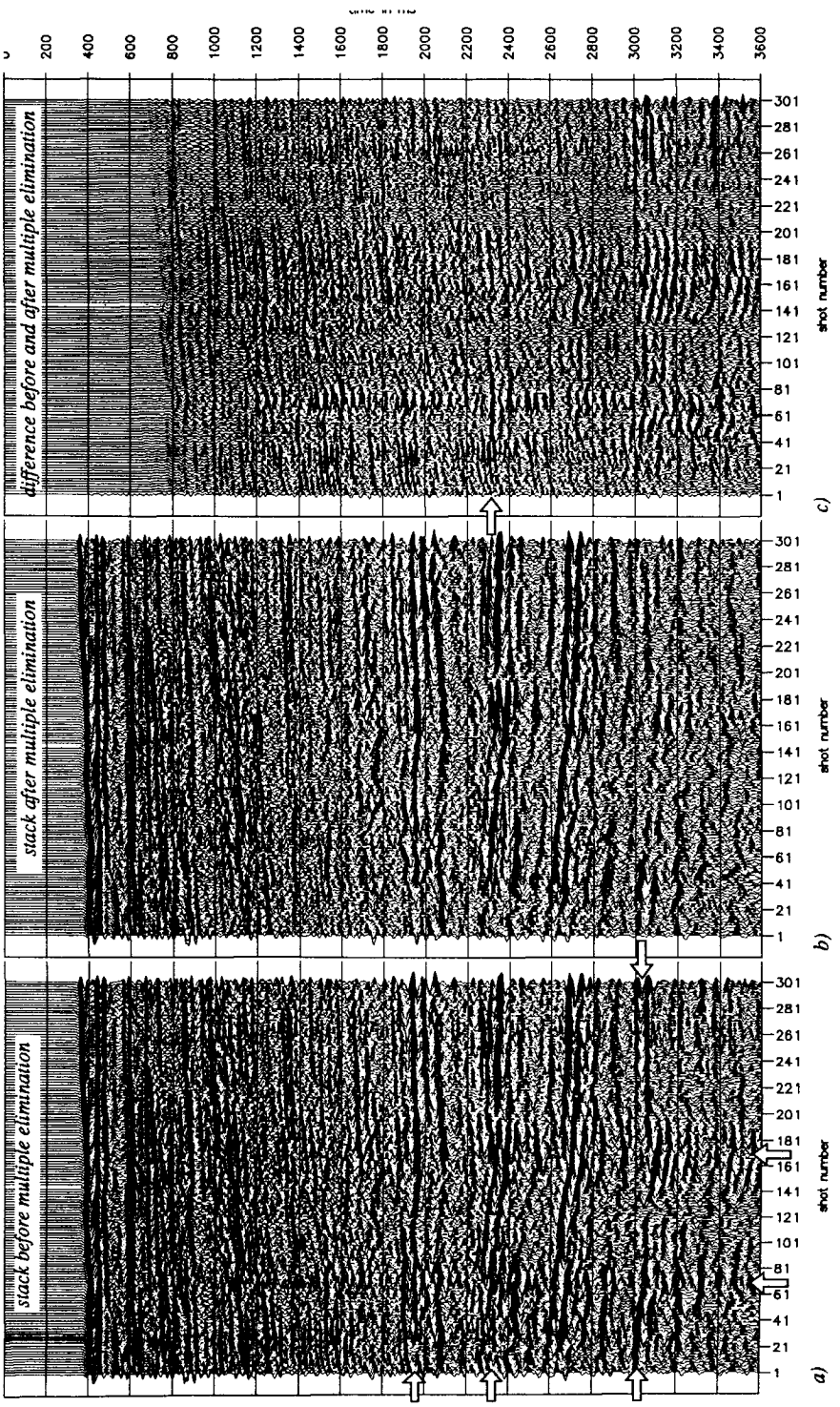

Fig. 7.10 *a) Stacked section with multiples. b) Stacked section after application of the surface-related multiple elimination. c) Difference before and after surface-related multiple elimination, i.e. the stacked surface-related multiples only.*

8

SURFACE-RELATED MULTIPLE ELIMINATION, A CMP VERSION

In this chapter an efficient version of the surface-related multiple elimination process is discussed, which acts on individual CMP-gathers. With this version the assumption of a (locally) 1D medium is made and each CMP gather is considered as the shot record of a true 1D medium. For a true 1D medium all shot records are equal, and multiple elimination can be carried out in the wave number or ray parameter domain as simple multiplications in stead of matrix multiplications. This speeds up the calculations considerably.

8.1 CMP-ORIENTED MULTIPLE ELIMINATION IN SLOWLY VARYING MEDIA

As the shot record-oriented multiple elimination process is rather time consuming, the method may be considered as a special processing tool (like pre-stack migration) rather than a standard processing tool at this moment. Therefore, it is interesting to have an efficient alternative, which can also be used as a standard processing tool, sacrificing some accuracy in the result compared to the full shot-record-oriented version.

To achieve this the following suggestion is made:

- Reorder the seismic data into CMP-gathers (which is always done in standard processing practice).

- Consider each CMP gather as a shot record and apply 1D multiple elimination per "shot record", using the benefits of going to the k_x-ω or p-ω domain where spatial convolutions (matrix multiplications) reduce to scalar multiplications.

The underlying principle is the fact that for a 1D subsurface model all shot records are equal. In this situation the multiple elimination can be carried out by transforming this one shot record to the k_x-ω or the p-ω domain.

Multiple elimination in the x-ω domain has been described by:

$$\mathbf{P}_0^-(z_0) = \mathbf{P}^-(z_0) - A(\omega)\{\mathbf{P}^-(z_0)\}^2 + A^2(\omega)\{\mathbf{P}^-(z_0)\}^3 - A^3(\omega)\{\mathbf{P}^-(z_0)\}^4 + \dots , \qquad (8.1)$$

with the surface factor $A(\omega)=r_0S^{-1}(\omega)$.
If the medium is 1D, yielding identical shot records at each position, the procedure can be carried out in the k_x-ω domain in the following way:

$$\tilde{P}_0^-(k_x,\omega;z_0) = \tilde{P}^-(k_x,\omega;z_0) - A(\omega)\{\tilde{P}^-(k_x,\omega;z_0)\}^2 +$$
$$A^2(\omega)\{\tilde{P}^-(k_x,\omega;z_0)\}^3 - A^3(\omega)\{\tilde{P}^-(k_x,\omega;z_0)\}^4 + \dots , \qquad (8.2)$$

with $\tilde{P}^-(k_x,\omega;z_0)$ the monochromatic shot record under consideration as a function of the horizontal wave number k_x, i.e. one column of the data matrix $\mathbf{P}^-(z_0)$ after a spatial Fourier transform. The matrix multiplications in equation (8.1) have been replaced by scalar multiplications in equation (8.2). A similar expression for the p-ω domain can be given, but at this moment we will focus on the application in the k_x-ω domain. In fact Koster (1991) uses a non-adaptive surface-related multiple elimination version in the p-ω domain for his pre-stack inversion of CMP-gathers.

As in practice the subsurface is never totally 1D the assumption that all shot records are equal does not hold. However, by considering CMP-gathers as shot records, the 1D assumption is better satisfied and the multiple elimination process may still produce good results if the medium (and especially the upper part which generates the multiples) is laterally slowly varying. Applying the method on individual CMP-gathers has two advantages:

- Calculations can be carried out by scalar multiplication in the k_x-ω domain in stead of matrix multiplications in the x-ω domain, which speeds up the processing time considerably (a factor of 10 can be gained).

- The processing can be done per individual CMP-gather , which saves a lot of computer memory and IO, compared to surface-related multiple elimination on shot records simultaneously, where for each multiple elimination step (elimination of one order of multiples) all data matrices have to be collected.
  As standard processing is done on CMP-gathers anyway, the reordering from shot records to monochromatic data matrices can be omitted.

8.2 SIMULATED DATA EXAMPLE

To see whether the CMP approach is acceptable a data set has been simulated for the subsurface model of Fig. 8.1. In this subsurface model the maximum dip of the reflectors is 5°, with a small synclinal structure (10 m depth, with also a maximum of 5° dip) and, from 1000 m onwards, with more globally dipping interfaces. As the model is rather shallow, the aperture of the simulated seismic data is large enough to see the influence of the inhomogeneities on the data. The amount of 101 shot records were simulated with a Kirchhoff extrapolation algorithm. The shot positions were located from 0 to 2000 m with steps of 20 m. Each shot record contains 101 traces in a split spread configuration with offsets from -1000 to 1000 m relative to the source position. On this dataset full 2D adaptive surface-related multiple elimination has been applied first. Fig. 8.2 shows the original source signature (solid line) and the estimated signature (dashed line). The source signature has been well estimated, within the frequency band of optimization from 10 to 30 Hz, especially the phase spectrum has been recovered almost perfectly. Note that the zero phase property of the source function has not been used in the optimization as a constraint.

If the zero offset section is extracted from the shot records before and after multiple elimination clearly a perfect removal of the surface multiples can be observed, leaving the three primaries (Fig. 8.3). The steeply dipping events crossing the data from the edges to the middle are edge effects from the multiple elimination, because of the finite number of shot records. This could have been prevented by applying a taper on the largest offsets.

The next step is to reorder the original shot records into CMP-gathers and apply the adaptive multiple elimination method on each CMP-gather separately, assuming that they are shot records over a 1D medium. There are twice as much CMP-gathers (202) as shot records with a twice as sparse trace sampling. To prevent spatial aliasing effects during multiple elimination, the CMP-gathers have been merged two by two, creating 101 CMP-gathers with the same trace spacing as in the shot gathers.

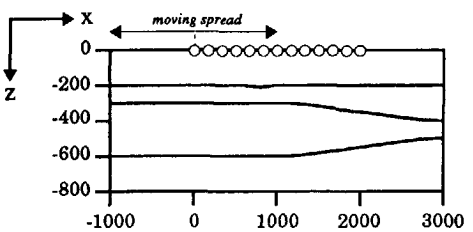

Fig. 8.1 Subsurface model with maximum 5° local dip.

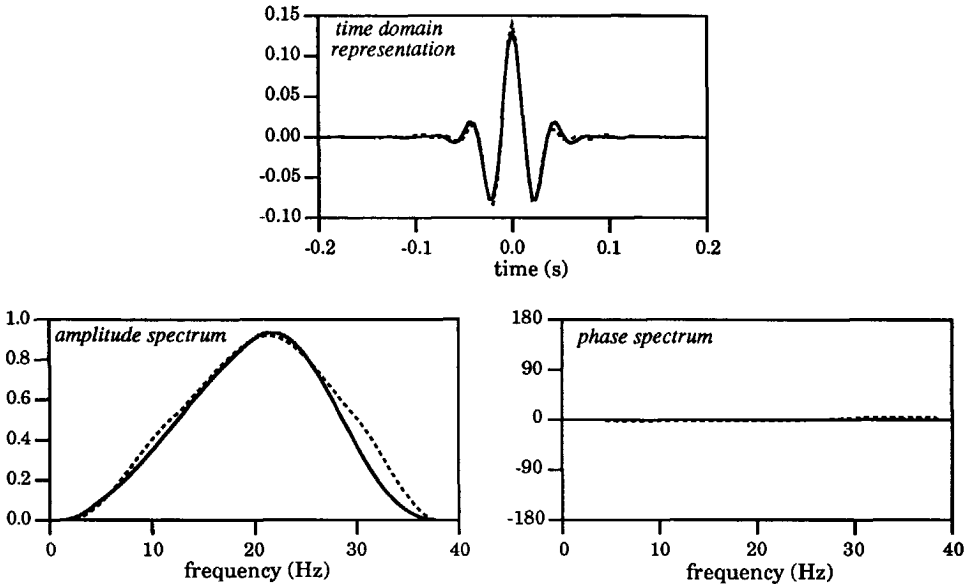

Fig. 8.2 *Original source signature used for modeling (plain line) and signature estimated with the full shot record-oriented multiple elimination (dashed line).*

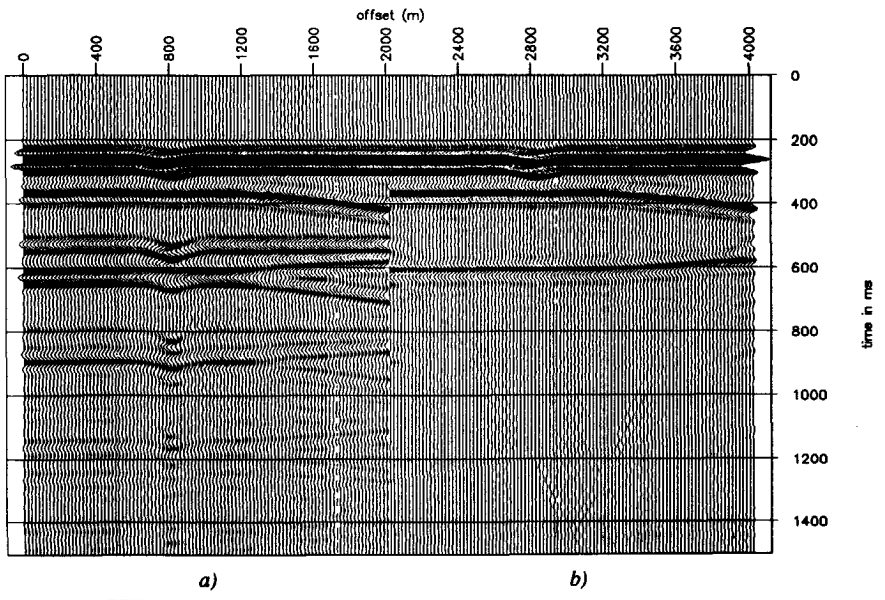

Fig. 8.3 *a) Zero offset section simulated in the subsurface model of Fig. 8.1 b) Zero offset section after shot record-oriented surface-related multiple elimination.*

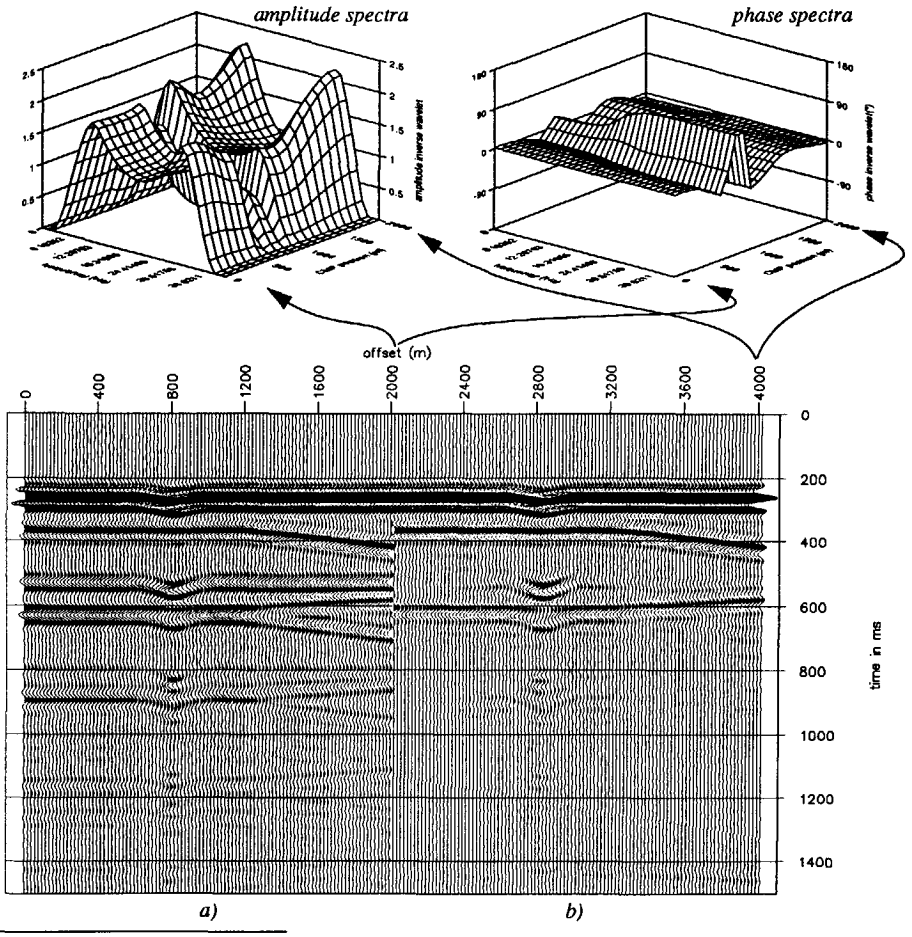

Fig. 8.4 *a) Zero offset section with multiples. b) Zero offset section after CMP-oriented surface-related multiple elimination. At the top the estimated inverse source functions per CMP-gather are given as amplitude and phase spectrum.*

From these CMP-gathers before and after CMP-oriented multiple elimination the zero offset traces have been selected (Fig. 8.4). Note that the zero offset section with multiples (Fig. 8.4a) is identical to Fig. 8.3a. The multiple elimination result is surprisingly good. In the global dipping region at the right hand side of the model, the multiples have been well suppressed. Below the small synclinal structure, the result is less good, because the subsurface variations are too fast there. So the local dip is not the only restriction, but also how *fast* the local dip changes. For laterally slowly varying media, the CMP-oriented method is a very good alternative for media with about 5 degree maximum dip. The effectiveness of the CMP-oriented multiple elimination can also be observed in the plot of the amplitude and phase spectra of the *inverse* source function, on the top of Fig. 8.4. The first estimated inverse source function (at offset 0 m) is the correct one, as the subsurface model is horizontally layered in that region.

Going from the low to the high CMP positions, a sudden decrease in amplitude and a deformation of the phase spectrum occurs around the synclinal structure at 800 m offset. Here the CMP-oriented multiple elimination cannot succeed to find one source function that can remove the multiples completely. Note that the estimated multiples are weighted with the *inverse* source function, being part of A(ω). So a *small* value of the estimated inverse source function in the CMP-oriented method indicates that the 1D assumption is severely violated.

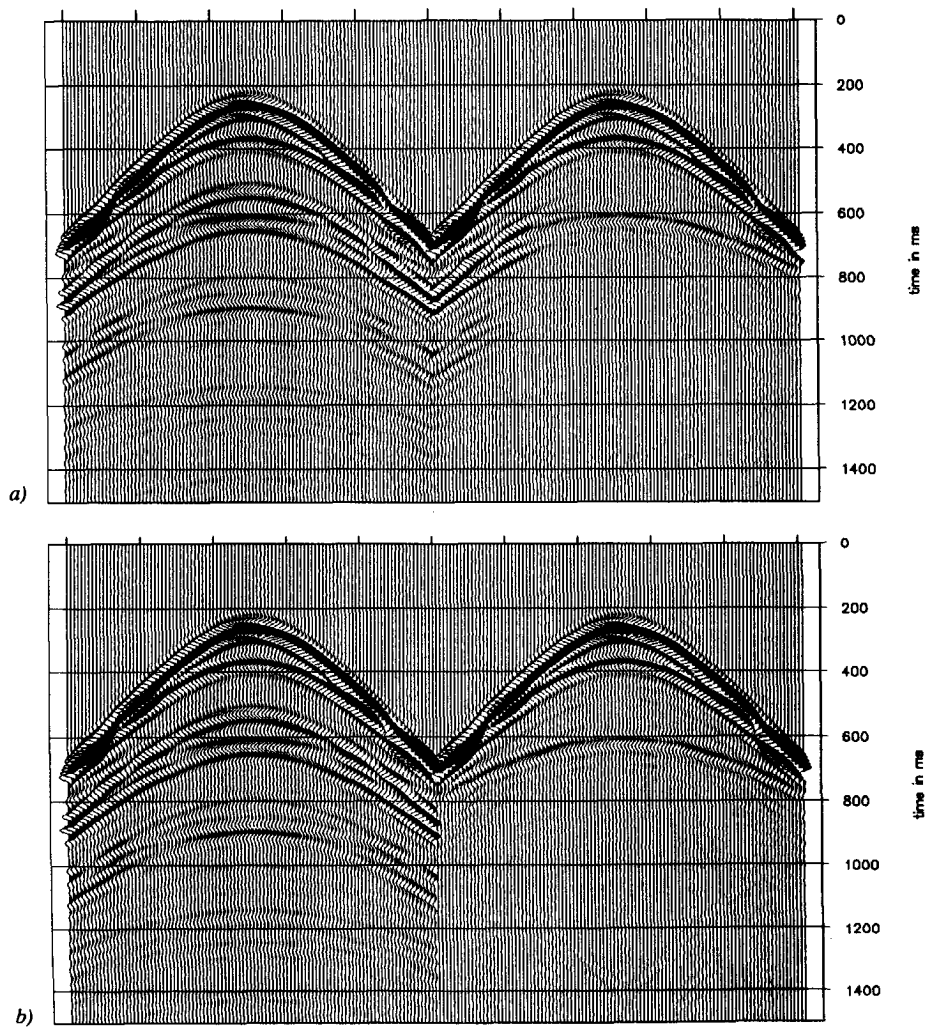

Fig. 8.5 *a) Shot record with source located at x=200 m before (left side) and after (right side) shot record-oriented multiple elimination b) CMP-gather at the same position before (left side) and after (right side) CMP-oriented multiple elimination.*

For a further comparison of the full pre-stack multiple elimination versus the CMP-oriented multiple elimination, the results are considered for three shot positions. Fig. 8.5 shows the result for the source position at 200 m, Fig. 8.6 the result for the source just above the syncline and Fig. 8.7 shows the result for the source at 1600 m. For the horizontal part of the model both the pre-stack as well as the CMP-oriented results are good (Fig. 8.5) as can be expected. For the shot record-oriented result there are remainings at the left side, as the coverage is insufficient for the first shot records. The CMP-oriented method is not sensitive for this coverage problem as only the CMP-gather itself is used for the multiple elimination.

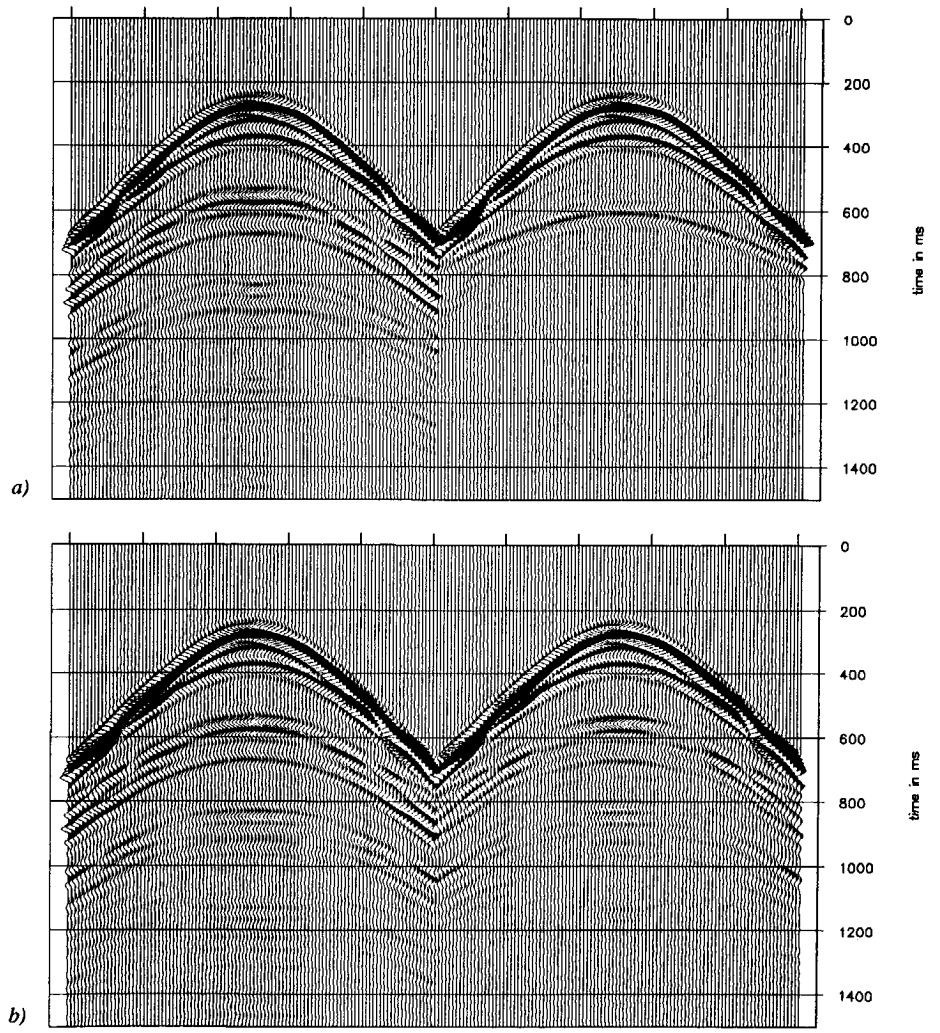

Fig. 8.6 *a) Shot record with source located at x=800 m before (left side) and after (right side) shot record-oriented multiple elimination b) CMP-gather at the same position before (left side) and after (right side) CMP-oriented multiple elimination.*

Above the syncline the CMP-oriented method encounters some problems (Fig. 8.6), as the multiples cannot be correctly predicted by the primaries. In the slowly dipping region (Fig. 8.7) both methods produce good results (except again the edge effects for the shot record-oriented method due to low coverage at the right hand side). The CMP-oriented method especially works well on the small offsets. For the larger offsets, where the influence of the dipping structure becomes larger, multiple energy is left. Fortunately, at the larger offset there are other methods (e.g. f-k filtering) that can easily remove these remnants.

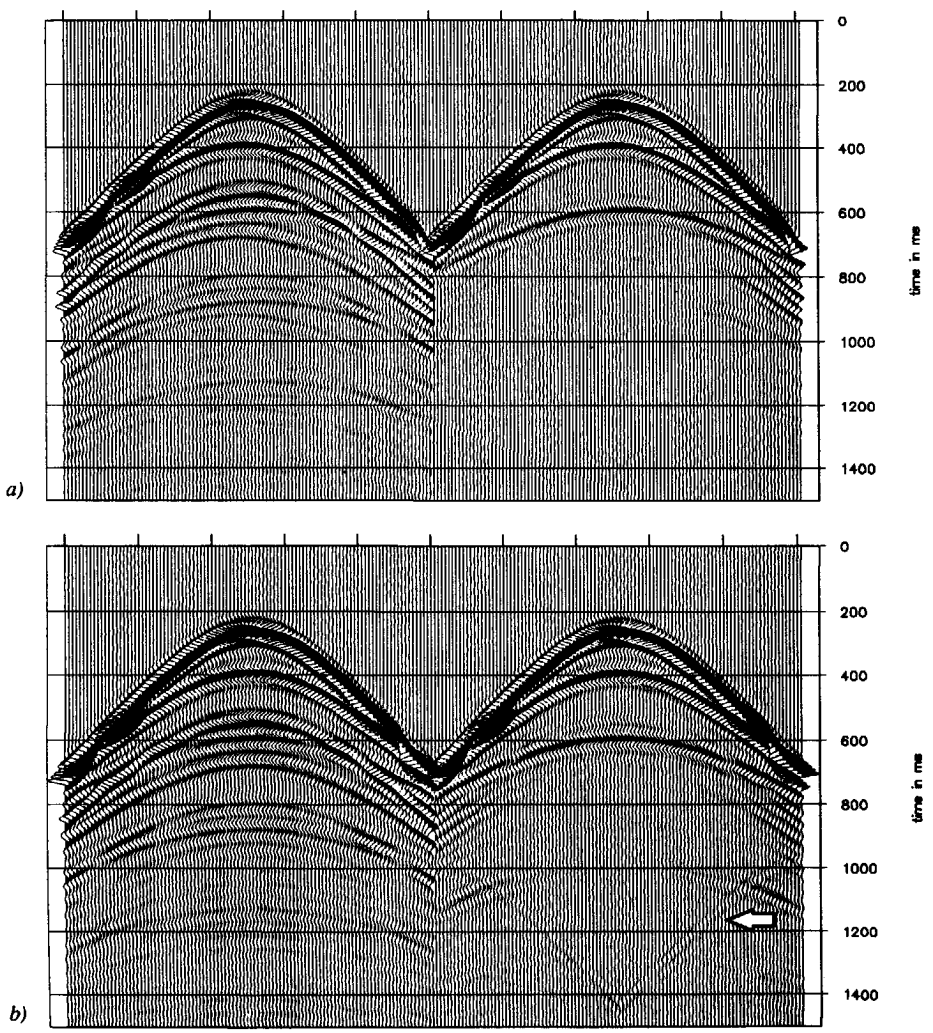

Fig. 8.7 *a) Shot record with source located at x=1600 m before (left side) and after (right side) shot record-oriented multiple elimination b) CMP-gather at the same position before (left side) and after (right side) CMP-oriented multiple elimination. The arrow points at an edge effect due to limited aperture.*

The arrow in Fig. 8.7b points at an edge effect due to the limited aperture of the data (see the discussion on missing far offsets in Chapter 5). In this example this effect is large as the primary has a large amplitude at the large offsets (see Fig. 8.7b at the right around 700 ms).

8.3 FIELD DATA EXAMPLE

On the second marine data example, as discussed in section 7.2, also the adaptive CMP-oriented multiple elimination method has been applied for the first 150 CMP-gathers in the section. As the medium is not completely one-dimensional and especially the multiple energy varies with the source position, this data serves as an interesting test case for the CMP-oriented multiple elimination procedure.

Fig. 8.8 shows the result for CMP-gather 41, with in Fig. 8.8a the original CMP-gather with multiples, in Fig. 8.8b the CMP-gather after CMP-oriented surface-related multiple elimination. For comparison the same CMP-gather extracted from the shot records after full shot record-oriented surface-related multiple elimination has been displayed in Fig. 8.8c. With the CMP-oriented multiple elimination process a lot of multiples have been removed indeed. The result is comparable to the full shot record-oriented process. However, small differences between the CMP-oriented result and the full shot record-oriented result can be observed. This can be expected, as discrepancies due to the non-one dimensionality of the medium become more noticeable for larger offsets. Consequently, a trade-off is found in the CMP-oriented application, with the total multiple reduction being a little less than the full shot record-oriented result. This can also be observed in the difference plot in Fig. 8.8d, showing the difference between the CMP-oriented result (Fig. 8.8b) and the full shot record-oriented result (Fig. 8.8c). These differences, however, are smaller than the amount of removed multiples, as can be seen by comparing Fig. 8.8d with Fig. 8.8e.

The application of the CMP-oriented multiple elimination procedure (without the estimation process) took about 2.5 CPU minutes per CMP-gather on the Convex C1, instead of the 15 minutes per shot record in the full shot record-oriented version. However, no effort has been put in optimizing the code for the CMP-oriented version. After optimization we expect the CMP-oriented version to be at least 10 times as fast as the full shot record-oriented version.

From all CMP-gathers before and after CMP-oriented surface-related multiple elimination a common offset section (for 600 m offset) has been extracted. Fig. 8.9a shows the common offset section with multiples, Fig. 8.9b shows the common offset section after the CMP-oriented surface-related multiple elimination. For comparison the common offset section extracted from the shot records after the full shot record-oriented surface-related multiple elimination process is displayed in Fig. 8.9c. It shows that with the CMP-oriented method a large amount of multiple energy can be suppressed. For example, the band of multiples at the left side in

Fig. 8.9a for the first 40 shot numbers is very well suppressed in Fig. 8.9b. However, for CMP gathers around shot number 70, where the small synclinal structure produces relatively strong multiples, the CMP-oriented method is not able to make a proper multiple prediction in the CMP domain. As expected, the full shot record-oriented method could remove these multiples very well (Fig. 8.9c). The same is true for the range of shot number 130 to 150.
Fig. 8.9d shows the difference between the CMP-oriented result (Fig. 8.10b) and the original common offset section (Fig. 8.9a). Fig. 8.10e shows the difference between the original data and the full shot record-oreirented result. Finally, Fig. 8.9f shows the difference between the CMP-oriented result (Fig. 8.9b) and the full shot record-oriented result (Fig. 8.9c). These difference plots show that the CMP-oriented method is partly effective, although especially in the upper part multiples are well suppressed.

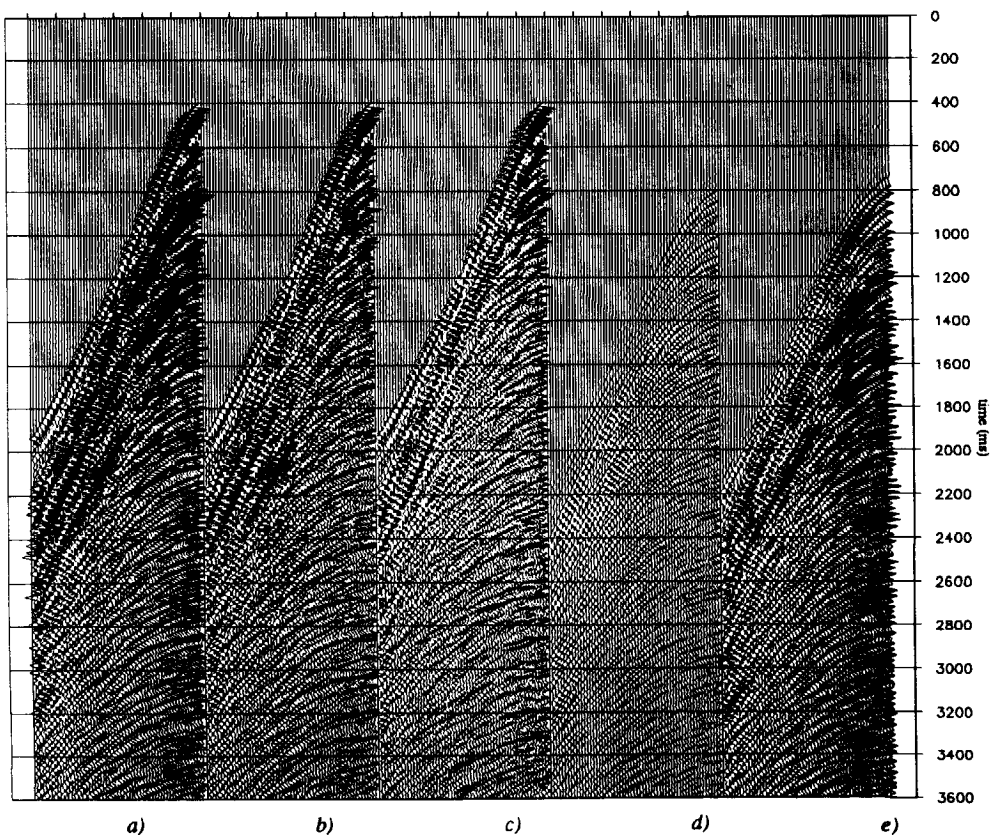

Fig. 8.8 *a) CMP-gather 41 with multiples b) CMP-gather 41 after adaptive CMP-oriented surface-related multiple elimination c) CMP-gather 41 after adaptive full shot record-oriented surface-related multiple elimination d) Difference between CMP-oriented and full shot record-oriented result e) Difference between input data and shot record-oriented result, i.e. the eliminated multiples.*

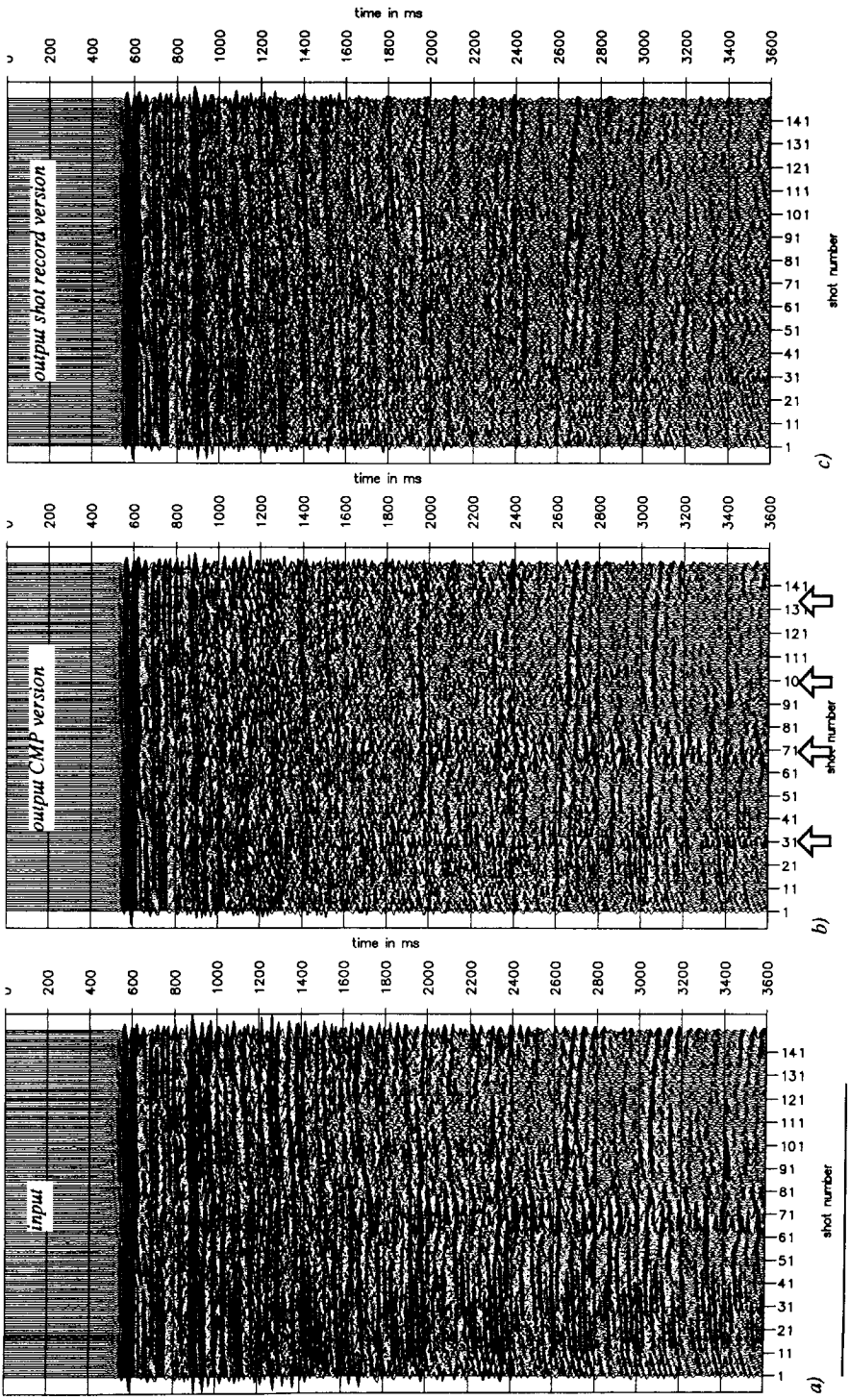

Fig. 8.9 *a) Common offset section with multiples b) Common offset section after CMP-oriented surface-related multiple elimination c) Common offset section after full shot record-oriented surface-related multiple elimination.*

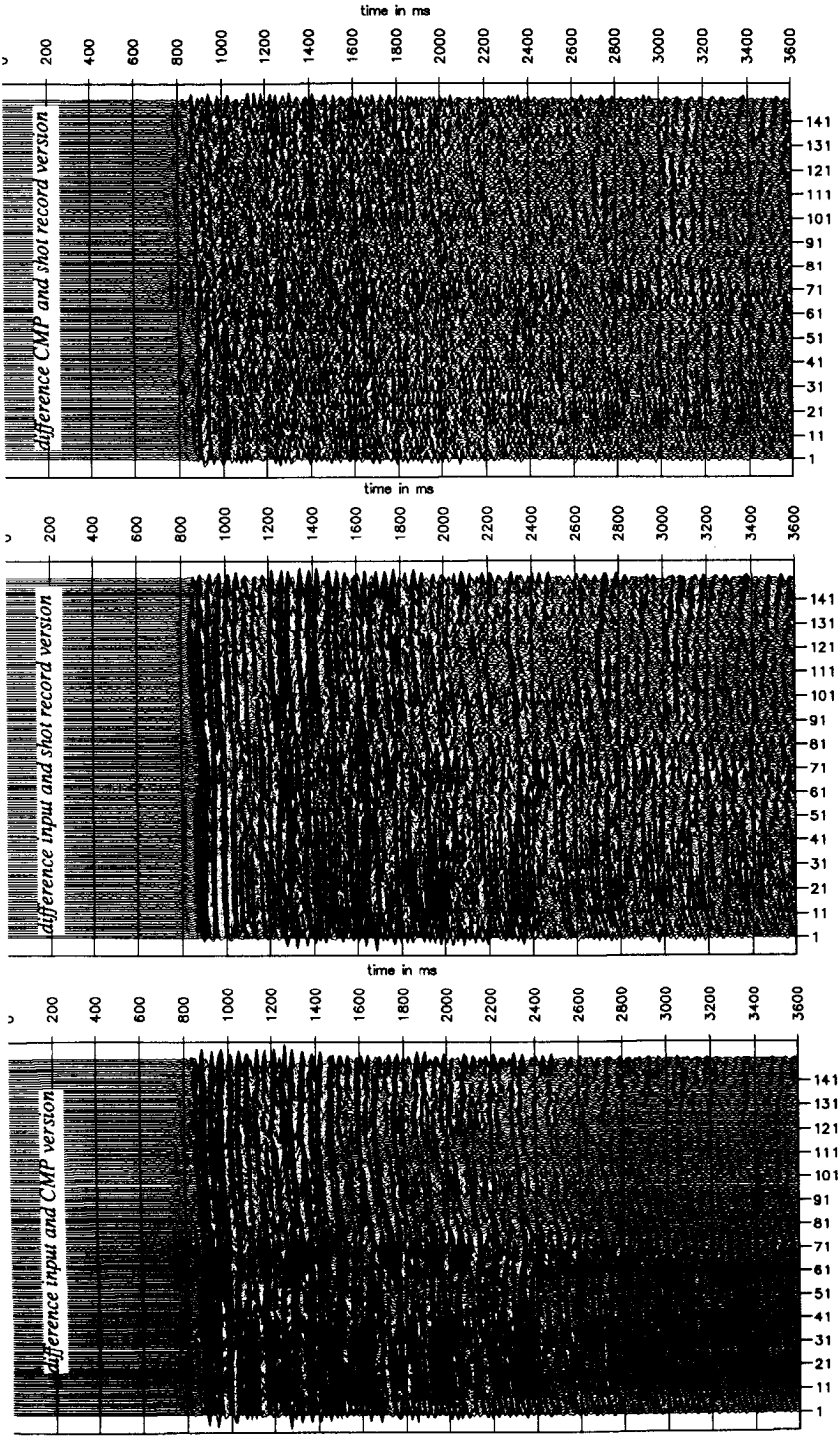

Fig. 8.9 (continued) d) Difference between original data (a) and CMP-oriented result (b) e) Difference between original data (a) and shot record-oriented result (c) f) Difference between CMP-oriented result (b) and shot record-oriented result (c).

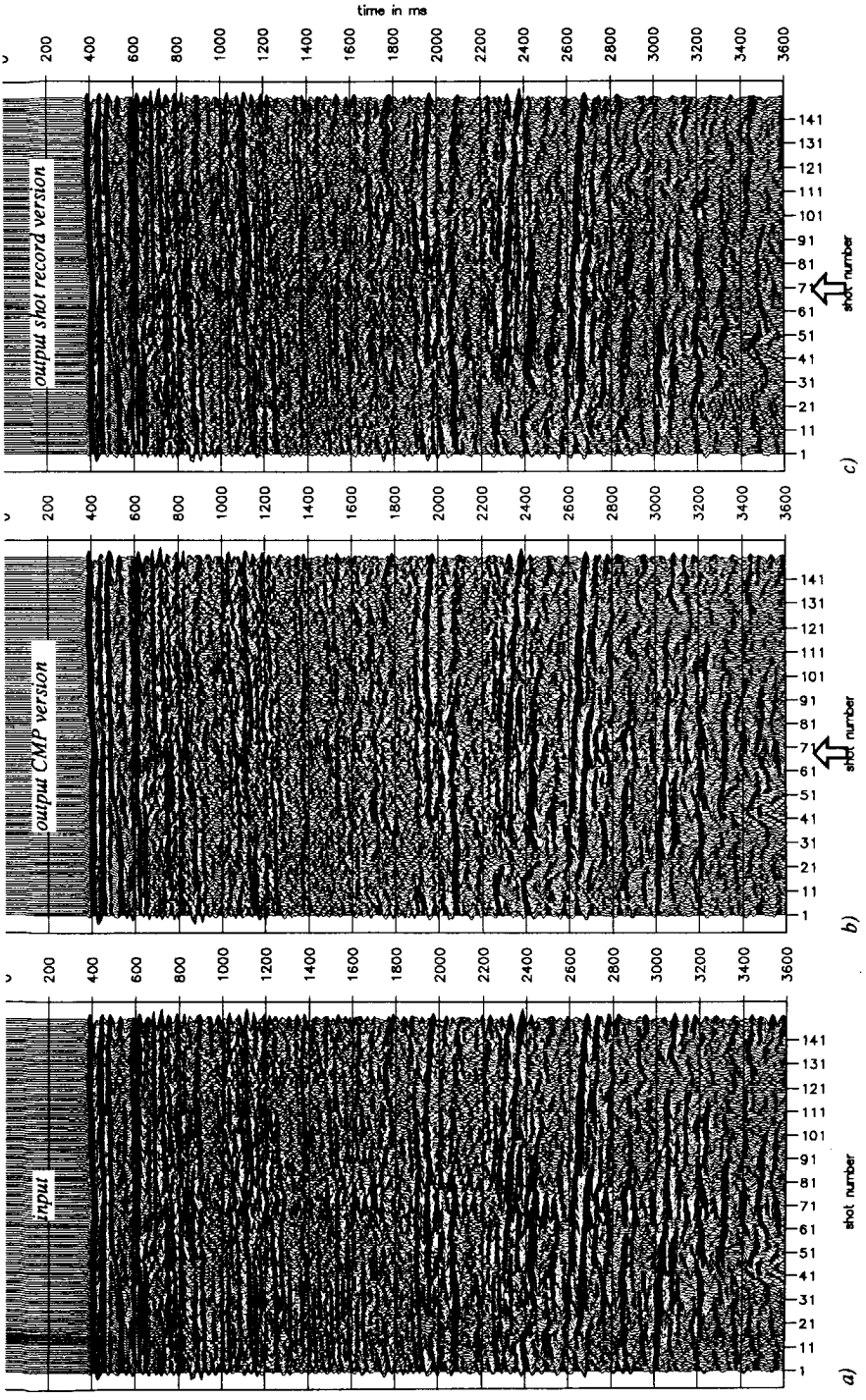

Fig. 8.10 a) Stack of first 150 CMP-gathers with multiples b) Stack after CMP-oriented surface-related multiple elimination c) Stack after full shot record-oriented surface-related multiple elimination.

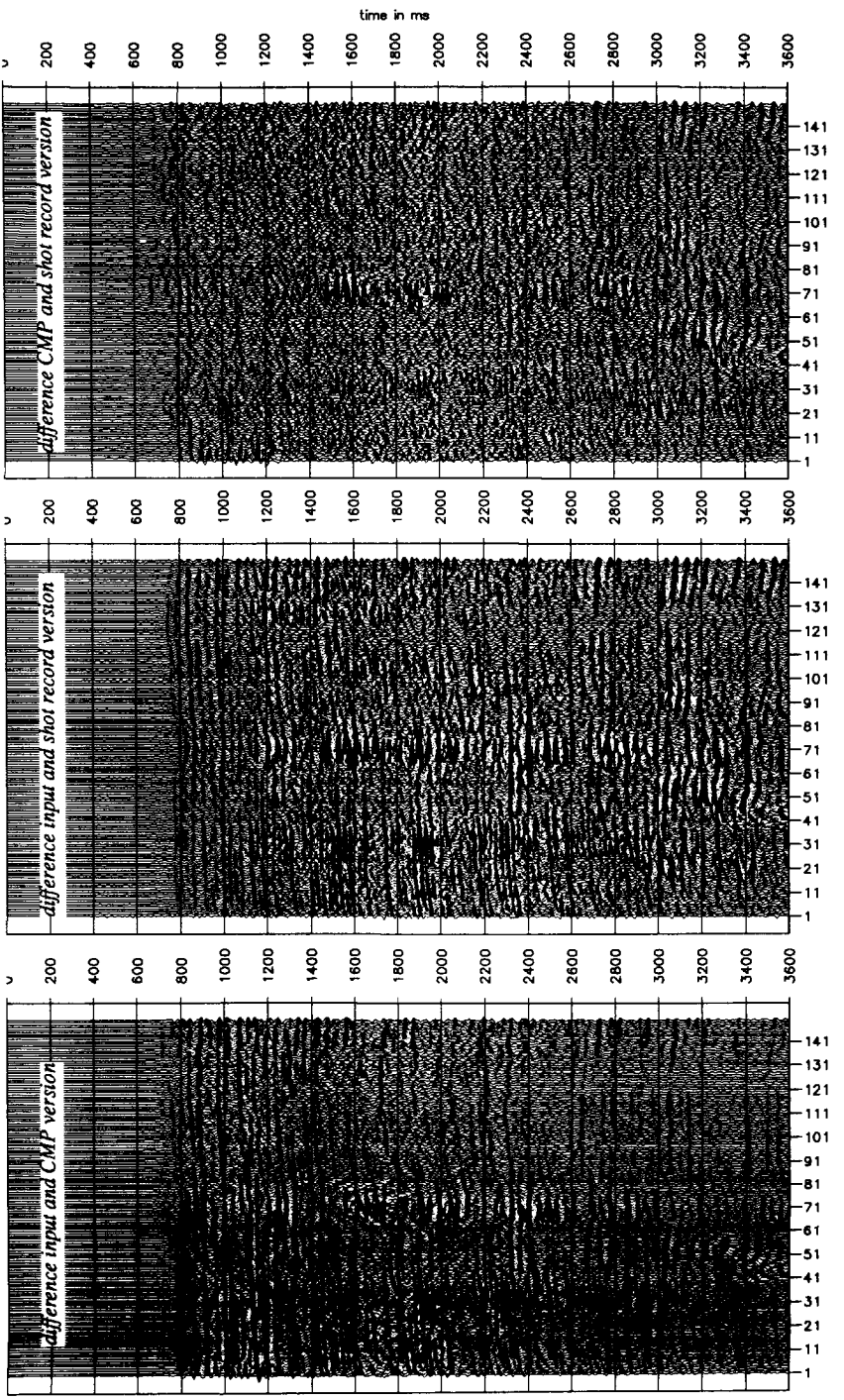

Fig. 8.10 (continued) d) Difference between original data (a) and CMP-oriented result (b) e) Difference between original data (a) and shot record-oriented result (c) f) Difference between CMP-oriented result (b) and shot record-oriented result (c).

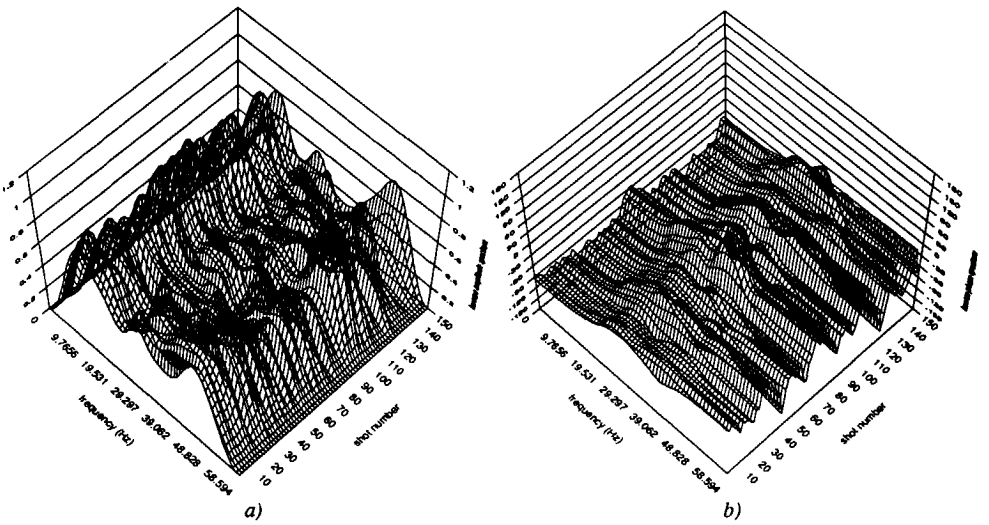

Fig. 8.11 Estimated inverse wavelet as a function of the shot number (or CMP-gather). a) Amplitude spectrum b) Phase spectrum.

After the CMP-oriented multiple elimination, the CMP-gathers have been stacked. In Fig. 8.10 three stacks are compared, of which 2 have already been showed in section 7.2. Fig. 8.10a shows the stack of the CMP-gathers without any multiple attenuation applied (although stacking itself reduces the multiples as well). In Fig. 8.10b the result of the CMP-oriented multiple elimination is displayed. It shows a very good agreement of the full shot record-oriented result, as shown in Fig. 8.10c. Fig. 8.10d shows the difference between the CMP-oriented result (Fig. 8.10b) and the full shot record-oriented result (Fig. 8.10c), which shows especially considerable residues in the indicated areas. As expected, differences between the stacks of the CMP-oriented results and the full shot record-oriented results of the multiple elimination process can be found especially around shot number 70 (see the arrows in Fig. 8.10). For a further comparison Fig. 8.10d shows the difference of the input data (Fig. 8.10a) and the CMP-oriented result (Fig. 8.10b). In Fig. 8.10e the difference between the input (Fig. 8.10a) and the full shot record oriented result (Fig. 8.10c) is displayed. Finally, Fig. 8.10f shows the difference between the CMP-oriented and the shot record-oriented result. As expected, the full shot record-oriented approach yields clearly the best results and is recommended for most practical applications.

The multiple elimination procedure has been applied *adaptively* per CMP-gather, yielding an estimated inverse wavelet for each CMP-gather. From these estimated inverse wavelets, the performance of the CMP-oriented multiple elimination can be controlled. Fig. 8.11 shows the estimated inverse wavelet per CMP-gather, both in an amplitude as well as a phase representa-

tion. In areas where the 1D approximation is not acceptable, the amplitude of the estimated inverse wavelet will become smaller, and the phase spectrum will show deviations. In fact both the amplitude and phase are varying for all CMP-gathers, indicating that the medium is not 1D. However, there are some ranges where especially the phase spectrum shows larger deviations. These deviations occur around shot number 30, around shot number 70 (where the synclinal structure is positioned), at shot number 100 and at the last 20 shot numbers (130-150). In the common offset sections in Fig. 8.10, these four areas (indicated with arrows in Fig. 8.10b) show that the multiple suppression with the CMP-oriented method does not yield as good results as the full shot record-oriented result in Fig. 8.10c.

The conclusion drawn from this example is that for an approximately 1D multiple generating layer system the CMP-oriented method is a good alternative, when full shot record-oriented surface-related multiple elimination is considered to be too expensive. However, local subsurface variations can disturb the result noticeably. The estimated inverse source signatures provide a measure to control the quality of the output from the CMP-oriented surface-related multiple elimination process. One could decide to apply the shot record oriented approach only in those areas were the CMP-oriented process shows via the estimated wavelet that the 1D approach is not acceptable.

The discrepancies that arise in the predicted multiples in areas where the 1D assumption is not valid might be overcome by introducing more parameters in the adaptive multiple elimination process, e.g. offset and time dependent weighting factors. With these extra parameters, a better adaptation of the predicted multiples to the true multiples can be achieved. However, some reservation has to be taken into account when introducing more parameters, as the primaries should not be affected by wrongly predicted multiples. It may be best to apply the CMP-oriented method in the p-ω domain, in stead of the k_x-ω domain, as each p-value corresponds to a certain *angle* in the data, independent of frequency. In that way, angle-dependent parameters can be easily introduced.

9

CONCLUSIONS AND DISCUSSION

In this chapter the main conclusions related to the theoretical and practical aspects of surface-related multiple elimination will be drawn. Next, it is argued that surface-related multiple elimination may start a new direction in seismic processing that involves inversion of *multiple* energy.

9.1 CONCLUSIONS

In this thesis we have investigated a *surface-related* multiple elimination method, which is applied as an *inversion* process to the seismic data. It has the following features:

- No information about the subsurface is needed, as the method uses the data itself as a multiple prediction operator. The seismic data implicitly contains *all* information of the subsurface that is needed to do a correct multiple prediction. Therefore, no assumption about the subsurface is made.
  As expected, for the 2D application out of plane multiples cannot be properly handled.

- The theory of the surface-related multiple elimination method can be derived for both the acoustic (marine data) as well as the elastic (land data) situation. In the latter case all surface-related multiples *and* conversions can be removed, provided *multi*-component data is available. For *single*-component land data, only the P-waves can be considered and all S-waves are ignored.

- Information of all parameters *at the surface* should be known, being the free surface reflectivity and the source and receiver characteristics. Using this information, the following pre-processing step is applied:

  * Removal of direct waves, surface waves and correlated noise events.

  * Removal of source and receiver characteristics.

  * Interpolation of missing traces

  * Spatial filtering to remove aliased data.

  * Amplitude scaling to 2D geometrical spreading (2D application).

  The output of the pre-processing step defines the actual multiple prediction operator.

- By applying the multiple prediction operator in an adaptive sense, the inverse source signature can be estimated. This means that multiple information is used to separate the source signature information from reflection information. The estimated inverse source signature can be optionally used to scale and deconvolve the multiple free data into a true amplitude impulse response.

- The method works on shot records. Therefore, application is time consuming, comparable with pre-stack redatuming methods.

- The surface-related multiple elimination process yields very good results on both simulated and field data. Primary energy can be recovered from severe interference with multiples. Especially in the lower part of the seismic sections, where the pre-stack energy of the surface-related multiples is often larger than the pre-stack energy of the primaries, results are excellent.

- As the number of parameters in surface-related multiple elimination is small, the user can be confident that the removed events are multiples indeed. This feature can be checked by the stationarity of the estimated source signature along the line. Non-stationary source functions, which cannot be explained by the actual acquisition, indicate problems due to out of plane effects or incorrect pre-processing.

- An efficient version of surface-related multiple elimination treats individual CMP-gathers in the k_x-ω or p-ω domain. For subsurfaces with small lateral variations in at least the multiple generating upper part, acceptable results can be achieved with an approximately 10 times faster scheme.

In summary, we may conclude that:

a) No *sub*surface information is needed to apply surface-related multiple elimination. Therefore the method can give excellent results in those areas were other methods fail, e.g. in areas with hardly any velocity discrimination between primaries and multiples, or in areas with complex subsurface structures.

b) It is possible to restore primaries that are masked by severe interference with multiples, especially in the deeper part of the section.

c) The source signature can be estimated together with the scaling factor in the data. No assumption about the property of the phase spectrum is required.

d) Computation time is significant, comparable to pre-stack redatuming.

9.2 DISCUSSION

9.2.1 Application on land data

So far, the surface-related multiple elimination procedure has been successfully applied to *marine* field data. No effort has yet been put on processing *land* field data. The theory for multi-component land data has been derived and tests on simulated data yield excellent results. However, application of the multiple elimination process on a land *field* data set requires the following extra attention:

- Strong surface waves may interfere with the subsurface reflections. Effective removal of the surface waves without distorting the reflections is essential.

- The source and receiver properties, including varying coupling effects, can be complex and should be taken into account.

- The influence of the weathered layer on the surface reflectivity is not yet fully understood.

Therefore, good pre-processing of land data is a pre-requisite for the success of the surface-related multiple elimination process. It is envisaged to include more parameters to the adaptive multiple elimination process, to correct for balancing and coupling problems. Note, however, that all requirements for successful surface-related multiple elimination are also requirements of high quality migration and/or inversion results.

9.2.2 Inversion of the multiple response, a new direction in seismic processing

In the field data examples most seismic energy consists of surface-related multiple energy (especially in the lower part of the section). The multiple response contains an abundant amount of propagation and reflection information of the subsurface, especially from the upper (multiple generating) part. For example, information of the first reflector (the sea bottom in marine data) is present in the multiple response *many times*, allowing an accurate determination of its position and reflectivity properties. Therefore, our work on surface-related multiple elimination has generated a new project that will use the "multiple section" for the extraction of subsurface information. This means that parallel to migration/inversion of the *multiple free* data, another migration/inversion path is added in the processing sequence, which uses the *multiple response* to contribute to the final subsurface image as well. The proposed processing scheme is shown in Fig. 9.1. The contribution of the multiple response to the final subsurface image can be accomplished by imaging along multiple paths, in stead of along primary paths only. One of the exiting aspects of multiple imaging is that in cases with a bad signal to noise ratio "multiple imaging" may be more promising than "primary imaging". In Chapter 5 it has been shown that the predicted multiples contain far less noise than the original data.

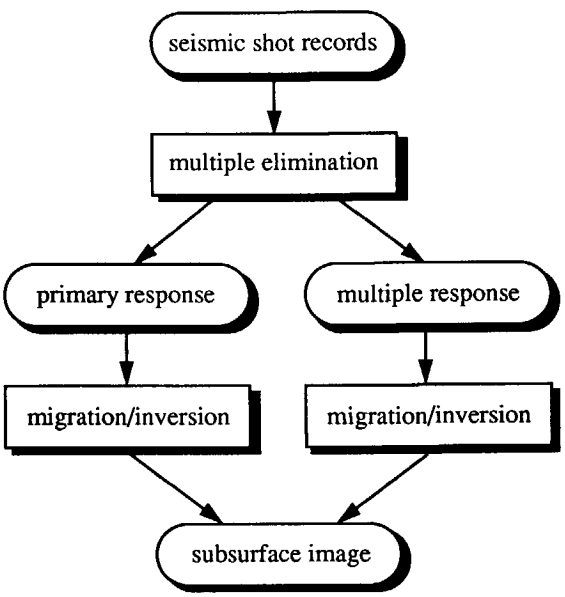

Fig. 9.1 *The multiple response, which has been removed from the total response by surface-related multiple elimination, can be separately included in the data processing sequence to get an improved image of the subsurface.*

9.2.3 Surface-related multiple elimination in 3D

In Chapter 5 it has been mentioned that a full 3D application of the surface-related multiple elimination procedure is not feasible at the moment due to the following two reasons:

- *Full* 3D surface-related multiple elimination would take an enormous amount of computation time, which is not practical at this moment.
- *Full* 3D multiple elimination requires 3D acquisition with a source at each grid point at the surface. At this moment, 3D acquisition is done with a more sparse source and receiver distribution at the surface.

The first problem will be overcome in the coming years when massive parallel MIMD computers become a practical preposition.

The second problem is not easily overcome. Seismic 3D acquisition with a dense source and receiver grid in both the x- and y-direction is economically not attractive. However, in special applications, such as monitoring of existing hydrocarbon fields, this way of data acquisition may be required to obtain the desired image quality.

9.2.4 Efficiency arguments

So far the surface-related multiple elimination procedure has been described as the exact solution of the multiple problem. The CMP-variant has been introduced as a way to make the method more efficient, but taking the risk of having a less good result.

Of course there can be other ways to make the procedure more efficient, without losing too much accuracy on the result.

An interesting suggestion may be to take only one or a few Taylor terms into account. The second Taylor term gives a correct prediction of the first order surface multiples, and an approximate prediction of higher order multiples (wrong amplitudes). The higher order Taylor terms are needed to bring each multiple back to the correct amplitude. If only the second Taylor term is used, in combination with a time and/or offset dependent scaling function, an attractive compromise may be found. In the two marine data examples described in Chapter 7 we have used about 6 or 7 terms in the multiple elimination procedure. If only the second term already yields satisfactory multiple elimination results a factor 5 in calculation time can be gained!

One could also think of taking only a small time window of the original data, which is used as operator to predict the multiples, if for example the water bottom multiples and reverberations are giving the most trouble in the data. In that situation the surface-related multiple elimination process is similar to the wave field based multiple prediction and subtraction technique, as described in section 1.2.3. However, in stead of using the depth and the contrast of the water bottom a windowed version of the true water bottom primary is used (thus the data itself). In

this case only the second Taylor term is needed, together with an appropriate scaling function to match the predicted multiples with the true multiples.

In practice, the total process should be applied adaptively for only a few shot records first. For this small amount of shot records some tests can be done to see how many terms of the Taylor series are needed. Also the source wavelet will be estimated for this range of shot records. If the user is satisfied with the results for those shot records, the multiple elimination process can be run for all shot records in a "hands off" mode.

APPENDIX A

MATRIX NOTATION

A.1 MATRIX NOTATION FOR SINGLE-COMPONENT DATA

A.1.1 Introduction

In this appendix the matrix notation, as has been introduced by Berkhout (1982), will be explained. The matrix notation originates from the fact that seismic measurements are *discrete* in both the time and the space direction. Therefore all wave theory based operations on seismic data are practically applied as discrete summations in stead of continuous integral operations. Applying an operator on a wave field means doing matrix-vector multiplications, which describe generalized lateral convolutions. Nice features of this matrix notation are its simplicity for the description of wave propagation and reflection and the close relation of this notation with the actual implementation in a computer algorithm.

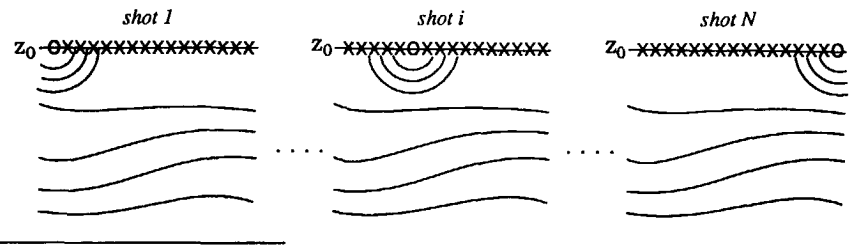

Fig. A.1 Seismic acquisition with N shot records with N detectors in a fixed spread configuration.

A.1.2 From shot records to data matrices

Let us consider a single-component seismic dataset consisting of N shot records in a fixed spread configuration with N detectors (see Fig. A.1). Suppose that each detector position also acts as source position once. This dataset is called $p(x_r,x_s,t;z_0)$, with x_r denoting the detector coordinate and x_s the source coordinate, t standing for time and z_0 indicating the depth level to which this response is related. All these variables are discrete, in fact we measure the numbers $p_{ijk}=p(i\Delta x_r,j\Delta x_s,k\Delta t;z_0)$ with i, j, k integers and Δx_r, Δx_s and Δt the sample interval of the receiver and source coordinate and the time axis respectively.

For each of these N shot records the N seismic traces are Fourier transformed from time to frequency with a discrete Fourier transform, yielding $P(i\Delta x_r,j\Delta x_s,k\Delta\omega)$ with $\Delta\omega$ denoting the temporal frequency interval. For each Fourier component $\omega_k=k\Delta\omega$ there are N^2 (complex) numbers, which describe the total seismic experiment for that independent frequency. These numbers $P(i\Delta x_r,j\Delta x_s;\omega=\omega_k)$ are stored into a matrix, called $\mathbf{P}(z_0)$. The variable z_0 indicates the depth level $z=z_0$ to which this matrix is related. Each time a matrix is used, such as $\mathbf{P}(z_0)$, it is implicitly assumed that we have such a matrix for each frequency component.

Fig. A.2 shows how the matrix is constructed from the seismic shot records. Each column of the data matrix corresponds to one Fourier component of one shot record.

Fig. A.3 shows how the measured wave fields are arranged in this matrix. Each column consists of a vector $\vec{P}(z_0)$ containing a discretized wave field corresponding to one Fourier component of one shot record.

Note that the matrix notation is a *multi-experiment* notation with in each column the common source gathers and in each row the common receiver gathers. The diagonals contain common offset data with the zero offset data on the main diagonal and the anti-diagonals contain common midpoint data, as shown in Fig. A.4.

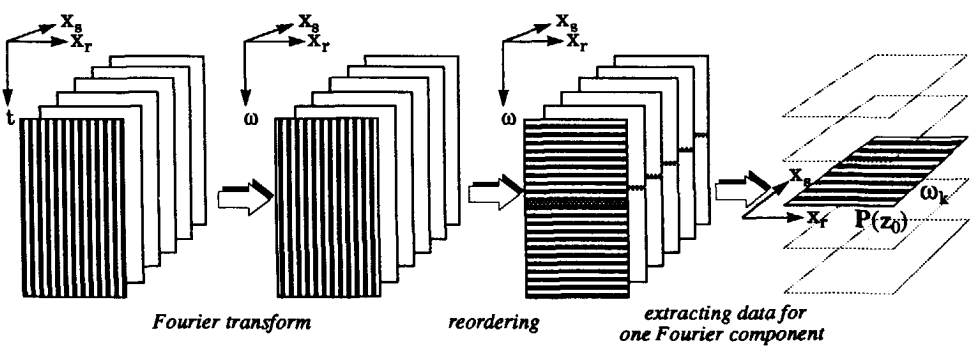

Fig. A.2 Constructing monochromatic data matrices from seismic shot records.

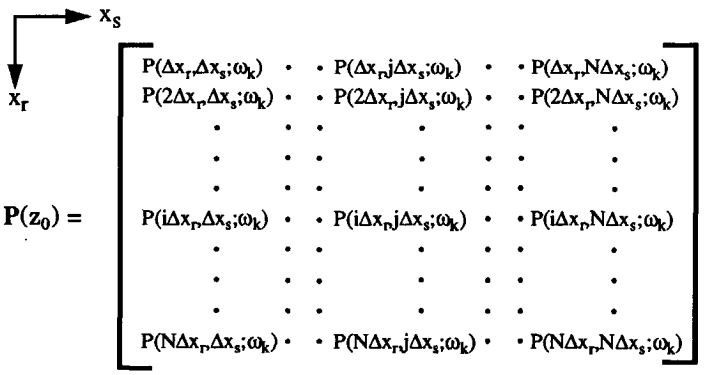

Fig. A.3 Matrix containing the prestack seismic data for one frequency component $\omega=\omega_k$.

In the description of the matrix notation the seismic acquisition was assumed to be done with N shot records of N traces in a fixed spread configuration. This acquisition gives a completely filled data matrix. However, for true seismic acquisition the configuration is generally different. For marine data a moving end of spread configuration is used, giving a matrix filling as shown in Fig. A.5a. With the reciprocity theorem (interchanging source and receiver) the other half of the matrix can be filled by mirroring the data in the main diagonal. However, the near offsets will remain unfilled. For land data (Fig. A.5b) also a moving spread is used in most situations, although the acquisition may be done split spread. In that case the reciprocity does not need to be applied. Also in land data, the near offsets are not measured in most applications, as they suffer from distorted input signals (being close to the source) or a lot of surface wave energy and other "noise".

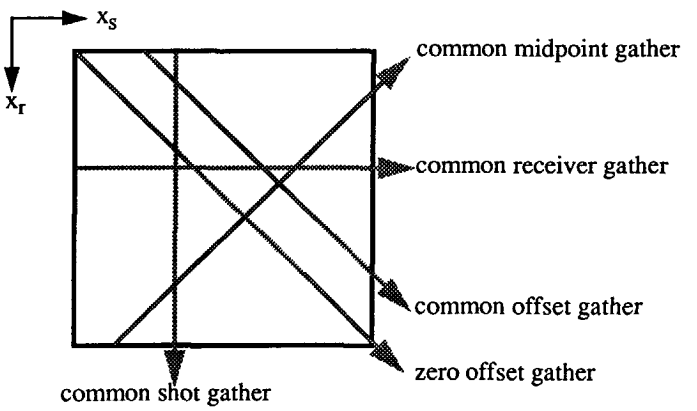

Fig. A.4 Different cross sections in a data matrix yield different seismic gathers for one Fourier component.

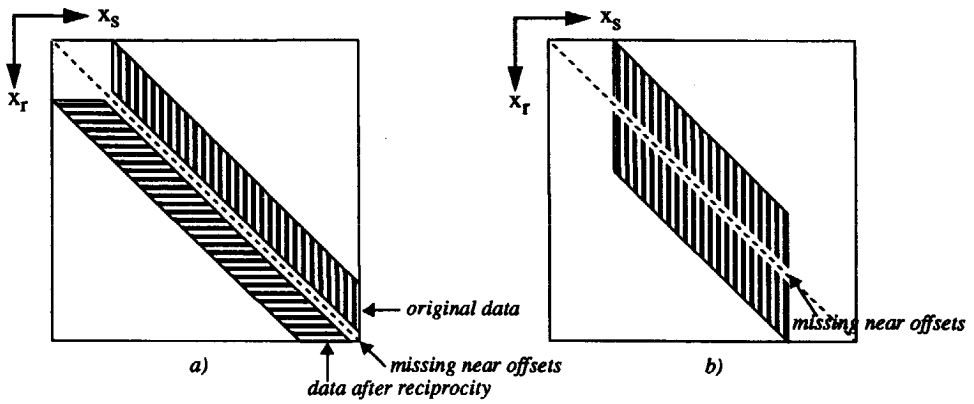

Fig. A.5 a) Moving end of spread configuration, which is typical for 2D marine acquisition. The other half of the data can be acquired using reciprocity. b) Moving split spread data, which is often used for land acquisition.

Note that reciprocity only applies if the source and receiver characteristics are equal. This assumption is normally not valid, using source and/or receiver arrays. Only after removing the source and receiver directivity effects, the reciprocity may be used.

A.1.3 Matrix multiplication and spatial convolution

If a wave field propagates through a part of the medium or interacts with inhomogeneities, this can be described by a spatial convolution of the wave field with an operator, as shown by Berkhout (1982). For the 2D situation, such an operation can be written with an integral like:

$$P^+(x_A,z_j;\omega) = \int W^+(x_A,z_j,x_k,z_i;\omega)\, P^+(x_k,z_i;\omega)\, dx_k\,, \qquad (A.1)$$

with $P^+(x_k,z_i;\omega)$ the (downgoing) wave field along depth level $z=z_i$, $W^+(x_A,z_j,x_k,z_i;\omega)$ the operator that describes a derivative of a Green's function from a point x_k at depth level z_i to the output point x_A at depth level z_j.

For example, equation (A.1) may describe a propagation from the wave field from a certain depth level to a point A (see Fig. A.6.). In this specific situation the operator $W^+(x_A,z_j,x_k,z_i;\omega)$ describes the propagation from depth level z_i to depth level z_j, and equation (A.1) represents the Rayleigh II integral.

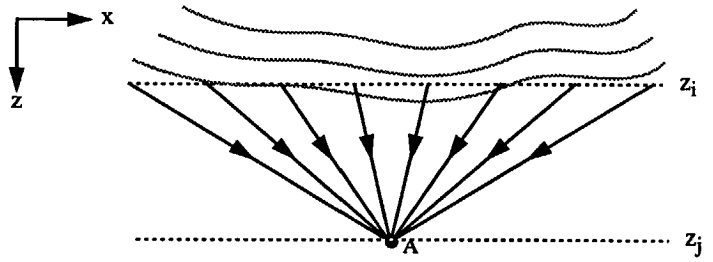

Fig. A.6 Propagation from depth level z_i to a point A at depth level z_j.

If the wave field at z_i has been discretized, the integral equation (A.1) modifies into a discrete summation in the space-frequency domain.

$$P^+(x_A,z_j;\omega) = \sum_k W^+(x_A,z_j,k\Delta x,z_i;\omega)\, P^+(k\Delta x,z_i;\omega)\, \Delta x\,. \tag{A.2}$$

In equation (A.2) $P^+(x_k,z_i;\omega)$ is the discretized wave field on which the discretized operator $W^+(x_A,z_j,x_k,z_i;\omega)$ is applied, yielding an output wave field in point A of $P^+(x_A,z_j;\omega)$.
If $P_k(z_i)=P^+(k\Delta x,z_i;\omega)$, $W_{lk}(z_j,z_i) = W^+(l\Delta x,z_j,k\Delta x,z_i;\omega)$ and $P_l(z_j)=P^+(l\Delta x,z_j;\omega)$, this summation may be written as:

$$P_l(z_j) = \sum W_{lk}(z_j,z_i)\, P_k(z_i)\,. \tag{A.3}$$

This can be rewritten as a matrix-vector multiplication (omitting the depth level annotation for the operator matrix elements):

$$\begin{bmatrix} P_1(z_j) \\ P_2(z_j) \\ . \\ . \\ P_N(z_j) \end{bmatrix} = \begin{bmatrix} W_{11} & W_{12} & . & . & W_{1N} \\ W_{21} & W_{22} & . & . & W_{2N} \\ . & . & . & . & . \\ . & . & . & . & . \\ W_{N1} & W_{N2} & . & . & W_{NN} \end{bmatrix} \begin{bmatrix} P_1(z_i) \\ P_2(z_i) \\ . \\ . \\ P_N(z_i) \end{bmatrix} \tag{A.4}$$

or,

$$\vec{P}^+(z_j) = \mathbf{W}^+(z_j,z_i)\, \vec{P}^+(z_i)\,. \tag{A.5}$$

For a multi-experiment description, the input and output vectors are combined into matrices, and equation (A.5) transforms into the matrix equation:

$$\mathbf{P}^+(z_j) = \mathbf{W}^+(z_j,z_i)\, \mathbf{P}^+(z_i)\,. \tag{A.6}$$

The matrix multiplication of the operator matrix $\mathbf{W}^+(z_j,z_i)$ with the data matrix $\mathbf{P}^+(z_i)$ describes a discretized multi-experiment generalized spatial convolution along the x-axis, which can be split into independent matrix-vector multiplications for each (independent) shot record experiment (each vector of the data matrix $\mathbf{P}^+(z_i)$).

Note that if the operator is position independent (for a horizontally homogeneous medium) all columns in the operator matrix $\mathbf{W}^+(z_j,z_i)$ are equal (with respect to the diagonal position), i.e. the matrix has a Toeplitz structure. The convolution operator is laterally invariant and the matrix-vector multiplications can be applied in the k_x-ω domain as scalar multiplications. To do this one column of the operator matrix should be Fourier transformed to the wave number domain and can be multiplied with the Fourier transforms of the data vectors:

$$\tilde{\mathbf{P}}^+(k_x;z_j,\omega) = \tilde{\mathbf{W}}^+(k_x;z_j,z_i,\omega)\,\tilde{\mathbf{P}}^+(k_x;z_i,\omega)\,, \tag{A.7}$$

with $\tilde{\mathbf{P}}^+(k_x;z_j,\omega)$ the spatial Fourier transform of the corresponding column of the output matrix.

Also reflection and transmission at inhomogeneities in the subsurface can be written as matrix multiplications. For example, if a reflection takes place at depth level z_i, the downgoing (multi-experiment) wave field $\mathbf{P}^+(z_i)$ and the reflected upgoing (multi-experiment) wave field $\mathbf{P}^-(z_i)$ are related in the following way:

$$\mathbf{P}^-(z_i) = \mathbf{R}^+(z_i)\,\mathbf{P}^+(z_i)\,, \tag{A.8}$$

with $\mathbf{R}^+(z_i)$ describing the reflectivity at depth level z_i. Each column of the matrix $\mathbf{R}^+(z_i)$ corresponds to one lateral position, as shown in Fig. A.7. If a dipping structure is crossing the depth level of interest, the reflectivity operator will have only non-zero columns around the lateral position where the crossing takes place. Note that the *diagonal* of the reflectivity matrix $\mathbf{R}^+(z_i)$, after summation for all frequencies, is the same as the result of "conventional" pre-stack depth migration for depth level z_i.

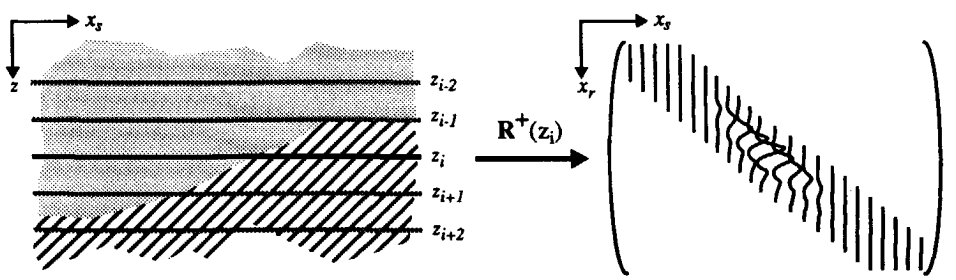

Fig. A.7 The reflectivity matrix related to a certain depth level contains the local reflectivity operator for each lateral position along the depth level.

A.2 MATRIX NOTATION FOR MULTI-COMPONENT DATA

In the case of multi-component data the matrix notation is extended to contain all multi-component shot records in one matrix. For the 2D situation with two components there are four possible shot records. Suppose we have a description in terms of P and S waves, than the multi-component data matrix is defined as:

$$\underset{\sim}{\mathbf{P}} = \begin{bmatrix} \mathbf{P}_{\varphi\varphi} & \mathbf{P}_{\varphi\psi} \\ \mathbf{P}_{\psi\varphi} & \mathbf{P}_{\psi\psi} \end{bmatrix}, \tag{A.9}$$

with each submatrix $\mathbf{P}_{ab}$, with $a,b=\phi$ or ψ, defined as a normal data matrix, containing the received a wave field due to b source wave fields. This multi-component matrix is also shown in Fig. A.8.

With this multi-component data matrix definition, matrix multiplications describe multi-component data operations, including the conversion. To show this, we consider the elastic reflection of a downgoing multi-component wave field, described by:

$$\underset{\sim}{\mathbf{P}}^{-}(z_i) = \underset{\sim}{\mathbf{R}}^{+}(z_i)\, \underset{\sim}{\mathbf{P}}^{+}(z_i) \tag{A.10}$$

with the multi-component reflectivity matrix defined as (omitting the depth level annotation in the submatrices)

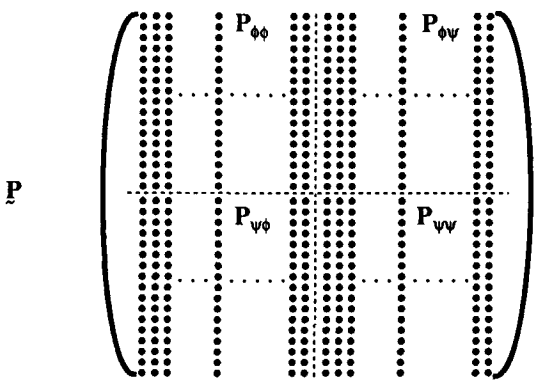

Fig. A.8 Multi-component data matrix for the 2 dimensional case. Each submatrix contains a pre-stack monochromatic experiment for one source and receiver component.

$$\underline{\mathbf{R}}^{+}(z_i) = \begin{bmatrix} \mathbf{R}^{+}_{\varphi\varphi} & \mathbf{R}^{+}_{\varphi\psi} \\ \mathbf{R}^{+}_{\psi\varphi} & \mathbf{R}^{+}_{\psi\psi} \end{bmatrix}, \tag{A.11}$$

which results into

$$\begin{bmatrix} \mathbf{P}^{-}_{\varphi\varphi} & \mathbf{P}^{-}_{\varphi\psi} \\ \mathbf{P}^{-}_{\psi\varphi} & \mathbf{P}^{-}_{\psi\psi} \end{bmatrix} = \begin{bmatrix} \mathbf{R}^{+}_{\phi\phi}\mathbf{P}^{+}_{\phi\phi} + \mathbf{R}^{+}_{\phi\psi}\mathbf{P}^{+}_{\psi\phi} & \mathbf{R}^{+}_{\phi\phi}\mathbf{P}^{+}_{\phi\psi} + \mathbf{R}^{+}_{\phi\psi}\mathbf{P}^{+}_{\psi\psi} \\ \mathbf{R}^{+}_{\psi\phi}\mathbf{P}^{+}_{\phi\phi} + \mathbf{R}^{+}_{\psi\psi}\mathbf{P}^{+}_{\psi\phi} & \mathbf{R}^{+}_{\psi\phi}\mathbf{P}^{+}_{\phi\psi} + \mathbf{R}^{+}_{\psi\psi}\mathbf{P}^{+}_{\psi\psi} \end{bmatrix}. \tag{A.12}$$

It can be easily verified from equation (A.12) that for the reflection the conversion is properly taken into account. Each matrix multiplication, which describes an interaction in the acoustic case, has its multi-component counterpart in which conversions can be taken into account.

If also the S-waves polarized in the y-direction are taken into account in the descriptions for multi-component data, the matrices become 3x3 matrices in stead of 2x2 matrices, yielding 9 submatrices per multi-component matrix, see also Wapenaar et al. (1990a).

A.3 MATRIX NOTATION FOR 3D DATA

In the case that a true 3D acquisition is carried out, it can also be captured in a 2D matrix notation, without violating the convolution properties being described by matrix multiplications. This 3D matrix notation has been described by Kinneging et al. (1989).

For the 3D matrix notation, we suppose that the acquisition has been carried out on a rectangular grid in the x-y plane, as displayed in Fig. A.9. Suppose there are N_x detector positions in the x and N_y detector positions in the y direction, yielding N_xN_y detectors per shot record. Also suppose that there are N_xN_y shot record experiments, with each grid point being a shot position once, and for each shot record at all N_xN_y detectors the signal is measured.

This results in $(N_xN_y)^2$ traces, which would describe a 5 dimensional data cube, instead of a 3 dimensional for the 2D acquisition case. In order to prevent 5 dimensional datasets, the 3D measurements are combined in a 3D cube, similar to the 2D case. Again all traces are Fourier transformed to the frequency domain, and data matrices per Fourier component are constructed. Each data matrix will now contain a full 3D acquisition for one Fourier component. To do this, the data for all receivers in the x-y plane for one shot record experiment are stored into one column of the data matrix, as shown in Fig. A.10. This is repeated for each source position, resulting into rectangular matrices with dimension N_x^2.

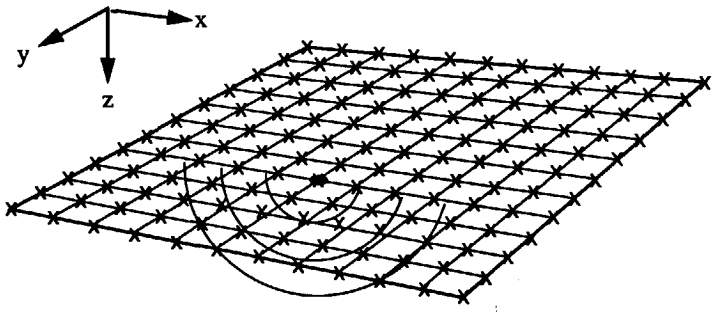

Fig. A.9 *3D acquisition on a perfect grid in the x-y plane, with all grid points being receivers and each grid point being a source position once.*

This means that the matrix can be thought to consist of submatrices with dimension N_x^2 containing a 2D experiment for all receivers of one line in the x-direction (for a fixed y-coordinate) and the source varying along another line in the x-direction with a fixed y-coordinate.

With this matrix notation, one column corresponds with a common source gather and one row with a common receiver gather. This guarantees that matrix multiplications now describe 2 dimensional spatial convolutions in the x- and y-direction. However, diagonals do not contain common offset information anymore, except for the main diagonal.

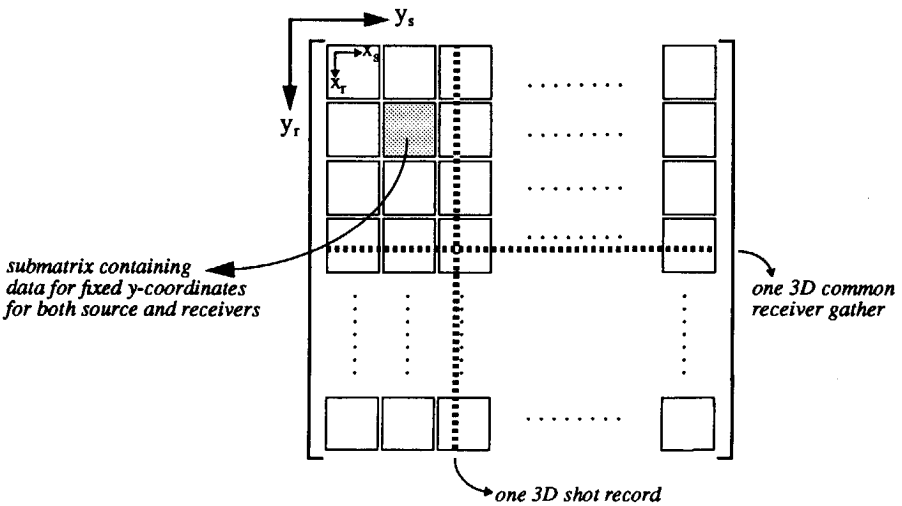

Fig. A.10 *A data matrix for a 3D acquisition on a grid in the x-y plane consists of a 2D submatrix for each y-source coordinate and for each receiver y-coordinate. One column still describes a 3D shot record, and one row describes a 3D common receiver gather.*

The nice feature about this matrix notation is that, as matrix multiplications still describe spatial convolutions, all formulations for the 2D situation equally describe the 3D situation without modification. Even the computer algorithms do not need to be adapted, going from 2D to full 3D. Only the construction for the data matrices is different.

APPENDIX B

SOURCE, RECEIVER AND REFLECTION MATRICES

This appendix will focus on the descriptions for the wave field of ideal source and receiver (array) responses, and how the corresponding matrices can be constructed. Also some operators related to the free surface are examined, with their expressions given in the wave number domain, like the composition and decomposition matrices and the free surface reflectivity matrices, which have been used in Chapter 2.

B.1 MONOPOLE AND DIPOLE RESPONSES IN HOMOGENEOUS MEDIA

B.1.1 Representation in the space and wave number domain

In Berkhout (1982) the expressions for the pressure wave field for a monopole or dipole pressure source in a 2D or 3D homogeneous acoustic medium can be found, which have been gathered in Table B.1. The variables distance r and angle φ are explained in Fig. B.1. It appears that the expressions in the wave number domain are identical for both the 3D and 2D situation. However, the definition of k_z is different; for the 2D case $k_z=\sqrt{(k^2-k_x^2)}$, for the 3D case $k_z=\sqrt{(k^2-k_x^2-k_y^2)}$.

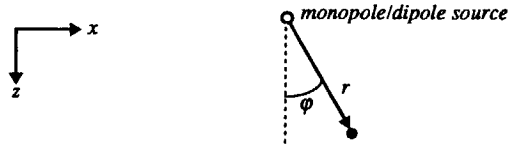

Fig. B.1 monopole or dipole source in a homogeneous medium.

Table B.1 Expressions for monopole and dipole responses in a homogeneous acoustic medium.

	3D		2D	
	monopole	dipole	monopole	dipole
x-ω exact	$\frac{e^{-jkr}}{r}$	$\frac{1+jkr}{r^2}\cos\varphi\ e^{-jkr}$	$-j\pi H_0^{(2)}(kr)$	$-jk\pi\cos\varphi H_1^{(2)}(kr)$
x-ω far field	$\frac{e^{-jkr}}{r}$	$\frac{jk}{r}\cos\varphi\ e^{-jkr}$	$\sqrt{\frac{2\pi}{jkr}}e^{-jkr}$	$\sqrt{\frac{2\pi jk}{r}}\cos\varphi\ e^{-jkr}$
k_x-ω exact	$-\frac{2\pi}{jk_z}e^{-jk_z\lvert z\rvert}$	$2\pi\,\mathrm{sign}(z)\,e^{-jk_z\lvert z\rvert}$	$-\frac{2\pi}{jk_z}e^{-jk_z\lvert z\rvert}$	$2\pi\,\mathrm{sign}(z)\,e^{-jk_z\lvert z\rvert}$

It appears that the response of a dipole source, has a flat spectrum in the k_x-ω domain (or k_x-k_y-ω domain for the 3D situation) for k_x (and k_y) values in the range (-k,k), and that for the response of a monopole source the amplitude in the k_x-ω domain (or k_x-k_y-ω domain) increases with the absolute value of k_x (and k_y) for the range (-k,k). In Fig. B.2 the amplitude spectrum in the k_x-ω domain (2D situation) of a monopole and a dipole response are shown related to three depth levels. It appears that the value outside the range (-k,k) decreases exponentially with depth. These fast decaying waves are the evanescent waves, which have almost disappeared for 100 m depth. Given the values for the velocity and frequency of 1500 m/s and 60 Hz respectively, 10 m corresponds to 0.4λ and 100 m corresponds to 4λ. The monopole response has a square root singularity for k_x=k.

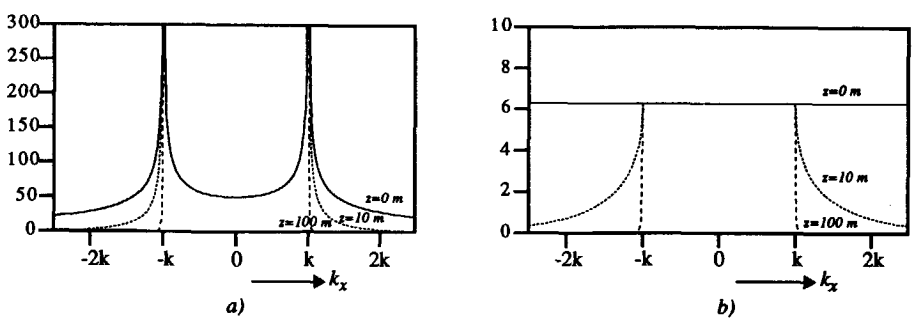

Fig. B.2 a) Amplitude spectrum of a monopole source for 60 Hz and a velocity of 1500 m/s in the k_x-ω domain (for the 2D situation) at depth 0 m (solid line), 10 m and 100 m (dashed lines) b) Amplitude spectrum of a dipole source for 60 Hz and a velocity of 1500 m/s in the k_x-ω domain at depth 0 m (solid line) 10 m and 100 m (dashed lines).

B.1.2 Constructing the source matrix

To construct the source matrix from the k_x-ω domain representations of the source (restricting ourselves to the 2D case), the response is inverse Fourier transformed to the space domain. For a downgoing wave field at z=0 of a dipole source , the k_x-ω domain response is equal to $2\pi S(\omega)$, $S(\omega)$ being the source signature. The space domain representation will be a scaled spatial delta function, with a non-zero value only at the source position (diagonal element of the source matrix). The value of the pulse depends on the frequency dependent signature $S(\omega)$. The space domain representation, after discretization, is stored in the column of the source matrix, corresponding to the source position, as visualized in Fig. B.3. This procedure can be repeated for each shot position.

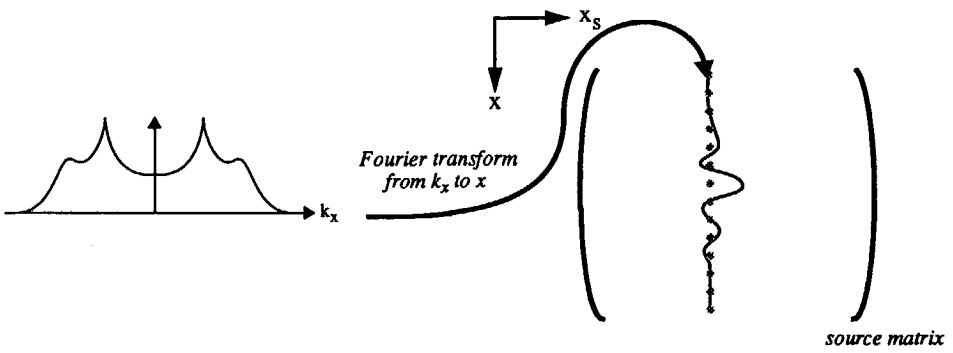

Fig. B.3 Construction of a source matrix. The k_x-ω domain response is Fourier transformed to the space domain, and the (discretized) result is stored into that column of the source matrix, that corresponds with the lateral shot position,.

B.2 LINEAR DESCRIPTION OF ARRAY AND GHOST RESPONSES

B.2.1 Array responses

In the case that acquisition is done using arrays of sources or receivers, the response can be predicted if a linear assumption is made. This means that the response of the total array can be assumed to be the superposition of the responses of each individual element. For receiver arrays this may be a valid assumption. For source arrays this linearity assumption is not valid, due to the interactions of the sources (marine data). However, Ziolkowski (1982) showed that any airgun array can be replaced by a new array with notional sources, for which the linear assumption is valid again. Therefore, a linear description for both source and receiver arrays can be applied in the k_x-ω domain.

Suppose there are N array elements, each of which are at a relative position x_i with respect to the central array position, and each element has an frequency dependent amplitude of $S_i(\omega)$. This results in a total response for the array $\tilde{D}_{array}(k_x,\omega)$ of:

$$\tilde{D}_{array}(k_x,\omega) = \sum_{i=1}^{N} S_i(\omega)\, e^{-jk_x x_i} . \qquad (B.1)$$

In Chapter 2 an example of a source and receiver array has already been shown. In general the effect of the array becomes more noticeable for the higher frequencies, as the wave length becomes shorter which means that the array length becomes relatively larger.

B.2.2 Ghost responses

The ghost operator is in fact an array in the z-direction, with two elements of opposite sign. Therefore the ghost operator for a source at depth z_s, below a water surface with reflectivity of -1, is given by:

$$\tilde{D}_s(k_x,\omega,z_s) = 1 - e^{-2jk_z\Delta z} , \qquad (B.2)$$

with, $\Delta z=|z_s-z_0|$, which is the expression related to depth level $z=z_s$. For an expression related to the surface z_0 an extra extrapolation has to be included, yielding:

$$\tilde{D}_s(k_x,\omega,z_0) = (1 - e^{-2jk_z\Delta z})\, e^{jk_z\Delta z} , \qquad (B.3a)$$

or, equivalently

$$\tilde{D}_s(k_x,\omega,z_0) = e^{jk_z\Delta z} - e^{-jk_z\Delta z} , \qquad (B.3b)$$

which can be written as

$$\tilde{D}_s(k_x,\omega,z_0) = 2j\sin(k_z\Delta z) . \qquad (B.3c)$$

For the receiver side there are similar expressions related to the receiver depth level z_r, with $\Delta z=|z_r-z_0|$.

As an example, we just show the response of the ghost operator for varying depths, to see when the dipole assumption is still valid for a monopole source with its ghost. Fig. B.4 shows the response of a monopole source or receiver positioned 1, 5 and 10 m below the free surface for frequencies 10, 20, 30, 40, 50 and 60 Hz. For the 1 m situation a perfect dipole response is the result (Fig. B.4a) for the given frequencies. When the monopole is at 5 m depth (Fig. B.4b) the response starts to slightly deform for the higher frequencies and small angles.

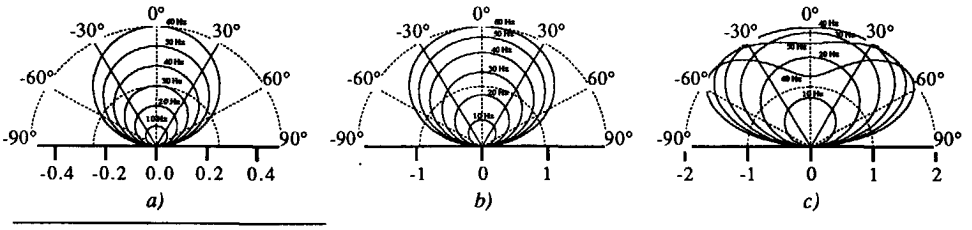

Fig. B.4 Ghost response for a unit valued monopole source or receiver positioned below the free surface. a) Ghost response for 1 m depth. b) Ghost response for 5 m depth. c) Ghost response for 10 m depth.

For the 10 m depth situation (Fig. B.4c) the frequencies above 30 Hz have a serious deviation from the dipole directivity. For small angles a reduction of the response is occurring. Note also that with varying depth, the global amplitude of the ghost response is changing, as can be observed from the horizontal amplitude axis in Fig. B.4. The shallower the depth, the smaller the global amplitude of the response. Therefore a too small depth of the sources or receivers is not desired in marine acquisition.

B.2.3 Total airgun array response

If the total airgun array response is to be calculated in the k_x-ω domain, the array response is combined with the ghost effect and the response of a monopole, as each airgun (approximately) behaves as a pressure monopole source. This has been vizualized in Fig. B.5. In Chapter 2 the downgoing source wave field has been gathered in the source matrix $\mathbf{S}^+(z_0)$, which contains the inverse Fourier transform of the array response in the k_x-ω domain in its columns. The basic airgun source signature $S(\omega)$ is defined as the airgun response for $k_x=0$ in the wave number domain, or as the integration along the lateral coordinate in the space domain of the aigun response. The remaining airgun array response, if the basic signature is separated from the total response, has been defined in Chapter 2 by $\mathbf{D}_{tot}^+(z_0,z_s)$. The basic source signature is put on the diagonal elements of the matrix $\mathbf{S}(z_s)$, resulting in

$$\mathbf{S}^+(z_0) = \mathbf{D}_{tot}^+(z_0,z_s)\,\mathbf{S}(z_s)\,. \tag{B.4}$$

In Chapter 2 the total normalized array response matrix $\mathbf{D}_{tot}^+(z_0,z_s)$ has been divided into $\mathbf{D}^+(z_0,z_s)$ and $\mathbf{D}_{array}(z_s)$. Matrix $\mathbf{D}_{array}(z_s)$ describes the array response itself (upper part of Fig. B.5) and $\mathbf{D}^+(z_0,z_s)$ monopole response and the ghost effect (lower part of Fig. B.5).

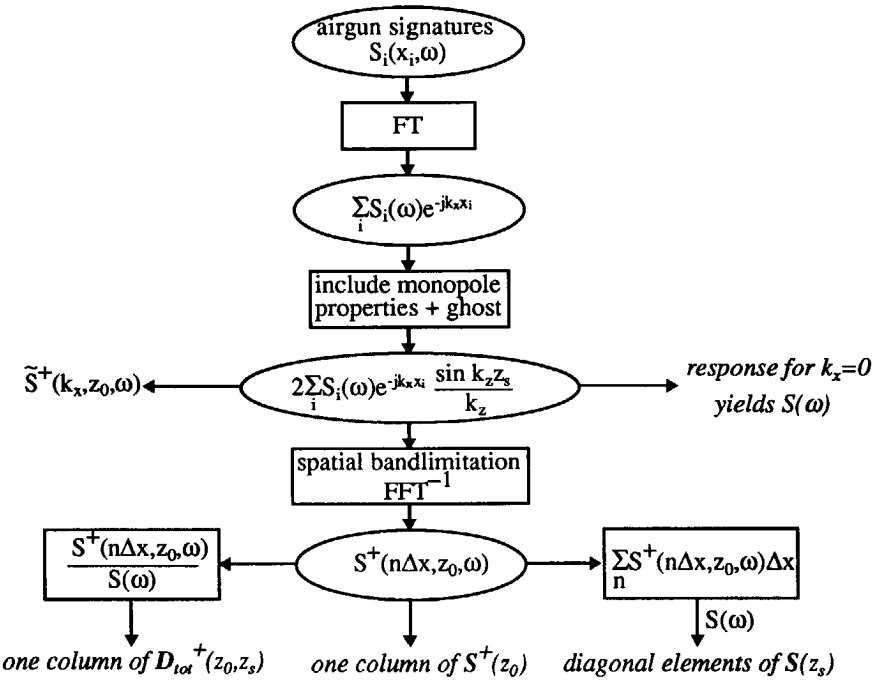

Fig. B.5 Total airgun array response consisting of the monopole response, the array effect and the ghost effect. The matrices at the bottom correspond the matrices mentioned in Chapter 2.

B.2.4 Removing the array and ghost effects

For removing the array and ghost effects, equation (B.1) and equation (B.3b) have to be inverted, and the Fourier transform of these operators from the wave number domain to the space domain should be stored in the columns of the inverse source or receiver matrices.

Note that the inversion of the source and detector matrices via the k_x-ω domain is only allowed if the properties do not vary (rapidly) from shot to shot record.

The inversion of the operators in the k_x-ω domain should always be stabilized, to prevent instabilities at notches in the spectrum.

For example, for the ghost operator the first notch appears when equation (B.3c) becomes zero, i.e when $k_z\Delta z=n\pi$, or $2\pi(f/c)\Delta z\cos\varphi=n\pi$, n=0,1,2,3, ... For $\varphi=0$ and c=1500 m/s and f=60 Hz this appears when $\Delta z=\lambda/2$, i.e. Δz=12.5 m. In Fig. B.4c, for Δz =10 m, we see that the notch is already appearing in the 60 Hz response. For 90° the response is always zero, which means that with a deghosting procedure the highest angles cannot be completely recovered. The deghosting operator in the k_x-ω domain reads:

$$\{\tilde{D}_s(k_x,\omega,z_0)\}^{-1} = 1/[2j\sin(k_z\Delta z)]\,. \tag{B.5a}$$

which can be best stabilized with a constant ε on the amplitude:

$$\{\tilde{D}_s(k_x,\omega,z_0)\}^{-1} = -j\sin(k_z\Delta z)/[\varepsilon + 2\sin^2(k_z\Delta z)]. \tag{B.5b}$$

B.3 REFLECTIVITY OF A THIN NEAR SURFACE LAYER IN THE K_X-ω DOMAIN

In section 2.5 the thin surface layer situation has been described, in which the free surface in combination with the thin layer is considered as one multiple generating system. The reflectivity of this thin layer system has been given by equation (2.29):

$$\mathbf{R}^-_{\omega}(z_1) = \mathbf{R}^-(z_1) + \mathbf{T}^+(z_1)\,\mathbf{W}^+(z_1,z_0)\,\mathbf{R}^-(z_0)\,\mathbf{T}^-(z_0,z_1)\,. \tag{B.6}$$

where $\mathbf{R}^-(z_1)$ described the reflection against the thin layer bottom from below, $\mathbf{T}^+(z_1)$ describes the downward transmission through the first layer bottom, $\mathbf{W}^+(z_1,z_0)$ contains the propagation from the surface to the thin layer bottom, $\mathbf{R}^-(z_0)$ contains the free surface reflectivity and finally $\mathbf{T}^-(z_0,z_1)$ describes the upward transmission through the first layer , including the reverberations within this layer. In the k_x-ω domain (so for a flat thin layer), the equivalent matrices read:

$$\tilde{R}^-(k_x,\omega,z_1) = -\frac{\rho_2 k_{z,1} - \rho_1 k_{z,2}}{\rho_2 k_{z,1} + \rho_1 k_{z,2}}\,, \tag{B.7a}$$

$$\tilde{T}^+(k_x,\omega,z_1) = 1 - \tilde{R}^-(k_x,\omega,z_1)\,, \tag{B.7b}$$

$$\tilde{W}^+(k_x,\omega,z_1,z_0) = e^{-jk_z|\,z_1 - z_0|}\,, \tag{B.7c}$$

$$\tilde{R}^-(k_x,\omega,z_0) = -1\,, \tag{B.7d}$$

$$\tilde{T}^-(k_x,\omega,z_0,z_1) = [1 - \tilde{W}^-(k_x,\omega,z_0,z_1)\tilde{R}^+(k_x,\omega,z_1)\tilde{W}^+(k_x,\omega,z_1,z_0)\tilde{R}^-(k_x,\omega,z_0)]^{-1}$$

$$\tilde{W}^-(k_x,\omega,z_0,z_1)\,\tilde{T}^-(k_x,\omega,z_1)\,, \tag{B.7e}$$

with

$$\tilde{W}^-(k_x,\omega,z_0,z_1) = \tilde{W}^+(k_x,\omega,z_1,z_0) \tag{B.7f}$$

$$\tilde{R}^{+}(k_x,\omega,z_1) = -\tilde{R}^{-}(k_x,\omega,z_1)\,, \tag{B.7g}$$

$$\tilde{T}^{-}(k_x,\omega,z_1) = 1 + \tilde{R}^{-}(k_x,\omega,z_1). \tag{B.7h}$$

This yields for the total reflectivity against the thin layer system from below:

$$\tilde{R}^{-}_{tot}(k_x,\omega,z_1) = \frac{\tilde{R}^{-}(k_x,\omega,z_1)+\{\tilde{W}^{+}(k_x,\omega,z_1,z_0)\}^2}{1+\tilde{R}^{-}(k_x,\omega,z_1)\{\tilde{W}^{+}(k_x,\omega,z_1,z_0)\}^2} \tag{B.8}$$

In Fig. B.6 the phase of the reflectivity operator $\tilde{R}^{-}_{tot}(k_x,\omega,z_1)$ has been displayed for 3 values of the thin layer thickness. Note that the absolute value of the amplitude is 1 for all angles, as the thin layer reflects all energy. The density and velocity in the thin layer have been chosen to be 1000 kg/m^3 and 1500 m/s, below this layer the density and velocity are 1700 kg/m^3 and 1800 m/s. Note the varying character for this reflectivity operator as a function of the thickness. If the thickness approaches zero, the phase will move to 180° for all angles of incidence.

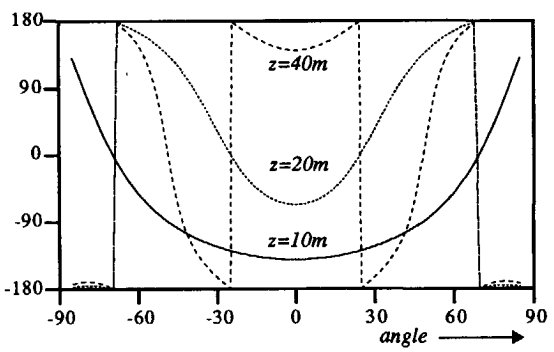

Fig. B.6 Phase of the reflectivity operator for a thin layer system as a function of angle. The operator has been displayed for 3 thicknesses of the thin layer.

B.4 COMPOSITION AND DECOMPOSITION OPERATORS

In Chapter 2 the relations between the total traction and particle velocity field and the up- and downgoing P- and S-wave potentials have been defined in equations (2.35) and (2.36), which read equivalently in the k_x-ω domain:

$$\begin{bmatrix} \tilde{\underline{T}} \\ \tilde{\underline{V}} \end{bmatrix} = \begin{bmatrix} \tilde{\underline{L}}_2^+ & \tilde{\underline{L}}_2^- \\ \tilde{\underline{L}}_1^+ & \tilde{\underline{L}}_1^- \end{bmatrix} \begin{bmatrix} \tilde{\underline{\Pi}}^+ \\ \tilde{\underline{\Pi}}^- \end{bmatrix}, \tag{B.9}$$

and

$$\begin{bmatrix} \tilde{\underline{\Pi}}^+ \\ \tilde{\underline{\Pi}}^- \end{bmatrix} = \begin{bmatrix} \tilde{\underline{M}}_2^+ & \tilde{\underline{M}}_2^- \\ \tilde{\underline{M}}_1^+ & \tilde{\underline{M}}_1^- \end{bmatrix} \begin{bmatrix} \tilde{\underline{T}} \\ \tilde{\underline{V}} \end{bmatrix}, \tag{B.10}$$

in which

* $\tilde{\underline{T}} = (\tilde{\tau}_{xz}, \tilde{\tau}_{zz})^T$ is the multi-component traction field vector,
* $\tilde{\underline{V}} = (\tilde{V}_x, \tilde{V}_z)^T$ is the multi-component particle velocity field vector,
* $\tilde{\underline{\Pi}}^- = (\tilde{\Phi}^-, \tilde{\Psi}^-)^T$ is the upgoing potential field vector and
* $\tilde{\underline{\Pi}}^+ = (\tilde{\Phi}^+, \tilde{\Psi}^+)^T$ is the downgoing potential field vector.

For a 3D description, the multi-component vectors consist of 3 components, see Wapenaar and Berkhout (1989). The expressions for the sub-matrcies in equations (B.9) and (B.10) can also be found in Wapenaar and Berkhout (1989), and read in the 2D situation:

$$\tilde{\underline{L}}_1^{\pm} = \frac{1}{\omega\rho} \begin{bmatrix} k_x & \pm \dfrac{-(k_S^2 - k_x^2)}{k_{z,S}} \\ \pm k_{z,P} & k_x \end{bmatrix}, \tag{B.11a}$$

$$\tilde{\underline{L}}_2^{\pm} = -\frac{\mu}{\omega^2\rho} \begin{bmatrix} \pm k_x k_{z,P} & -(k_S^2 - 2k_x^2) \\ (k_S^2 - 2k_x^2) & \pm 2k_x k_{z,S} \end{bmatrix}, \tag{B.11b}$$

$$\tilde{\underline{M}}_1^{\pm} = \frac{\mu}{2\omega} \begin{bmatrix} 2k_x & \pm \dfrac{(k_S^2 - 2k_x^2)}{k_{z,P}} \\ \pm \dfrac{-(k_S^2 - 2k_x^2)}{k_{z,S}} & 2k_x \end{bmatrix}, \tag{B.11c}$$

$$\tilde{\underline{M}}_2^{\pm} = -\frac{1}{2}\begin{bmatrix} \pm\dfrac{k_x}{k_{z,P}} & 1 \\ -1 & \pm\dfrac{k_x}{k_{z,S}} \end{bmatrix} . \qquad \text{(B.11d)}$$

In these expressions $k_P=\omega/c_P$, with c_P the velocity of the P-waves, $k_S=\omega/c_S$, with c_S the velocity of the S-waves, $k_{z,P}=\sqrt{(k_P^2-k_x^2)}$ and $k_{z,S}=\sqrt{(k_S^2-k_x^2)}$.

B.5 ELASTIC FREE SURFACE REFLECTIVITY OPERATORS

In Chapter 2 the expressions for the free surface reflectivity operators for different descriptions of the wave field have been given, see section 2.6.4. If the wave field is described in terms of tractions, the free surface reflectivity matrix is simply a negative unit matrix (see equation (2.65)):

$$\underline{\mathbf{R}}_T^-(z_0) = -\ \underline{\mathbf{I}} \ . \qquad \text{(B.12)}$$

For a description in down- and upgoing P- and S-wave potentials, the free surface reflectivity operator is given by (see equation (2.60a)):

$$\underline{\mathbf{R}}_\Pi^-(z_0) = -[\underline{\mathbf{L}}_2^+(z_0)]^{-1}\,\underline{\mathbf{L}}_2^-(z_0) \ . \qquad \text{(B.13)}$$

In the k_x-ω domain the elastic free surface reflectivity matrix in terms of P- and S-wave potentials can be found using equations (B.11a) and (B.11b):

$$\tilde{\underline{\mathbf{R}}}_\Pi = \begin{bmatrix} \tilde{R}_{PP} & \tilde{R}_{PS} \\ \tilde{R}_{SP} & \tilde{R}_{SS} \end{bmatrix} =$$

$$\frac{1}{4k_x^2k_{z,P}k_{z,S} + (k_S^2-2k_x^2)^2}\begin{bmatrix} 4k_x^2k_{z,P}k_{z,S} - (k_S^2-2k_x^2)^2 & 4k_xk_{z,S}(k_S^2-2k_x^2) \\ -4k_xk_{z,P}(k_S^2-2k_x^2) & 4k_x^2k_{z,P}k_{z,S} - (k_S^2-2k_x^2)^2 \end{bmatrix} \qquad \text{(B.14)}$$

Note that the density of the medium does not influence the free surface reflectivity. Also note that the reflectivity for P to P-wave and S to S-wave reflection is identical *as a function of* k_x. As a function of the angle of incidence, the two reflectivity operators are different.

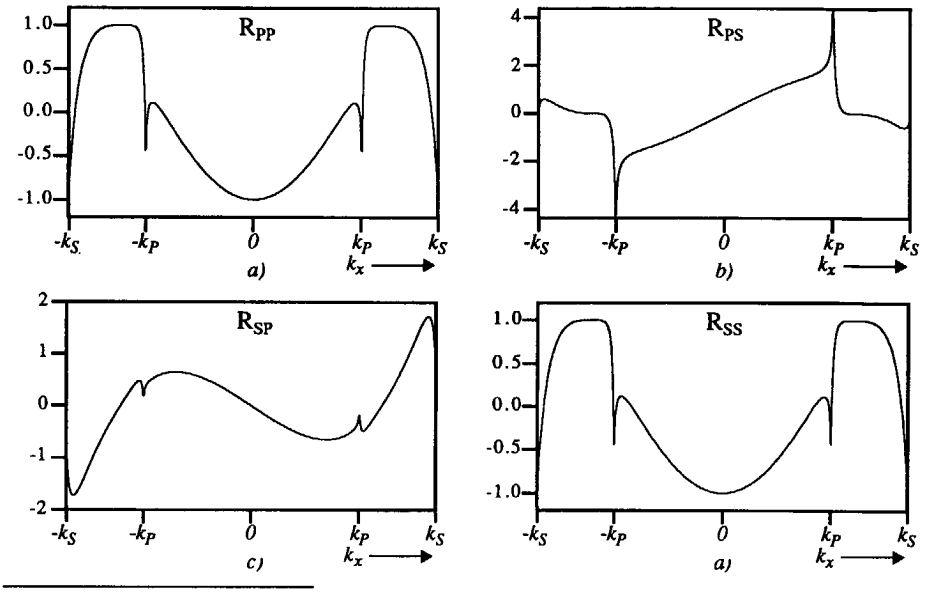

Fig. B.7 *Real part of the free surface reflectivity as a function of k_x for a medium with P-wave velocity of 2400 m/s and an S-wave velocity of 1400 m/s. a) P to P-wave reflection b) S to P-wave reflection c) P to S-wave reflection d) S to S-wave reflection.*

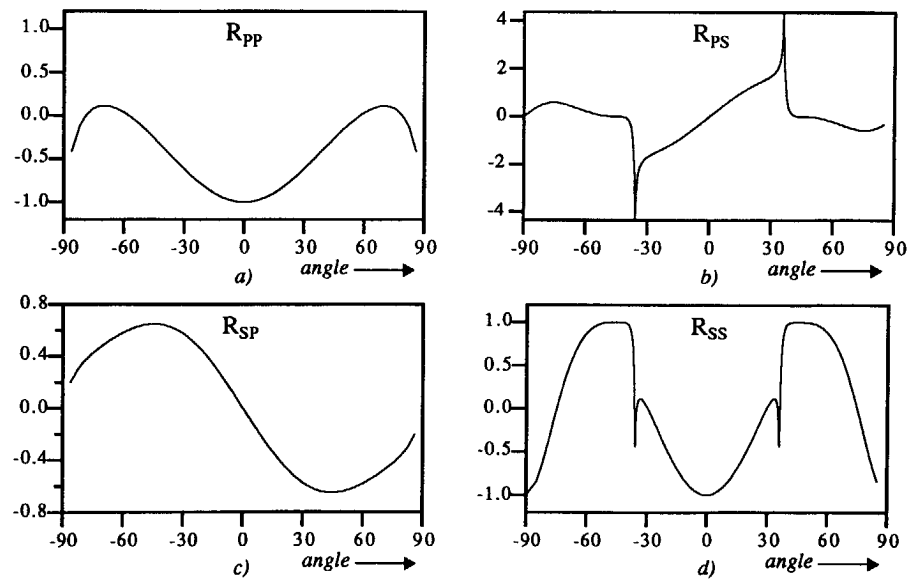

Fig. B.8 *Real part of the free surface reflectivity as a function of angle of incidence for a medium with P-wave velocity of 2400 m/s and an S-wave velocity of 1400 m/s. a) P to P-wave reflection b) S to P-wave reflection c) P to S-wave reflection d) S to S-wave reflection.*

As an example the (real part) reflectivity operators for the free surface with a P-wave velocity being 2400 m/s and an S-wave velocity of 1400 m/s are displayed in Fig. B.7. The velocities are corresponding to the first layer in the elastic example of Chapter 4. To construct the reflectivity matrices in the space domain, the operators are Fourier transformed from k_x to x and stored in the columns of the matrix. If the medium velocities near the surface do not vary laterally, all columns are identical. Optionally, the range of k_x-values outside $(-k_S,k_S)$, which is not used for propagating waves, can be used to adapt the reflectivity operator to a smooth one, in order to make the x-domain operator as short as possible.
Using the P- and S-wave velocities, the k_x-axis can be transformed to an angle axis. Fig. B.8 shows the same reflectivity operators, but as a function of the angle of incidence. Here we see that the P-P and the S-S reflection are not identical.

From (B.14) can be concluded that the free surface reflectivity only depends on the *ratio* of the P-wave and S-wave velocity. If the top of the subsurface consists of a so-called weathered layer, the ratio of the P- and S-wave velocities (which is normally in the range of 1.5 to 2) can be increased to even 4. Therefore, also an example of the elastic free surface reflectivity for a P- to S-wave ratio of 4 is shown in Fig. B.8. The P to P-wave reflection is almost -1 over the whole range of angles. Consequently, the amplitudes of the conversion reflectivities are also smaller than in the previous example. As the P- and S-wave velocity ration is that large, the critical S-wave angle is at 14.5°.

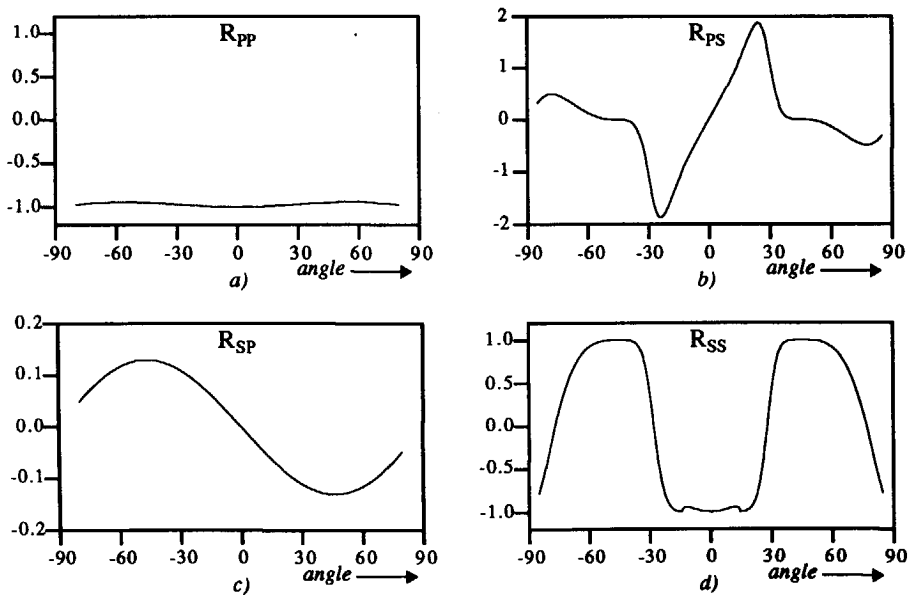

Fig. B.9 Real part of the free surface reflectivity as a function of angle of incidence for a medium with P-wave velocity of 800 m/s and an S-wave velocity of 200 m/s.a) P to P-wave reflection b) S to P-wave reflection c) P to S-wave reflection d) S to S-wave reflection.

REFERENCES

Aki, K.and Richards, P.G., 1980, Quantitative Seismology: W.H. Freeman and Co.

Anstey, N.A., and Newman, P., 1967, Part I: The sectional auto-correlogram and part II: The sectional retro-correlogram, Geophysical Prospecting, Volume 14, 391-426.

Anstey, N.A., 1981, Seismic Prospecting Instruments, Volume 1: Signal characteristics and instrument specifications, Gebrüder Borntraeger, Berlin.

Backus, M. M., 1959, Water reverberations - their nature and elimination: Geophysics, Volume 24, 233-261.

Baeten, G.J.M., 1989, Theoretical and practical aspects of the vibroseis method: Ph.D. thesis, Delft Univ. of Tech.

Baeten, G.J.M., Ziolkowski, A. M., Link, J.H., and Fokkema, J.T., 1990, Estimation of the dynamite wavelet from postcritical seismic data: presented at the 52nd Ann. Internat. Mtg., Euro. Assn. Expl. Geophys.

Beresford-Smith, G., and Rango, R., 1989, Suppression of ground roll by windowing in two domains: First Break, Volume 7, 55-63.

van den Berg, P.M., and Fokkema, J.T., 1980, The Rayleigh hypothesis in the theory of diffraction by a perturbation in a plane surface, Radio Science, Volume 15, 723-732.

Berkhout, A.J., 1982, Seismic migration: Imaging of acoustic energy by wave field extrapolation. A. Theoretical aspects, second edition: Elsevier Science Publ. Co., Inc.

Berkhout, A.J., 1984, Seismic migration: Imaging of acoustic energy by wave field extrapolation. B. Practical aspects: Elsevier Science Publ. Co., Inc.

Berkhout, A.J., 1985, Seismic migration: Imaging of acoustic energy by wave field extrapolation. A. Theoretical aspects, third edition: Elsevier Science Publ. Co., Inc.

Berkhout, A.J., 1987, Applied seismic wave theory: Elsevier Science Publ. Co., Inc.

Berkhout, A.J., and Wapenaar, C.P.A., 1990, DELPHI: Delft philosophy on acoustic and elastic inversion, The Leading Edge, Volume 9, No. 2, p.30-34.

Bernth, H., and Sonneland, L., 1983, Wave field extrapolation techniques for prestack attenuation of water reverberations: presented at the 53rd Ann. Internat. Mtg., Soc. Explor. Geophys.

Berryhill, J.R., and Kim, Y.C., 1986, Deep-water peglegs and multiples: emulation and suppression, Geophysics, Volume 51, 2177-2184.

de Bruin, C.G.M, Wapenaar, C.P.A, and Berkhout, A.J., 1990, Angle-dependent reflectivity by means of prestack migration, Geophysics, Volume 55, 1223-1234.

Darche, G., 1990, Spatial interpolation using a fast parabolic transform: presented at the 60th Ann. Internat. Mtg., Soc. Explor. Geophys.

Duijndam, A.J.W., 1988, Bayesian inversion of seismic data. Part I, Geophysical Prospecting, Volume 36, 878-898.

Durrani, J.A., 1991, Multiple attenuation by predictive deconvolution in the p-τ domain: presented at the 53rd Ann. Mtg., European Association of Explor. Geophys.

Fokkema, J.T., and Ziolkowski, A., 1987, The critical reflection theorem: Geophysics, Volume 52, 965-972.

Fokkema, J.T., Baeten, G.J.M., and Vaage, S., 1990, Directional deconvolution in the f-x domain: presented at the 60th Ann. Internat. Mtg., Soc. Explor. Geophys.

Fuchs, K., and Muller, G., 1971, Computation of synthetic seismograms with the reflectivity method and comparison of observations: Geophysical Journal of the Royal Astronomical Society, Volume 23, 417-433.

Gelfand, V., and Larner, K., 1983, Seismic lithology modeling: Leading Edge, Volume 3, 30-35.

Hampson, D., 1986, Inverse velocity stacking for multiple elimination: presented at the 56th Ann. Internat. Mtg., Soc. Explor. Geophys.

Hardy, R.J.J., and Hobbs, R.W., 1991, A strategy for multiple suppression, First Break, Volume 9, No. 4.

Julien, P., and Raoult, J., J., 1989, Adaptive subtraction of emulated multiples: presented at the 60th Ann. Internat. Mtg., Soc. Explor. Geophys.

Kelamis, P.G., Chiburis, E.F., and Shahryar, S., 1990, Radon multiple elimination, a practical methodology for land data: presented at the 60th Ann. Internat. Mtg., Soc. Explor. Geophys.

Kennett, B.L.N., 1979, The suppression of surface multiples on seismic records, Geophysical Prospecting, Volume 27, 584-600.

Kinneging, N.A., Budejicky. V., Wapenaar, C.P.A. and Berkhout, A.J., 1989, Efficient 2D and 3D shot record redatuming, Geophysical Prospecting, Volume 37, 493-530.

Koster, J.K., 1991, A direct layer-stripping approach to the inversion of marine seismic data, Ph.D. thesis.

Martinson, D.G., and Hopper, J. R., 1990, Nonlinear seismic trace interpolation: presented at the 60th Ann. Internat. Mtg., Soc. Explor. Geophys.

Monk, D.J., 1991,Wave equation multiple-suppression using constrained cross equalization: presented at the 53rd Ann. Mtg., European Association of Explor. Geophys.

Ongkiehong, L., and Askin, H.J., 1988, Towards the universal seismic acquisition technique, First Break, Volume 6, No. 2.

Parkes, G.E., Ziolkowski, A., Hatton, L., and Haugland, T., 1984, The signature of an air gun array: Computation from near-field measurements including interactions- Practical considerations, Geophysics, Volume 49, 105-111.

Robinson, E.A., and Treitel, S., 1980, Geophysical signal analysis, Prentice-Hall Signal Processing series, Prentice-Hall, Inc., Englewood Cliffs, N.J.

Rosenbaum, J. M., 1974, Synthetic microseismograms: Logging in porus formations: Geophysics, Volume 39, 14-32.

Ryu, J.V., 1982, Decomposition (DECOM) approach applied to wave-field analysis with seismic reflection records, Geophysics, Volume 47, 869-883.

Spitz, S, 1989, Trace interpolation beyond aliasing and without picking: presented at the 59th Ann. Internat. Mtg., Soc. Explor. Geophys.

Taner, M.T., 1980, Long period sea floor multiples and their suppression: Geophysical Prospecting, Volume 28, 30-48.

Taner, M.T., and O'Doherty, R.F., 1990, Conjugate gradient X-T deconvolution: presented at the 60th Ann. Internat. Mtg., Soc. Explor. Geophys.

Tarantola, A., 1987, Inverse problem theory, methods for data fitting and model parameter estimation: Elsevier Science Publ. Co., Inc.

Thybo, H., 1989, Wrap-around removal from one-dimensional synthetic seismograms: Geophysics, Volume 54, 911-915.

Ursin, B., 1983, Review of elastic and electromagnetic wave propagation in horizontally layered media: Geophysics, Volume 48, 1063-1081.

Verschuur, D.J., Berkhout, A.J., and Wapenaar, C.P.A., 1989, Wavelet estimation by prestack multiple elimination: presented at the 59th Ann. Internat. Mtg., Soc. Explor. Geophys.

Wapenaar, C.P.A., and Berkhout, A.J., 1989, Elastic wave field extrapolation: Redatuming of single- and multi-component seismic data: Elsevier Science Publ. Co., Inc.

Wapenaar, C.P.A., Herrmann, P., Verschuur, D.J., and Berkhout, A.J., 1990a, Decomposition of multi-component seismic data into primary P and S wave responses, Geophysical Prospecting, Volume 38, 633-661.

Wapenaar, C.P.A., Verschuur, D.J., and Herrmann, P., 1990b, Amplitude preprocessing of 2-D seismic data, presented at the 60th Ann. Internat. Mtg., Soc. Explor. Geophys.

Wiggins, J.W., 1988, Attenuation of complex water-bottom multiples by wave-equation based prediction and subtraction, Geophysics, Volume 53, 1527-1539.

Yilmaz, O., 1987, Seismic data processing, Soc. Explor. Geophys., Tulsa.

Yilmaz, O.,1989, Velocity stack processing: Geophysical prospecting, Volume 37, 357-382.

Ziolkowski, A. M., Parkes, G.E., Hatton, L., and Haugland, T., 1982, The signature of an air gun array: Computation from near-field measurements including interactions, Geophysics, Volume 47, 1413-1421.

Ziolkowski, A. M., 1991, Why don't we measure seismic signatures?, Geophysics, Volume 56, 190-201.

SUMMARY

In seismic processes such as migration and inversion, the input data is assumed to consist of *primary* reflections only. Therefore, multiple reflections should be removed in one of the pre-processing steps.

It is not always realized that the *free surface* acts as the major multiple generating interface. Therefore, removing the surface-related multiples will solve the multiple problem to a large extend.

This thesis starts with an overview of the most popular multiple elimination methods, being predictive deconvolution, velocity filtering and wave field based dereverberation. Next, the newly developed surface-related multiple elimination method is introduced. If the subsurface structures are complex and/or if velocity discrimination is not possible and/or if true *pre-stack* primary amplitudes are desired, the surface-related method is to be preferred. Furthermore, if the target is rather deep in the section (say below 2s) the multiple problem is often not defined by reverberations in the first layer, but by *other* surface-related multiples. In that situation, the surface-related multiple elimination method is the only method to be used.

The surface-related multiple elimination method is derived as an *inversion* process on the seismic surface data. An inverse operator is applied to the data, the operator parameters being determined by the free surface reflectivity and the source and receiver characteristics. Application involves pre-stack convolutions of the seismic data with itself. No knowledge about the *sub*surface is required.

In a first step the source and receiver array effects are optionally removed and the data is decomposed into an upgoing response due to a downgoing source wave field. The source signature is estimated in a true amplitude sense by applying the surface-related multiple elimina-

tion process *adaptively*. As a criterion to decide whether the multiples have been optimally removed, the energy in the output is used.

The theory for surface-related multiple elimination can be extended to the *elastic* case, using multi-component data. Similar to the acoustic case, after removing the source and receiver characteristics, decomposition into down- and upgoing elastic wave fields is applied. By including the elastic reflectivity of the free surface, all surface-related multiples *and conversions* can be eliminated.

The surface-related multiple elimination procedure in the acoustic mode (marine data) yields very good results on both simulated as well as field data. In the elastic mode (land data) good results have been achieved on a simulated multi-component data set.

An important advantage of surface-related multiple elimination is the fact that no information about the subsurface is required to eliminate *all* surface-related multiples. The data itself contains implicitly all information to accurately predict the surface-related multiples.

A disadvantage of surface-related multiple elimination is the large amount of calculations that have to be applied; it is comparable to pre-stack redatuming. Another disadvantage is the fact that the result of the surface-related multiple elimination process depends on the input data quality, i.e. any missing or extra events in the data are translated in a wrongly predicted multiple field. However, this can be overcome by applying a *pre-processing* step that removes direct waves and carefully generates missing traces by inter- or extrapolation.

For more or less one dimensional subsurfaces, the method can be applied to individual CMP--gathers. In this CMP-variant the CMP-gathers are assumed to be shot records in a (approximately) horizontally layered medium. It allows application of the method in the wave number or slowness domain. In those domains matrix multiplications (corresponding with lateral convolutions) reduce to scalar multiplications. A speed up of about a factor 10 can be expected for practical applications. The CMP-variant shows acceptable results for a field data set that has been recorded in the North Sea.

The results in this thesis show that the surface-related multiple elimination process (including pre-processing) solves the seismic signal-to-noise problem to a very large extend.

SAMENVATTING

In seismische processen, zoals migratie en inversie, wordt de input data verondersteld alleen uit primaire reflekties te bestaan. Multiple reflekties dienen daarom verwijderd te worden in één van de voorbewerkingsstappen.

Het is niet algemeen bekend dat het *vrije aardoppervlak* de belangrijkste multiple generator is. Daarom zal het verwijderen van de multiples die door het vrije aardoppervlak gegenereerd worden ("oppervlakte multiples"), het multiple probleem voor het grootste gedeelte oplossen.

Dit proefschrift begint met een overzicht van de meest gebruikte multiple eliminatie methoden: prediktieve deconvolutie, snelheid gebaseerde filtering en golfveld gebaseerde dereverberatie. Daarna wordt de nieuw ontwikkelde oppervlakte-multiple eliminatie methode geïntroduceerd.
Als de strukturen in de ondergrond ingewikkeld zijn en/of de scheiding op basis van snelheid niet mogelijk is en/of nauwkeurige *pre-stack* amplituden in de primaire reflekties gewenst zijn, heeft de oppervlakte-multiple eliminatie methode de voorkeur. Als bovendien de reflekties van de interessante strukturen zich vrij diep in de seismische sectie bevinden (zeg boven de 2 s), dan wordt het multiple probleem vaak niet bepaald door de reverberaties in de eerste laag, maar door de *overige* oppervlakte-multiples. In dat geval is de oppervlakte-multiple eliminatie methode de enige oplossing.

De nieuwe multiple eliminatie methode kan worden afgeleid als een *inversie* proces voor de seismische data. Een inverse operator wordt toegepast op de data, waarbij de parameters van deze operator bepaald worden door de reflektie eigenschappen van het vrije oppervlak en door de bron- en ontvangerkarakteristieken. Toepassing van de methode omvat pre-stack convoluties van de seismische data met zichzelf. Hierbij is geen enkele informatie van de *ondergrond* nodig.

In een eerste stap wordt er, indien noodzakelijk, voor de bron en ontvanger array-effekten gecorrigeerd en wordt de data vertaald in een opgaand gereflekteerd golfveld ten gevolge van een neergaand bronveld. Door vervolgens de multiple eliminatie methode *adaptief* op de resulterende data toe te passen kan het bronsignaal geschat worden met de correcte amplitude schaling. Hierbij wordt de totale energie van het resultaat na multiple eliminatie gebruikt als kriterium om te beslissen of de multiples optimaal geëlimineerd zijn.

De theorie van de nieuwe multiple eliminatie methode kan uitgebreid worden voor de *elastische* situatie (landdata), gebruik makend van multi-component data. Zoals ook in het akoestische geval gedaan wordt, vindt na het verwijderen van de bron- en ontvangerkarakteristieken een decompositie plaats in neer- en opgaande golfvelden. Als ook de elastische reflektie eigenschappen van het vrije oppervlak worden meegenomen, kunnen alle oppervlaktemultiples en *conversies* geëlimineerd worden.

De nieuwe multiple eliminatie methode in de akoestische variant (voor marinedata) levert zeer goede resultaten op zowel gesimuleerde als echte data. In de elastische variant (voor landdata) zijn goede resultaten verkregen op een gesimuleerde multi-component dataset (finite difference data). De evaluatie op echte landdata heeft nog niet plaatsgevonden.

Een belangrijk voordeel van de nieuwe multiple eliminatie methode is het feit dat geen enkele informatie over de ondergrond nodig is om *alle* oppervlakte multiples te verwijderen. De data zelf bevat impliciet de noodzakelijke informatie om nauwkeurig alle oppervlakte multiples te voorspellen.

Een nadeel van de nieuwe multiple eliminatie methode is de grote hoeveelheid berekeningen die gedaan moet worden, vergelijkbaar met pre-stack redatuming. Een ander nadeel is het feit dat het resultaat van het multiple eliminatie proces afhangt van de kwaliteit van de input data; elk missend of extra event in de data wordt vertaald in verkeerd voorspelde multiples. Dit kan echter voorkomen worden door een voorbewerkingsstap op de data uit te voeren waarbij het direkte veld verwijderd wordt en de missende informatie nauwkeurig wordt opgevuld met behulp van interpolatie- of extrapolatietechnieken.

Als de ondergrond min of meer ééndimensionaal is kan de nieuwe methode ook toegepast worden op individuele CMP-gathers. In deze CMP variant worden de CMP-gathers als schot registraties van een (bij benadering) horizontaal gelaagd medium verondersteld. Op deze manier kan de procedure in het golfgetal- of ray-parameterdomein worden uitgevoerd. In deze domeinen vereenvoudigen de matrix vermenigvuldigingen in het plaatsdomein (die overeenkomen met laterale convoluties) tot scalaire vermenigvuldigingen. Op deze manier kan een verbetering in rekentijd met ongeveer een faktor 10 verwacht worden. De toepassing van de CMP-variant op een dataset uit de Noordzee laat bevredigende resultaten zien.

De resultaten uit dit proefschrift laten zien dat eliminatie van de, door het aardoppervlak gegenereerde, multiples het probleem van de seismische signaal-ruis verhouding grotendeels oplost.

CURRICULUM VITAE

Naam	Verschuur, Dirk Jacob
Geboortedatum	1 september 1964
Geboorteplaats	Alphen aan den Rijn
OPLEIDING	
1970 - 1976	Basisonderwijs te Alphen aan den Rijn
1976 - 1982	Atheneum B aan het Chr. Lyceum te Alphen aan den Rijn
1982 - 1986	Technische Natuurkunde aan de Technische Universiteit Delft
	Afstudeeronderzoek: "On the Wigner distributions of loudspeaker responses in a room" in samenwerking met het Philips Natuurkundig Laboratorium in Eindhoven.
WERKERVARING	
1986 - 1991	Wetenschappelijk onderzoeker aan de Technische Universiteit Delft, Vakgroep Akoestiek en Seismiek, STW projekt DTN 58.0879.